TECHNICAL REPORTS OF THE METEOROLOGICAL RESEARCH INSTITUTE

Documentation of the Meteorological Research Institute / Numerical Prediction Division Unified Nonhydrostatic Model

BY

Kazuo Saito, Teruyuki Kato, Hisaki Eito
and
Chiashi Muroi

気象研究所技術報告

第42号

気象研究所/数値予報課統一非静力学モデル

斉藤和雄・加藤輝之・永戸久喜
室井ちあし

気 象 研 究 所

METEROLOGICAL RESEARCH INSTITUTE, JAPAN

MARCH 2001

The *Technical Reports of the Meteorological Research Institute* has been issued at irregular intervals by the Meteorological Research Institute since 1978 as a medium for the publication of technical reports, data reports and comprehensive reports on meteorology, oceanography, seismology and related earth sciences (hereafter referred to as reports) contributed by the members of the MRI and the collaborating researches.

The Editing Committee reserves the right of decision on acceptability of manuscripts and is responsible for the final editing.

Documentation of the Meteorological Research Institute / Numerical Prediction Division Unified Nonhydrostatic Model

BY

Kazuo Saito, Teruyuki Kato, and Hisaki Eito
Forecast Research Department, Meteorological Research Institute
1-1 Nagamine, Tsukuba, Ibaraki, 305-0052 Japan

and

Chiashi Muroi
Numerical Prediction Division, Japan Meteorological Agency
1-3-4 Otemachi, Chiyoda-ku, Tokyo, 100-8122 Japan

Contents

気象研究所/数値予報課統一非静力学モデル

斉藤和雄*・加藤輝之*・永戸久喜*
室井ちあし†

この技術報告は気象研究所予報研究部と気象庁数値予報課が共同開発している多目的非静力学モデルについて記述する。このモデルは，気象研究所予報研究部で開発された非静力学メソスケールモデルと気象庁数値予報課で開発された非静力モデルの統合モデルの第一歩として作成されたものである。

気象研究所予報研究部では，1991 年に技術報告「気象研究所予報研究部で開発された非静水圧モデル(Ikawa and Saito, 1991)」を刊行した後，モデルを用いたメソスケール現象の機構解明についての研究とモデルの改良に取り組んできた。モデルはまず，気象庁領域モデルとのネスティングにより再現実験が可能なモデルに改良された。当初は支配方程式系として非弾性方程式系が用いられていたが，その後マップファクターを含む完全圧縮方程式系に改良され，さらに物理過程の強化や新しい工夫の追加などにより，本格的なメソスケールモデル（MRI-NHM）へと発展してきている（斉藤・加藤，1999)。

気象庁数値予報課では，1997 年から格子点法を用いる非静力学予報モデルの開発を開始し，データ同化手法や新しい計算機環境の下で現業に適した高い実行効率を達成するための計算手法などに配慮しながら，モデル開発を行ってきた（室井，1998；1999a)。

気象研究所と数値予報課では，これまでもソースプログラムを含む様々な技術情報の交換を積極的に行ってきたが，メソモデル開発については上記のようにそれぞれの機関である程度独立して行われてきた歴史的経緯があった。限られた人的資源の中で，近年の数値モデルの巨大化と計算機環境の急速な変化に対応していくために，モデルを出来る限り共有することによって両機関でより密接な協力体制を持つことが望まれるようになっていた。

このような情勢に鑑み，非静力学モデルについては，1999 年 2 月に両機関のモデルを統合する方向で基本合意が成立し，いくつかのプランが検討された。最初のステップとして，MRI-NHM に数値予報課非静力モデルで開発されたスプリットイクスプリシット時間積分法（HE-VI スキーム）を組み込むことにより統合モデル（MRI/NPD-NHM）を作成した（室井ほか，1999)。今後，このモデルをベースに，次世代の計算機環境にも対応した現業予報と研究の双方に資する統一メソモデルを共同開発していくことで作業が始まっている。これらの意味において，この技術報告に記述されているモデルは，その一部は気象研究所予報研究部で開発されてきた MRI-NHM のいわば最後のバージョンであり，また一方で，全体としては両機関でのモデル共同開発のスタートラインとしての統合モデルの最初のバージョンでもある。

本モデルにはまだ多くの改良すべき点が残されている。分散主記憶型並列計算機への対応と最適化，現業予報モデルとしても用いるための環境の整備や高速化と計算安定性の保証，など喫緊なテーマがある。標準的コーディングルールに準拠した FORTRAN90 への書き換えなども必要になってくるだろう。また力学フレームや境界条件，物理過程についても，多くの改良課題が残っている。これらのいくつかについては既に取り組みが始まっている。気象庁のモデル公開の方針を受けて，近い将来，このモデル

* 気象研究所予報研究部
† 気象庁数値予報課（気象研究所予報研究部に併任）

は所定の手続きを経て気象庁内外の気象官署や大学などでも研究用に利用できるように体制が整備される予定になっている。今後，このモデルがより多くの人に利用され新しい研究成果を生み出す助けになるとともに，更にグレードアップしたモデルが将来新たな報告として刊行されることを期待している。

このモデルの開発にあたっては，非常に多くの方の協力・助力を頂いた。気象研究所では，長谷川隆司，古賀晴成，大塚伸，吉住禎夫の歴代の予報研究部長，および近藤洋輝(現気候研究部長)，丸山健人(現東京学芸大学)，和田美鈴（故人）の前予報研究部第一研究室長にいろいろお世話になった。吉崎正憲現予報研究部第一研究室長には，モデル開発とメソ現象の理解について特に多くのご指導を頂いた。さらに中村一，青梨和正，瀬古弘，栗原和夫(現気象庁気候情報課)，田宮久一郎，藤部文昭，金久博忠，上野充，村田昭彦，益子渉，清野直子，山本哲，村上正隆の各氏にも多くのご助力を頂いた。気象庁数値予報課では，佐藤信夫，岩崎俊樹，露木義の歴代の数値予報班長にいろいろお世話になったほか，中村誠臣，永田雅，郷田治稔，山田和孝の各氏にも，さまざまなご助力を頂いた。このモデルの物理過程のいくつかは，気象庁数値予報課で開発されたJSMやRSMのソースプログラムを参考にしている。このモデルの力学コアや物理過程の重要な部分のいくつかは，1991年に急逝された気象研究所の故猪川元興主任研究官の仕事が基になっている。故人のご功労に改めて深い敬意を表するものである。

本書の構成は以下のとおりとなっている。B章では，総説としてモデルの現時点での仕様が述べられる。C章では，モデルの基礎方程式系と気圧方程式の定式化が述べられる。D章では，モデルの差分表現と気圧方程式の数値解法が述べられる。E章とF章では，モデルの初期条件と境界条件についてを記述している。G章では，Ikawa and Saito (1991) より後に新たに追加された物理過程について説明している。H章ではモデルの検証と計算例をいくつか示した。I章ではモデルの構造を，J章では関連するユーティリティを記述した。K章は，モデルを実際に走らせるためのユーザーガイドである。L章には，現在進行中の取り組みのうち，分散主記憶型並列計算機への対応するための並列化の取り組みについてと気象庁の現業用メソモデルの開発についての数値予報課との共同の取り組みについて簡単に言及した。また最近開始した将来の全球非静力学モデルに向けての開発のための取り組みとしての球面直交曲線座標系バージョンについても簡単に紹介した。本報告は，C-2-4，C-3-4，D-2-3，G-1-2，G-1-3，G-1-4，G-2-2，G-5-1，H-3，J-3-2，K-5-2を主に加藤が，G-5-2，H-4を主に永戸が，C-3-2，L-2を主に室井が，I-2を全員が，それ以外を主に斉藤が書いた。図の作成に関して，筑波大学の佐藤友徳氏の協力を頂いた。

最後に，本原稿を精読して有益なコメントを下さった査読者の方々にも感謝したい。

A. Preface

This technical report describes a multipurpose nonhydrostatic atmospheric model developed by the Forecast Research Department of the Meteorological Research Institute and the Numerical Prediction Division of the Japan Meteorological Agency. This work was accomplished as a first step in the collaboration between MRI and NPD to develop a unified mesoscale model.

In MRI, "Nonhydrostatic model developed at the Forecast Research Department of MRI (Ikawa and Saito, 1991)" was published in the MRI Technical Report. Ikawa and Saito's (1991) model was developed as a research tool and used for simulations of mountain flow (Saito, 1993 ; Saito et al., 1994) and orographic snowfall (Saito et al., 1996). The model was modified to a nesting model to realistically simulate mesoscale phenomena (Saito and Ikawa, 1992 ; Saito, 1994a). For its basic equations, fully compressible equations including a map factor (Saito and Kato, 1996 ; Saito, 1997) replaced anelastic equations, where the linearlization using the reference atmosphere was removed. The semi-implicit time integration scheme (HI-VI scheme) was employed. Furthermore, the Box-Lagrangian rain drop scheme (Kato, 1995), the moist convective adjustment (Kato and Saito, 1995), the prediction of ground temperature (Kato, 1996), the modified centered difference advection scheme (Kato, 1998), two atmospheric radiation schemes (Kato, 1999 ; Eito et al., 1999), *etc.,* were also incorporated into the model. These modifications extended the model to a full-scale mesoscale model called "MRI-NHM (Saito and Kato, 1999)" that has been used for several studies in MRI (*e.g.,* Fujibe et al., 1999 ; Seko et al., 1999 ; Yoshizaki et al., 2000).

In NPD, a spectral nonhydrostatic model was developed by Goda and Kurihara (1991). Development of another fully compressible grid model was begun in 1997, and its numerics were reported by Muroi (1998). The split-explicit time integration scheme (HE-VI scheme) was employed, considering the computational efficiency in the next generation computing facilities. Muroi (1999a) experimented a nested run with 10 km horizontal resolution by the NPD nonhydrostatic model, supposing future numerical prediction in JMA.

Collaboration between MRI and NPD should be promoted to prepare for the rapid change of computer environments and to accelerate nonhydrostatic modeling for both research and operational objectives (Muroi, 1999b). From this viewpoint, the two modeling centers agreed to unify the two mesoscale models, and joint work was started in February 1999. As the first step, the HE-VI time integration scheme was incorporated into MRI-NHM by Muroi et al. (1999), and the first version of the unified model, "MRI/NPD-NHM," was completed in July 1999. Further collaboration on this prototypical model is currently under way to develop the next generation system (Muroi et al., 2000). Under these circumstances, the model described in this technical report is the final version of MRI-NHM and, simultaneously, the first version of the MRI/NPD community model, which is the starting point of mutual modeling work at MRI and NPD.

Many aspects of our model must be revised, including code parallelization to accommodate distributed memory parallel computers and optimization as an operational model, which are urgently needed. The code should be refined using FORTRAN 90 based on new programming standards. Several points must also be improved in the dynamic frame, boundary conditions and physical processes. Some revisions of the above points have already been started, as mentioned in Chapter L. In addition, a number of university scientists are currently expressing interest in participating in our modeling work. We hope that this model will be used more widely in the Japanese research community and that new reports on further upgraded models will be published in the future.

A large number of scientists have contributed to developing this model. We thank the staff of MRI and NPD for supporting our modeling work. Specifically, M. Yoshizaki, Head of the First Laboratory of the Forecast Research Department of MRI, gave us invaluable comments and continuous encouragement. We also thank R. Hasegawa, H. Koga, S. Otsuka, S. Yoshizumi, H. Kondo, T. Maruyama, M. Wada, H. Nakamura, K. Aonashi, H. Seko, K. Kurihara, T. Tamiya, F. Fujibe, H. Kanehisa, M. Ueno, A. Murata, W. Mashiko, N. Seino, A. Yamamoto and M. Murakami of MRI for their help and discussions. We also express our appreciation to N. Sato, T. Iwasaki, T. Tsuyuki, M. Nakamura, M. Nagata, H. Gouda and K. Yamada of NPD for their help and courtesy in referring to the NPD operational models. Some source codes of this nonhydrostatic model were developed with reference to the program of JSM. We express our deepest respect for the achievements of the late Dr. M. Ikawa, who passed away in 1991 after dedicating half his life to developing a nonhydrostatic model in MRI.

The organization of this report is as follows. Chapter B presents an overview of the model. Chapter C gives the governing equations and pressure equations. Chapter D describes their finite discretization form and relevant pressure equation solver. Chapters E and F introduce the initiation procedures and boundary conditions. Chapter G explains newly incorporated physical processes after Ikawa and Saito (1991) and diffusion processes. Chapter H presents examples of numerical simulation. Chapters I and J describe the model code structure and relevant utilities. Chapter K is the user's guide to running the model. In Chapter L, we briefly refer to current and future programs for code parallelization and joint programs of MRI and NPD to develop a regional model of JMA for numerical prediction. A spherical curvilinear orthogonal coordinate version under development to realize a global nonhydrostatic model in the future is also briefly introduced.

Sections C-2-4, C-3-4, D-2-3, G-1-2, G-1-3, G-1-4, G-2-2, G-5-1, H-3, J-3-2 and K-5-2 were mainly written by T. Kato; sections G-5-2 and H-4, by H. Eito; and sections C-3-2 and L-2, by C. Muroi. Section I-2 was written by all authors. Other sections were mainly written by K. Saito.

Finally, we would like to extend our gratitude to the anonymous reviewers, whose valuable comments improved the manuscript significantly.

B. Overview of the model

The MRI/NPD unified nonhydrostatic model is a multipurpose mesoscale model being developed by the Forecast Research Department of the Meteorological Research Institute and the Numerical Prediction Division of the Japan Meteorological Agency for both research and operational forecasting. Fully compressible equations with conformal mapping or anelastic approximation (AE) can be selected as the basic equations. The fully compressible model doesn't contain approximations, such as the linearlization using the reference atmosphere and/or omitting the diabatic heating term in the pressure equation. In addition to the semi-implicit scheme (HI-VI scheme) employed in MRI-NHM, the split-explicit scheme (HE-VI scheme) developed at NPD has been incorporated into the model for the computational scheme. Accordingly, three dynamic cores (HI-VI, HE-VI and AE) are available and can be selected by a mode switch.

future.

A large number of scientists have contributed to developing this model. We thank the staff of MRI and NPD for supporting our modeling work. Specifically, M. Yoshizaki, Head of the First Laboratory of the Forecast Research Department of MRI, gave us invaluable comments and continuous encouragement. We also thank R. Hasegawa, H. Koga, S. Otsuka, S. Yoshizumi, H. Kondo, T. Maruyama, M. Wada, H. Nakamura, K. Aonashi, H. Seko, K. Kurihara, T. Tamiya, F. Fujibe, H. Kanehisa, M. Ueno, A. Murata, W. Mashiko, N. Seino, A. Yamamoto and M. Murakami of MRI for their help and discussions. We also express our appreciation to N. Sato, T. Iwasaki, T. Tsuyuki, M. Nakamura, M. Nagata, H. Gouda and K. Yamada of NPD for their help and courtesy in referring to the NPD operational models. Some source codes of this nonhydrostatic model were developed with reference to the program of JSM. We express our deepest respect for the achievements of the late Dr. M. Ikawa, who passed away in 1991 after dedicating half his life to developing a nonhydrostatic model in MRI.

The organization of this report is as follows. Chapter B presents an overview of the model. Chapter C gives the governing equations and pressure equations. Chapter D describes their finite discretization form and relevant pressure equation solver. Chapters E and F introduce the initiation procedures and boundary conditions. Chapter G explains newly incorporated physical processes after Ikawa and Saito (1991) and diffusion processes. Chapter H presents examples of numerical simulation. Chapters I and J describe the model code structure and relevant utilities. Chapter K is the user's guide to running the model. In Chapter L, we briefly refer to current and future programs for code parallelization and joint programs of MRI and NPD to develop a regional model of JMA for numerical prediction. A spherical curvilinear orthogonal coordinate version under development to realize a global nonhydrostatic model in the future is also briefly introduced.

Sections C-2-4, C-3-4, D-2-3, G-1-2, G-1-3, G-1-4, G-2-2, G-5-1, H-3, J-3-2 and K-5-2 were mainly written by T. Kato; sections G-5-2 and H-4, by H. Eito; and sections C-3-2 and L-2, by C. Muroi. Section I-2 was written by all authors. Other sections were mainly written by K. Saito.

Finally, we would like to extend our gratitude to the anonymous reviewers, whose valuable comments improved the manuscript significantly.

B. Overview of the model

The MRI/NPD unified nonhydrostatic model is a multipurpose mesoscale model being developed by the Forecast Research Department of the Meteorological Research Institute and the Numerical Prediction Division of the Japan Meteorological Agency for both research and operational forecasting. Fully compressible equations with conformal mapping or anelastic approximation (AE) can be selected as the basic equations. The fully compressible model doesn't contain approximations, such as the linearlization using the reference atmosphere and/or omitting the diabatic heating term in the pressure equation. In addition to the semi-implicit scheme (HI-VI scheme) employed in MRI-NHM, the split-explicit scheme (HE-VI scheme) developed at NPD has been incorporated into the model for the computational scheme. Accordingly, three dynamic cores (HI-VI, HE-VI and AE) are available and can be selected by a mode switch.

Table B-1 MRI/NPD-NHM Specifications.

Category	Specification	Optional choice
Basic equations	Fully compressible with a map factor (Saito, 1997) Fall-out of precipitable water substances is considered in continuity equation	Anelastic (Ikawa, 1988) Quasi-compressible (Ikawa, 1988) Hydrostatic (Kato and Saito, 1995)
Vertical coordinate	Terrain-following	
Horizontal coordinate	Conformal map projection (Saito, 2000)	Cartesian
Vertical grid structure	Lorenz type	
Horizontal grid structure	Arakawa C	
Advection term	Flux form, second order	Modified centered difference (Kato, 1998)
	Box-Lagrangian scheme for rainfall (Kato, 1995)	Advective form with third/fourth order (Saito, 1998)
Treatment of sound waves	HI-VI (Saito, 1997) HE-VI (Muroi et al., 1999)	Anelastic filtering (AE)
Time differencing	Semi-implicit (for HI-VI) Split-explicit (for HE-VI)	Leap-frog for AE
Turbulent closure	Deardorff level 2.5 (Saito and Ikawa, 1991; Saito, 1993)	
Cloud microphysics	Predict qv, qc, qr, qi, qs, qg (Ikawa *et al.,* 1991)	Predict number density of cloud ice, snow and graupel (Ikawa *et al.,* 1991)
Cumulus parameterization	Moist convective adjustment (Kato and Saito, 1995)	
Atmospheric radiattion	Long- and short-wave radiation specified by relative humidity (Kato, 1999)	Specified by cloud micro-physical properties (Eito *et al.,* 1999)
Surface layer (land)	Monin-Obukhov (Sommeria, 1976)	Free slip
(sea)	Kondo (1975)	
Lower boundary	Prognostic ground temperature (Kato, 1996)	Specified ground temperature
Upper boundary	Rigid lid, thermally insulated Rayleigh friction layer	
Lateral Boundary	Radiative nesting boundary condition (Saito, 1994a)	Open (Orlanski, 1976) Cyclic
Initialization	Hydrostatic interpolation from JSM or RSM	Variational calculus for AE scheme (Saito, 1994a)
Numerical diffusion	4-th order linear damping	Nonlinear damping

C. Model equations

C-1. Governing equations

C-1-1 Basic equations in Cartesian coordinates

For dry air, the atmospheric state is described by six fundamental variables; pressure p, density ρ, temperature T, and three wind components u, v and w. These six variables are governed by the following six equations.

a) Momentum equations

$$\frac{du}{dt}+\frac{1}{\rho}\frac{\partial p}{\partial x}=dif.u, \tag{C1-1-1}$$

$$\frac{dv}{dt}+\frac{1}{\rho}\frac{\rho p}{\partial y}=dif.v, \tag{C1-1-2}$$

$$\frac{dw}{dt}+\frac{1}{\rho}\frac{\partial p}{\partial z}+g=dif.w. \tag{C1-1-3}$$

b) Continuity equation

$$\frac{\partial \rho}{\partial t}+\frac{\partial \rho u}{\partial x}+\frac{\partial \rho v}{\partial y}+\frac{\partial \rho w}{\partial z}=0. \tag{C1-1-4}$$

c) Thermodynamic equation

$$\frac{d\theta}{dt}=\frac{Q}{C_p\pi}+dif.\theta. \tag{C1-1-5}$$

d) State equation

$$p=\rho RT. \tag{C1-1-6}$$

Here, $dif.\phi$ stands for the diffusion term for field variable ϕ. Q is the diabatic heating rate, C_p the specific heat of dry air at constant pressure, and R the gas constant for dry air.

θ is the potential temperature, and π the Exner function defined as

$$\pi\equiv\left(\frac{p}{p_0}\right)^{R/C_p}, \tag{C1-1-7}$$

$$\theta\equiv\frac{T}{\pi}. \tag{C1-1-8}$$

For moist air, taking account of the partial pressure of water vapor, the state equation is replaced by

$$p=\rho_a RT_v, \tag{C1-1-9}$$

where ρ_a is the density of air, which is the sum of the density of dry air and water vapor, and T_v is the virtual temperature defined as

$$T_v\equiv(1+0.61q_v)\,T. \tag{C1-1-10}$$

Here, q_v is the mixing ratio of water vapor. Virtual potential temperature is defined in the same manner as in (C1-1-8) by

$$\theta_v\equiv\frac{T_v}{\pi}=\frac{(1+0.61q_v)\,T}{\pi}=(1+0.61q_v)\,\theta. \tag{C1-1-11}$$

Using (C1-1-7) and (C1-1-8), the state equation (C1-1-9) is rewritten in the following formula.

$$\rho_a=\frac{p_0}{R\theta_v}\left(\frac{p}{p_0}\right)^{C_v/C_p}. \tag{C1-1-12}$$

C-1-2 Mass-virtual potential temperature

a) Definition of the density and the state equation

When water substances exist, we define the density as the sum of the masses of moist air and the water substances per unit volume as

$$\rho \equiv \rho_d + \rho_v + \rho_c + \rho_r + \rho_i + \rho_s + \rho_g$$
$$= \rho_a + \rho_c + \rho_r + \rho_i + \rho_s + \rho_g, \qquad \text{(C1-2-1)}$$

where subscripts c, r, i, s, g stand for the cloud water, rain, cloud ice, snow, and graupel. ρ_d is the density of dry air and ρ_v, that of water vapor. In terms of the mixing ratio q, we can express the above formula as

$$\rho = \rho_d (1 + q_v + q_c + q_r + q_i + q_s + q_g)$$
$$\cong \rho_a (1 + q_c + q_r + q_i + q_s + q_g). \qquad \text{(C1-2-2)}$$

In the second expression, q is not the *mixing ratio* but the *specific value,* which is defined by the ratio of the mass of water substance to moist air. In this technical report, we neglect the difference between the two technical terms, following a custom in mesoscale numerical modeling (this is a matter of terminology rather than approximation).

As q is sufficiently small compared with unity (on the order of 10^{-3}), we can approximate (C1-2-2) with sufficient accuracy as

$$\rho_a = \rho (1 + q_c + q_r + q_i + q_s + q_g)^{-1}$$
$$\cong \rho (1 - q_c - q_r - q_i - q_s - q_g). \qquad \text{(C1-2-3)}$$

Considering that the state equation is an equation for substances in gas phase, we obtain the following equation by substituting (C1-2-3) into the left-hand side of (C1-1-12),

$$\rho = \frac{p_0}{R\theta_v} \left(\frac{p}{p_0}\right)^{C_v/C_p} (1 - q_c - q_r - q_i - q_s - q_g)^{-1}$$
$$= \frac{p_0}{R\theta_m} \left(\frac{p}{p_0}\right)^{C_v/C_p}. \qquad \text{(C1-2-4)}$$

Here, θ_m is the *mass-virtual potential temperature* defined by

$$\theta_m \equiv \theta_v (1 - q_c - q_r - q_i - q_s - q_g)$$
$$= \theta (1 + 0.61 q_v)(1 - q_c - q_r - q_i - q_s - q_g). \qquad \text{(C1-2-5)}$$

This quantity was introduced in Ikawa and Saito (1991) to expand the fundamental equations, but was not used in the actual programming. In this model, we use (C1-2-4) and compute buoyancy directly and exactly by the perturbation of density.

b) Continuity equation

When we define the density by (C1-2-4), we must consider the fall-out of water substances. We regard the rain, snow and graupel as the precipitable water substances and neglect the fall-out of the cloud water and cloud ice. Using mass-weighted bulk terminal velocity V, the time tendency of the density can be expressed as

$$\frac{\partial \rho}{\partial t} = -\left(\frac{\partial \rho u}{\partial x} + \frac{\partial \rho u}{\partial y} - \frac{\partial}{\partial z}\{(\rho_a + \rho_c + \rho_i) w\}\right.$$
$$\left. + \frac{\partial}{\partial z}\{\rho_r (V_r - w) + \rho_s (V_s - w) + \rho_g (V_g - w)\}\right. \qquad \text{(C1-2-6)}$$

Thus, the continuity equation is replaced by

$$\frac{\partial\rho}{\partial t}+\frac{\partial\rho u}{\partial x}+\frac{\partial\rho v}{\partial y}+\frac{\partial\rho w}{\partial z}=\frac{\partial}{\partial z}(\rho_r V_r+\rho_s V_s+\rho_g V_g)$$

$$=\frac{\partial}{\partial z}(\rho_a V_r q_r+\rho_a V_s q_s+\rho_a V_g q_g). \qquad \text{(C1-2-7)}$$

In the model, the reference value of the density is used for the air-density in the right-hand side of (C1-2-7) for simplicity.

C-1-3 Fundamental equations in conformal map projection

In Ikawa and Saito (1991), terms relating to mapping projection were neglected in the basic equations. In the new model, the map factor relating to arbitrary conformal map projections (see in J-1-3) is taken into account in the basic equations. For example, in Polar stereographic projection, the horizontal coordinates in the model (x, y) corresponding to the Earth's surface of the latitude and longitude (φ, λ) are given by

$$\begin{pmatrix} x \\ y \end{pmatrix}=\begin{pmatrix} x_p+ma\cos\varphi\sin\Delta\lambda \\ y_p-ma\cos\varphi\cos\Delta\lambda \end{pmatrix}, \qquad \text{(C1-3-1)}$$

where (x_p, y_p) is the position of the north pole, $\Delta\lambda$ the deflection of longitude from the standard longitude λ_0, and a the radius of the Earth (Fig. J1-3-1). m is the map factor[1] and becomes unity at the standard latitude φ_0,

$$m=\frac{1+\sin\varphi_0}{1+sin\varphi}. \qquad \text{(C-1-3-2)}$$

Distance on the polar projection map (dx, dy) can be derived by differentiating (C1-3-1):

$$\begin{pmatrix} dx \\ dy \end{pmatrix}=ma\begin{pmatrix} -(1+\sin\varphi)^{-1}\cos\varphi d\varphi\cos\varphi\sin\Delta\lambda-\sin\varphi d\varphi\sin\Delta\lambda+\cos\varphi\cos\Delta\lambda d\lambda \\ (1+\sin\varphi)^{-1}\cos\varphi d\varphi\cos\varphi\cos\Delta\lambda+\sin\varphi d\varphi\cos\Delta\lambda+\cos\varphi\sin\Delta\lambda d\lambda \end{pmatrix}$$

$$=ma\begin{pmatrix} -d\varphi\sin\Delta\lambda+\cos\varphi\cos\Delta\lambda d\lambda \\ d\varphi\cos\Delta\lambda+\cos\varphi\sin\Delta\lambda d\lambda \end{pmatrix}=ma\begin{pmatrix} -\sin\Delta\lambda & cos\Delta\lambda \\ \cos\Delta\lambda & sin\Delta\lambda \end{pmatrix}\begin{pmatrix} d\varphi \\ \cos\varphi d\lambda \end{pmatrix}. \qquad \text{(C1-3-3)}$$

Considering the real distance on the Earth's surface, (dx_s, dy_s) is

$$\begin{pmatrix} dx_s \\ dy_s \end{pmatrix}=\begin{pmatrix} a\cos\varphi d\lambda \\ ad\varphi \end{pmatrix}. \qquad \text{(C1-3-4)}$$

The relationship between the differentials is given by the following rotational transformation:

$$\begin{pmatrix} dx \\ dy \end{pmatrix}=m\begin{pmatrix} \cos\Delta\lambda & -\sin\Delta\lambda \\ \sin\Delta\lambda & \cos\Delta\lambda \end{pmatrix}\begin{pmatrix} dx_s \\ dy_s \end{pmatrix}. \qquad \text{(C1-3-5)}$$

Since the velocity is written in the (x, y) coordinate system as

$$u=\frac{1}{m}\frac{dx}{dt}, \qquad \text{(C1-3-6)}$$

$$v=\frac{1}{m}\frac{dy}{dt}, \qquad \text{(C1-3-7)}$$

the relationship between the winds $\{u_s=dx_s/dt,\ v_s=dy_s/dt\}$ in the spherical coordinate system and $\{u, v\}$ is given by

[1]Strictly speaking, the map factor depends on the height h as

$$m'=\frac{1}{1+h/a}m. \qquad \text{(C1-3-2)}'$$

In this model, we neglect h/a to 1 and substitute m *for* m'.

$$\begin{pmatrix} u \\ v \end{pmatrix} = \begin{pmatrix} \cos\Delta\lambda & -\sin\Delta\lambda \\ \sin\Delta\lambda & \cos\Delta\lambda \end{pmatrix} \begin{pmatrix} u_s \\ v_s \end{pmatrix} \tag{C1-3-8}$$

Taking the third coordinate z in the upward vertical direction and defining w as $w = dz/dt$, the momentum equations in (x, y, z) are written as follows:

$$\frac{du}{dt} = Cor_1 + Crv_1 - \frac{1}{\rho} m \frac{\partial p}{\partial x} + Dif_1, \tag{C1-3-9}$$

$$\frac{dv}{dt} = Cor_2 + Crv_2 - \frac{1}{\rho} m \frac{\partial p}{\partial y} + Dif_2, \tag{C1-3-10}$$

$$\frac{dw}{dt} = Cor_3 + Crv_3 - \frac{1}{\rho} m \frac{\partial p}{\partial z} + Dif_3, \tag{C1-3-11}$$

where Dif stands for the diffusion terms, and the subscripts 1, 2 and 3 correspond to components x, y and z. Cor and Crv are the following Coriolis and curvature terms[2] (*e.g.,* Kikuchi. 1975).

$$Cor_1 = 2\Omega\sin\varphi v - 2\Omega\cos\varphi\cos\lambda w, \tag{C1-3-12}$$

$$Cor_2 = -2\Omega\cos\varphi\sin\Delta\lambda w - 2\Omega\sin\varphi u, \tag{C1-3-13}$$

$$Cor_3 = 2\Omega\cos\varphi\cos\Delta\lambda u + 2\Omega\cos\varphi\sin\Delta\lambda v, \tag{C1-3-14}$$

$$Crv_1 = m^2 v\{v\frac{\partial}{\partial x}(\frac{1}{m}) - u\frac{\partial}{\partial y}(\frac{1}{m})\} - \frac{uw}{a}, \tag{C1-3-15}$$

$$Crv_2 = m^2 u\{u\frac{\partial}{\partial y}(\frac{1}{m}) - v\frac{\partial}{\partial x}(\frac{1}{m})\} - \frac{vw}{a}, \tag{C1-3-16}$$

$$Crv_3 = \frac{u^2 + v^2}{a}. \tag{C1-3-17}$$

With no precipitation, the continuity equation becomes

$$\frac{1}{\rho}\frac{d\rho}{dt} + m^2\{\frac{\partial}{\partial x}(\frac{u}{m}) + \frac{\partial}{\partial y}(\frac{v}{m})\} + \frac{\partial w}{\partial z} + \frac{2w}{a} = 0. \tag{C1-3-18}$$

For Lambert conformal projection and Mercator projection, map factors are given by (J1-3-7) and (J1-3-13), respectively. For these projections, the form of Eqs. (C1-3-5) - (C1-3-18) is not altered, except that $\Delta\lambda$ becomes $c\Delta\lambda$, where c is given by (J1-3-8) for Lambert projection and zero for Mercator projection.

C-1-4 Fundamental equations in flux form

From (C1-3-6) and (C1-3-7), the total derivative in conformal map projection is given by

$$\frac{d}{dt} = \frac{\partial}{\partial t} + \frac{dx}{dt}\frac{\partial}{\partial x} + \frac{dy}{dt}\frac{\partial}{\partial y} + \frac{dz}{dt}\frac{\partial}{\partial z} = \frac{\partial}{\partial t} + m(u\frac{\partial}{\partial x} + v\frac{\partial}{\partial y}) + w\frac{\partial}{\partial z}. \tag{C1-4-1}$$

Substituting (C1-4-1), the continuity equation (C1-3-18) becomes

$$\frac{\partial\rho}{\partial t} + m(u\frac{\partial\rho}{\partial x} + v\frac{\partial\rho}{\partial y}) + w\frac{\partial\rho}{\partial z} + \rho m^2\{\frac{\partial}{\partial x}(\frac{u}{m}) + \frac{\partial}{\partial y}(\frac{v}{m})\} + \rho\frac{\partial w}{\partial z}$$

$$= \frac{\partial\rho}{\partial t} + m^2\{\frac{\partial}{\partial x}(\frac{\rho u}{m}) + \frac{\partial}{\partial y}(\frac{\rho v}{m})\} + \frac{\partial}{\partial z}(\rho w) = 0. \tag{C1-4-2}$$

Here, we neglected the last term of (C1-3-18), assuming the vertical scale of the motion is considerably smaller

[2]The last terms in (C1-3-15), (C1-3-16) and (C1-3-17) are proportional to $\frac{1}{m^2}\frac{\partial m'}{\partial z}$, and are absent in the limit of $a \to \infty$. However, these terms should be retained so that the set of basic equations approaches that in the spherical coordinates in the limit of $h/a \to 0$ (see L-3).

than the radius of the Earth. With the fall-out of precipitating substances, the above continuity equation becomes

$$\frac{\partial \rho}{\partial t}+m^2\{\frac{\partial}{\partial x}(\frac{\rho u}{m})+\frac{\partial}{\partial y}(\frac{\rho v}{m})\}+\frac{\partial}{\partial z}(\rho w)=Prc, \qquad \text{(C1-4-3)}$$

where Prc is the right-hand side of (C1-2-7).

For arbitrary variable ϕ, the total derivative can be written from (C1-4-1) as

$$\frac{\rho}{m^2}\frac{d\phi}{dt}=\frac{\rho}{m^2}\frac{\partial \phi}{\partial t}+\frac{\rho u}{m}\frac{\partial \phi}{\partial x}+\frac{\rho v}{m}\frac{\partial \phi}{\partial y}+\frac{\rho w}{m^2}\frac{\partial \phi}{\partial z}. \qquad \text{(C1-4-4)}$$

From (C1-4-3), we obtain

$$\frac{\phi}{m^2}\frac{\partial \rho}{\partial t}+\phi\{\frac{\partial}{\partial x}(\frac{\rho u}{m})+\frac{\partial}{\partial y}(\frac{\rho v}{m})\}+\frac{\phi}{m^2}\frac{\partial}{\partial z}(\rho w)-\frac{\phi}{m^2}Prc=0. \qquad \text{(C1-4-5)}$$

Consequently, the total derivative can be written as

$$\frac{\rho}{m^2}\frac{d\phi}{dt}=\frac{1}{m^2}\frac{\partial}{\partial t}(\rho\phi)+\frac{\partial}{\partial x}(\frac{\rho u\phi}{m})+\frac{\partial}{\partial y}(\frac{\rho v\phi}{m})+\frac{1}{m^2}\frac{\partial}{\partial z}(\rho w\phi)-\frac{\phi}{m^2}Prc, \qquad \text{(C1-4-6)}$$

or, assuming (C1-3-2), as

$$\frac{\rho}{m}\frac{d\phi}{dt}=\frac{\partial}{\partial t}(\frac{\rho\phi}{m})+m\{\frac{\partial}{\partial x}(\frac{\rho v\phi}{m})+\frac{\partial}{\partial y}(\frac{\rho v\phi}{m})\}+\frac{\partial}{\partial z}(\frac{\rho w\phi}{m})-\frac{\phi}{m}Prc. \qquad \text{(C1-4-7)}$$

Using (C1-4-7)[3], equations (C1-3-9) to (C1-3-11) become

$$\frac{\partial}{\partial t}(\frac{\rho u}{m})+Adv.U+\frac{\partial p}{\partial x}=Crv.U+Cor.U+Dif.U, \qquad \text{(C1-4-8)}$$

$$\frac{\partial}{\partial t}(\frac{\rho v}{m})+Adv.V+\frac{\partial p}{\partial y}=Crv.V+Cor.V+Dif.V, \qquad \text{(C1-4-9)}$$

$$\frac{\partial}{\partial t}(\frac{\rho w}{m})+Adv.W+\frac{1}{m}(\frac{\partial p}{\partial z}+\rho g)=Crv.W+Cor.W+Dif.W. \qquad \text{(C1-4-10)}$$

Here, $Adv.$ corresponds to the second to last terms on the right-hand side of (C1-4-7), *e.g.*, it is expressed for u as

$$Adv.U=m\{\frac{\partial}{\partial x}(\frac{\rho uu}{m})+\frac{\partial}{\partial y}(\frac{\rho vu}{m})\}+\frac{\partial}{\partial z}(\frac{\rho wu}{m})-\frac{u}{m}Prc. \qquad \text{(C1-4-11)}$$

$Cor.U$, $Cor.V$ and $Cor.W$ are Coriolis terms (C1-3-12) to (C1-3-14) multiplied by ρ/m. The curvature terms $Crv.U$, $Crv.V$ and $Crv.W$ are expressed by

$$Crv.U=\frac{\rho v}{m}(u\frac{\partial m}{\partial y}-v\frac{\partial m}{\partial x})-\frac{\rho u}{m}\frac{w}{a}, \qquad \text{(C1-4-12)}$$

$$Crv.V=\frac{\rho u}{m}(u\frac{\partial m}{\partial y}-v\frac{\partial m}{\partial x})-\frac{\rho v}{m}\frac{w}{a}, \qquad \text{(C1-4-13)}$$

$$Crv.W=\frac{m}{\rho a}\{(\frac{\rho u}{m})^2+(\frac{\rho v}{m})^2\}. \qquad \text{(C1-4-14)}$$

[3]Ikawa and Saito's (1991) nonhydrostatic model used the following relation.

$$\bar\rho\frac{\partial \phi}{dt}=\frac{\partial \bar\rho\phi}{\partial t}+\frac{\partial \bar\rho u\phi}{\partial x}+\frac{\partial \bar\rho v\phi}{\partial y}+\frac{\partial \bar\rho w\phi}{\partial z}. \qquad \text{(C1-4-7')}$$

The above relationship is correct only for anelastic equations but yields errors for quasi-compressible elastic equations. Ikawa (1988) suggested that the errors caused practically no trouble if the sound wave mode was sufficiently damped. However, they may cause computational instability in some cases when a longer time step is used (Saito, 1994b).

The thermodynamic equation is

$$\frac{d\theta}{dt}=\frac{\partial\theta}{\partial t}+Adv.\theta=\frac{Q}{C_p\pi}+Dif.\theta. \qquad \text{(C1-4-15)}$$

where the advection term in flux form is given as

$$Adv.\theta=[m\{\frac{\partial}{\partial x}(\frac{\rho u\theta}{m})+\frac{\partial}{\partial y}(\frac{\rho v\theta}{m})\}+\frac{\partial}{\partial z}(\frac{\rho w\theta}{m})-\frac{\theta}{m}\underline{(Prc-\frac{\partial\rho}{\partial t})}]\frac{m}{\rho}. \qquad \text{(C1-4-16)}$$

The underlined term is the divergence (sum of the second to fourth terms on the left-hand side of (C1-4-3)).

C-2. Fundamental equations in terrain-following coordinates

C-2-1 Equations in terrain-following coordinates

Following Gal-Chen and Somerville (1975) and Clark (1977), we introduce the terrain-following vertical coordinate

$$z^*=\frac{H(z-z_s)}{H-z_s}, \qquad \text{(C2-1-1)}$$

and components of the metric tensor for the coordinate transformations:

$$G^{\frac{1}{2}}=1-\frac{z_s}{H}, \qquad \text{(C2-1-2)}$$

$$G^{\frac{1}{2}}G^{13}=(\frac{z^*}{H}-1)\frac{\partial z_s}{\partial x}, \qquad \text{(C2-1-3)}$$

$$G^{\frac{1}{2}}G^{23}=(\frac{z^*}{H}-1)\frac{\partial z_s}{\partial y}. \qquad \text{(C2-1-4)}$$

Here, z_s is the surface height and H is the model top height. Applying the chain rule for the coordinate transformation from (x, y, z) to (x, y, z^*), the following relations are obtained for any arbitrary variable ϕ:

$$G^{\frac{1}{2}}\frac{\partial\phi}{\partial x}=\frac{\partial}{\partial x}(G^{\frac{1}{2}}\phi)+\frac{\partial}{\partial z^*}(G^{\frac{1}{2}}G^{13}\phi), \qquad \text{(C2-1-5)}$$

$$G^{\frac{1}{2}}\frac{\partial\phi}{\partial y}=\frac{\partial}{\partial y}(G^{\frac{1}{2}}\phi)+\frac{\partial}{\partial z^*}(G^{\frac{1}{2}}G^{23}\phi), \qquad \text{(C2-1-6)}$$

$$G^{\frac{1}{2}}\frac{\partial\phi}{\partial z}=\frac{\partial\phi}{\partial z^*}. \qquad \text{(C2-1-7)}$$

The cotinuity equation (C1-4-3) is rewritten as follows:

$$G^{\frac{1}{2}}\frac{\partial\rho}{\partial t}+DIVT(U,V,W)=PRC, \qquad \text{(C2-1-8)}$$

where U, V, and W are wind components multiplied by $\rho G^{1/2}/m$. These are taken as the prognostic variables:

$$U=\frac{\rho G^{\frac{1}{2}}u}{m}, \qquad \text{(C2-1-9)}$$

$$V=\frac{\rho G^{\frac{1}{2}}v}{m}, \qquad \text{(C2-1-10)}$$

$$W=\frac{\rho G^{\frac{1}{2}}w}{m}, \qquad \text{(C2-1-11)}$$

and $DIVT$ is the total divergence in z^* coordinate calculated by

$$DIVT(U,V,W)=m^2(\frac{\partial U}{\partial x}+\frac{\partial V}{\partial y})+m\frac{\partial W^*}{\partial z^*}. \qquad \text{(C2-1-12)}$$

W^* is the vertical momentum in z^* coordinate defined by

$$W^* = \frac{\rho G^{\frac{1}{2}}}{m}\frac{dz^*}{dt} = \frac{1}{G^{\frac{1}{2}}}\{W + m(G^{\frac{1}{2}}G^{13}U + G^{\frac{1}{2}}G^{23}V)\}, \qquad \text{(C2-1-13)}$$

and PRC is the divergence of the fall-out of water substances written in z^* coordinate:

$$PRC = \frac{\partial}{\partial z^*}(\rho_a V_r q_r + \rho_a V_s q_s + \rho_a V_g q_g). \qquad \text{(C2-1-14)}$$

Momentum equations (C1-4-8) to (C1-4-10) are rewritten as follows:

$$\frac{\partial U}{\partial t} + \frac{\partial P}{\partial x} + \frac{\partial G^{\frac{1}{2}}G^{13}P}{G^{\frac{1}{2}}\partial z^*} = -ADVU + RU, \qquad \text{(C2-1-15)}$$

$$\frac{\partial V}{\partial t} + \frac{\partial P}{\partial y} + \frac{\partial G^{\frac{1}{2}}G^{13}P}{G^{\frac{1}{2}}\partial z^*} = -ADVU + RV, \qquad \text{(C2-1-16)}$$

$$\frac{\partial W}{\partial t} + \frac{1}{mG^{\frac{1}{2}}}\frac{\partial P}{\partial z^*} = \frac{1}{m}BUOY - ADVW + RW, \qquad \text{(C2-1-17)}$$

where P denotes $(p\text{-}\bar{p})G^{1/2}$. $BUOY$ is the buoyancy term, which is defined by the deviation of the density as

$$BUOY = -(\rho - \bar{\rho})gG^{\frac{1}{2}}. \qquad \text{(C2-1-18)}$$

Here, overbars indicate the variables of the reference atmosphere in which we assume hydrostatic balance. *ADVU, ADVV* and *ADVW* are the advection terms for *U, V* and *W*. For example, *ADVU* is given as

$$ADVU = m\{\frac{\partial Uu}{\partial x} + \frac{\partial Vu}{\partial y}\} + \frac{\partial W^*u}{\partial z^*} - \frac{u}{m}PRC. \qquad \text{(C2-1-19)}$$

RU, RV and *RW* represent the residual terms including the curbature, Coriolis and diffusion terms:

$$RU = f_3 V - f_2 W + V(u\frac{\partial m}{\partial y} - v\frac{\partial m}{\partial x}) - U\frac{w}{a} + DIF.U, \qquad \text{(C2-1-20)}$$

$$RV = f_1 W - f_3 U - U(u\frac{\partial m}{\partial y} - v\frac{\partial m}{\partial x}) - V\frac{w}{a} + DIF.V, \qquad \text{(C2-1-21)}$$

$$RW = f_2 U - f_1 V + \frac{m}{\rho G^{\frac{1}{2}}}\frac{(U^2 + V^2)}{a} + DIF.W. \qquad \text{(C2-1-22)}$$

The pressure prognostic equation is obtained from (C1-2-4) and (C2-1-8) as

$$\frac{\partial P}{\partial t} + C_m{}^2(-PFT + DIVT - PRC) = dif.P, \qquad \text{(C2-1-23)}$$

where $dif.P$ is an additional term that comes from Rayleigh damping in pressure, and C_m is

$$C_m{}^2 = \frac{C_p}{C_v}R\theta_m(\frac{p}{p_0})^{R/C_p}. \qquad \text{(C2-1-24)}$$

If there are no precipitable water substances, C_m is reduced to the speed of sound waves given by (C2-2-8). *PFT* represents the thermal expansion of air[1], which is expressed as

$$PFT = \frac{\rho G^{\frac{1}{2}}}{\theta_m}\frac{\partial \theta_m}{\partial t}. \qquad \text{(C2-1-25)}$$

[1]Some nonhydrostatic models (e.g., Klemp and Wilhemson, 1978; Pielke et al., 1992; Dudhia, 1993) omit this term from the pressure equations to save computation time and to avoid numerical problems. However, this term represents a substantial part of the state equation and is important to evaluate density perturbation (=buoyancy in our model) accurately. As Doms and Schaettler (1997) mentioned, omitting this term may cause significant problems in numerical weather prediction and the associated data assimilation cycle.

There is no change in the thermodynamic equation.

$$\frac{d\theta}{dt}=\frac{\partial\theta}{\partial t}+ADV.\theta=\frac{Q}{C_p\pi}+Dif.\theta, \tag{C2-1-26}$$

except the following modification of the advection term;

$$ADV.\theta=\{m(\frac{\partial U\theta}{\partial x}+\frac{\partial V\theta}{\partial y})+\frac{\partial W^*\theta}{\partial z^*}\frac{\theta}{m}(PRC-G^{\frac{1}{2}}\frac{\partial\rho}{\partial t})\}\frac{m}{\rho G^{\frac{1}{2}}}$$
$$=\{m^2(\frac{\partial U\theta}{\partial x}+\frac{\partial V\theta}{\partial y})+m\frac{\partial W^*\theta}{\partial z^*}-\theta DIVT(U,V,W)\}/\rho G^{\frac{1}{2}}. \tag{C2-1-27}$$

C-2-2 Quasi-compressible approximation

A quasi-compressible approximated version is historically developed as an elastic version of Ikawa and Saito (1991)'s nonhydrostatic model. The field variables $\phi(x, y, z, t)$ are divided into a horizontally uniform reference basic state $\bar{\phi}(z)$ and residual perturbation $\phi'(x, y, z, t)$ as follows:

$$\phi(x,y,z,t)=\bar{\phi}(z)+\phi'(x,y,z,t). \tag{C2-2-1}$$

Note that $\phi(z)$ depends on not only z^* but also on x and y, in the terrain-following coordinate system; $\bar{\phi}(z)=\phi(x, y, z^*)$. The set of quasi-compressible equations is obtained by setting $m=1$, $PRC=0$, and $\rho(x, y, z, t)=\bar{\rho}(z)$ in (C2-1-9) to (C2-1-27) except for $BUOY$ in (C2-1-17):

$$G^{\frac{1}{2}}\frac{\partial\rho}{\partial t}+DIVT(U,V,W)=0, \tag{C2-2-2}$$

$$U=\bar{\rho}G^{\frac{1}{2}}u,$$
$$V=\bar{\rho}G^{\frac{1}{2}}v, \tag{C2-2-3}$$
$$W=\bar{\rho}G^{\frac{1}{2}}w,$$

$$\frac{\partial U}{\partial t}+\frac{\partial P}{\partial x}+\frac{\partial G^{\frac{1}{2}}G^{13}P}{G^{\frac{1}{2}}\partial z^*}=ADVU+RU, \tag{C2-2-4}$$

$$\frac{\partial V}{\partial t}+\frac{\partial P}{\partial y}+\frac{\partial G^{\frac{1}{2}}G^{23}P}{G^{\frac{1}{2}}\partial z^*}=ADVV+RU. \tag{C2-2-5}$$

Hire, $ADVU$, $ADVV$, and $ADVW$ are defined as[2]

$$ADVU=\frac{\partial Uu}{\partial x}+\frac{\partial Vu}{\partial y}+\frac{\partial W^*u}{\partial z^*}. \tag{C2-2-6}$$

A density perturbation in the vertical equation is divided into two components by the following approximations:

$$-\rho' g\cong\{\bar{\rho}(\frac{\theta_v'}{\bar{\theta}_v}-q_c-q_r-q_s-q_g-q_i)-\frac{p'}{C_s^2}\}g, \tag{C2-2-7}$$

where

$$C_s^2=\frac{C_p}{C_v}R\bar{\theta}_v(\frac{p}{p_0})^{R/C_p}, \tag{C2-2-8}$$

Using the above, the vertical momentum equation becomes

$$\frac{\partial W}{\partial t}+\frac{1}{G^{\frac{1}{2}}}\frac{\partial P}{\partial z^*}+\frac{P}{C_s^2}g=BUOY'-ADVW+RW, \tag{C2-2-9}$$

where the buoyancy term is given by

[2]As mentioned in C-1-4, this form requires the anelastic relation (C2-3-1) and is not exact for (C2-2-2).

$$BUOY' \equiv \bar{\rho} G^{\frac{1}{2}} \left(\frac{\theta_v'}{\bar{\theta}_v} - q_c - q_r - q_s - q_g - q_i \right) g. \tag{C2-2-10}$$

The pressure equation is as follows

$$\frac{\partial P}{\partial t} + C_s^2 (-PFT + DIVT) = dif.P, \tag{C2-2-11}$$

where

$$PFT = \frac{1}{g} \frac{\partial BUOY'}{\partial t}. \tag{C2-2-12}$$

C-2-3 Anelastic approximation

In the anelastic system, the first term of the continuity equation (C2-2-2) is neglected in order to remove the sound waves following Ogura and Phillips (1962),

$$DIVT(U, V, W) = 0, \tag{C2-3-1}$$

where $m=1$ is set in (C2-1-12) and the three components of the momentum are defined by (C2-2-3) as in the quasi-compressible model. The linearized momentum equations are the same as in (C2-2-4), (C2-2-5) and (C2-2-9), and the flux form (C2-2-6) is exact for (C2-3-1). Pressure is diagnosed by the anelastic continuity equation and momentum equations (see C-3).

C-2-4 Hydrostatic version of the anelastic model

The hydrostatic version of the anelastic model is obtained by degenerating the vertical momentum equation (C2-2-9) into the hydrostatic approximation as

$$\frac{1}{G^{\frac{1}{2}}} \frac{\partial P}{\partial z^*} + \frac{P}{C_s^2} g = BUOY'. \tag{C2-4-1}$$

Vertical momentum W is determined by the continuity equation (C2-3-1). The method for calculating the pressure is presented in subsection C-3-4.

C-3. Pressure equations

Since elastic nonhydrostatic models include sound waves in their solutions, the maximum time step is restricted by the speed of sound waves if a simple leap-frog time integration scheme is used. To overcome this problem, current nonhydrostatic models treat sound waves in two schemes: one that treats sound waves implicitly in the vertical direction and explicitly in the horizontal (HE-VI scheme; *e.g.,* Klemp and Wilhelmson, 1978) and another that treats sound waves implicitly in both the horizontal and vertical directions (HI-VI scheme; *e.g.,* Tapp and White, 1976). Generally, a time-splitting scheme whereby high-frequency terms are evaluated at a shorter time step level is used in the HE-VI scheme.

The explicit treatment of sound waves in the horizontal directions presumes that the horizontal resolution is much finer than the vertical resolution. Consequently, the HE-VI scheme may need a very short time step when the horizontal grid interval becomes as small as the vertical grid interval. On the other hand, the time step in the HI-VI scheme is not restricted by the sound wave speed, but it is necessary to solve a three-dimensional Helmholtz equation for pressure. This characteristic feature of the HI-VI scheme may become a disadvantage in massive computation using a distributed memory parallel computer.

From the above point of view, some recent nonhydrostatic models tend to prepare two options to treat sound waves. For example, an HI-VI version of Lokal-modell (Doms and Schaettler, 1997) of the Deutscher Wetterdienst was recently developed by Thomas et al. (1999), and an HI-VI option is being developed in the WRF model project at NCEP. In JMA, a new HE-VI scheme was incorporated into the MRI nonhydrostatic model as the first step to develop the MRI/NPD unified nonhydrostatic model.

Most operational hydrostatic models, as well as some nonhydrostatic models (*e.g.,* Tanguay *et al.,* 1990; Golding, 1992), treat gravity waves implicitly to maintain computational stability and efficiency. Implicit treatment of the gravity waves is one of our future subjects, though it may deform not only the high-frequency gravity waves but also the low-frequency gravity waves.

C-3-1 Pressure tendency equation in HI-VI scheme

In this model, we treat implicitly only the sound waves following the E-HI-VI scheme described in Ikawa (1988) and Ikawa and Saito (1991) for their quasi-compressible model. Before presenting the formulation, we redefine the buoyancy term $BUOY$ in this section in order to unify the two expressions of buoyancy (C2-1-18) and (C2-2-10). Introducing a switching parameter σ, which takes zero for direct computation of the buoyancy from density perturbation and unity for conventional computation by the temperature perturbation, the term can be rewritten as

$$BUOY \equiv \sigma \frac{\rho G^{\frac{1}{2}} \theta_m'}{\theta_m} g + (1-\sigma)(\bar{\rho}-\rho) g G^{\frac{1}{2}}. \qquad \text{(C3-1-1)}$$

Usually, σ is zero for the fully compressible mode and unity for quasi-compressible approximation (in this case, the first term on the right-hand side becomes (C2-2-10). Using σ, vertical momentum equations can be expressed as

$$\frac{\partial W}{\partial t} + \frac{1}{mG^{\frac{1}{2}}}\frac{\partial P}{\partial z^*} + \sigma \frac{P}{mC_m{}^2} g = \frac{1}{m} BUOY - ADVW + RW. \qquad \text{(C3-1-2)}$$

In the E-HI-VI scheme, momentum equations (C2-1-15), (C2-1-16) and (C3-1-2) are represented in finite difference form as follows:

$$\frac{U^{it+1}-U^{it-1}}{2\Delta t} + \frac{\partial \bar{P}^t}{\partial x} + -(ADVU - RU + \frac{\partial G^{\frac{1}{2}} G^{13} P}{G^{\frac{1}{2}} \partial z^*}), \qquad \text{(C3-1-3)}$$

$$\frac{V^{it+1}-V^{it-1}}{2\Delta t} + \frac{\partial \bar{P}^t}{\partial y} + -(ADVV - RV + \frac{\partial G^{\frac{1}{2}} G^{23} P}{G^{\frac{1}{2}} \partial z^*}), \qquad \text{(C3-1-4)}$$

$$\frac{W^{it+1}-W^{it-1}}{2\Delta t} + \overline{\overline{\frac{1}{mG^{\frac{1}{2}}}}}\frac{\partial \bar{P}^t}{\partial z^*} + \overline{\overline{\frac{g}{mC_m{}^2}}}\bar{P}^t$$

$$= \frac{1}{m} BUOY - (ADVW - RW) + (\overline{\overline{\frac{1}{mG^{\frac{1}{2}}}}} - \frac{1}{mG^{\frac{1}{2}}})\frac{\partial P}{\partial z^*} + (\overline{\overline{\frac{g}{mC_m{}^2}}} - \sigma \frac{g}{mC_m{}^2}) P. \qquad \text{(C3-1-5)}$$

Here, terms marked with a double overbar denote averaged quantity on a z^* surface and superscripts $it+1$ and $it-1$ represent the time levels in the leap-frog integration. Terms marked with a single overbar together with superscript t denote the weighted averaged values between $it+1$ and $it-1$ time levels defined by

$$\bar{A}^t \equiv \frac{1+\alpha}{2} A^{it+1} + \frac{1-\alpha}{2} A^{it-1} \equiv \frac{\Delta^2 A}{2} + A^{it}, \qquad \text{(C3-1-6)}$$

where α is the weight parameter, which is currently set to 0.5. The last terms on the left-hand and right-hand sides of (C3-1-5) are pressure perturbation components in the buoyancy term, which must be treated implicitly to maintain computational stability. Thermodynamic equation (C2-1-26) is represented in a simple difference form since the gravity waves are not treated implicitly in our model.

Pressure prognostic equation (C2-1-23) is represented in finite difference form as

$$\frac{\partial P}{\partial t}+\overline{\overline{C_m^2}}DIVS(\overline{U^t},\overline{V^t},\overline{W^t})$$
$$=C_m^2(PFT-DIVT(U,V,W)+PRC)+\overline{\overline{C_m^2}}DIVS(U,V,W)+dif.P, \qquad \text{(C3-1-7)}$$

where $DIVS$ is the linearized separable part of the total divergence, which is defined by

$$DIVS(U,V,W)=\overline{\overline{m^2}}(\frac{\partial U}{\partial x}+\frac{\partial V}{\partial y})+\overline{\overline{\frac{m}{G^{\frac{1}{2}}}}}\frac{\partial W}{\partial z^*}. \qquad \text{(C3-1-8)}$$

Substituting the following relation

$$\frac{A^{it+1}-A^{it-1}}{2\Delta t}=\frac{\Delta^2 A}{2(1+\alpha)\Delta t}+\frac{A^{it}-A^{it-1}}{(1+\alpha)\Delta t}, \qquad \text{(C3-1-9)}$$

into (C3-1-3) to (C3-1-5) and (C3-1-7), we obtain the following formulas:

$$\frac{\Delta^2 U}{(1+\alpha)\Delta t}+\frac{\partial\Delta^2 P}{\partial x}=-2ADVU', \qquad \text{(C3-1-10)}$$

$$\frac{\Delta^2 V}{(1+\alpha)\Delta t}+\frac{\partial\Delta^2 P}{\partial y}=-2ADVV', \qquad \text{(C3-1-11)}$$

$$\frac{\Delta^2 W}{(1+\alpha)\Delta t}+\overline{\overline{\frac{1}{mG^{\frac{1}{2}}}}}\frac{\partial\Delta^2 P}{\partial z^*}+\overline{\overline{\frac{g}{mC_m^2}}}\Delta^2 P=-2ADVW', \qquad \text{(C3-1-12)}$$

$$\frac{\Delta^2 P}{(1+\alpha)\Delta t}+\overline{\overline{C_m^2}}DIVS(\Delta^2 U,\Delta^2 V,\Delta^2 W)=-\overline{\overline{C_m^2}}2ADVP', \qquad \text{(C3-1-13)}$$

where the right-hand sides are the modified advection terms:

$$ADVU'=ADVU-RU+\frac{U^{it}-U^{it-1}}{(1+\alpha)\Delta t}+\frac{\partial P^{it}}{\partial x}+\frac{\partial G^{\frac{1}{2}}G^{13}P^{it}}{G^{\frac{1}{2}}\partial z^*}, \qquad \text{(C3-1-14)}$$

$$ADVV'=ADVV-RV+\frac{V^{it}-V^{it-1}}{(1+\alpha)\Delta t}+\frac{\partial P^{it}}{\partial y}+\frac{\partial G^{\frac{1}{2}}G^{23}P^{it}}{G^{\frac{1}{2}}\partial z^*}, \qquad \text{(C3-1-15)}$$

$$ADVW'=ADVW-RW-\frac{1}{m}BUOY+\frac{W^{it}-W^{it-1}}{(1+\alpha)\Delta t}+\frac{1}{m}(\frac{1}{G^{\frac{1}{2}}}\frac{\partial}{\partial z^*}+\sigma\frac{g}{C_m^2})P^{it}, \qquad \text{(C3-1-16)}$$

$$ADVP'=\frac{1}{\overline{\overline{C_m^2}}}\{\frac{P^{it}-P^{it-1}}{(1+\alpha)\Delta t}-C_m^2(PFT-DIVT(U,V,W)+PRC)-dif.P\}. \qquad \text{(C3-1-17)}$$

Substitution of (C3-1-10) to (C3-1-12) into (C3-1-13) to eliminate $\Delta^2 U$, $\Delta^2 V$, and $\Delta^2 W$, yields

$$\frac{\Delta^2 P}{\overline{\overline{C_m^2}}(1+\alpha)^2(\Delta t)^2}-DIVS(2ADVU'+\frac{\partial\Delta^2 P}{\partial x},2ADVV'+\frac{\partial\Delta^2 P}{\partial y},2ADVW'+\overline{\overline{\frac{1}{mG^{\frac{1}{2}}}}}\frac{\partial\Delta^2 P}{\partial z^*}+\overline{\overline{\frac{g}{mC_m^2}}}\Delta^2 P)$$
$$=-\frac{2}{(1+\alpha)\Delta t}ADVP'. \qquad \text{(C3-1-18)}$$

Arranging the above, we obtain the following Helmholtz-type pressure tendency equation:

$$\overline{\overline{m^2}}(\frac{\partial^2\Delta^2 P}{\partial x^2}+\frac{\partial^2\Delta^2 P}{\partial y^2})+\overline{\overline{\frac{m}{G^{\frac{1}{2}}}}}\,\overline{\overline{\frac{1}{mG^{\frac{1}{2}}}}}\frac{\partial^2\Delta^2 P}{\partial z^{*2}}+\overline{\overline{\frac{m}{G^{\frac{1}{2}}}}}\frac{\partial}{\partial z^*}(\overline{\overline{\frac{g}{mC_m^2}}}\Delta^2 P)$$
$$-\frac{\Delta^2 P}{\overline{\overline{C_m^2}}(1+\alpha)^2(\Delta t)^2}=2\{\frac{ADVP'}{(1+\alpha)\Delta t}-DIVS(ADVU',ADVV',ADVW')\}. \qquad \text{(C3-1-19)}$$

This equation is solved directly by the Dimension Reduction Method discussed in D-3. In Saito (1997), the model assumed

$$\overline{\overline{m^2}}\cong 1,\ \overline{\overline{\frac{m}{G^{\frac{1}{2}}}}}\cong\overline{\overline{\frac{1}{mG^{\frac{1}{2}}}}}\cong\overline{\overline{\frac{1}{G^{\frac{1}{2}}}}},\ \overline{\overline{\frac{g}{mC_m{}^2}}}\cong\overline{\overline{\frac{g}{C_m{}^2}}}, \tag{C3-1-20}$$

for simplicity on the understanding that the standard latitude φ_0 in (C1-3-2) is taken at the center of the model domain. However, the above approximation (premise) was removed in the latest version (Saito, 2000).

C-3-2 Formulation of HE-VI scheme

Referring to the E-HE-VI scheme described in Ikawa and Saito (1991), the time-splitting, horizontally explicit version of the MRI mesoscale nonhydrostatic model is presented in the following. The Numerical Prediction Division of JMA incorporated this new scheme into MRI-NHM as a joint program with MRI to develop the MRI/NPD unified mesoscale model (Muroi et al., 1999) (see L-2).

In the E-HE-VI scheme, the time integration procedure is divided into two parts to avoid severe restriction of time interval for integration. Terms related to the sound mode are treated explicitly in the horizontal direction and implicitly in the vertical direction. These terms are integrated with a short time step ($\Delta\tau$). The other terms that include the advection term, friction term and physical processes are integrated with long time step (Δt). In the short time step integration, the horizontal velocity is integrated first with a forward scheme. The vertical velocity and pressure field are then solved with a backward scheme. In the long time step integration, a three-time level scheme with a time filter is applied.

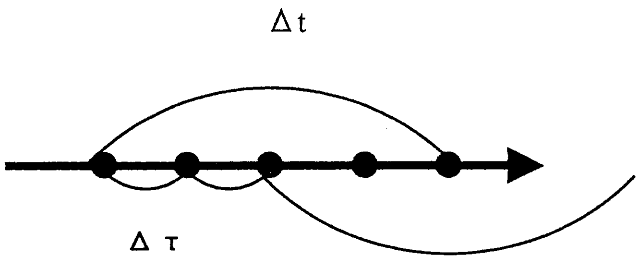

Forward time integration of (C2-1-15) and (C2-1-16) and backward integration of (C3-1-2) and (C2-1-23) are represented in finite difference form as

$$\frac{U^{\tau+\Delta t}-U^{\tau}}{\Delta\tau}+\frac{\partial P^{\tau}}{\partial x}+\frac{\partial G^{\frac{1}{2}}G^{13}P^{\tau}}{G^{\frac{1}{2}}\partial z^*}=-(ADVU+RU), \tag{C3-2-1}$$

$$\frac{V^{\tau+\Delta t}-V^{\tau}}{\Delta\tau}+\frac{\partial P^{\tau}}{\partial y}+\frac{\partial G^{\frac{1}{2}}G^{23}P^{\tau}}{G^{\frac{1}{2}}\partial z^*}=-(ADVV+RV), \tag{C3-2-2}$$

$$\frac{W^{\tau+\Delta\tau}-W^{\tau}}{\Delta\tau}+\frac{1}{mG^{\frac{1}{2}}}\frac{\partial P^{\beta}}{\partial z^*}+\frac{g}{mC_m{}^2}P^{\beta}=\frac{1}{m}BUOY-(ADVW-RW)+(1-\sigma)\frac{g}{mC_m{}^2}P, \tag{C3-2-3}$$

$$\frac{P^{\tau+\Delta t}-P^{\tau}}{\Delta\tau}+C_m{}^2(-PFT+m^2(\frac{\partial U^{\gamma}}{\partial x}+\frac{\partial V^{\gamma}}{\partial y})$$

$$+m\frac{\partial}{\partial z^*}[\frac{1}{G^{\frac{1}{2}}}\{W^{\beta}+m(G^{\frac{1}{2}}G^{13}U^{\gamma}+G^{\frac{1}{2}}G^{23}V^{\gamma})\}]-PRC)=dif.P, \tag{C3-2-4}$$

where

$$U^{\gamma}=\frac{1+\gamma}{2}U^{\tau+\Delta\tau}+\frac{1-\gamma}{2}U^{\tau}, \tag{C3-2-5}$$

$$V^{\gamma}+\frac{1+\gamma}{2}V^{\tau+\Delta\tau}+\frac{1-\gamma}{2}V^{\tau}, \tag{C3-2-6}$$

$$W^{\beta}=\frac{1+\beta}{2}W^{\tau+\Delta\tau}+\frac{1-\beta}{2}W^{\tau}$$

$$=\frac{\Delta\tau(1+\beta)}{2}\left(\frac{W^{\tau+\Delta\tau}-W^{\tau}}{\Delta\tau}\right)+W^{\tau}=\frac{\Delta\tau(1+\beta)}{2}\delta W+W^{\tau}. \tag{C3-2-7}$$

Here, the left-hand sides are calculated in the short time step integration, and the right-hand sides are evaluated in the long time step integration. P^{β} is similar to (C3-2-7). $\sigma=1$, $\beta=0.5$ and $\gamma=0$ are used in the current version of the model.

Substituting the above equations into (C3-2-4), we obtain

$$\frac{2}{\Delta\tau(1+\beta)}(P^{\beta}-P^{\tau})+C_m^2((-PFT+m^2DIVH(U^{\gamma},V^{\gamma})$$

$$\underline{+m\frac{\partial}{\partial z^*}[\frac{1}{G^{\frac{1}{2}}}\{\frac{\Delta\tau(1+\beta)}{2}}\delta W+W^{\tau}\}]-PRC))=dif.P, \tag{C3-2-8}$$

where $DIVH$ stands for horizontal divergence

$$DIVH(U,V)\equiv\frac{\partial U}{\partial x}+\frac{\partial V}{\partial y}+\frac{\partial}{\partial z^*}(G^{13}U+G^{23}V). \tag{C3-2-9}$$

The under-lined part of (C3-2-8) becomes

$$-\left(\frac{1}{G^{\frac{1}{2}}}\right)^2\frac{\Delta\tau(1+\beta)}{2}\frac{\partial^2P^{\beta}}{\partial z^*}-\frac{1}{G^{\frac{1}{2}}}\frac{\Delta\tau(1+\beta)}{2}\frac{\partial}{\partial z^*}\left(\frac{g}{C_m^2}P^{\beta}\right)$$

$$+\frac{m}{G^{\frac{1}{2}}}\frac{\Delta\tau(1+\beta)}{2}\frac{\partial}{\partial z^*}\{r.h.s.\,(\text{C3-2-3})\}. \tag{C3-2-10}$$

Finally, we obtain the following one-dimensional Helmholtz-type pressure equation

$$\frac{\partial^2P^{\beta}}{\partial z^{*2}}+G^{\frac{1}{2}}\frac{\partial}{\partial z^*}\left(\frac{g}{C_m^2}P^{\beta}\right)-(G^{\frac{1}{2}})^2\left\{\frac{2}{C_m\Delta\tau(1+\beta)}\right\}^2P^{\beta}=FP.HE.INV+FP.HE.VAR, \tag{C3-2-11}$$

where $FP.HE.INV$ is the invariable term during short time step integration in the forcing terms

$$PP.HE.INV=\frac{2(G^{\frac{1}{2}})^2}{\Delta\tau(1+\beta)}\left(PFT+PRC+\frac{dif.P}{C_m^2}\right)$$

$$+G^{\frac{1}{2}}\frac{\partial}{\partial z^*}\{BUOY-m(ADVW-RW)+(1-\sigma)\frac{g}{C_m^2}P\}, \tag{C3-2-12}$$

and $FP.HE.VAR$ is the variable term during short time step integration in the forcing terms

$$FP.HE.VAR=\frac{2(G^{\frac{1}{2}})^2}{\Delta\tau(1+\beta)}\left\{m^2DIVH(U^{\gamma},\ V^{\gamma})+\frac{m}{G^{\frac{1}{2}}}\frac{\partial W^{\tau}}{\partial z^*}\right\}-\left\{\frac{2G^{\frac{1}{2}}}{C_m\Delta\tau(1+\beta)}\right\}^2P^{\tau}. \tag{C3-2-13}$$

The upper boundary condition may be obtained from $\delta W=0$ as

$$\left(\frac{1}{mG^{\frac{1}{2}}}\frac{\partial}{\partial z^*}+\frac{g}{mC_m^2}\right)P^{\beta}=-(ADVW-RW)+\frac{1}{m}\{BUOY+(1-\sigma)\frac{g}{C_m^2}P\}. \tag{C3-2-14}$$

The lower boundary condition is the same as in (C3-2-14), while in free-slip case, the right-hand side requires the following extra term

$$-\delta W=m(G^{\frac{1}{2}}G^{13}\delta U+G^{\frac{1}{2}}G^{23}\delta V)=m\left(G^{\frac{1}{2}}G^{13}\frac{U^{\tau+\Delta t}-U^{\tau}}{\Delta\tau}+G^{\frac{1}{2}}G^{23}\frac{V^{\tau+\Delta t}-V^{\tau}}{\Delta\tau}\right)$$

$$=\frac{1}{\Delta\tau}\{W^{\tau}+m(G^{\frac{1}{2}}G^{13}U^{\tau+\Delta\tau}+G^{\frac{1}{2}}G^{23}V^{\tau+\Delta\tau}),\tag{C3-2-15}$$

in order to satisfy the kinematic condition

$$\delta W^{*}=\delta W+m(G^{\frac{1}{2}}G^{13}\delta U+G^{\frac{1}{2}}G^{23}\delta V)=0,$$
$$W^{*\tau}=W^{\tau}+m(G^{\frac{1}{2}}G^{13}U^{\tau}+G^{\frac{1}{2}}G^{23}V^{\tau})=0.\tag{C3-2-16}$$

C-3-3 Pressure diagnostic equation in anelastic version

Pressure in the anelastic system is described in Ikawa and Saito (1991). Here, we present it for discussion in later chapters. Substituting (C2-2-4), (C2-2-5) and (C2-2-9) into (C2-3-1) to eliminate time tendencies of U, V and W, we obtain

$$-\frac{\partial DIVT(U,V,W)}{\partial t}=DIVT(\frac{\partial P}{\partial x}+\frac{\partial G^{\frac{1}{2}}G^{13}P}{G^{\frac{1}{2}}\partial z^{*}}+ADVU-RU,$$
$$\frac{\partial P}{\partial y}+\frac{\partial G^{\frac{1}{2}}G^{23}P}{G^{\frac{1}{2}}\partial z^{*}}+ADVV-RV,\frac{1}{G^{\frac{1}{2}}}\frac{\partial P}{\partial z^{*}}+\frac{P}{C_m^{2}}g+ADVW-RW-BUOY'),\tag{C3-3-1}$$

where we assume $m=1$ for the anelastic model. Introducing a residual part of the total divergence to the separable part

$$DIVR(U,V,W)=DIVT(U,V,W)-DIVS(U,V,W)$$
$$=\frac{\partial}{\partial z^{*}}\frac{1}{G^{\frac{1}{2}}}\{W+G^{\frac{1}{2}}G^{13}U+G^{\frac{1}{2}}G^{23}V\}-\overline{\overline{\frac{1}{G^{\frac{1}{2}}}}}\frac{\partial W}{\partial z^{*}}$$
$$=\frac{1}{G^{\frac{1}{2}}}\frac{\partial}{\partial z^{*}}(G^{\frac{1}{2}}G^{13}U+G^{\frac{1}{2}}G^{23}V)+(\frac{1}{G^{\frac{1}{2}}}-\overline{\overline{\frac{1}{G^{\frac{1}{2}}}}})\frac{\partial W}{\partial z^{*}},\tag{C3-3-2}$$

we obtain the following Poisson-type pressure diagnostic equation:

$$DIVS(\frac{\partial P}{\partial x},\frac{\partial P}{\partial y},\overline{\overline{\frac{1}{G^{\frac{1}{2}}}}}\frac{\partial P}{\partial z^{*}}+\overline{\overline{\frac{g}{C_s^{2}}}}P)+DIVR(\frac{\partial P}{\partial x},\frac{\partial P}{\partial y},\overline{\overline{\frac{1}{G^{\frac{1}{2}}}}}\frac{\partial P}{\partial z^{*}}+\overline{\overline{\frac{g}{C_s^{2}}}}P)$$
$$+DIVT\{\frac{\partial G^{\frac{1}{2}}G^{13}P}{G^{\frac{1}{2}}\partial z^{*}},\frac{\partial G^{\frac{1}{2}}G^{23}P}{G^{\frac{1}{2}}\partial z^{*}},(\frac{1}{G^{\frac{1}{2}}}\frac{\partial}{\partial z^{*}}+\frac{g}{C_s^{2}}-\overline{\overline{\frac{1}{G^{\frac{1}{2}}}}}\frac{\partial}{\partial z^{*}}-\overline{\overline{\frac{g}{C_s^{2}}}})P\}$$
$$+DIVT(ADVU-RU,ADVV-RV,ADVW-RW-BUOY')$$
$$=\frac{1}{2\Delta t}DIVT(U^{\tau-1},V^{\tau-1},W^{\tau-1}),\tag{C3-3-3}$$

The right-hand side of the above equation represents the residual divergence computed at the former time level, which is theoretically zero in the anelastic system but non-zero numerically due to computation errors. This term is important for satisfying the continuity equation at the next time level and stabilizing the computation (Clark, 1977; Ikawa and Saito, 1991).

C-3-4 Pressure equation in anelastic hydrostatic version

The hydrostatic model is a degenerate version of the non-hydrostatic model developed by Ikawa and Saito (1991). Clark and Hall (1991) also made a hydrostatic version of their non-hydrostatic model by using almost the same method as used in this subsection. Since the vertical momentum flux W is a diagnostic variable, W is determined by the anelastic continuity equation. The pressure is calculated as follows.

Combining (C2-2-4), (C2-2-5), and (C2-4-1) leads to a diagnostic equation for p' as

$$\frac{\partial^2 p'}{\partial x^2}+\frac{\partial^2 (G^{13}p')}{\partial x \partial z^*}+\frac{\partial^2 p'}{\partial y^2}+\frac{\partial^2 (G^{23}p')}{\partial y \partial z^*}=-\frac{\partial Fx}{\partial x}-\frac{\partial Fy}{\partial y}+\frac{1}{2\Delta t}\frac{\partial (W^{m+1}-W^{m-1})}{\partial z}, \tag{C3-4-1}$$

where Δt is the time step interval, and the superscript 'm' denotes the value at the time step 'm'. From (C2-4-1), p'_k at the k-th vertical level can be expressed with the pressure at the upper boundary p'_{nz} as

$$p'_k = a_k p_{nz} + b_k, \tag{C3-4-2}$$

where

$$a_k=\sum_{k=k}^{nz}\frac{G^{\frac{1}{2}}-\Delta z_{k+\frac{1}{2}}\frac{g}{C_s^2}}{G^{\frac{1}{2}}+\Delta z_{k+\frac{1}{2}}\frac{g}{C_s^2}} \tag{C3-4-3}$$

and

$$b_k=-\sum_{k=k}^{nz}\frac{\Delta z_{k+\frac{1}{2}}BOUY'_{k+\frac{1}{2}}}{G^{\frac{1}{2}}+\Delta z_{k+\frac{1}{2}}\frac{g}{C_s^2}}. \tag{C3-4-4}$$

Summing (C3-4-1) in the vertical column results in the following diagnostic column pressure equation:

$$\begin{aligned}&\frac{\partial^2}{\partial x^2}\sum_k \Delta z_k p'_k+\frac{\partial}{\partial x}(G^{13}p'_{nz}-G^{13}p'_1)+\frac{\partial^2}{\partial y^2}\sum_k \Delta z_k p'_k+\frac{\partial}{\partial y}(G^{23}p'_{nz}-G^{23}p'_1)\\ &\qquad=-\sum_k \Delta z_k\left(\frac{\partial Fx}{\partial x}+\frac{\partial Fy}{\partial y}\right)_k+\frac{\{(W^{m+1}-W^{m-1})_{nz}-(W^{m+1}-W^{m-1})_1\}}{2\Delta t},\end{aligned} \tag{C3-4-5}$$

where Δz_k is the k-th vertical grid interval and the subscripts 1 and nz denote the values at the lower and upper boundaries, respectively. The second term on the right-hand side of (C3-4-5) should theoretically be zero because of the lower and upper boundary conditions. However, since W^{m-1}_{nz} calculated from (C2-3-1) becomes non-zero due to round-off errors in numerical simulations, this term remains in (C3-4-5) to guarantee $W^{m+1}_{nz}=0$. Substitution of (C3-4-2) into (C3-4-5) results in the horizontal elliptic equation for p'_{nz}, which can be solved by the same method as in the non-hydrostatic model (see subsection D-3-3).

D. Finite discretization form and pressure equation solver

D-1. Grid structure

The model grid structure is the Arakawa-C type in the horizontal direction and the Lorenz-type in the vertical direction, which is the same as in Ikawa and Saito (1991). This chapter briefly describes the structure of the staggered grid, supplementing Ikawa and Saito (1991)

D-1-1 Structure of the staggered grid

All variables, other than velocity components, advection terms and metric tensors, are defined at the "scalar" grid point indexed by integer (i, j, k). Velocity components U, V and W (as well as W^*) are located at the grid points indexed by the half integer $(i+1/2, j, k)$, $(i, j+1/2, k)$, $(i, j, k+1/2)$. Advection terms $ADVU$, $ADVV$ and $ADVW$ are computed at the same points as U, V and W, respectively. Metric tensor $G^{1/2}$ is defined at the grid point (i, j) independently of k, while $G^{1/2}G^{13}$ and $G^{1/2}G^{23}$ are computed at $(i+1/2, j, k+1/2)$, $(i, j+1/2, k+1/2)$, respectively (Fig. D1-1-1).

Figures D1-1-2 and D1-1-3 present horizontal and vertical cross sections of the grid mesh of the model. The physical boundaries are located at $x=1+1/2$ and $x=nx$-1/2 in the x-direction, where the x-component of velocity is $U(2,,)$ and $U(NX,,)$. It is also the case in the y-direction, and the y-component of velocity is $V(,2,)$ and $V(,NY,)$ at $y=1+1/2$ and $y=ny$-1/2. However, in the vertical direction, the physical upper and lower boundaries are located at $z=1+1/2$ and $z=nz$-1/2, where the z-components of velocity are $W(,,1)$ and $W(,,NZ$-1).

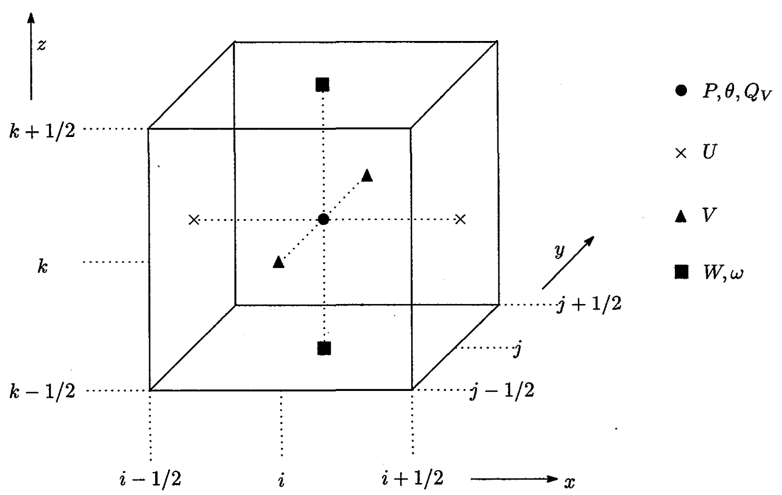

Fig. D1-1-1 Staggered grid. Reproduced from Ikawa and Saito (1991).

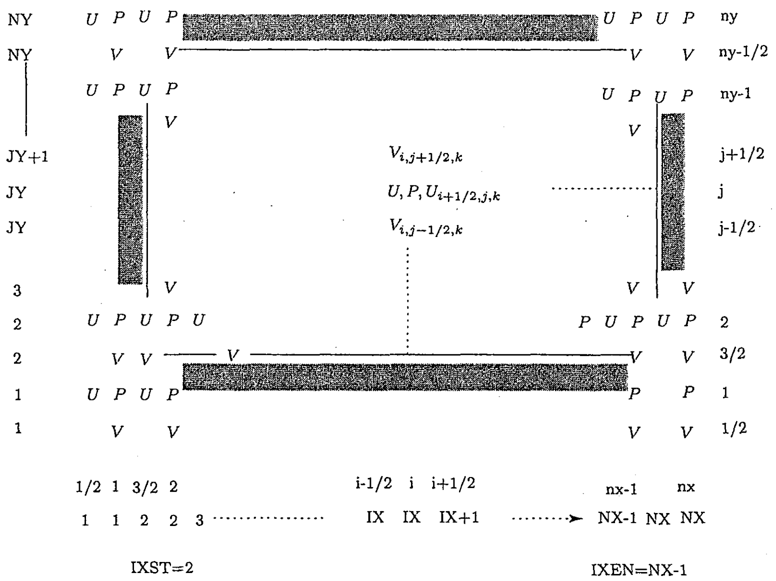

Fig. D1-1-2 Horizontal cross section of the grid mesh and the domain boundary. Reproduced from Ikawa and Saito (1991).

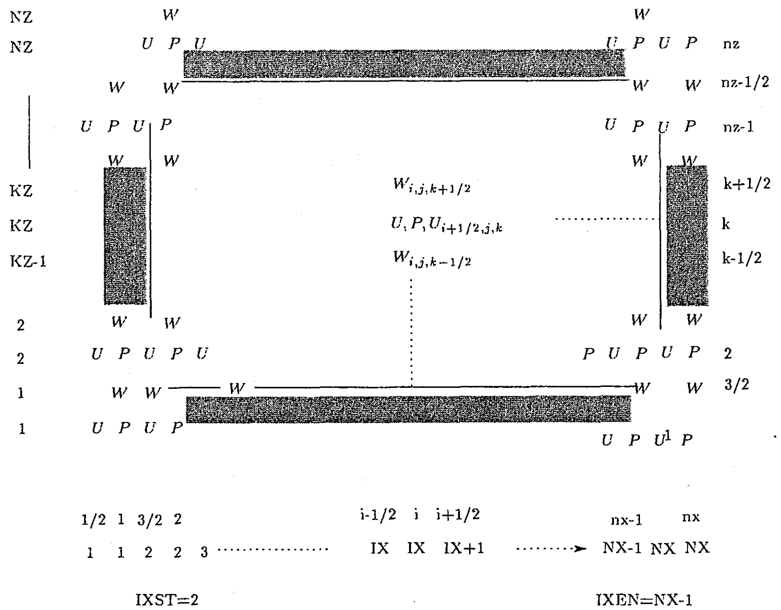

Fig. D1-1-3 Vertical cross section of the grid mesh and the domain boundary. Reproduced from Ikawa and Saito (1991).

D-1-2 Variable vertical grid

Figure D1-2-1 shows the variable grid structure in the z-direction. Two kinds of grid intervals are defined. Δz_k represents the grid intervals between the two grid points (i, j, k-1/2) and (i, j, k+1/2). In the program, this grid interval is denoted by *VDZ(K)*, which corresponds to the interval between the levels of $W(,,K)$ and $W(,,K+1)$. $\Delta z_{k+1/2}$ represents the grid intervals between the two grid points (i, j, k) and (i, j, k+1). In the program, this grid interval is denoted by *VDZ2(K)*, which corresponds to the interval between the levels of $P(,,K)$ and $P(,,K+1)$. As shown in Fig. D1-2-1, the half level is located at the center of the full level, and Δz_k and $\Delta z_{k+1/2}$ are related

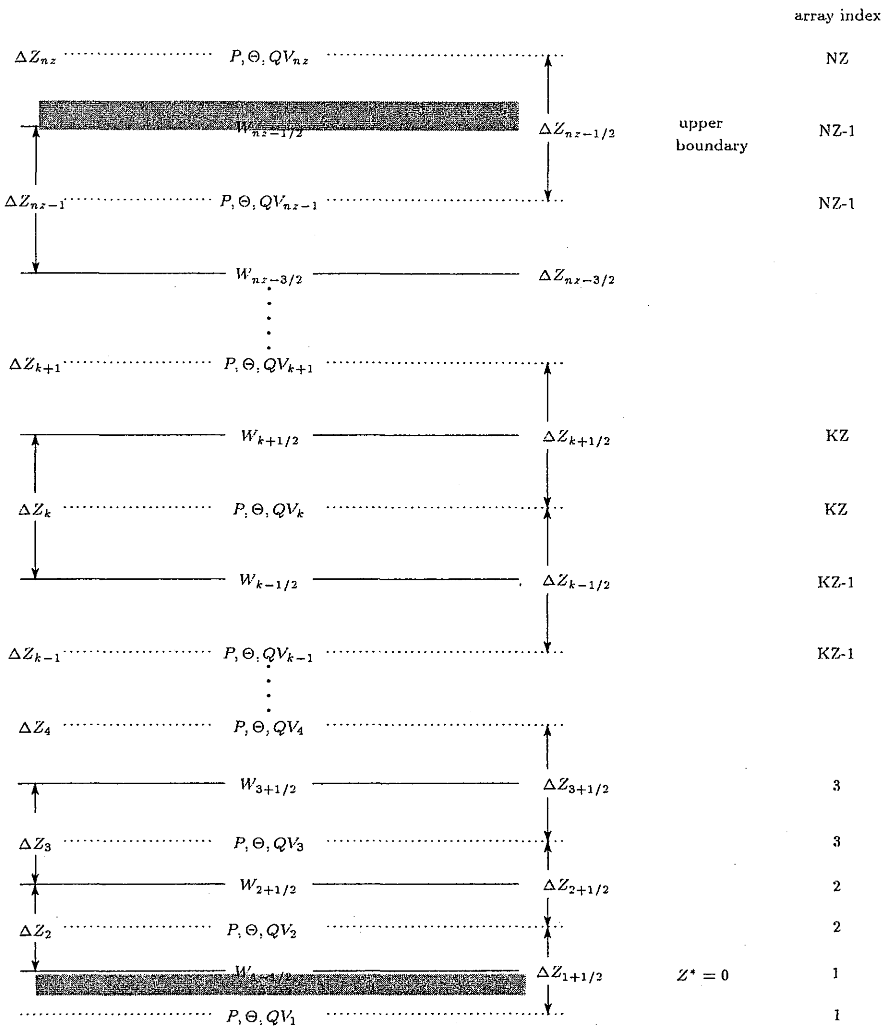

Fig. D1-2-1 Variable grid structure in the z-direction. Reproduced from Ikawa and Saito (1991).

as follows:

$$\Delta z_k = \frac{\Delta z_{k-1/2} + \Delta z_{k+1/2}}{2}, \tag{D1-2-1}$$

that is,

$$VDZ(K) = 0.5 * \{VDZ2(K-1) + VDZ2(K)\}. \tag{D1-2-2}$$

The heights of levels k and $k+1/2$ are denoted by *ZRP(KZ)* and *ZRW(KZ)*,. The relations between the variables are given by

$$Z_{3/2} = ZRW(1) = 0, \tag{D1-2-3}$$

$$Z_{k+1/2} = Z_{k-1/2} + \Delta z_k$$

$$= ZRW(K) = \sum_{KZ=2}^{k} VDZ(KZ), \tag{D1-2-4}$$

and

$$Z_1 = ZRP(1) = -\frac{\Delta z_{3/2}}{2} = -0.5 * VDZ2(1), \tag{D1-2-5}$$

$$Z_k = Z_{k-1} + \Delta z_{k-1/2}$$

$$= ZRP(K) = -0.5 * VDZ2(1) + \sum_{KZ=1}^{K-1} VDZ2(KZ). \quad \text{(D1-2-6)}$$

Note that physical intervals between grid points (i, j, k) must be computed by multiplying $G^{1/2}(i, j)$ for both Δz_k and $\Delta z^{k+1/2}$ when the orography exists.

Program Guide (hereafter, abbreviated as P.G.)

The variable grid distances are set in sub.VRGDIS where "sub" denotes subroutine. The arrays *ZRP* and *ZRW* are defined in sub.SETZRP and sub.SETZRW.

The variable grid structure in the x- and y-directions is shown in Fig. D1-2-2. The structure is similar to that in the z-direction, but the array indexes for U and V are different from that for W in the z-direction corresponding to the locations of the lateral boundaries. For example, in the x-direction, the relations between the variables are given by

$$\Delta x_i = \frac{\Delta x_{i-1/2} + \Delta x_{i+1/2}}{2},$$

$$= VDX(I) = 0.5 * \{VDX2(I) + VDX2(I+1)\}, \quad \text{(D1-2-7)}$$

$$X_{3/2} = 0, \quad \text{(D1-2-8)}$$

$$X_{i+1/2} = X_{i-1/2} + \Delta x_i$$

$$= XRU(I+1) = \sum_{IX=2}^{I} VDX(IX), \quad \text{(D1-2-9)}$$

$$X_1 = -0.5 * VDX2(2), \quad \text{(D1-2-10)}$$

$$X_i = X_{i-1} + \Delta x_{i-1/2}$$

$$= XRP(I) = -0.5 * VDX2(2) + \sum_{IX=2}^{I} VDX2(IX). \quad \text{(D1-2-11)}$$

The arrays *XRP* and *XRU* are defined in relevant utilities such as initial file setting and plot, but are not currently set in the model computation. The relations in the y-direction are the same as in the x-direction.

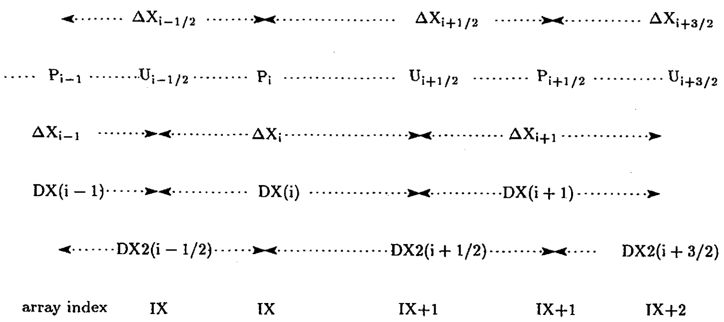

Fig. D1-2-2 Variable grid structure in x-direction. Reproduced from Ikawa and Saito (1991).

D-2. Finite discretization form

D-2-1 Finite discretization form for basic equations

Following Ikawa and Saito (1991), the averaging operator in the x-direction is defined for any variable F defined at the scalar point by

$$\overline{F}^{x}_{i+1/2}=\frac{F_i+F_{i+1}}{2}, \tag{D2-1-1}$$

and another averaging operator for any variable U defined at the grid point of a half integer by

$$\overline{U}^{x}_{i}=\frac{\Delta x_{i+1/2}U_{i-1/2}+\Delta x_{i-1/2}U_{i+1/2}}{\Delta x_{i-1/2}+\Delta x_{i+1/2}}$$

$$=\frac{\Delta x_{i+1/2}U_{i-1/2}+\Delta x_{i-1/2}U_{i+1/2}}{2\Delta x_i}. \tag{D2-1-2}$$

Averaging operators in the y- and z-directions are defined in the same way.

Finite differencing operators are defined by

$$\partial_x F_{i-1/2}=\frac{F_i-F_{i-1}}{\Delta x_{i-1/2}}, \tag{D2-1-3}$$

$$\partial_{2x} F_{i}=\frac{F_{i+1}-F_{i-1}}{2\Delta x_{i}}, \tag{D2-1-4}$$

$$\partial_x U_{i}=\frac{U_{i+1/2}-U_{i-1/2}}{\Delta x_{i}}. \tag{D2-1-5}$$

Using these operators, the governing equations in chapter C2 are expressed in the finite discretization form. For (C2-1-3) and (C2-1-4):

$$G^{\frac{1}{2}}G^{13}{}_{i+1/2,j,k+1/2}=(\frac{z^*{}_{k+1/2}}{H}-1)\,\partial_x z_{s_{i+1/2,j}}, \tag{D2-1-6}$$

$$G^{\frac{1}{2}}G^{23}{}_{i,j+1/2,k+1/2}=(\frac{z^*{}_{k+1/2}}{H}-1)\,\partial_y z_{s_{i,j+1/2}}. \tag{D2-1-7}$$

For (C2-1-9) - (C2-1-11):

$$U_{i+1/2,j,k}=\frac{\overline{(\rho G^{\frac{1}{2}})}^{x}}{\overline{m}^{x}}u, \tag{D2-1-8}$$

$$V_{i,j+1/2,k}=\frac{\overline{(\rho G^{\frac{1}{2}})}^{y}}{\overline{m}^{y}}v, \tag{D2-1-9}$$

$$W_{i,j,k+1/2}=\frac{\overline{(\rho G^{\frac{1}{2}})}^{z}}{m}w. \tag{D2-1-10}$$

For (C2-1-12) and (C2-1-13):

$$DIVT\,(U,V,W)_{i,j,k}=m^2(\partial_x U+\partial_y V)+m\partial_z W^*, \tag{D2-1-11}$$

$$W^*{}_{i,j,k+1/2}=\frac{1}{G^{\frac{1}{2}}}\{W+m(\overline{G^{\frac{1}{2}}G^{13}\overline{U}^{z}}^{x}+\overline{G^{\frac{1}{2}}G^{23}\overline{V}^{z}}^{y})\}. \tag{D2-1-12}$$

For (C2-1-15) - (C2-1-17):

$$(\frac{\partial U}{\partial t})_{i+1/2,j,k}+\partial_x P+\partial_z\{G^{\frac{1}{2}}G^{13}\overline{(\overline{P}^{z}/G^{\frac{1}{2}})}^{x}\}=-ADVU_{i+1/2,j,k}+RU_{i+1/2,j,k}, \tag{D2-1-13}$$

$$(\frac{\partial V}{\partial t})_{i,j+1/2,k}+\partial_y P+\partial_z\{G^{\frac{1}{2}}G^{23}\overline{(\overline{P}^{z}/G^{\frac{1}{2}})}^{y}\}=-ADVV_{i,j+1/2,k}+RV_{i,j+1/2,k}, \tag{D2-1-14}$$

$$\left(\frac{\partial W}{\partial t}\right)_{i,j,k+1/2}+\frac{1}{mG^{\frac{1}{2}}}\partial_z P=\frac{1}{m}\overline{BUOY}^{z}-ADVW_{i,j,k+1/2}+RW_{i,j,k+1/2}. \tag{D2-1-15}$$

Here,

$$ADVU_{i+1/2,j,k}=\overline{m}^{x}\{\partial_x(m\overline{U}^{x}\overline{u'}^{x})+\partial_y(m\overline{V}^{x}\overline{u'}^{y})\}+\partial_z(m\overline{W^*}^{x}\overline{u'}^{z})-\frac{u}{\overline{m}^{x}}\overline{PRC}^{x}, \tag{D2-1-16}$$

$$ADVV_{i,j+1/2,k}=\overline{m}^{y}\{\partial_x(m\overline{U}^{y}\overline{v'}^{x})+\partial_y(m\overline{V}^{y}\overline{v'}^{y})\}+\partial_z(m\overline{W^*}^{y}\overline{v'}^{z})-\frac{v}{\overline{m}^{y}}\overline{PRC}^{y}, \tag{D2-1-17}$$

$$ADVW_{i,j,k+1/2}=m\{\partial_x(m\overline{U}^{x}\overline{w'}^{x})+\partial_y(m\overline{V}^{z}\overline{w'}^{y})\}+\partial_z(m\overline{W^*}^{z}\overline{w'}^{z})-\frac{w}{m}PRC, \tag{D2-1-18}$$

$$RU_{i+1/2,j,k}=\overline{f_3}^{x}\overline{V}^{xy}-\overline{f_2}^{x}\overline{W}^{xz}+\frac{\overline{m}^{x}}{\overline{(\rho G^{\frac{1}{2}})}^{x}}\{\overline{V}^{xy}(U\partial_{2y}\overline{m}^{x}-\overline{V}^{xy}\partial_x m)-\frac{\overline{UW}^{xz}}{\alpha}\}+DIF.U, \tag{D2-1-19}$$

$$RV_{i,j,k+1/2}=\overline{f_1}^{y}\overline{W}^{yz}-\overline{f_3}^{y}\overline{U}^{xy}-\frac{\overline{m}^{y}}{\overline{(\rho G^{\frac{1}{2}})}^{y}}\{\overline{U}^{xy}(\overline{U}^{xy}\partial_y m-V\partial_{2x}\overline{m}^{y})+\frac{\overline{VW}^{yz}}{\alpha}\}+DIF.V, \tag{D2-1-20}$$

$$RW_{i,j,k+1/2}=f_2\overline{U}^{xz}-f_1\overline{V}^{yz}+\frac{m}{\overline{(\rho G^{\frac{1}{2}})}^{z}}\frac{(\overline{U}^{xy^2}+\overline{V}^{yz^2})}{\alpha}+DIF.W. \tag{D2-1-21}$$

and

$$u'=\frac{U}{\overline{(\rho G^{\frac{1}{2}})}^{x}},\quad v'=\frac{V}{\overline{(\rho G^{\frac{1}{2}})}^{y}},\quad w'=\frac{W}{\overline{(\rho G^{\frac{1}{2}})}^{z}}. \tag{D2-1-22}$$

PFT in (C2-1-25) is computed directly from the virtual potential temperature.[1]

For (C2-1-26), the advection term of potential temperature is discretized as

$$ADV.\theta_{i,j,k}=\{m(\partial_x(U\overline{\theta}^{x})+\partial_y(V\overline{\theta}^{y}))+\partial_z(W^*\overline{\theta}^{z})\}\frac{m}{\rho G^{\frac{1}{2}}}-\frac{\theta DIVT(U,V,W)}{\rho G^{\frac{1}{2}}}. \tag{D2-1-23}$$

At lateral boundaries, all the advection terms are computed by one-sided differences.

P.G. Advection terms for U, V and W are computed in sub.CADV4UV and sub.CADVC4W.

D-2-2 Higher order discretization for advection terms

For a function $f(x)$, $f(x\pm\Delta x)$ is expanded in the following Taylor series,

$$f(x\pm\Delta x)=f(x)\pm f'(x)\Delta x+f''(x)\frac{(\Delta x)^2}{2!}\pm f^{(3)}(x)\frac{(\Delta x)^3}{3!}+\cdots \tag{D2-2-2}$$

That is,

$$f(x+\Delta x)-f(x-\Delta x)=f'(x)2\Delta x+f^{(3)}(x)\frac{2(\Delta x)^3}{3!}+f^{(5)}(x)\frac{2(\Delta x)^5}{5!}+\cdots \tag{D2-2-3}$$

Rearranging (D2-2-3) gives

$$f'(x)_{\Delta x}=\frac{f(x+\Delta x)-f(x-\Delta x)}{2\Delta x}-f^{(3)}(x)\frac{(\Delta x)^2}{3!}-f^{(5)}(x)\frac{(\Delta x)^4}{5!}-\cdots \tag{D2-2-4}$$

The first term on the right-hand side is the second-order centered difference that contains errors of higher order

---

[1]In Ikawa and Saito's (1991) quasi-compressible model, PFT was defined by (C2-2-12) and discretized by

$$PFT=\frac{1}{g}\frac{\partial\overline{BUOY'}^{z}}{\partial t}.$$

In addition to the linearization, this expression contained errors due to double averaging of potential temperature because $BUOY'$ is defined at a half level.

than $(\Delta x)^2$. For the advection term, this error affects the phase speed of the quantity, which causes a dispersion.

Substituting $2\Delta x$ for Δx in (D2-2-4), we obtain

$$f'(x)_{2\Delta x}=\frac{f(x+2\Delta x)-f(x-2\Delta x)}{4\Delta x}-f^{(3)}(x)\frac{4(\Delta x)^2}{3!}-f^{(5)}(x)\frac{16(\Delta x)^4}{5!}-\cdots \tag{D2-2-5}$$

Computing $f'(x)$ by $\{4\times(\text{D2-2-4})-(\text{D2-2-5})\}\div 3$ gives

$$\begin{aligned} f'(x)&=\frac{3}{4}f'(x)_{\Delta x}-\frac{1}{3}f'(x)_{2\Delta x} \\ &=\frac{-f(x+2\Delta x)+8f(x+\Delta x)-8f(x-\Delta x)+f(x-2\Delta x)}{12\Delta x}+f^{(5)}(x)\frac{4(\Delta x)^4}{5!}+\cdots \end{aligned} \tag{D2-2-6}$$

The first term on the right-hand side is the fourth-order centered difference derived by the four-point method.

Higher order advection terms of scalar variables are computed in advective form as

$$ADV.\theta_{i,j,k}=\{m(\overline{U}^x\partial_{x4}\theta+\overline{V}^z\partial_{y4}\theta)+\overline{W^*}^z\partial_{2z}\theta\}\frac{m}{\rho G^{\frac{1}{2}}}, \tag{D2-2-7}$$

where, assuming uniform grid intervals, the fourth-order gradient is defined by

$$\partial_{x4}\theta=\frac{-\theta_{i+2,j,k}+8\theta_{i-1,j,k}+\theta_{i-2,j,k}}{12\Delta x}. \tag{D2-2-8}$$

In the same manner, the third-order upstream gradient is defined by

$$\begin{aligned} \partial_{x3}\theta&=\frac{2\theta_{i+1,j,k}+3\theta_{i,j,k}-6\theta_{i-1,j,k}+\theta_{i-2,j,k}}{6\Delta x} \quad for\overline{U}^x\geq 0, \\ \partial_{x3}&=\frac{-\theta_{i+2,j,k}+6\theta_{i+1,j,k}-3\theta_{i,j,k}-2\theta_{i-1,j,k}}{6\Delta x} \quad for\overline{U}^x<0, \end{aligned} \tag{D2-2-9}$$

For the wind component, the fourth-order gradient (D2-2-8) is directly applied to (D2-1-16) - (D2-1-18), *e.g.,*

$$ADVU_{i+1/2,j,k}=\overline{m}^x\{\partial_{x4}(m\overline{U}^x\overline{u'}^x)+\partial_{y4}(m\overline{V}^x\overline{u'}^y)\}+\partial_z(m\overline{W^*}^x\overline{u'}^z)-\frac{u}{\overline{m}^x}PRC^x, \tag{D2-2-10}$$

At the lateral boundaries, all the advection terms are computed by one-sided differences, and just inside the lateral boundaries, the advection terms are computed by the second order accuracy.

The fourth-order advection scheme described in this chapter was used for the GCSS CASE-1 model intercomparison, where a TOGA-COARE observed squall line was simulated (Redelsperger *et al.,* 1999). Currently, this option works for off-line ideal simulation but is instable for simulations in real situations. Further testing should be done to use a higher order scheme for real case simulation with nesting.

D-2-3 Modified centered difference scheme for advection

A new advection scheme has been developed to remove the numerical errors that the centered-difference advection scheme produces on the upstream side. These errors increase rapidly as the grid size decreases, which causes significant problems, especially in a high-resolution model with a horizontal grid size of less than 5 km. For positive prediction values, Smolarkiewicz (1983) and Hsu and Arakawa (1990) developed a more accurate advection scheme. Regardless of the sign of predicted values, the present scheme is designed so that values calculated by the centered-difference advection scheme lie between the maximum and minimum of those in the upstream neighboring grid boxes.

This new scheme is outlined for a two-dimensional case. The second-order centered-difference advection scheme for a predicted value F is given as

$$F^{m+1}_{i,j}=F^{m-1}_{i,j}-2\Delta t\left(\frac{U^{m}_{i+\frac{1}{2},j}F^{m}_{i+\frac{1}{2},j}-U^{m}_{i-\frac{1}{2},j}F^{m}_{i-\frac{1}{2},j}}{\Delta x}+\frac{V^{m}_{i,j+\frac{1}{2}}F^{m}_{i,j+\frac{1}{2}}-V^{m}_{i,j-\frac{1}{2}}F^{m}_{i,j-\frac{1}{2}}}{\Delta x}\right), \qquad \text{(D2-3-1)}$$

where the superscript m denotes the m-th time level, U and V are the momentum fluxes, Δx and Δy are the grid intervals in the x- and y-directions, and Δt is the time step. First, the rates of advection from the upstream side are calculated as

$$\begin{aligned}
UP&=Max\,(Min\,(-\frac{2\Delta t U^{m}_{i+\frac{1}{2},j}}{\Delta x},1.0),0.0),\\
UM&=Max\,(Min\,(-\frac{2\Delta t U^{m}_{i-\frac{1}{2},j}}{\Delta x},1.0),0.0),\\
VP&=Max\,(Min\,(-\frac{2\Delta t V^{m}_{i+\frac{1}{2},j}}{\Delta y},1.0),0.0),\\
VM&=Max\,(Min\,(-\frac{2\Delta t V^{m}_{i-\frac{1}{2},j}}{\Delta y},1.0),0.0),
\end{aligned} \qquad \text{(D-2-3-2)}$$

and

$$V\mathrm{max}=Max\,(UP,UM,VP,VM).$$

Here, these rates are zero for the advection from the downstream side, and Vmax is the rate in the direction where the maximum advection is determined. The value in the neighboring grid box in this direction at the time level m-1 is denoted as $F0$. Next, the acceptable maximum Fx and the minimum Fn of the value considered by advection are determined as

$$\begin{aligned}
Fx_{i,j}=Max\,(F^{m-1}_{i,j},\ &F0+({}^{m-1}_{i+1,j}-F0)\frac{UP}{V\mathrm{max}},\ F0+(F^{m-1}_{i,j+1}-F0)\frac{VP}{V\mathrm{max}},\\
&F0+({}^{m-1}_{i-1,j}-F0)\frac{UM}{V\mathrm{max}},\ F0+(F^{m-1}_{i,j-1}-F0)\frac{VM}{V\mathrm{max}},
\end{aligned}$$

and (D2-3-3)

$$\begin{aligned}
Fn_{i,j}=Min\,(F^{m-1}_{i,j},\ &F0+({}^{m-1}_{i+1,j}-F0)\frac{UP}{V\mathrm{max}},\ F0+(F^{m-1}_{i,j+1}-F0)\frac{VP}{V\mathrm{max}},\\
&F0+({}^{m-1}_{i-1,j}-F0)\frac{UM}{V\mathrm{max}},\ F0+(F^{m-1}_{i,j-1}-F0)\frac{VM}{V\mathrm{max}},
\end{aligned}$$

When the value calculated by (D2-3-1) does not fall between Fx and Fn (*i.e.*, $F^{m+1}_{i,j}-Fx_{i,j}>0$ or $F^{m+1}_{i,j}-Fn_{i,j}<0$), it is replaced by either Fx or Fn. The difference produced by this replacement is distributed among the neighbor grid boxes as follows. The difference between the value calculated by (D2-3-1) and Fx (Fn) is denoted as

$$F1_{i,j}=-F^{m+1}_{i,j}+Fx_{i,j}\,(=F^{m+1}_{i,j}-Fn_{i,j}). \qquad \text{(D2-3-4)}$$

The total acceptable amount of the neighboring grid boxes FS is calculated as

$$FS_{i,j}=Max\,(F1_{i+1,j},0.0)+Max\,(F1_{i-1,j},0.0)+Max\,(F1_{i,j+1},0.0)+Max\,(F1_{i,j-1},0.0). \qquad \text{(D2-3-5)}$$

Therefore, the values of the neighboring grid boxes in which the value calculated by (D2-3-1) is between Fx and Fn are adjusted as

$$R=\frac{Max(FS_{i,j}+F1_{i,j},0.0)}{F1_{i,j}},$$

$$F1^*_{i\pm1,j}=R\times F1_{i\pm1,j},\quad for\quad F1_{i\pm1,j}>0,$$

and (D2-3-6)

$$F1^*_{i,j\pm1}=R\times F1_{i,j\pm1},\quad for\quad F1_{i,j\pm1}>0,$$

where $F1^*_{i,j}$ is the adjusted value of $F1_{i,j}$. By substituting $F1^*_{i,j}$ into the left-hand side of (D2-3-4), we can calculate the adjusted value of $F^{m+1}{}_{i,j}$. For $FS_{i,j}+F1_{i,j}<0$, the total amount of predicted values cannot be exactly preserved, but the validation test of this scheme indicates that this error is very small (see Fig. 11.12 in Saito and Kato, 1999).

D-3. Pressure equation solver

The basic concept of the pressure equation solver on a variable grid was reviewed in B-6 of Ikawa and Saito (1991), but the expression was simplified assuming $G^{1/2}=1$. In this technical report, we describe the details of the pressure solver of HI-VI again following the programming code including the map factor.

D-3-1 Unified expression of the pressure equation

As shown in chapter C-3, the pressure equations take the following form for the E-HI-VI scheme

$$\alpha_{HI}\left(\frac{\partial^2\Delta^2P}{\partial x^2}+\frac{\partial^2\Delta^2P}{\partial y^2}\right)+\frac{\partial^2\Delta^2P}{\partial z^2}+\frac{\partial}{\partial z}(h_{HI}\Delta^2P)+e_{HI}\Delta^2P=FP.HI, \tag{D3-1-1}$$

where

$$\alpha_{HI}=\frac{\overline{\overline{m^2}}}{\overline{\overline{\frac{m}{G^{\frac{1}{2}}}\frac{1}{mG^{\frac{1}{2}}}}}}, \tag{D3-1-2}$$

$$h_{HI}=\frac{1}{\overline{\overline{\frac{1}{mG^{\frac{1}{2}}}}}}\overline{\overline{\frac{g}{mC^2_m}}}, \tag{D3-1-3}$$

$$e_{HI}=-\frac{1}{\overline{\overline{\frac{m}{G^{\frac{1}{2}}}\frac{1}{mG^{\frac{1}{2}}}}}}\frac{1}{\overline{\overline{C^2_m}}(1+\alpha)^2(\Delta t)^2}, \tag{D3-1-4}$$

$$FP.HI=\frac{1}{\overline{\overline{\frac{m}{G^{\frac{1}{2}}}\frac{1}{mG^{\frac{1}{2}}}}}}\left\{\frac{ADVP'}{(1+\alpha)\Delta t}DIVS(ADVU',ADVV',ADVW')\right\}, \tag{D3-1-5}$$

For the AE scheme,

$$\alpha_{AE}\left(\frac{\partial^2P}{\partial x^2}+\frac{\partial^2P}{\partial y^2}\right)+\frac{\partial^2P}{\partial z^2}+\frac{\partial}{\partial z}(h_{AE}P)=FP.AE.INV+FP.AE.VAR, \tag{D3-1-6}$$

where

$$\alpha_{AE}=(\overline{\overline{G^{\frac{1}{2}}}})^2, \tag{D3-1-7}$$

$$h_{AEI}=\frac{g}{C^2_s}\overline{\overline{G^{\frac{1}{2}}}}\approx\frac{\overline{\overline{gG^{\frac{1}{2}}}}}{C^2_s}, \tag{D3-1-8}$$

$$FP.AE.INV = -\overline{\overline{(G^{\frac{1}{2}})}}^{2} DIVT(ADVU-RU, ADVV-RV, ADVW-RW-BUOY')$$

$$+\frac{\overline{\overline{(G^{\frac{1}{2}})}}^{2}}{2\Delta t} DIVT(U^{\tau-1}, V^{\tau-1}, W^{\tau-1}), \tag{D3-1-9}$$

$$FP.AE.VAR = -\overline{\overline{(G^{\frac{1}{2}})}}^{2} DIVR\left(\frac{\partial P}{\partial x}, \frac{\partial P}{\partial y}, \overline{\overline{\frac{1}{G^{\frac{1}{2}}}}}\frac{\partial P}{\partial z^*}+\frac{P}{C_s^2}g\right)$$

$$-\overline{\overline{(G^{\frac{1}{2}})}}^{2} DIVT\left\{\frac{\partial G^{\frac{1}{2}}G^{13}P}{G^{\frac{1}{2}}\partial z^*}, \frac{\partial G^{\frac{1}{2}}G^{23}P}{G^{\frac{1}{2}}\partial z^*}, \left(\frac{1}{G^{\frac{1}{2}}}\frac{\partial}{\partial z^*}+\frac{g}{C_s^2}-\overline{\overline{\frac{1}{G^{\frac{1}{2}}}}}\frac{\partial}{\partial z^*}-\frac{g}{C_s^2}\right)P\right\}. \tag{D3-1-10}$$

For the E-HE-VI scheme, the pressure equations are given by (C3-2-11) to (C3-2-13).

Here, (D3-1-1) is the three-dimensional Helmholtz equation for $\Delta^2 P$, (D3-1-6) is the three-dimensional Poisson equation for P, and (C3-2-11) is the one-dimensional Helmholtz equation for P^{β}. Following Ikawa and Saito (1991), the 3-D elliptic equations can be reduced to a one-dimensional elliptic equation by the Dimension Reduction Method, which is described in D-3-3.

D-3-2 Finite discretization form for the pressure equation

In the finite discretization of second-order accuracy, the centered differences may be written as

$$\frac{\partial}{\partial x}(\phi)_j = (\phi_x)_j = \frac{1}{\Delta x_j}\{(\phi)_{j+\frac{1}{2}} - (\phi)_{j-\frac{1}{2}}\}, \tag{D3-2-1}$$

$$\frac{\partial^2}{\partial x^2}(\phi)_j = \frac{1}{\Delta x_j}\{(\phi_x)_{j+\frac{1}{2}} - (\phi_x)_{j-\frac{1}{2}}\}$$

$$= \frac{1}{\Delta x_j}\left\{\frac{(\phi)_{j+1}-(\phi)_j}{\Delta x_{j+\frac{1}{2}}} - \frac{(\phi)_j-(\phi)_{j-1}}{\Delta x_{j-\frac{1}{2}}}\right\}$$

$$= \frac{(\phi)_{j+1}}{\Delta x_j \Delta x_{j+\frac{1}{2}}} - \frac{(\phi)_j}{\Delta x_j}\left(\frac{1}{\Delta x_{j+\frac{1}{2}}}+\frac{1}{\Delta x_{j-\frac{1}{2}}}\right) + \frac{(\phi)_{j-1}}{\Delta x_j \Delta x_{j-\frac{1}{2}}}. \tag{D3-2-2}$$

Thus, (D3-1-1) and (D3-1-6) may be discretized for a grid point (i, j, k) as

$$a\left\{\frac{P_{i,j,k}}{\Delta x_i \Delta x_{i+\frac{1}{2}}} - \frac{P_{i,j,k}}{\Delta x_j}\left(\frac{1}{\Delta x_{i+\frac{1}{2}}}+\frac{1}{\Delta x_{i-\frac{1}{2}}}\right) + \frac{P_{i-1,j,k}}{\Delta x_i \Delta x_{i-\frac{1}{2}}}\right.$$

$$+\frac{P_{i,j+1,k}}{\Delta y_j \Delta y_{j+\frac{1}{2}}} - \frac{P_{i,j,k}}{\Delta y_j}\left(\frac{1}{\Delta y_{j+\frac{1}{2}}}+\frac{1}{\Delta y_{j-\frac{1}{2}}}\right) + \frac{P_{i,j-1,k}}{\Delta y_j \Delta y_{j-\frac{1}{2}}}$$

$$+\frac{1}{\Delta z_k}\left\{\frac{1}{\Delta z_{i+1/2}}(P_{i,j,k+1}-P_{i,j,k}) - \frac{1}{\Delta z_{k-1/2}}(P_{i,j,k-1})\right\}$$

$$+\frac{1}{\Delta z_k}\left(h_{i,j,k+\frac{1}{2}}\frac{P_{i,j,k+1}P_{i,j,k}}{2} - h_{i,j,k-\frac{1}{2}}\frac{P_{i,j,k}+P_{i,j,k-1}}{2}\right)$$

$$+eP_{i,j,k} = F_{i,j,k}. \tag{D3-2-3}$$

Here, h is given at a half level. In the above expression, $\Delta^2 P$ in (D3-1-1) is replaced with P and subscripts are omitted for a unified description.

At the boundaries, we assume the following Neumann-type boundary conditions.

$$\frac{\partial P}{\partial x} = B_x, \tag{D3-2-4}$$

$$\frac{\partial P}{\partial y}=B_y, \tag{D3-2-5}$$

$$\frac{\partial P}{\phi z}+hP=B_z. \tag{D3-2-6}$$

The detailed formulation of B is discussed in F-1. In the finite discretization form, the above equations are written as

$$\frac{1}{\Delta x_{1+\frac{1}{2}}}(P_{2,j,k}-P_{1,j,k})=B_{1,j,k},$$

$$\frac{1}{\Delta x_{nx-\frac{1}{2}}}(P_{nx,j,k}-P_{nx-1,j,k})=B_{nx,j,k}, \tag{D3-2-7}$$

$$\frac{1}{\Delta y_{1+\frac{1}{2}}}(P_{i,2,k}-P_{i,1,k})=B_{i,1,k},$$

$$\frac{1}{\Delta y_{nx+\frac{1}{2}}}(P_{i,ny,k}-P_{i,ny-1,k})=B_{i,ny,k}, \tag{D3-2-8}$$

$$\frac{1}{\Delta z_{1+1/2}}(P_{i,j,2}-P_{i,j,1})+\frac{h_{i,j,1+\frac{1}{2}}}{2}(P_{i,j,2}+P_{i,j,1})=B_{i,j,1},$$

$$\frac{1}{\Delta z_{nz-1/2}}(P_{i,j,nz}-P_{i,j,nz-1})+\frac{h_{i,j,nz-\frac{1}{2}}}{2}(P_{i,j,nz}+P_{i,j,nz-1})=B_{i,j,nz}. \tag{D3-2-9}$$

Here, (nx, ny, nz) is the model dimension, and the boundary values $B_{1,j,k}$, $B_{nx,j,k}$, $B_{i,1,k}$, $B_{i,ny,k}$, $B_{i,j,1}$, $B_{i,j,nz}$ are given at the locations $x=1+1/2$, nx-1/2, $y=1+1/2$, ny-1/2, $z=1+1/2$, nz-1/2, respectively.

Incorporating the boundary condition (D3-2-7), the finite discretization in the x-direction of the first term on the left-hand side of (D3-2-3) is expressed as

$$\alpha Y_A^{-1}A\Pi_{,j,k}=\Phi_{j,k}, \tag{D3-2-10}$$

for i running from 2 to nx-1. Here,

$$Y_A^{-1}=\begin{pmatrix} \frac{1}{\Delta x_2} & 0 & & \\ 0 & \frac{1}{\Delta x_3} & 0 & \\ \cdots & \cdots & & \cdots \\ 0 & \frac{1}{\Delta x_{nx-2}} & & 0 \\ & 0 & & \frac{1}{\Delta x_{nx-1}} \end{pmatrix}, \tag{D3-2-11}$$

$$A=\begin{pmatrix} -\frac{1}{\Delta x_{2+\frac{1}{2}}} & \frac{1}{\Delta x_{2+\frac{1}{2}}} & & & \\ \frac{1}{\Delta x_{3-\frac{1}{2}}} & -(\frac{1}{\Delta x_{3+\frac{1}{2}}}+\frac{1}{\Delta x_{3-\frac{1}{2}}}) & \frac{1}{\Delta x_{3+\frac{1}{2}}} & & \\ & \cdots & \cdots & \cdots & \\ & & \frac{1}{\Delta x_{nx-2+\frac{1}{2}}} & -(\frac{1}{\Delta x_{nx-2+\frac{1}{2}}}+\frac{1}{\Delta x_{nx-2-\frac{1}{2}}}) & \frac{1}{\Delta x_{nx-2+\frac{1}{2}}} \\ & & & \frac{1}{\Delta x_{nx-1-\frac{1}{2}}} & -\frac{1}{\Delta x_{nx-1-\frac{1}{2}}} \end{pmatrix}, \tag{D3-2-12}$$

$$\Pi_{,j,k}=\begin{pmatrix} P_{2,j,k} \\ P_{3,j,k} \\ \cdots \\ P_{nx-2,j,k} \\ P_{nx-1,j,k} \end{pmatrix}, \tag{D3-2-13}$$

$$\Phi_{j,k}=\begin{pmatrix} F_{2,j,k} \\ F_{3,j,k} \\ \cdots \\ F_{nz-2,j,k} \\ F_{nz-1,j,k} \end{pmatrix}, \tag{D3-2-14}$$

and

$$\begin{aligned} F'_{2,j,k} &= F_{2,j,k}+aB_{1,j,k}/\Delta x_2, \\ F'_{nx-1,j,k} &= F_{nx-1,j,k}-aB_{nx,j,k}/\Delta x_{nx-1}. \end{aligned} \tag{D3-2-15}$$

For a uniform grid, the product of (D3-2-11) and (D3-2-12) is simply rewritten as

$$Y_A^{-1}A=A_u=\left(\frac{1}{\Delta x}\right)^2\begin{pmatrix} -1 & 1 & & & \\ 1 & -2 & 1 & & \\ & \cdots & \cdots & \cdots & \\ & & 1 & -2 & 1 \\ & & & 1 & -1 \end{pmatrix}, \tag{D3-2-16}$$

If the boundary condition is cyclic, the matrix has the following form

$$A_c=\left(\frac{1}{\Delta x}\right)^2\begin{pmatrix} -2 & 1 & & & 1 \\ 1 & -2 & 1 & & \\ & \cdots & \cdots & \cdots & \\ & & 1 & -2 & 1 \\ 1 & & & 1 & -2 \end{pmatrix}, \tag{D3-2-17}$$

with $B_{1,j,k}$ and $B_{nx,j,k}$ vanishing in (D3-2-15).

Under Dirichlet-type boundary conditions (not implemented in the model yet), (D3-2-10) becomes

$$a\left(\frac{1}{\Delta x}\right)^2\begin{pmatrix} -2 & 1 & & & 0 \\ 1 & -2 & 1 & & \\ & \cdots & \cdots & \cdots & \\ & & 1 & -2 & 1 \\ 0 & & & 1 & -2 \end{pmatrix}\begin{pmatrix} P_{2,j,k} \\ P_{3,j,k} \\ \cdots \\ P_{nx-2,j,k} \\ P_{nx-1,j,k} \end{pmatrix}=\begin{pmatrix} F_{2,j,k}-a\dfrac{P_{1,j,k}}{(\Delta x)^2} \\ F_{3,j,k} \\ \cdots \\ F_{nx-2,j,k} \\ F_{nx-1,j,k}-a\dfrac{P_{nx,j,k}}{(\Delta x)^2} \end{pmatrix} \tag{D3-2-18}$$

Hereafter, we use $njx=nx-2$, $njy=ny-2$ for expression. Since (D3-2-3) is separable in the x- and y-directions, applying the same manner in the y-direction yields

$$a\begin{pmatrix} A_u & & & & \\ & A_u & & & \\ & & \cdots & & \\ & & & A_u & \\ & & & & A_u \end{pmatrix}\begin{pmatrix} \Pi_{,2,k} \\ \Pi_{,3,k} \\ \cdots \\ \Pi_{,ny-2,k} \\ \Pi_{,ny-1,k} \end{pmatrix}+a\left(\frac{1}{\Delta y}\right)^2\begin{pmatrix} -I_{njx} & I_{njx} & & & \\ I_{njx} & -2I_{njx} & I_{njx} & & \\ & \cdots & \cdots & \cdots & \\ & & I_{njx} & -2I_{njx} & I_{njx} \\ & & & I_{njx} & -I_{njx} \end{pmatrix}\begin{pmatrix} \Pi_{,2,k} \\ \Pi_{,3,k} \\ \cdots \\ \Pi_{,ny-2,k} \\ \Pi_{,ny-1,k} \end{pmatrix}=\begin{pmatrix} \Phi_{2,k}' \\ \Phi_{3,k} \\ \cdots \\ \Phi_{ny-2,k} \\ \Phi_{ny-1,k}' \end{pmatrix} \tag{D3-2-19}$$

for each level discretization. Here, I_{njx} is a unit matrix whose dimensions are (njx, njx). Introducing a tensor product operator for (m, m) matrix M and (n, n) matrix N

$$M \otimes N \equiv \begin{pmatrix} m_{11}N & m_{12}N & \cdots & m_{1m}N \\ m_{21}N & m_{22}N & & m_{2m}N \\ & & & \\ m_{m1}N & & & m_{mm}N \end{pmatrix} \tag{D3-2-20}$$

(D3-2-19) can be written in the following form

$$a(I_{njy} \otimes Y_A^{-1}A + Y_B^{-1}B \otimes I_{njx})\Pi_{,,k} = \Phi_{,,k}. \tag{D3-2-21}$$

Here, I_{njy} is a unit matrix of (njy, njy), B is a matrix of (njy, njy) that is similar to A, and $\Pi_{,,k}$ and $\Phi_{,,k}$ are $(njx{*}njy, 1)$ matrices consisting of $P_{,j,k}$ and $F_{,j,k}$ (incorporating the boundary conditions).

Finally, the finite discretization (D3-2-3) is written in the following form

$$a(I_{njy} \otimes Y_A^{-1}A + Y_B^{-1}B \otimes I_{njx})\Pi_{,,k} + r_k\Pi_{,,k-1} + (s_k + e_k)\Pi_{,,k} + t_k\Pi_{,,k+1} = \Phi_{,,k}, \tag{D3-2-22}$$

for $2 \leqq k \leqq nz-1$. Here,

$$r_k = \frac{1}{\Delta z_k}\left(\frac{1}{\Delta z_{k-\frac{1}{2}}} - \frac{h_{k-\frac{1}{2}}}{2}\right),$$

$$s_k = \frac{1}{\Delta z_k}\left(\frac{1}{\Delta z_{k+\frac{1}{2}}} - \frac{1}{\Delta z_{k-\frac{1}{2}}} + \frac{h_{k+\frac{1}{2}} - h_{k-\frac{1}{2}}}{2}\right),$$

$$t_k = \frac{1}{\Delta z_k}\left(\frac{1}{\Delta z_{k+\frac{1}{2}}} + \frac{h_{k+\frac{1}{2}}}{2}\right). \tag{D3-2-23}$$

The upper and lower boundary conditions (D3-2-9) are rewritten as

$$\left(-\frac{1}{\Delta z_{1+\frac{1}{2}}} + \frac{h_{1+\frac{1}{2}}}{2}\right)\Pi_{,,1} + \left(\frac{1}{\Delta z_{1+\frac{1}{2}}} + \frac{h_{1+\frac{1}{2}}}{2}\right)\Pi_{,,2} = \Phi_{,,1},$$

$$\left(-\frac{1}{\Delta z_{nz-\frac{1}{2}}} + \frac{h_{nz-\frac{1}{2}}}{2}\right)\Pi_{,,nz-1} + \left(\frac{1}{\Delta z_{nz-\frac{1}{2}}} + \frac{h_{nz-\frac{1}{2}}}{2}\right)\Pi_{,,nz} = \Phi_{,,nz}. \tag{D3-2-24}$$

Here, $\Phi_{,,1}$ and $\Phi_{,,nz}$ are $(njx{*}njy, 1)$ matrices consisting of $B_{i,j,1}$ and $B_{i,j,nz}$. These equations are rewritten as

$$t_1\Pi_{,,2} + s_1\Pi_{,,1},$$

$$r_{nz}\Pi_{,,nz-1} + s_{nz}\Pi_{,,nz} = \Phi_{,,nz}. \tag{D3-2-25}$$

D-3-3 Dimension Reduction Method

The dimension reduction method described in Ikawa and Saito (1991) is used to solve (D3-2-22). This method projects the pressure equation onto the horizontal eigen space, and leaves a one-dimensional vertical equation. Here, we focus primarily on a uniform grid (D3-2-16) since the usual computation is done with a uniform grid. A detailed description of the dimension reduction method for a variable grid is presented in Ikawa and Saito (1991).

For a uniform grid, the eigen value matrix and eigen function for A_u (D3-2-16) are given as

$$\Lambda_a = \frac{1}{(\Delta x)^2}\begin{pmatrix} 0 & 0 & & & \\ 0 & \cdots & 0 & & \\ & & -4\sin^2\frac{k-1}{2njx}\pi & & \\ & & 0 & \cdots & 0 \\ 0 & & & 0 & -4\sin^2\frac{njx-1}{2njx}\pi \end{pmatrix}, \tag{D3-3-1}$$

and

$$P=\frac{\sqrt{2}}{\sqrt{njx}}\begin{pmatrix} \frac{1}{\sqrt{2}} & \cdots & \cos\frac{(k-1)(1-1/2)}{njx}\pi & \cdots & \cos\frac{(njx-1)(1-1/2)}{njx}\pi \\ \cdots & & \cdots & & \\ \frac{1}{\sqrt{2}} & \cdots & \cos\frac{(k-1)(m-1/2)}{njx}\pi & \cdots & \cos\frac{(njx-1)(m-1/2)}{njx}\pi \\ \cdots & & \cdots & & \\ \frac{1}{\sqrt{2}} & \cdots & \cos\frac{(k-1)(njx-1/2)}{njx}\pi & \cdots & \cos\frac{(njx-1)(njx-1/2)}{njx}\pi \end{pmatrix}. \quad \text{(D3-3-2)}$$

Under the cyclic boundary condition, as described in Ikawa (1981), they are

$$\Lambda_a=\frac{1}{(\Delta x)^2}\begin{pmatrix} 0 & & & & & & \\ & \cdots & & & & & \\ & & 4\sin^2\frac{k-1}{njx}\pi & & & & \\ & & & -4\sin^2\frac{\pi}{2} & & & \\ & & & & -4\sin^2\frac{\pi}{2} & & \\ & & & & & \cdots & \\ & & & & & -\sin^2\frac{2(k-njx/2-1)}{njx}\pi & \\ & & & & & & 4\sin^2\frac{njx-1}{2njx}\pi \end{pmatrix}, \quad \text{(D3-3-3)}$$

$$P=\frac{\sqrt{2}}{\sqrt{njx}}\begin{pmatrix} \frac{1}{\sqrt{2}} & 1 & \cdots & 1 & 0 & \cdots & 0 \\ \frac{1}{\sqrt{2}} & \cos\frac{2\pi}{njx} & \cdots & \cos\frac{2\pi}{njx}\frac{njx}{2} & \sin\frac{2\pi}{njx} & \cdots & \sin\frac{2\pi}{njx}(\frac{njx}{2}-1) \\ \cdots & \cdots & & \cdots & \cdots & & \cdots \\ \frac{1}{\sqrt{2}} & \cos\frac{2\pi}{njx}m & \cdots & \cos\frac{2\pi}{njx}\frac{njx}{2}m & \sin\frac{2\pi}{njx}m & & \sin\frac{2\pi}{njx}(\frac{njx}{2}-1)m \\ \cdots & \cdots & & \cdots & \cdots & & \\ \frac{1}{\sqrt{2}} & \cos\frac{2\pi}{njx}(njx-1) & \cdots & \cos\frac{2\pi}{njx}\frac{njx}{2}(njx-1) & \sin\frac{2\pi}{njx}(njx-1) & & \sin\frac{2\pi}{njx}(\frac{njx}{2}-1)(njx-1) \end{pmatrix}, \quad \text{(D3-3-4)}$$

respectively. For the Diriclet boundary condition, see Ogura (1969).

Using the following property of a tensor product

$$(U_1\otimes U_2)(U_3\otimes U_4)=(U_1U_3)\otimes(U_2U_4). \quad \text{(D3-3-5)}$$

and operating $Q^{-1}\otimes P^{-1}$, the coefficients of $\Pi_{,,k}$ in (D3-2-22) become

$$\begin{aligned} &Q^{-1}\otimes P^{-1}(I_{njy}\otimes A_u+B_u\otimes I_{njx})(Q\otimes P)Q^{-1}\otimes P^{-1} \\ &=(Q^{-1}I_{njy}Q\otimes P^{-1}A_uP+Q^{-1}B_uQ\otimes P^{-1}I_{njx}P)Q^{-1}\otimes P^{-1} \\ &=(I_{njy}\otimes\Lambda_a+\Lambda_b\otimes I_{njz})Q^{-1}\otimes P^{-1}, \end{aligned} \quad \text{(D3-3-6)}$$

where Q and Λ_b are the eigen function and eigen value matrix of B_u.

Thus, (D3-2-22) becomes

$$\begin{aligned} &a(I_{njy}\otimes\Lambda_u+\Lambda_b\otimes I_{njx})Q^{-1}\otimes P^{-1}\Pi_{,,k} \\ &+r_kQ^{-1}\otimes P^{-1}\Pi_{,,k-1}+(s_k+e_k)Q^{-1}\otimes P^{-1}\Pi_{,,k} \\ &+t_kQ^{-1}\otimes P^{-1}\Pi_{,,k+1}=Q^{-1}\otimes P^{-1}\Phi_{,,k}. \end{aligned} \quad \text{(D3-3-7)}$$

If we define

$$\hat{\Pi}_{,,k} \equiv Q^{-1} \otimes P^{-1} \Pi_{,,k},$$
$$\hat{\Phi}_{,,k} \equiv Q^{-1} \otimes P^{-1} \Phi_{,,k}, \tag{D3-3-8}$$

(D3-3-7) becomes

$$r_k \hat{\Pi}_{,,k-1} + \{a(I_{njy} \otimes \Lambda_a + \Lambda_b \otimes I_{njx}) + s_k + e_k\} \hat{\Pi}_{,,k} + t_k \hat{\Pi}_{,,k+1} = \Phi_{,,k}. \tag{D3-3-9}$$

That is, for $\hat{\Phi}_{i,j,k}$

$$\begin{pmatrix} s_1 & t_1 & & & & \\ r_2 & s_2+e_2+a(\lambda a_i+\lambda b_j) & t_2 & & & \\ & \cdots & \cdots & \cdots & & \\ & & r_k & s_k+e_k+a(\lambda a_i+\lambda b_j) & t_k & \\ & & & \cdots & \cdots & \\ & & & & r_{nz} & s_{nz} \end{pmatrix} \begin{pmatrix} \hat{\Pi}_{i,j,1} \\ \hat{\Pi}_{i,j,2} \\ \cdots \\ \hat{\Pi}_{i,j,k} \\ \cdots \\ \hat{\Pi}_{i,j,nz} \end{pmatrix} = \begin{pmatrix} \hat{\Phi}_{i,j,1} \\ \hat{\Phi}_{i,j,2} \\ \cdots \\ \hat{\Phi}_{i,j,k} \\ \cdots \\ \hat{\Phi}_{i,j,nz} \end{pmatrix}. \tag{D3-3-10}$$

where λa_i and λb_j are i-th and j-th components of Λ_a and Λ_b. This is a one-dimensional Helmholtz equation, similar to (C3-2-11). When $\hat{\Pi}_{,,k}$ is given, $\Pi_{,,k}$ can be obtained by inverse transform

$$\Pi_{,,k} = Q \otimes P \hat{\Pi}_{,,k}. \tag{D3-3-11}$$

D-3-4 Pressure equation solver with the Gaussian elimination

(D3-3-10) can be solved by the Gaussian elimination if the (nz, nz) coefficients matrix is not singular. For simplicity, we omit suffixes i,j from the expression, and rewriting $s_k+e_k+a(\lambda a_i+\lambda b_j)$ as s_k for $2 \leqq k \leqq nz-1$ and express the coefficients of the tri-diagonal matrix as

$$\begin{pmatrix} s_1 & t_1 & & & & \\ r_g & s_2 & t_2 & & & \\ & \cdots & \cdots & \cdots & & \\ & & r_k & s_k & t_k & \\ & & & \cdots & \cdots & \\ & & & & r_{nz} & s_{nz} \end{pmatrix} \begin{pmatrix} p_1 \\ p_2 \\ \\ p_k \\ \\ p_{nz} \end{pmatrix} = \begin{pmatrix} f_1 \\ f_2 \\ \\ f_k \\ \\ f_{nz} \end{pmatrix}. \tag{D3-4-1}$$

Multiplying the first line of (D3-4-1) by $a_1 = 1/s_1$, and setting $b_1 = -t_1 a_1$, $g_1 = f_1 a_1$ yields

$$\begin{pmatrix} 1 & -b_1 & & & & \\ r_2 & s_2 & t_2 & & & \\ & \cdots & \cdots & \cdots & & \\ & & r_k & s_k & t_k & \\ & & & \cdots & \cdots & \\ & & & & r_{nz} & s_{nz} \end{pmatrix} \begin{pmatrix} p_1 \\ p_2 \\ \\ p_k \\ \\ p_{nz} \end{pmatrix} = \begin{pmatrix} g_1 \\ f_2 \\ \\ f_k \\ \\ f_{nz} \end{pmatrix}. \tag{D3-4-2}$$

Subtracting $r_2 \times$(first line) from the second line and multiplying by $a_2 = 1/(s_2 + r_2 b_1)$ gives

$$\begin{pmatrix} 1 & -b_1 & & & & \\ 0 & 1 & -b_2 & & & \\ & \cdots & \cdots & \cdots & & \\ & & r_k & s_k & t_k & \\ & & & \cdots & \cdots & \\ & & & & r_{nz} & s_{nz} \end{pmatrix} \begin{pmatrix} p_1 \\ p_2 \\ \\ p_k \\ \\ p_{nz} \end{pmatrix} = \begin{pmatrix} g_1 \\ g_2 \\ \\ f_k \\ \\ f_{nz} \end{pmatrix}, \tag{D3-4-3}$$

where $b_2 = -t_2 a_2$, $g_2 = (f_2 - r_2 g_1) a_2$. In the same manner, by setting $a_k = 1/(s_k + r_k b_{k-1})$, $b_k = -t_k a_k$, $g_k = (f_k - r_k g_{k-1}) a_k$, the above formula becomes

$$\begin{pmatrix} 1 & -b_1 & & & & \\ & \cdots & \cdots & & & \\ & & 1 & -b_k & & \\ & & & \cdots & \cdots & \\ & & & & 1 & -b_{nz-1} \\ & & & & 0 & 1 \end{pmatrix} \begin{pmatrix} p_1 \\ \\ p_k \\ \\ p_{nz-1} \\ p_{nz} \end{pmatrix} = \begin{pmatrix} g_1 \\ \\ g_k \\ \\ g_{nz-1} \\ g_{nz} \end{pmatrix}. \tag{D3-4-4}$$

The solution is given by $p_{nz}=g_{nz}$, ..., $p_k=g_k+b_k p_{k+1}$, ... $p_1=g_1+b_1 p_2$. The coefficients a_k and b_k can be prepared in advance since they are independent of p_k or f_k.

As seen in (D3-3-1), $\lambda a_1=\lambda b_1=0$ for $(i, j)=(1, 1)$, thus, for an anelastic model ($e_k=0$), from (D3-2-23) to (D3-2-25), the following relation is satisfied:

$$(1 \quad \Delta z_2 \quad \cdots \quad \Delta z_k \quad \cdots \quad 1) \begin{pmatrix} s_1 & t_1 & & & & \\ r_2 & s_2 & t_2 & & & \\ & \cdots & \cdots & \cdots & & \\ & & r_k & s_k & t_k & \\ & & & \cdots & \cdots & \\ & & & & r_{nz} & s_{nz} \end{pmatrix} = 0, \tag{D3-4-5}$$

which means the (nz, nz) coefficient matrix becomes singular. As mentioned in Ikawa and Saito (1991), this corresponds to the non-uniqueness of the horizontal averaged pressure field in the anelastic model. To avoid this situation, the constraint

$$\hat{\Pi}_{1,1,nz-1}+\hat{\Pi}_{1,1,nz}=0, \tag{D3-4-6}$$

is imposed. In our case, we set $r_{nz}=s_{nz}=1$ for $(i, j)=(1, 1)$, which means that the horizontal averaged pressure in the anelastic model takes the same value of the reference atmosphere at the upper boundary.

P.G. The boundary conditions for pressure equations are set in sub.CFPBDV, and the forcing terms are set in sub.CPFORI and sub.CPFRV1. Eigen vector functions are set in sub.INIVG1 for a variable grid and sub.INIVG2 for a uniform grid. The Helmholtz equation is solved in sub.VHELMH where the Gaussian elimination is done in TRIDGH.

E. Initiation of the model

E-1. Reference atmosphere and initial environmental field

E-1-1 Stand-alone case

For the stand-alone case (without nesting), the input parameter card specifies vertical profiles of horizontal wind (u, v), potential temperature (θ) and mixing ratio of water vapor (q_v) (see Section K). In Ikawa and Saito (1991), the reference atmosphere was given by a simple algebraic function, while in the new model, the vertical profile given by the input parameter card is used for the reference atmosphere without any deformation except vertical interpolation into the model levels. For given θ and q_v, the pressure and density of the reference atmosphere are given by

$$\overline{\theta_v}=\overline{\theta}(1+0.61\overline{q_v}), \tag{E1-1-1}$$

$$\overline{\pi_g}=(\frac{\overline{p_s}}{p_0})^{R/C_p}, \tag{E1-1-2}$$

$$\overline{\pi}=\overline{\pi_g}-\frac{g}{C_p}\int_0^z\frac{1}{\overline{\theta_v}}dz, \tag{E1-1-3}$$

$$\overline{p}=p_0\overline{\pi}^{C_p/R}, \tag{E1-1-4}$$

$$\overline{\rho}=\frac{p_0}{R\overline{\theta_v}}(\frac{p}{p_0})^{C_v/C_p}, \tag{E1-1-5}$$

where $\bar{p}_s$ is the averaged pressure at $z=0$. Once $\bar{\rho}(z)$ is obtained, the reference atmosphere is interpolated on the z^* coordinate

$$\begin{aligned}&\overline{\theta_v}(z)\rightarrow\overline{\theta_v}(x,y,z^*),\\&\overline{p}(z)\rightarrow\overline{p}(x,y,z^*),\\&\overline{\rho}(z)\rightarrow\overline{\rho}(x,y,z^*),\end{aligned} \tag{E1-1-6}$$

In order to satisfy $DIVT(U,\ V,\ W)=0$ and $W^*=0$ in entire model domains, the initial momentum as the prognostic variables U, V and W is set by

$$\begin{aligned}&U(z^*)=\overline{\rho}(z)u(z),\\&V(z^*)=\overline{\rho}(z)v(z),\end{aligned} \tag{E1-1-7}$$

$$W(x,y,z^*)=-(G^{\frac{1}{2}}G^{13}U+G^{\frac{1}{2}}G^{23}V). \tag{E1-1-8}$$

Here we assumed $m=1$ for the stand-alone case. Note that, U and V in (E1-1-7) differ from the alternative expression by their original definition:

$$\begin{aligned}&U(x,y,z^*)=\rho(x,y,z^*)G^{\frac{1}{2}}u(z),\\&V(x,y,z^*)=\rho(x,y,z^*)G^{\frac{1}{2}}v(z),\end{aligned} \tag{E1-1-9}$$

Expression (E1-1-7) gives constant values for U and V at the z^* surface, that is, greater values than (E1-1-9) are used for the initial horizontal wind components if there are mountains. This modification is important for achieving a smooth start-up.

E-1-2 Nested case

When the non-hydrostatic model is used as the nested model, initial fields are prepared by interpolating the field of the outer model. As described in Saito (1994), two different interpolation procedures are employed. For the horizontal wind and the specific humidity, vertical interpolation is performed using the z^* coordinate in each model so that the boundary layer structure of the outer model is retained in the nested model. For the potential temperature, vertical interpolation is performed using the z coordinate to prevent artificial buoyancy due to the difference in the orographic heights between the models.

Once the specific humidity and potential temperature are interpolated, their horizontal average is computed to make the reference atmosphere:

$$\overline{\theta}(x,y,z^*) \rightarrow \overline{\theta}(z),$$
$$\overline{q_v}(x,y,z^*) \rightarrow \overline{q_v}(z), \tag{E1-2-1}$$

where averaging is performed strictly on the horizontal coordinate, not on the terrain-following model coordinate. Once θ and q_v are computed, the reference atmosphere is set by (E1-1-1) to (E1-1-5), and interpolated into the model planes by (E1-1-6). Pressure and density at the initial field at each grid point are computed by

$$\pi_g = \left(\frac{p_g}{p_0}\right)^{R/C_p}, \tag{E1-2-2}$$

$$\pi = \pi_g - \frac{gG^{\frac{1}{2}}}{C_p}\int_0^z \frac{1}{\theta_v} dz^*, \tag{E1-2-3}$$

$$P(x,y,z^*) = (p_0 \pi^{C_p/R} - \overline{p})\, G^{\frac{1}{2}}, \tag{E1-2-4}$$

where $p_0 = 1000$ hPa, θ_v is the interpolated virtual potential temperature of the outer model, and p_g is the pressure at the ground surface of the nested model, which is evaluated by

$$p_g = p_{go}\left\{1 - \frac{\Gamma(z_s - z_{so})}{T_{go}}\right\}^{\frac{g}{R\Gamma}}. \tag{E1-2-5}$$

Here, p_{go} is the interpolated surface pressure of the outer model, and z_s and z_{so} denote the ground heights of the nested model and outer model, respectively. T_{go} is the ground temperature of the outer model. The ground temperature of the nested model is derived from the outer model but is adjusted according to the difference of the heights between the two models. We use 6.5×10^{-3} deg/m for Γ, the temperature lapse rate near the surface. When the pressure is determined, the density is calculated by

$$\rho(x,y,z^*) = \frac{p_0}{R\theta_m}\left(\frac{\overline{p} + P/G^{\frac{1}{2}}}{p_0}\right)^{C_v/C_p}. \tag{E1-2-6}$$

Currently, the water quantities, other than water vapor, are regarded as zero in the initial field, so θ_v is used instead of the mass-virtual potential temperature in the denominator of (E1-2-6).

Using (C2-1-9) and (C2-1-10), the initial guess of the horizontal winds is calculated from the interpolated horizontal wind field of the outer model (u_0, v_0) as

$$U_0 = \frac{\rho G^{\frac{1}{2}}}{m} u_0,$$
$$V_0 = \frac{\rho G^{\frac{1}{2}}}{m} v_0, \tag{E1-2-7}$$

In the initiation procedure, the above initial guess of the horizontal winds is modified as described in the next subsection.

P.G. The vertical profile of the reference atmosphere is set by sub.SETREF for the stand-alone case and by HRMEAN for the nesting case. The profile is interpolated into model planes by sub.CPTRFT.

E-2. Start-up procedure

E-2-1 Adjustment of the horizontal wind components

In anelastic models, mass conservation in the entire model domain becomes the solvability condition for the Poisson type pressure diagnostic equation, as Ikawa and Saito (1991) discussed. In a fully compressible model, the conservation of mass is not the solvability condition for the pressure equation, but total mass flux through lateral boundaries is still very important for maintaining the total mass in the model domain.

Volume integrating the continuity equation (C2-1-8), we obtain the following relation between the time tendency of total mass in the entire model domain and the mass flux through the lateral boundaries:

$$\frac{\partial}{\partial t}\iiint \frac{\rho G^{\frac{1}{2}}}{m^2} dxdydz^* = (\iint Udydz^*)_{x=0} - (\iint Udydz^*)_{x=X}$$
$$+ (\iint Vdxdz^*)_{y=0} - (\iint Vdxdz^*)_{y=Y}$$
$$- \iint \frac{1}{m^2}(\rho_a V_r q_r + \rho_a V_s q_s + \rho_a V_g q_g)_{z^*=0} dxdy, \qquad \text{(E2-1-1)}$$

where X and Y denote the dimensions of the nested model domain for x and y directions and we assume that W^* becomes zero at the lower and upper boundaries. The last term on right-hand side of above equation comes from the volume integration of PRC in (C2-1-8), which corresponds to the total surface precipitation in the model domain.[1]

In the nesting procedure, simple application of the interpolated wind of the mother model (E1-2-7) does not satisfy the above relation due to interpolation errors, differences of upper boundary conditions between the two models, and treatment of the PRC term in the nonhydrostatic model. In order to satisfy (E2-1-1), the interpolated winds U_0 and V_0 are adjusted by

$$U_0'(x,y,z^*) = U_0(x,y,z^*) + \frac{X-2x}{X} ADJ,$$
$$V_0'(x,y,z^*) = V_0(x,y,z^*) + \frac{Y-2y}{Y} ADJ, \qquad \text{(E2-1-2)}$$

where ADJ is the difference between the expected change of total mass and the right-hand side of (E2-1-1):

$$ADJ = \frac{1}{2(S_{xz}+S_{yz})}\{S_{xy}\frac{\partial}{\partial t}\frac{\overline{p_s}-\overline{p_H}}{g} - (\iint U_0 dydz^*)_{x=0} + (\iint U_0 dydz^*)_{x=X},$$
$$-(\iint V_0 dxdz^*)_{y=0} + (\iint V_0 dxdz^*)_{y=Y}$$
$$+\iint \frac{1}{m^2}(\rho_a V_r q_r + \rho_a V_s q_s + \rho_a V_g q_g)_{z^*=0} dxdy\}. \qquad \text{(E2-1-3)}$$

Here, S_{xz} and S_{yz} are the square measures of the lateral planes of the nested model at the north-south and the east-west boundaries respectively, and S_{xy} is the area of the model domain. $\overline{p_s}$ and $\overline{p_H}$ are the averaged pressures

[1] Saito (1997) neglected this term. However, this term is not necessarily negligible in case of heavy precipitation or long-term simulation since mean precipitation of 10 mm corresponds to a pressure decrease of 1 hPa. For the GCSS WG4 Case-1 squall line simulation (Saito and Yamasaki, 1997; Redelsperger *et al.*, 2000), neglect of this term resulted in about a 2 hPa deficit of the mean pressure (Saito, 1998). More strictly, we should consider the surface vapor fluxes too, but currently neglect them.

of the outer model at the surface and top of the nested model. This adjustment is applied not only at the initial time of the nested model but also at all output times of the outer model.

E-2-2 Vertical wind component

The first guess of the vertical wind is calculated from the interpolated horizontal wind field of the outer model (U_0, V_0) using the continuity equation. In order to satisfy the boundary conditions of $W^*=0$ at the upper and lower boundaries, the following weighted mean vertical velocity ω_0 is introduced:

$$W^*_0(z^*) = W^*_u \frac{H-z^*}{H} + W^*_d \frac{z^*}{H}, \tag{E2-2-1}$$

where W^*_u and W^*_d are the vertical velocities obtained by the upward and downward integration of the continuity equation:

$$W^*_u(z^*) = -m \int_0^{z^*} \left(\frac{\partial U_0'}{\partial x} + \frac{\partial V_0'}{\partial y}\right) dz_0^*, \tag{E2-2-2}$$

$$W^*_d(z^*) = m \int_{z^*}^{H} \left(\frac{\partial U_0'}{\partial x} + \frac{\partial V_0'}{\partial y}\right) dz_0^*. \tag{E2-2-3}$$

W^*_0 given by (E2-2-1) is mainly derived by upward integration near the surface and by downward integration near the upper boundary.

E-2-3 Mass-consistent variational calculus

The *hybrid* vertical wind W^*_0 given by (E2-2-1) does not necessarily satisfy the continuity equation. In order to obtain a three-dimensional, mass-consistent wind field, the variational calculus method (Saito, 1994) is available as an optional choice in the start-up procedure of the anelastic system.

The function needed to minimize the variance of the difference between the adjusted and the interpolated wind is described by the following equation (Sherman, 1978):

$$J = \int_V \{\alpha_1^2(U-U_0') + \alpha_1^2(V-V_0')^2 + \alpha_2^2(W^*-W^*_0)^2 + \lambda DIVT(U,V,W)\} dxdydz^*. \tag{E2-3-1}$$

Here, α_1 and α_2 are weight parameters that depend on the accuracy of the initial field, and λ is the Lagrange multiplier and is a function of x, y, and z^*. The variation of J is

$$\delta J = \int_V \{\alpha_1^2 2(U-U_0')\delta U + \alpha_1^2 2(V-V_0')\delta V + \alpha_2^2 2(W^*-W^*_0)\delta W^* + \lambda\left(\frac{\partial \delta U}{\partial x} + \frac{\partial \delta V}{\partial y} + \frac{\partial \delta W^*}{\partial z^*}\right)\} dxdydz^*. \tag{E2-3-2}$$

Note that the map factor is neglected in the divergence of the anelastic system (see C-2-3). Taking partial integration of (E2-3-2) and assuming boundary conditions

$$(\lambda\delta U)|_{0,x}=0, \quad (\lambda\delta V)|_{0,Y}=0, \quad (\lambda\delta W^*)|_{0,H}=0, \tag{E2-3-3}$$

we obtain the following associated Euler-Lagrange equations whose solution minimizes (E2-3-1):

$$2\alpha_1^2(U-U_0') - \frac{\partial \lambda}{\partial x} = 0, \tag{E2-3-4}$$

$$2\alpha_1^2(V-V_0') - \frac{\partial \lambda}{\partial y} = 0, \tag{E2-3-5}$$

$$2\alpha_2^2(W^* - W^*_0) - \frac{\partial \lambda}{\partial z^*} = 0. \tag{E2-3-6}$$

Substituting the above relations into the constraint (C2-3-1), the equation of λ is obtained by solving the following Poisson equation:

$$\frac{\partial^2 \lambda}{\partial x^2} + \frac{\partial^2 \lambda}{\partial y^2} + \frac{\alpha_1^2}{\alpha_2^2}\frac{\partial^2 \lambda}{\partial z^{*2}} = -2\alpha_1^2 DIVT(U_0', V_0', W_0'), \tag{E2-3-7}$$

The boundary conditions of (E2-3-7) are $\lambda = 0$ at the lateral boundaries, and $\partial\lambda/\partial z^* = 0$ at the upper and lower boundaries. In the model, $\alpha_1 = 1$ and $\alpha^2 = \alpha_1^2/\alpha_2^2$ are usually used, and the solution of (E2-3-7) is obtained by the Successive Over-Relaxation method.

E-2-4 Initialization of pressure in elastic models

The variational calculus presented in the former section is applied only to anelastic systems. For an elastic model, the divergence in the initial field causes sound waves that are soon reduced and do not affect the later simulation results in most cases. The initial pressure field of the compressible model is given by (E1-2-4). For another way to initiate the pressure field, the model has an option in which the pressure field is given by solving the Poisson type pressure diagnostic equation for an anelastic system. This option efficiently smoothes start-up and minimizes the sound waves; it is suitable for cases in which the surface pressure field of the outer model is not reliable. Currently, this option is not complete for initialization of the regional prediction model since the map factor is not considered in the anelastic pressure equation.

P.G. The wind field is adjusted according to the total mass tendency in sub.ADJFLX. Variational calculus is performed in sub.RELAX and sub.CADJP1.

F. Boundary Conditions

F-1. Boundary conditions for the pressure equation

F-1-1 E-HI-VI scheme

In section D-3, we discussed the pressure solver for the Neumann boundary conditions (D3-2-4) to (D3-2-6). The definite expressions of B_x, B_y and B_z were obtained by computing the pressure gradient terms in the relevant momentum equations.

For the E-HI-VI scheme, the lateral boundary conditions are given from (C3-1-10) and (C3-1-11) as

$$\frac{\partial \Delta^2 P}{\partial x} = -\frac{\Delta^2 U}{(1+\alpha)\Delta t} - 2ADVU'$$

$$= -2\{ADVU' + \frac{\partial U}{\partial t} - \frac{U^{it} - U^{it-1}}{(1+\alpha)\Delta t}\}, \qquad \text{(F1-1-1)}$$

$$\frac{\partial \Delta^2 P}{\partial y} = -\frac{\Delta^2 V}{(1+\alpha)\Delta t} - 2ADVV'$$

$$= -2\{ADVV' + \frac{\partial V}{\partial t} - \frac{V^{it} - V^{it-1}}{(1+\alpha)\Delta t}\}. \qquad \text{(F1-1-2)}$$

The right-hand sides of the above equations include the time tendency of wind speed at the boundaries. Since the modified advection terms ($ADVU'$; $ADVV'$, ..) defined in (C3-1-14) and (C3-1-15) include surface friction and Coriolis forces as in (C2-1-20) and (C2-1-21), the model gives a kinematically balanced pressure field as the solution. We will refer to the time tendency of horizontal winds again in section F-2-2.

The upper boundary condition from (C3-1-12) is

$$\left(\frac{\partial}{\partial z^*} + \frac{1}{\overline{\overline{\frac{1}{mG^{\frac{1}{2}}}}}}\overline{\overline{\frac{g}{mC_m{}^2}}}\right)\Delta^2 P = \left(-\frac{\Delta^2 W}{(1+\alpha)\Delta t} - 2ADVW'\right) / \overline{\overline{\frac{1}{mG^{\frac{1}{2}}}}}$$

$$= -2\{ADVW' + \frac{\partial W}{\partial t} - \frac{W^{it} - W^{it-1}}{(1+\alpha)\Delta t}\} / \overline{\overline{\frac{1}{mG^{\frac{1}{2}}}}}$$

$$= -2\{ADVW' + \frac{EXT.W - W^{it-1}}{2\Delta t} - \frac{W^{it} - W^{it-1}}{(1+\alpha)\Delta t}\} / \overline{\overline{\frac{1}{mG^{\frac{1}{2}}}}}. \qquad \text{(F1-1-3)}$$

Here, $EXT.W$ is the expected value of W at the upper boundary, which is currently set to zero.

The lower boundary condition is given by setting

$$G^{\frac{1}{2}}\Delta^2 W^* = \Delta^2 W + m(G^{\frac{1}{2}}G^{13}\Delta^2 U + G^{\frac{1}{2}}G^{23}\Delta^2 V) = 0, \qquad \text{(F1-1-4)}$$

and substituting it into (F1-1-3) with (C3-1-10) and (C3-1-11) as

$$\left(\frac{\partial}{\partial z^*} + \frac{1}{\overline{\overline{\frac{1}{mG^{\frac{1}{2}}}}}}\overline{\overline{\frac{g}{mC_m{}^2}}}\right)\Delta^2 P = \{-2ADVW' - 2m(G^{\frac{1}{2}}G^{13}ADVU' + G^{\frac{1}{2}}G^{23}ADVV')\} / \overline{\overline{\frac{1}{mG^{\frac{1}{2}}}}}$$

$$\underline{-mG^{\frac{1}{2}}G^{13}\frac{\partial \Delta^2 P}{\partial x} + G^{\frac{1}{2}}G^{23}\frac{\partial \Delta^2 P}{\partial y}) / \overline{\overline{\frac{1}{mG^{\frac{1}{2}}}}}}. \qquad \text{(F1-1-5)}$$

An iterative procedure is necessary to solve (D3-1-1), since the under-lined term in the above equation is not separable. However, if the model includes surface friction and we assume $W=0$ at the ground surface, we can use

$$\left(\frac{\partial}{\partial z^*}+\frac{1}{\overline{\overline{\frac{1}{mG^{\frac{1}{2}}}}}}\overline{\overline{\frac{g}{mC_m{}^2}}}\right)\Delta^2 P=-2ADVW'/\overline{\overline{\frac{1}{mG^{\frac{1}{2}}}}}, \tag{F1-1-6}$$

for the lower boundary condition instead of (F1-1-5), and then the iterative procedure is no longer required.

<u>P.G.</u> Lateral boundary conditions for pressure equations are set in the array PFORCE in sub.CFPBDV.

F-1-2 AE scheme

The boundary conditions for an anelastic model are the same as described by Ikawa and Saito (1991). The lateral boundary conditions are, from (C2-2-4) and (C2-2-5),

$$\frac{\partial P}{\partial x}=-\frac{\partial U}{\partial t}-\frac{\partial G^{\frac{1}{2}}G^{13}P}{G^{\frac{1}{2}}\partial z^*}-ADVU+RU, \tag{F1-2-1}$$

$$\frac{\partial P}{\partial y}=-\frac{\partial V}{\partial t}-\frac{\partial G^{\frac{1}{2}}G^{23}P}{G^{\frac{1}{2}}\partial z^*}-ADVV+RV, \tag{F1-2-2}$$

where the right-hand sides of the above equations include the time tendency of wind speed at the boundaries, as well as surface friction and Coriolis forces as the forcing functions. The second terms on the right-hand side come from the residual terms of the horizontal pressure gradient forces in the chain rule. The inner values of P just adjacent to the boundaries at the former time step are used in these terms.

The upper boundary condition is obtained from (C2-2-9) as

$$\begin{aligned}\left(\frac{\partial}{\partial z^*}+\frac{gG^{\frac{1}{2}}}{C_s{}^2}\right)P&=G^{\frac{1}{2}}\left(-\frac{\partial W}{\partial t}-ADVW+BUOY'+RW\right)\\ &=G^{\frac{1}{2}}\left(-\frac{EXT.W-W^{it-1}}{2\Delta t}-ADVW+BUOY'+RW\right),\end{aligned} \tag{F1-2-3}$$

where $EXT.W$ is currently set to zero.

The lower boundary condition is given by setting

$$G^{\frac{1}{2}}\frac{\partial W^*}{\partial t}=\frac{\partial W}{\partial t}+G^{\frac{1}{2}}G^{13}\frac{\partial U}{\partial t}+G^{\frac{1}{2}}G^{23}\frac{\partial V}{\partial t}=0, \tag{F1-2-4}$$

and substituting it into (F1-2-3) with (C2-2-4) and (C2-2-5) as

$$\begin{aligned}\left(\frac{\partial}{\partial z^*}+\frac{gG^{\frac{1}{2}}}{C_s{}^2}\right)P=G^{\frac{1}{2}}\Big\{&G^{\frac{1}{2}}G^{13}\left(-\frac{\partial p}{\partial x}-\frac{\partial G^{\frac{1}{2}}G^{13}P}{G^{\frac{1}{2}}\partial z^*}-ADVU+RU\right)\\ &+G^{\frac{1}{2}}G^{23}\left(-\frac{\partial p}{\partial y}-\frac{\partial G^{\frac{1}{2}}G^{23}P}{G^{\frac{1}{2}}\partial z^*}-ADVV+RV\right)-ADVW+BUOY'+RW\Big\}.\end{aligned} \tag{F1-2-5}$$

In order to maintain separability, the above equation is arranged as

$$\begin{aligned}\left(\frac{\partial}{\partial z^*}+\overline{\overline{\frac{gG^{\frac{1}{2}}}{C_s{}^2}}}\right)P=&G^{\frac{1}{2}}\{BUOY'-ADVW+RW-G^{\frac{1}{2}}G^{13}(ADVU-RU)-G^{\frac{1}{2}}G^{23}(ADVV-RV)\}\\ &\underline{+\left(\overline{\overline{\frac{gG^{\frac{1}{2}}}{C_s{}^2}}}\right)-\frac{gG^{\frac{1}{2}}}{C_s{}^2})P-G^{\frac{1}{2}}\{G^{\frac{1}{2}}G^{13}\left(\frac{\partial P}{\partial x}+\frac{\partial G^{\frac{1}{2}}G^{23}P}{G^{\frac{1}{2}}\partial z^*}\right)+G^{\frac{1}{2}}G^{23}\left(\frac{\partial P}{\partial y}+\frac{\partial G^{\frac{1}{2}}G^{23}P}{G^{\frac{1}{2}}\partial z^*}\right)\}},\end{aligned} \tag{F1-2-6}$$

where the underlined terms are the variable part in the iterative application of the direct method.

<u>P.G.</u> Lateral boundary conditions for pressure equations are set in the array PFORCE in sub.CFPBDV.

F-2. Lateral boundary conditions

F-2-1 Cyclic boundary condition

As described in B-7-1 of Ikawa and Saito (1991), the cyclic boundary conditions are available in x- and/or y- directions. For the x-direction cyclic boundary condition,

$$\phi_{1,,}=\phi_{nx-1,,},$$
$$\phi_{nx,,}=\phi_{2,,}, \tag{F2-1-1}$$

are imposed for all field variables ϕ. Similar conditions are applied to the y-direction for the y-direction cyclic condition.

As described in B-7-2 of Ikawa and Saito (1991), the free-slip wall lateral boundary condition is an option.

P.G. The cyclic condition is employed when MSWSYS(14)=1 or 2 ; the wall lateral boundary condition is used when MSWSYS(14)=-1 or -2. See sub.LTRLB2, LTRLBU, LTRLBV, LTRLUV and ADJ2D1.

F-2-2 Open boundary condition

a) Normal wind

Orlanski's (1976) radiation condition is used for wind normal to the lateral boundaries. According to the Sommerfeld radiation condition, the phase velocity of the inner gravity wave is evaluated by

$$C^{\tau}_{\phi_b}=-\frac{\phi_b{}^{\tau+1}-\phi_b{}^{\tau-1}}{2\Delta t}\Bigg/\frac{\dfrac{\phi_b{}^{\tau+1}+\phi_b{}^{\tau-1}}{2}-\phi^{\tau}_{in}}{\Delta x}$$
$$=-\frac{\phi_b{}^{\tau+1}-\phi_b{}^{\tau-1}}{\phi_b{}^{\tau+1}+\phi_b{}^{\tau-1}-2\phi_{in}{}^{\tau}}\frac{\Delta x}{\Delta t}. \tag{F2-2-1}$$

Here, the subscripts b and in indicate variables at the boundary and inner adjacent points. This phase velocity C is replaced by the smoothed phase velocity C^* that is averaged at three inner grid points at the former time step, and we choose the smaller value compared to $\Delta x/\Delta t$ as

$$\mathrm{C}_{\phi}{}^*=\min\left(\frac{1}{3}\sum_{i=1}^{3}\mathrm{C}^{\tau-1}_{\phi_{b-i}},\frac{\Delta x}{\Delta t}\right). \tag{F2-2-2}$$

The radiative value ϕ_{RAD} at the outflow boundary is then given as

$$\phi_{RAD}=\frac{1-\dfrac{\Delta t}{\Delta x}C_{\phi}{}^*}{1+\dfrac{\Delta t}{\Delta x}C_{\phi}{}^*}\phi^{\tau-1}_{in}+\frac{2\dfrac{\Delta t}{\Delta x}C_{\phi}{}^*}{1+\dfrac{\Delta t}{\Delta x}C_{\phi}{}^*}\phi^{t}_{in} \quad for\ C_{\phi}{}^*>0. \tag{F2-2-3}$$

At the inflow boundary, ϕ_{RAD} is assumed to be the same as the boundary value at the former time step:

$$\phi_{RAD}=\phi_b{}^{\tau-1} \qquad for\ C_{\phi}{}^*\leq 0. \tag{F2-2-4}$$

The value at the boundary is finally determined by the following weighted averaging procedure using ϕ_{EXT} and ϕ_{RAD} as

$$\phi^{\tau+1}_{BND}=\alpha\phi_{EXT}+(1-\alpha)\phi_{RAD}, \tag{F2-2-5}$$

where ϕ_{EXT} is the external reference value, and α is a weighting parameter.

Three values of α,

α_{in} ; *for* $U < 0$ *and* $C_\phi^* \leq 0$,

α_{out1} ; *for* $U \geq 0$ *and* $C_\phi^* \leq 0$,

α_{out2} ; *for* $C_\phi^* > 0$, (F2-2-6)

are employed depending on the directions of the normal wind and gravity waves. In the nesting case, these values should be determined according to the reliability of the prediction of the outer model. If maximum values such as $\alpha_{in} = \alpha_{out1} = \alpha_{out2} = 1$ are used, the lateral boundary values of the nested model are strictly determined by the outer model only, and the radiative condition becomes meaningless. If the smallest values, such as $\alpha_{in} = \alpha_{out1} = \alpha_{out2} = 0$, are used, the lateral boundary values are determined only by the radiation condition, which means that the inner model can no longer incorporate the time change of the environmental field from the outer model. In most nested runs, a value greater than 0.5 is used for α_{in}, while relatively smaller values are employed for α_{out1} and α_{out2}.

Using (F2-2-5), the time tendency of the normal wind component at the lateral boundary is *tentatively* given as

$$\left(\frac{\partial \phi}{\partial t}\right)_b^{\tau *} = \frac{\phi_{BND}^{\tau+1} - \phi_b^{\tau-1}}{2\Delta t}. \qquad \text{(F2-2-7)}$$

This tentative time tendency of the normal wind is modified so that it guarantees the conservation of the total mass in the model domain as discussed in F-2-3.

b) for other variables

For variables other than the wind component normal to the lateral boundaries, gradient extrapolation is usually used at the outflow boundary. The inflow and outflow are distinguished by the direction of the normal wind component :

$$\phi_{RAD} = 2\phi_{in}^{\tau} - \phi_{in-1}^{\tau-1} \quad for\ U \geq 0, \qquad \text{(F2-2-8)}$$

$$\phi_{RAD} = \phi_{out}^{\tau-1} \quad for\ U < 0. \qquad \text{(F2-2-9)}$$

Here, ϕ means the prognostic variables of the model such as the wind component parallel to the lateral boundaries, potential temperature, and water vapor mixing ratio. Since their locations are placed on a staggered grid (Fig. D1-1-2), subscripts *out* and *in* mean the external and internal values just adjacent to the lateral boundary. The external value just adjacent to the lateral boundary at the next time level is determined using a weighted averaging procedure similar to (F2-2-5) :

$$\phi_{out}^{\tau+1} = \beta\phi_{EXT} + (1-\beta)\,\phi_{RAD}, \qquad \text{(F2-2-10)}$$

Three values of β are available, depending on the directions of wind and gravity waves, similar to (F2-2-6), though usually β_{out2} is set equal to β_{out1}. The potential temperature is extrapolated using the deviation from the reference potential temperature as

$$\theta_{out}^{\tau+1} = \beta_{out}\theta_{EXT} + (1-\beta_{out})\,[\overline{\theta} + \{2(\overline{\theta} - \theta_{in}^{\tau}) - (\overline{\theta} - \theta_{in-1}^{\tau-1})\}], \qquad \text{(F2-2-11)}$$

to prevent artificial buoyancy, considering the steepness of the orography at the boundary.

<u>P.G.</u> Normal wind is extrapolated in sub.EXTNUH and sub.EXTNVH ; tangential wind is extrapolated in sub. EXTUY2 and sub.EXTVX2. Other variables are extrapolated in sub.EXTRX1, EXTRY1, EXTRX2 and

EXTRY2.

F-2-3 Mass flux adjustment for radiative nesting

The relation between the time tendency of the total mass within the entire model domain and the total mass flux through the lateral boundaries (E2-1-1) must be satisfied not only for the initial conditions but also for the entire simulation period. Although U_0' and V_0' in (E2-1-2) satisfy (E2-1-1) for each output time of the outer model, the normal wind components determined by the radiation condition (F2-2-5) are not necessarily consistent with (E2-1-1). A simple adjustment scheme for an anelastic model was given in Ikawa and Saito (1991). In a fully compressible nesting model, the time tendency of the normal wind should be modified so that the mass flux at each model boundary conforms to the mass flux of the outer model as closely as possible while satisfying (E2-1-1).

For the given adjusted interpolated horizontal wind (*e.g.*, $U_0'(,,,KT)$ and $U_0'(,,,KT+\Delta KT)$) of the outer model, the external wind at t and its tendency between KT and $KT+\Delta KT$ are given by

$$U_{EXT}(,,,t) = U_0'(,,,KT) + (t-KT)\frac{\partial}{\partial t}U_{EXT}, \tag{F2-3-1}$$

$$\frac{\partial}{\partial t}U_{EXT} = \frac{U_0'(,,,KT+\Delta KT) - U_0'(,,,KT)}{\Delta KT}. \tag{F2-3-2}$$

The time tendency of the mass-flux through each lateral plane that satisfies the total mass conservation is obtained as follows:

$$\frac{\partial MFX1}{\partial t} = \frac{\partial}{\partial t}(\iint U_{EXT}dydz^*)_{x=0}$$
$$= \frac{\iint U_0'(2,,,KT+\Delta KT)\,dydz^* - \iint U_0'(2,,,KT)\,dydz^*}{\Delta KT}, \tag{F2-3-1}$$

$$\frac{\partial MFX2}{\partial t} = \frac{\partial}{\partial t}(\iint U_{EXT}dydz^*)_{x=X}$$
$$= \frac{\iint U_0'(nx,,,KT+\Delta KT)\,dydz^* - \iint U_0'(nx,,,KT)\,dydz^*}{\Delta KT}, \tag{F2-3-2}$$

$$\frac{\partial MFY1}{\partial t} = \frac{\partial}{\partial t}(\iint V_{EXT}dxdz^*)_{y=0}$$
$$= \frac{\iint V_0'(,2,,KT+\Delta KT)\,dxdz^* - \iint V_0'(,2,,KT)\,dxdz^*}{\Delta KT}, \tag{F2-3-3}$$

$$\frac{\partial MFY2}{\partial t} = \frac{\partial}{\partial t}(\iint V_{EXT}dxdz^*)_{y=Y}$$
$$= \frac{\iint V_0'(,ny,,KT+\Delta KT)\,dxdz^* - \iint V_0'(,ny,,KT)\,dxdz^*}{\Delta KT}. \tag{F2-3-4}$$

Finally, the time tendencies of the normal wind component in each model plane given by (F2-2-7) are adjusted by

$$(\frac{\partial U}{\partial t})_0^\tau = (\frac{\partial U}{\partial t})_0^{\tau*} + \{\frac{\partial MFX1}{\partial t} - \int_s(\frac{\partial U}{\partial t})_0^{\tau*}dydz^*)\}/S_{yz}, \tag{F2-3-5}$$

$$(\frac{\partial U}{\partial t})_{X_L}^\tau = (\frac{\partial U}{\partial t})_{X_L}^{\tau*} + \{\frac{\partial MFX2}{\partial t} - \int_s(\frac{\partial U}{\partial t})_{X_L}^{\tau*}dydz^*)\}/S_{yz}, \tag{F2-3-6}$$

$$(\frac{\partial V}{\partial t})_0^\tau = (\frac{\partial U}{\partial t})_0^{\tau*} + \{\frac{\partial MFY1}{\partial t} - \int_s(\frac{\partial V}{\partial t})_0^{\tau*}dxdz^*)\}/S_{xz}, \tag{F2-3-7}$$

$$(\frac{\partial V}{\partial t})^{\tau}_{Y_L}=(\frac{\partial V}{\partial t})^{\tau}_{Y_L}{}^{*}+\{\frac{\partial MFY2}{\partial t}-\int_s(\frac{\partial V}{\partial t})^{\tau}_{Y_L}{}^{*}dxdz^{*})\}/S_{yz}, \qquad \text{(F2-3-8)}$$

where S_{yz} and S_{xz} are the areas of the lateral plane of the model at the east-west and north-south lateral boundaries, respectively. The above wind speed adjustment is only order of 10^{-4} m/s^2 in most cases, but is crucial for maintaining a reasonable average pressure field of the nested model. The above time tendencies of normal winds are used for the Neumann-type boundary conditions for pressure diagnostic equations (F1-1-1) and (F1-1-2). For an AE scheme, similar procedures are done assuming the left-hand side of (E2-1-1) as zero, and the time tendencies are used for the first terms of *r.h.s.* in (F1-2-1) and (F1-2-2).

P.G. The time tendency of the mass-flux through each model plane is computed in sub.CDMFDT2. The time tendency is adjusted in sub.UVPBD.

F-2-4 Boundary relaxation

Rayleigh damping, which enforces the external values of the prognostic variables, can be imposed near the lateral boundaries. In Ikawa and Saito's (1991) model, the external values were fixed to those of a one-dimensional reference atmosphere. In the new model, time-dependent three-dimensional values interpolated from the outer model are used for the boundary relaxation.

Rayleigh damping

$$D_R=-\frac{1}{\Delta t}\frac{D_{xy}}{m_g}\{\phi(x,y,z,t)-\phi_{EXT}(x,y,z,t)\}, \qquad \text{(F2-4-1)}$$

is added to the time tendency of ϕ, where m_R is the coefficient that determines the $1/e$-folding time. D_{xy} is a function given by

$$D(x,x_d,X_L)=\frac{x_d-x}{x_d} \quad for\ x<x_d,$$

$$D(x,x_d,X_L)=\frac{x-(X_L-x_d)}{x_d} \quad for\ x>X_L-x_d, \qquad \text{(F2-4-2)}$$

$$D_{xy}(x,y,x_d)=\max\{D(x,x_d,X_L),\ D(x,x_d,Y_L)\}. \qquad \text{(F2-4-3)}$$

Here x_d is the width of the sponge layer where the boundary relaxation is enforced. At $x=0$ and $x=X_L$, the $1/e$-folding time of (F2-4-1) becomes $m_R\Delta t$.

P.G. Parameters m_R and x_d are given by RLDMPX and IDIFX in the parameter card. D_{xy} is set in sub.SETDCF and used in sub.RLDAMP3.

F-3. Upper and lower boundary conditions

F-3-1 Velocity and potential temperature

From (D2-1-12), the kinematic condition

$$W^{*}=\frac{1}{G^{\frac{1}{2}}}\{W+m(\overline{G^{\frac{1}{2}}G^{13}\overline{U}^{z}}^{x}+\overline{G^{\frac{1}{2}}G^{23}\overline{V}^{z}}^{y})\}=0, \qquad \text{(F3-1-1)}$$

is imposed for W at $k=1+1/2$ and $k=nz-1/2$. For U and V, a free-slip condition is imposed for the upper boundary and lower boundary, if there is no friction. Under non-slip conditions, sub-grid scale momentum fluxes are given from the resistance law as in B-10-2 of Ikawa and Saito (1991).

F-3-2 Absorbing layer

Rayleigh damping, which enforces the external values to the prognostic variables, is imposed near the upper boundary. In Ikawa and Saito's model (1991), the external values were fixed to those of a one-dimensional reference atmosphere. In the new model, time-dependent three-dimensional values given by the outer model are available for nesting.

Rayleigh damping

$$D_{Rz} = -\frac{1}{\Delta t}\frac{D_z}{m_{Rz}}\{\phi(x,y,z,t) - \phi_{EXT}(x,y,z,t)\}, \qquad \text{(F3-2-1)}$$

is added to the time tendency of ϕ, where m_{Rz} is the coefficient that determines the e-folding time. D_z is a function given by

$$D_z(z,z_d,H) = \frac{1+\cos\left(\frac{H-z}{H-z_d}\pi\right)}{2} \quad for\ z > z_d. \qquad \text{(F3-2-2)}$$

Here, x_d is the width of the sponge layer where the boundary relaxation is enforced. At $z=H$, the e-folding time of (F3-2-1) becomes $m_{Rz}\Delta t$.

P.G. Parameters m_{Rz} and z_d are given by RLDMPZ and KZDST in the parameter card. D_z is set in sub.SETDCF and used in sub.RLDAMP3.

G. Physical processes and diffusion

G-1. Cloud microphysics

G-1-1 General features of cloud microphysics

The explicit cloud scheme of the model is basically the same as that in Ikawa *et al.* (1991) and Ikawa and Saito (1991), where the water substances are categorized into six species (water vapor, cloud water, rain, cloud ice, snow and graupel). The cloud microphysical processes are illustrated in Fig. G1-1-1. This scheme is based on the formulation of Lin *et al.* (1983) but has an option that predicts not only the mixing ratios of the six water species but also the number concentrations of three ice species (cloud ice, snow and graupel), referring to Murakami (1990). For the details, see B-11 of Ikawa and Saito (1991).

G-1-2 Box-Lagrangian raindrop scheme

When a prognostic explicit scheme is employed in numerical models with a horizontal grid size larger than 10 km, the rain terminal velocity V, not the air horizontal velocity, restricts the time step interval Δt. In those models, Δt must be chosen independent of horizontal grid spacing Δx to satisfy the Courant-Friedrich-Lewy (CFL) condition for rain falling ($V\Delta t/\Delta z<1$, where Δz is the vertical grid interval). Especially when many vertical layers are employed in the lower part of the domain to express the atmospheric boundary layer in detail, Δt has to be so reduced to calculate stable rain fall. Actually, for 10 to 20 km grid-resolution models in which

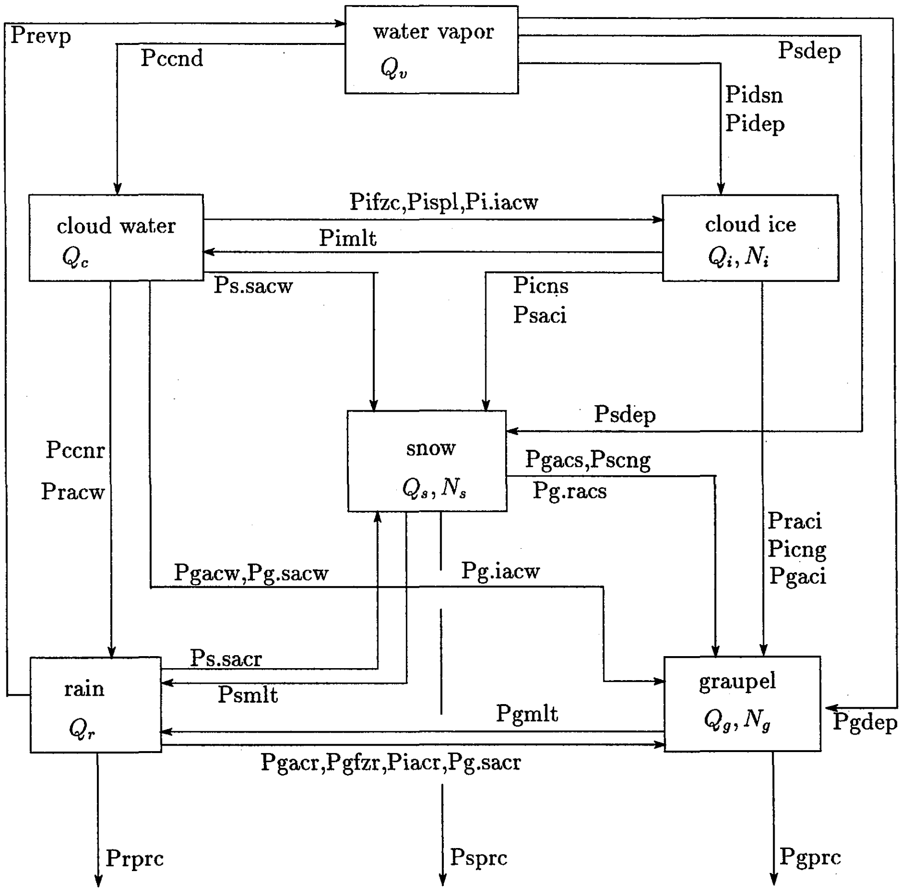

Fig. G1-1-1 Cloud microphysical processes in the model. Reproduced from Ikawa and Saito (1991). For explanation of the symbols, see B-11-1 in Ikawa and Saito (1991).

a prognostic explicit scheme is employed, $\Delta t=15$ to 30 sec has been used (*e.g.,* Yamasaki, 1977 ; Kato and Saito, 1995).

In numerical models with a grid size larger than 10 km, to use the time step interval calculated from the CFL condition for air advection (*i.e.,* $Va\ \Delta t/\Delta x<1$, where Va is the absolute value of air horizontal velocity), a new raindrop scheme named the Box-Lagradian raindrop scheme was developed (Kato, 1996). This new scheme is described in this section. First, a raindrop scheme is designed from the following equation when it is assumed anelastic.

$$\rho\frac{dq}{dt}=\rho\frac{\partial q}{\partial t}-\frac{\partial(\rho qV)}{\partial z}=0. \qquad \text{(G1-2-1)}$$

Here, ρ is the air density, q is the mixing ratio of rainwater and V is the rain terminal velocity defined as $V=Aq^n$, where A and n are positive constants. In numerical models, the amount at the next time step is generally calculated from $\rho\frac{\partial q}{\partial t}=\frac{\partial(\rho qV)}{\partial z}$ (the Eulerian method), but a method that searches for dropping points after a time step interval by using the left-hand side of (G1-2-1) (the Lagrangian method) is considered. The new raindrop scheme is based on the Lagrangian method, but it drops the bulk of rainwater in a vertical gird box, not the rainwater at a vertical grid point. Figure G1-2-1 outlines the new scheme. It is designed so that the bulk of rainwater $\rho q\Delta z$ in a vertical grid box, which is defined by two vertical layers, is preserved while keeping V

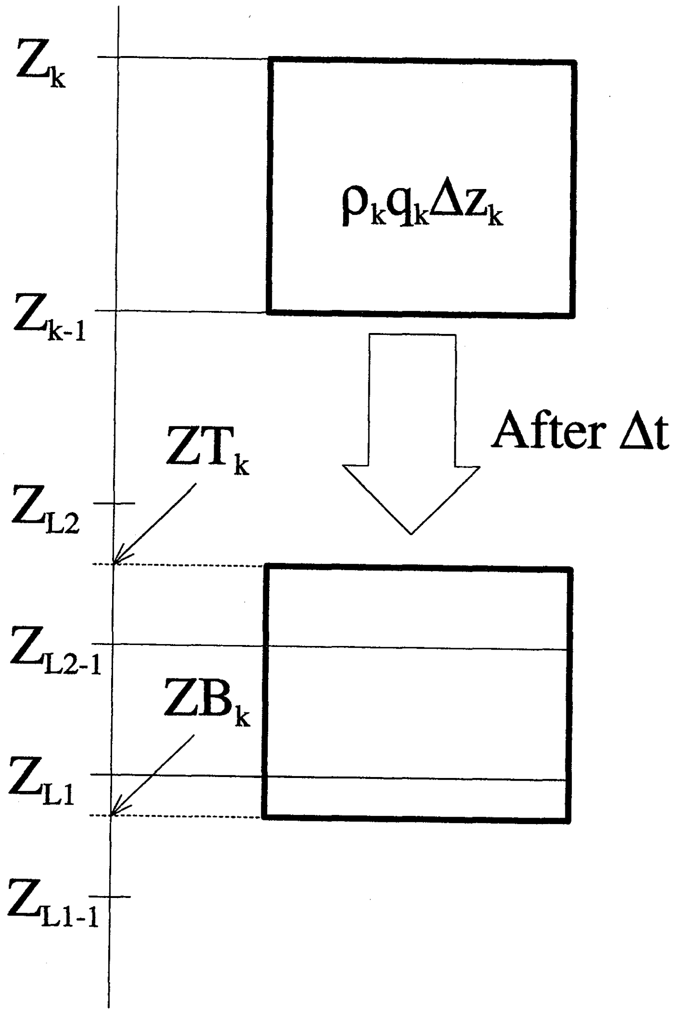

Fig. G1-2-1 Outline of box-Lagrangian raindrop scheme (from Kato, 1996).

constant during a time step interval Δt. The k-th vertical grid box is displaced downward during a time step interval, and the heights of the top ZT_k, and the bottom ZB_k of the k-th grid box after displaced are determined first.

The vertical layer where ZT_k or ZB_k exists is then searched:

$$\begin{aligned} & ZT_k^m = Z_k - V_k^m \Delta t \quad \in [Z_{L2-1}, Z_{L2}], \\ \text{and} \quad & \\ & ZB_k^m = Z_{k-1} - V_k^m \Delta t \quad \in [Z_{L1-1}, Z_{L1}], \end{aligned} \tag{G1-2-2}$$

where Z_k is the top height of the k-th vertical grid box, the superscript 'm' denotes the value at the time step 'm' and the brackets $[T,B]$ represent the interval in space between T and B.

Next, the dropped bulk of rainwater is partitioned into vertical grid boxes between ZT_k and ZB_k. When the displaced box interacts with the ground surface, the rainwater below it is removed from the model domain as precipitation. For $L1 \neq L2$,

$$P_{L1,k}^{m+1} = \rho_k q_k^m (Z_{L1} - ZB_k),$$

$$P_{L,k}^{m+1} = \rho_k q_k^m (Z_L - Z_{L-1}) \qquad \text{for } L1 < L < L2,$$

and (G1-2-3)

$$P_{L2,k}^{m+1} = \rho_k q_k^m (ZT_k - Z_{L2-1}),$$

for $L1 = L2$,

$$P_{L1,k}^{m+1} = \rho_k q_k^m \Delta z_k, \tag{G1-2-4}$$

where $P_{L,k}^{m+1}$ is the dropped rainwater in the L-th grid box at the next time step from the k-th grid box, and the subscript 'k' denotes the value at the k-the vertical grid point. Summing the dropped rainwater from all vertical grid boxes, the mixing ratio of rainwater at the next time step is calculated as

$$q_L^{m+1} = \frac{\sum_k P_{L,k}^{m+1}}{\rho_L (Z_L - Z_{L-1})}. \tag{G1-2-5}$$

When the CFL condition ($\Delta z > V\Delta t$) is satisfied, $L1 = k-1$ and $L2 = k$ are obtained from (G1-2-2). By substituting $L1 = k-1$ and $L2 = k$ into (G1-2-3) and (G1-2-5), the change of q per unit time, $\left(\frac{\partial q}{\partial t}\right)_k^m$, is obtained as

$$\left(\frac{\partial q}{\partial t}\right)_k^m = \frac{\dfrac{P_{k,k+1}^{m+1} + P_{k,k}^{m+1}}{\rho_k (Z_k - Z_{k-1})} - q_k^m}{\Delta t} = \frac{\rho_{k+1} q_{k+1}^m V_{k+1}^m - \rho_k q_k^m V_k^m}{\rho_k (Z_k - Z_{k-1})}. \tag{G1-2-6}$$

In contrast, from (G1-2-1), $\left(\frac{\partial q}{\partial t}\right)_k^m$ in the Eulerian raindrop scheme is given as

$$\left(\frac{\partial q}{\partial t}\right)_k^m = \frac{\partial (\rho q V)_k^m}{\rho_k \partial z_k} = \frac{(\rho q V)_{k+1}^m - (\rho q V)_k^m}{\rho_k \Delta z_k}. \tag{G1-2-7}$$

Thus, from (G1-2-6) and (G1-2-7), the box-Lagrangian and the Eulerian schemes coincide with each other when the CFL condition is satisfied.

G-1-3 Moist convective adjustment

The moist convective adjustment was originally proposed by Manabe *et al.* (1965). A scheme modified by Gadd and Keers (1970) is adopted in the MRI-NHM. The modified scheme has the following processes. If the temperature lapse rate exceeds the critical value Γ_c and the relative humidity RH exceeds its intermediate value

RH_i (0.5 is used in the model), temperature and specific humidity are adjusted so that the lapse rate becomes Γ_c while conserving relative humidity and total thermal energy. Γ_c is a function of relative humidity defined as

$$\Gamma_c=\frac{1}{1-RH_i}(\Gamma_d(1-RH)+\Gamma_s(RH-RH_i)) \quad for \quad RH_i<RH, \tag{G1-3-1}$$

where Γ_d and Γ_s are the dry adiabatic lapse rate and the saturated lapse rate. If only a moist convective adjustment scheme is employed in the model as a rain-generation process, the supersaturation Δs produced by the adjustment of specific humidity is forced to drop to the ground during the time step interval. In the MRI-NHM, however, Δs can be held on the grid scale since the moist convective adjustment scheme can be used in conjunction with the prognostic explicit scheme. Therefore, the following two cases are examined.

Case 1. The supersaturation Δs yielded by the moist convective adjustment is instantaneously removed from the model grids as precipitation.

Case 2. Δs is shared equally to the mixing ratio of cloud water q_c in adjusted grids as follows:

$$q_{c,k} \rightarrow q_{c,k}+\frac{\Delta s}{\sum_{n=k1}^{k2}\rho_n\Delta Z_n}, \quad \Delta s=\sum_{n=k1}^{k2}\rho_n\Delta q_n\Delta Z_n, \quad for \quad k1\leq k\leq k2, \tag{G1-3-2}$$

where Δq_k is the adjusted amount at the k-th vertical layer and $k1$ and $k2$ indicate the bottom and top of adjusted layers, respectively.

When a moist convective adjustment scheme is used in conjunction with an explicit precipitation scheme, the temperature change ΔT adjusted by the former scheme must be modified dependently on the model grid-resolution Δx and the convective time scale so that the conjunction scheme is reduced to an explicit scheme for small Δx and Δt:

$$\Delta T \rightarrow \frac{\Delta x-1km}{19km}\times\frac{\Delta t}{20 \text{ min}}\times\Delta T \quad for \quad 1km<\Delta x<20km,$$

and

$$\Delta T \rightarrow \frac{\Delta t}{20 \text{ min}}\times\Delta T \quad for \quad \Delta x\geq 20km, \tag{G1-3-3}$$

where Δt is the time step interval.

G-1-4 Cloud amount prediction scheme

Cloud water advected by saturated air flow never evaporates if the temperature of the air is not increased. In the computational domain where a grid method is used, cloud water that moves into a grid box where the air is not saturated is instantly evaporated. This often occurs in grid boxes neighboring a cloud. In order to suppress this erroneous evaporation, cloud amounts are employed as follows.

For convenience, the one-dimensional case is described here. The cloud amount C_m is advected by using a modified upstream scheme as

$$C_{m,j}^{m+1}=Min\left(1.0,\ C_{m,j}^{m-1}-2\Delta t\frac{N_{i+\frac{1}{2}}^{m}u_{i+\frac{1}{2}}^{m}-N_{i-\frac{1}{2}}^{m}u_{i-\frac{1}{2}}^{m}}{\Delta x}\right), \tag{G1-4-1}$$

where the superscript "m" denotes the m-th time step, Δx is the grid interval, and Δt is the time step interval.

The value of N is determined by the following conditions as

$$N^{m}_{i-\frac{1}{2}}=0 \quad for \quad C^{m-1}_{m,j-1}\neq 1, \quad C^{m-1}_{m,j}=0, \quad u^{m}_{i-\frac{1}{2}}>0,$$

$$N^{m}_{i+\frac{1}{2}}=0 \quad for \quad C^{m-1}_{m,j+1}\neq 1, \quad C^{m-1}_{m,j}=0, \quad u^{m}_{i-\frac{1}{2}}<0,$$

and (G1-4-2)

$$N^{m}_{i\pm\frac{1}{2}}=1 \quad for \ other \ cases.$$

When the air in a grid box is determined as saturated after calculating condensation and evaporation between water vapor q_v and cloud water q_c using an "instantaneous adjustment procedure," C_m is set to 1.0 independently of the advection result. When C_m becomes negative after calculation by (G1-4-1), C_m and q_c are adjusted as follows. C_m is set to 0.0, and q_c is moved into the neighboring grid box on the windward side when the air in the box is saturated; otherwise, C_m is set to 1.0 in order to accelerate the evaporation of cloud water. For two- or three-dimension simulation, when there are several neighboring grid boxes into which q_c can be moved, q_c is equally divided among these grid boxes.

The evaporation of cloud water during the "instantaneous adjustment procedure" is restricted by C_m. The values of cloud water $q_c{}^*$ and cloud amount $C_m{}^*$ after this evaporation are calculated as

$$q^*_c=Max\,(q_c-(q_{vs}-q_v)\,C_m,\ q_c(1.0-C_m)), \qquad \text{(G1-4-3)}$$

$$C^*_m=C_m\frac{q^*_c}{q_c}, \qquad \text{(G1-4-4)}$$

where q_{vs} is the saturated mixing ratio of water vapor. For $C_m=1.0$, (G1-4-3) gives the original values. The first term on the right-hand side of (G1-4-3) means that the evaporation of cloud water is restricted to only the region where cloud water exists in a grid box. The second term determines the maximum evaporation of cloud water. Furthermore, cloud water is restricted to evaporate only in downdrafts. Under these restrictions, the finite difference form for the advection of cloud water is modified as

$$q^{m+1}_{c,i}=q^{m-1}_{c,i}-2\Delta t\frac{N^{m}_{i+\frac{1}{2}}u^{m}_{i+\frac{1}{2}}q^{m}_{c,j+\frac{1}{2}}-N^{m}_{i-\frac{1}{2}}u^{m}_{i-\frac{1}{2}}q^{m}_{c,j-\frac{1}{2}}}{\Delta x}. \qquad \text{(G1-4-5)}$$

G-2. Surface Boundary layer

G-2-1 Surface fluxes

A surface boundary layer is assumed at the lower boundary, where the resistance law gives surface heat and momentum fluxes. Over the sea, exchange coefficients are determined from the formula by Kondo (1975); over land, they are based on Monin and Obukhov's similarity law with Sommeria's (1976) formula, depending on the ground roughness and ground (sea-surface) temperature. The above formulations are the same as in B-10-2 of Ikawa and Saito (1991), while the ground temperatures of four soil layers are predicted as described in next subsection.

P.G. The surface fluxes are computed in sub.CRSTUV. The drag coefficients are calculated in sub.KONDOH and sub.GRDFXH on the sea and land, respectively.

G-2-2 Ground temperature

According to Segami *et al.* (1989), we use the four-layer model shown in Fig. G.2.1 to predict ground temperature. The predictive equation of underground temperature T is given as

$$\rho_c \frac{\partial T}{\partial t} = -\frac{\partial G}{\partial z}, \tag{G2-2-1}$$

$$G = -\lambda \frac{\partial T}{\partial z}, \tag{G2-2-2}$$

where λ is the thermal conductivity and ρ_c, the heat capacity. Finite discretization forms of (G2-2-1) and (G2-2-2) are expressed as follows.

$$G_k = 2\lambda \frac{T_{k-1} - T_k}{\Delta z_{k-1} + \Delta z_k}, \tag{G2-2-3}$$

$$\frac{\partial T_k}{\partial t} = -\frac{G_k - G_{k-1}}{\rho_c \Delta z_k}, \tag{G2-2-4}$$

where Δz_k is the depth of the k-th layer. T_4 is assumed constant during the forecast. The heat balance at the ground surface G_1 is given as

$$G_1 = -\varepsilon\sigma T_1{}^4 - H - LE + (1-\alpha) R_s + R_L, \tag{G2-2-5}$$

where ε (=0.95) is the emissivity of the ground surface, σ the Stefan-Boltzman constant, H the latent heat, LE the sensitive heat, α the albedo of the ground surface, R_s the solar radiation reaching the ground, and R_L the downward long wave radiation at the ground surface. H and LE are calculated from Eqs. 8-7 and 8-8 in Ikawa and Saito (1991), respectively. R_s and R_L are obtained by using an atmospheric radiation scheme described in section G-5. When the atmospheric radiation is not calculated in the model, R_s and R_L are expressed as the following formula proposed by Kondo (1976):

$$R_s = S(1-0.7C_L)(1-0.6C_M)(1-0.3C_H), \tag{G2-2-6}$$

$$S = S_\infty \cos\zeta \{0.57 - 0.016e - 0.06\log_{10}e + (0.43+0.016e) \times 10^{-0.13\sec\zeta}\}, \tag{G2-2-7}$$

$$\cos\zeta = \sin\theta \sin\theta_s + \cos\theta \cos\theta_s \cos\phi_t, \tag{G2-2-8}$$

$$R_L = \varepsilon\sigma T_a^4 [1 + (-0.49+0.066e)\{1-(0.75-0.0005e)(C_L + 0.85C_M + 0.5C_H)\}], \tag{G2-2-9}$$

where S_∞ is the solar constant, θ the latitude, θ_s the declination, ϕ_t the hour angle, e the water vapor pressure near the ground surface, and T_a the temperature near the ground surface. C_L, C_M and C_H indicate the amount of low, middle and high clouds. They are calculated with the relative humidity averaged between the ground surface and 1.5 km height (low cloud), 1.5 and 5.0 km height (middle cloud), and 5.0 and 10.0 km height (high cloud) by using the empirical formula proposed by Ohno and Isa (1984).

The surface temperature at the time step "$m+1$" T_1^{m+1} can be calculated from (G2-2-3) and (G2-2-4), after G_1^m and G_1^{m+1} are obtained from (G2-2-5) for a given T_4. Here G_1^{m+1} is calculated by using the trapezoid implicit method shown below.

$$G_1^{m+1} = G_1^m + \left(\Delta t \frac{\partial G_1}{\partial t}\right)^{m+\frac{1}{2}} = G_1^m + \left(\Delta t \frac{\partial G_1}{\partial T_1}\frac{\partial T_1}{\partial t}\right)^{m+\frac{1}{2}} \approx G_1^m + \left(\frac{\partial G_1}{\partial T_1}\right)^m (T_1^{m+1} - T_1^m). \tag{G2-2-10}$$

The orographic steepness increases or decreases the solar radiation reaching the ground. To introduce this effect into the model, the zenith angle ζ is modified in a north-south direction based on the alteration of latitude (Fig. G2-2-2a) as

$$\theta \to \theta + \tan^{-1}\frac{\partial z}{\partial y} \tag{G2-2-11}$$

and in an east-west direction based on the alteration of hour angle (Fig. G2-2-2b) as

$$\phi_t \to \phi_t + \tan^{-1}\frac{\partial z}{\partial x}, \tag{G2-2-12}$$

Here, ζ is not modified for $\cos\zeta < 0$ (*i.e.*, the grids on which the Earth throws a shadow).

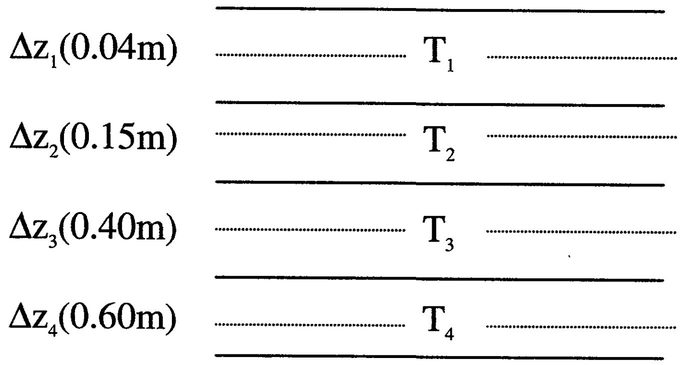

Fig. G2-2-1 Layers underground. T_k and Δz_k are the underground temperature and the depth of the k-th layer.

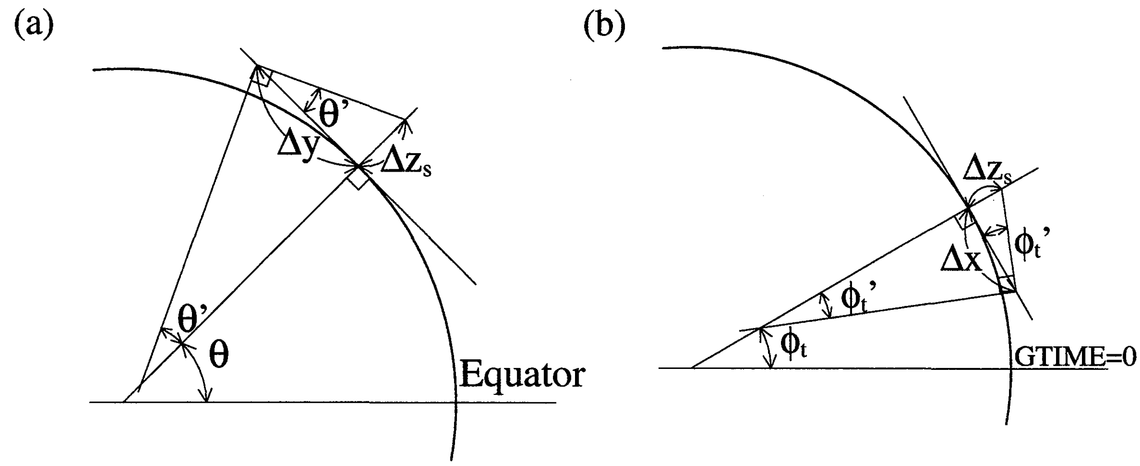

Fig. G2-2-2 Alteration of (a) latitude and (b) hour angle for the modification of the zenith angle.

G-3. Turbulent closure model

The turbulent closure model that predicts the turbulent kinetic energy is employed to determine the diffusion coefficients. The formulation is based on Klemp and Wilhelmson (1978) and Deardorff (1980), but slightly modified. For details, see B-10-1 of Ikawa and Saito (1991). In the model, the linear stability condition

$$K < K_{\max}(z) = 0.1 \left(\cong \frac{1}{\pi^2}\right) \frac{(\Delta z)^2}{\Delta t}, \tag{G3-1}$$

is imposed for the eddy diffusion coefficients K_m, K_e and K_h in order to maintain a stable run.

P.G. The surface fluxes are computed in sub.CRSTUV. The turbulent energy is computed in sub.CETUR5. K_{max} is set in sub.SETEMX.

G-4. Computational diffusion

A nonlinear damper, a fourth-order linear damper, and Asselin's time filter are employed to suppress the computational noise, adding to the Rayleigh damping (F2-4-1) and (F3-2-1).

a. Non- linear damper

Nonlinear damping (Nakamura, 1978)

$$D_{NL}=\frac{1}{m_{NL}\Delta t}\{(\Delta x)^3\frac{\partial}{\partial x}(\left|\frac{\partial\phi}{\partial x}\right|\frac{\partial\phi}{\partial x})+(\Delta y)^3\frac{\partial}{\partial y}(\left|\frac{\partial\phi}{\partial y}\right|\frac{\partial\phi}{\partial y})\}, \tag{G4-1}$$

is added to the diffusion term of ϕ, where m_{NL} is the coefficient that determines the $1/e$-folding time. For two-grid noises of amplitude a, (G4-1) gives the equivalent $1/e$-folding time $m_{NL}\Delta t/8a$. In above expression, the uniform horizontal grid distances are assumed.

b. Fourth-order linear damper

Fourth-order linear damping

$$D_{2D}=-\frac{1}{m_{2D}\Delta t}\{(\Delta x)^4\frac{\partial^4\phi}{\partial x^4}+(\Delta y)^4\frac{\partial^4\phi}{\partial y^4}\}, \tag{G4-2}$$

where m_{2D} is the coefficient which determines the e-folding time, is added to the diffusion term of ϕ to suppress primarily two-grid noises. For two-grid noises whose amplitude is a, (G4-2) gives the equivalent $1/e$-folding time $m_{2D}\Delta t/16$. In the above expression, the uniform grid distances are assumed horizontally. C urrently, this diffusion is not employed at the lateral boundaries and their inner next grid points in order to assure symmetry.

c. A sselin's time filter

After the time integration, all quantities of prognostic variables at the time step '*it*' are modified according to the Asselin's time filter (Robert, 1966),

$$\phi(,,,it)\rightarrow\phi(,,,it)+0.5\nu(\phi(,,,it+1)-2\phi(,,,it)+\phi(,,,it)+\phi(,,,it-1)\}, \tag{G4-3}$$

where ν is the coefficient set by the input parameter card (usually 0.2). Near the upper boundary ($kz>0.7*\mathrm{NZ}$), ν is increased linearly up to three times of the original value.

P.G. Linear and nonlinear dampers are computed in sub.DAMPCN. The time filter is employed in sub. TSMOTH, using the quantities at the time step "*it*-1" that is set by sub.OSAVEH.

G-5. Atmospheric Radiation

G-5-1 Atmospheric radiation calculated using relative humidity.

The basic framework of the radiation scheme was described by Sugi *et al.* (1990), and the introduced scheme in MRI-NHM was developed with reference to the software package in JSM. Full computation of long wave radiation is made with an interval that can be determined by a control parameter card (see subsection K-4-3). The following description is referred to subsection 3.2.3 in NPD/JMA (1997). Only long-wave flux radiated from the ground surface is considered in every time step. The temperature tendency relates to radiative fluxes

$$\left(\frac{\partial T}{\partial t}\right)_{rad}=-\frac{RT}{C_p p}\frac{\partial F}{\partial z}, \tag{G5-1-1}$$

where F is the net upward flux.

(a) Long-wave flux

The long-wave flux F can be written as

$$F = C(z,z_s)\,\tau(s,T_s)\{\pi B(T_g) - \pi B(T_s)\} + C(z,z_t)\,\tau(s_t - s,\ T_t)\,\pi B(T_t)$$

$$+\int_{T_t}^{T_s} C(z,z')\,\tau^*(|s-s'|,\ T')\frac{d\pi B(T')}{dT'}dT', \tag{G5-1-2}$$

where $C(z,\ z')$ is the ratio of the clear line of sight between levels of z and z', T_g the soil temperature at the ground surface, T_s the air temperature at the ground surface, and T_t the air temperature at the top. This ratio is unity when there are no clouds. The scheme assumes that clouds are fully opaque and overlap randomly in the vertical direction. The transmission function τ and $B(T)$ are given by

$$\tau(s,T) = \frac{1}{B(T)}\int_0^\infty \tau_v(s)\,B_v(T)\,dv \tag{G5-1-3}$$

$$\tau^*(s,T) = \frac{1}{\frac{dB(T)}{dT}}\int_0^\infty \tau_v(s)\frac{\partial B_v(T)}{\partial T}dv \tag{G5-1-4}$$

and

$$\pi B(T) = \pi\int_0^\infty B_v(T)\,dv = \sigma T^4. \tag{G5-1-5}$$

where $B_v(T)$ is the Planck function. In the model, $\tau(s,\ T)$ and $\tau^*(s,\ T)$ are selected from tables prepared in advance. To make the tables, τ_v is evaluated for each absorber assuming Goody's random model (1952). Parameters used in the random model are found in Roger and Walshaw (1966) for water vapor, Goldman and Kyle (1968) for ozone, and Houghton (1977) for carbon dioxide. The pressure broadening of each absorber (i) is considered using the scaling

$$s_i = 1.66\int_0^z \left(\frac{p}{1000hPa}\right)^n \rho_i dz, \tag{G5-1-6}$$

where the constant n is 1.0 for water vapor, 0.9 for carbon dioxide, and 0.4 for ozone. The diffusive factor of 1.66 comes from the average over all directions. is The continuum band by dimer $(H_2O)_2$ is an exception to (G5-1-6). Since the dimer is composed of two molecules, the optical density is quadratic to water vapor density (Roberts *et al.*, 1976). The transmission function is calculated in each band shown in Fig. G5-1-1 and combined

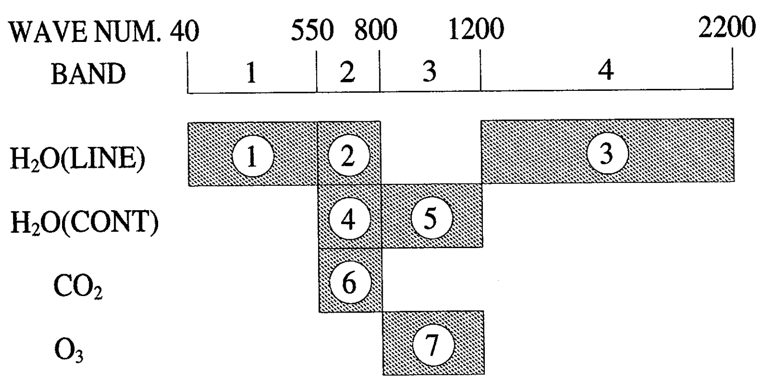

Fig. G5-1-1 Division of the wave number region for computing the transmission function. H_2O(LINE) denotes absorption due to water vapor absorption lines. H_2O(CONT) denotes the continuum band of water vapor (dimer).

to yield the total transmissivity including overlapping effects of different absorbers. In the present scheme, the absorption of dimers with wave numbers between 800 and 1200 is neglected. However, since this absorption is not small, the scheme should be modified in the near future.

(b) Short waves

The radiative processes of solar short waves are separately parameterized for wavelengths less than 0.9 μm (almost visible) and wavelengths greater than 0.9 μm (near infrared).

As to visible radiation, the scheme considers the absorption by ozone, Rayleigh scattering by air, and Mie scattering by cloud droplets. The absorber ozone exists mainly in the stratosphere. In the troposphere, complicated scattering takes place, but the heating rate due to visible radiation is quite small. Thus, the important matter for the visible radiation scheme is to evaluate precisely the reflectivity of the whole troposphere, which affects the upward stratospheric flux.

Absorbers of the near infrared band considered in the model are water vapor and cloud droplets. Lacis and Hansen (1974) expanded the transmission due to water vapor for a sum of the several bands with respect to absorption coefficients

$$\tau=\sum a_i \exp(-\lambda_i S). \qquad \text{(G5-1-7)}$$

The cloud droplets contribute both to absorption and scattering. The single scattering albedo ω_0 is assumed to be constant.

$$\omega_0=\frac{\delta_c}{(\delta_{wv}+\delta_c+\delta_l)}, \qquad \text{(G5-1-8)}$$

where the spectral dependence is neglected. Here, δ is the optical thickness, wv the absorption by water vapor, c the scattering by clouds, and l the absorption by clouds. The total thickness for near infrared radiation is

$$\delta=\delta_{wv}+\delta_c+\delta_l. \qquad \text{(G5-1-9)}$$

Both absorption and scattering are significant in the tropospheric radiative processes in the near-infrared band. These processes are calculated with the two-stream method (δ-Eddington approximation), assuming a horizontally uniform distribution of cloud droplets within each grid.

(c) Cloud fraction

The cloud fraction is one of the key factors of long- and short-wave radiative processes. The model parameterizes the cloud fraction using a quadratic function of relative humidity

$$Cloud\ fraction \propto \begin{cases} (RH-RHCC)^2 & RH>RHCC \\ 0 & RH \leq RHCC \end{cases}, \qquad \text{(G5-1-10)}$$

where the critical relative humidity $RHCC$ is empirically determined through comparison with satellite observations for the Far East region (Saito and Baba, 1988). The $RHCC$ should be re-determined for other regions. The proportional constant of (G5-1-10) is tuned for the model to reproduce realistic outgoing long-wave radiation and planetary albedo.

G-5-2 Atmospheric radiation for cloud resolving model

This radiation scheme was originally proposed by Yamamoto and Satomura (1994). The basic framework of this scheme is almost the same as that of subsection G-5-1. MRI-NHM calculates cloud properties directly, so parameterization of the radiative properties of clouds can be introduced. In this scheme, the liquid water path (LWP) and ice water path (IWP) are used as the basic parameters for computing the radiative properties of clouds.

(a) Shortwave parameterization

In this parameterization of the solar radiative properties of clouds, optical thickness τ is expressed in terms of LWP or IWP. Formulations by Stephens (1978) are used for water clouds. In this scheme, τ and LWP are related as follows:

(i) Wavelength $<0.9\ \mu$m (almost visible)

$$\log_{10} \tau = 0.2633 + 1.7095 \ln(\log_{10} LWP). \qquad \text{(G5-2-1)}$$

(ii) Wavelength $>0.9\ \mu$m (near infrared).

$$\log_{10} \tau = 0.3492 + 1.6518 \ln(\log_{10} LWP). \qquad \text{(G5-2-2)}$$

From Liou (1992), the parameterization of optical thickness involving ice clouds is written in the form

$$\tau = IWP(-6.6560 \times 10^{-3} + 3.6860 \times 10^{0}/D_e), \qquad \text{(G5-2-3)}$$

where D_e is the mean effective radius; that value is fixed to 100 μm in this model.

(b) Longwave parameterization

In this scheme, cloud emittance is calculated from LWP or IWP, and it substitutes for cloud coverage in the scheme of subsection G-5-1. Neglecting the scattering contribution and applying the gray approximation, the broadband emittance ε of clouds may be expressed by

$$\varepsilon \cong 1 - \exp(-k^c W/\bar{\mu}) \qquad \text{(G5-2-4)}$$

where k^c is the wave-number-averaged mass absorption coefficient, and W denotes either LWP or IWP. $1/\bar{\mu}$ is referred to as the diffusivity factor, and a value of 1.66 is used.

In this model, k^c values of 0.158 for the downward emittance of water clouds and 0.130 for the upward one, computed by Stephens (1978), are used. For ice clouds, a k^c value of 0.06 (Liou, 1992) is adopted.

H. Examples of numerical simulations

This chapter presents examples of numerical simulation. All simulations are conducted using the fully compressible version of the nonhydrostatic model with the HI-VI scheme (e.g., "MRI-NHM").

H-1. Basic verification against 3-D linear mountain waves[1]

Ikawa and Saito (1991) verified the model-simulated mountain flow over a three-dimensional mountain. However, at that time, the anelastic-scheme with the Boussinesq approximation was used for the model. In this chapter, we show the basic verification once again to demonstrate the model's progress after publication of Ikawa and Saito (1991). The design of verification is almost the same as in Ikawa and Saito (1991), but the fully compressible version is employed and the amplification effect of the mountain waves due to decrease of the density of the reference atmosphere is considered both in the numerical simulation and the analytic solution.

H-1-1 Linear analytic solution of 3-D mountain waves

For steady state, stratified Boussinesq fluid, the vertical displacement of streamlines $\delta(x, y, z)$ of linear mountain waves is given as

$$\frac{\partial^2}{\partial x^2}\left(\frac{\partial^2}{\partial x^2}+\frac{\partial^2}{\partial y^2}+\frac{\partial^2}{\partial z^2}\right)\delta+\frac{N^2}{U^2}\left(\frac{\partial^2}{\partial x^2}+\frac{\partial^2}{\partial y^2}\right)\delta=0, \qquad \text{(H1-1-1)}$$

where U is the environmental wind speed and N, the Brunt-Vaisala frequency:

$$N^2=\frac{g}{\bar{\theta}}\frac{d\bar{\theta}}{dz}. \qquad \text{(H1-1-2)}$$

Here, θ is the potential temperature of the environmental atmosphere.

With constant N and U, the solution of (H1-1-1) is obtained by using double-Fourier transform analysis (Smith, 1980):

$$\delta(x,y,z)=\iint_{-\infty}^{\infty}H(k,l)\,e^{imz}e^{i(kx+ly)}dkdl, \qquad \text{(H1-1-3)}$$

where $H(k,l)$ is the double-Fourier transform of the orography height $h(x,y)$ defined as

$$H(k,l)=\frac{1}{4\pi^2}\iint_{-\infty}^{\infty}h(x,y)\,e^{-i(kx+ly)}dxdy. \qquad \text{(H1-1-4)}$$

Here, m in (H1-1-3) is calculated by the horizontal wave number vector (k,l) as

$$m^2=\frac{k^2+l^2}{k^2}\left(\frac{N^2}{U^2}-k^2\right). \qquad \text{(H1-1-5)}$$

For the upper radiation condition, the positive imaginary root of (H1-1-5) is chosen for $k^2>N^2/U^2$, while the sign of m is chosen to be the same as that of k for $k^2<N^2/U^2$. Once δ is obtained, the vertical wind component w is given by the following linear relation for steady flow:

$$w=U\frac{\partial\delta}{\partial x}. \qquad \text{(H1-1-6)}$$

In this study, in order to express the amplification effect of the mountain waves due to the decrease of density of the reference atmosphere ρ, we multiply the amplitude of the w-field by the following amplification

[1]Part of this section was extracted from the results reported in Saito *et al.* (1998).

factor :

$$\left(\frac{\bar{\rho}}{\bar{\rho}_0}\right)^{-\frac{1}{2}}=[e^{-Sz}\{1-\frac{g}{c_p\theta_0 S}(1-e^{-Sz})\}^{\frac{c_v}{R}}]^{-\frac{1}{2}}. \qquad \text{(H1-1-7)}$$

Here, S is the static stability $(=N^2/g)$, g the gravity acceleration, c_p the specific heat of air at constant pressure, R the gas-constant, and subscripts 0 express the values at the ground surface. (H1-1-7) can be obtained by the following relation for a non-Boussinesq atmosphere with constant stability :

$$\bar{\theta}=\theta_0 e^{Sz}. \qquad \text{(H1-1-8)}$$

In computing the analytic solution, an isolated 3-D mountain with circular contours

$$Z_s(x,y)=\frac{h_m}{\{1+(\frac{x}{a})^2+(\frac{y}{a})^2\}^{\frac{3}{2}}}, \qquad \text{(H1-1-9)}$$

is employed according to Smith (1980) and Saito *et al.* (1998). The mountaintop height is set to $h_m=100$ m, and its shape is discretized on a grid mesh with $\Delta x=\Delta y=a/3$. The mesh size $(Nx, Ny)=(128, 128)$ is used for the hydrostatic case, while the domain size for the x-direction is enlarged to $(Nx, Ny)=(256, 128)$ for nonhydrostatic case because, in a nonhydrostatic case, the mountain wave extends leeward and the analytic solution is contaminated due to the periodic nature of the Fourier transform if the domain size is not sufficient. For the environmental atmospheric state, $U=8$ ms^{-1} and $N=0.01$ s^{-1} are chosen as in Saito *et al.* (1998).

H-1-2 Comparison between numerical and analytic solutions

Numerical solutions by the two models are computed with the following conditions :

1) Horizontal grid interval $\Delta x=\Delta y=a/3$, and model domain $(Nx, Ny)=(62, 42)$.
2) 32 vertical levels with stretched grid interval $\Delta z=40$ m to 1200 m.
3) Rayleigh damping layers are imposed on the upper five levels.
4) Constant temperature/potential temperature lapse rate $d\theta/dz=3.0$ K/km is given. This lapse rate corresponds to the atmospheric stability $N=0.01$ s^{-1}.

a. Almost hydrostatic case

First, we show the result for the case of $\Delta x=2$ km. In this case, the horizontal scale of the mountain is $a=$ 6 km, and the product of the Scorer number N/U and a is 7.5, which means the horizontal scale of the mountain is much larger than the horizontal wave length of the buoyancy oscillation, and the nonhydrostatic effect is small. Figure H1-2-1 shows the vertical wind w obtained by the nonhydrostatic analytic solution (a and b), and the numerical model (c and d). In these figures, each scale on the horizontal axis represents the horizontal grid, and the mountaintop is located at $x=y=21.5$. The scale of the vertical axes of Figs. a and c is 400 m. As shown in these figures, the model simulates the characteristics of the analytic solution of the mountain wave well. The amplitude of simulated mountain waves is smaller than that of the analytic solution in upper layers. This underestimation of mountain waves near the upper boundaries is primarily attributed to the Rayleigh damping layer imposed near the model top (above $z=12$ km). Compared with Fig. C-1-3c of Ikawa and Saito (1991), the model solution is modified significantly in terms of the amplitude in the upper layers.

Another reason for the underestimation in the model solution may be the finite difference approximation.

Figure H1-2-2 shows the model solution when the horizontal advection terms are computed using the optional fourth-order accuracy scheme instead of the original second-order scheme. The simulated mountain wave is stronger in upper layers compared with Figs. H1-2-1c and d, and approaches the analytic solution more closely.

b. Nonhydrostatic case

Next, we show the results for $\Delta x = 0.4$ km. In this case, the horizontal scale a is 1.2 km. The product of the Scorer number and a is 1.5, which means that the nonhydrostatic effect is significant. Figure H1-2-3 shows vertical wind w obtained by the nonhydrostatic analytic solution, and the numerical model. Again, the numerical model simulates the characteristics of the analytic solution of the nonhydrostatic mountain wave very well. The radiation condition of the model works successfully, and the mountain wave propagates leeward through the right-side lateral boundary. Compared with Fig. C-1-3f of Ikawa and Saito (1991), the progress of the nonhydrostatic model is obvious.

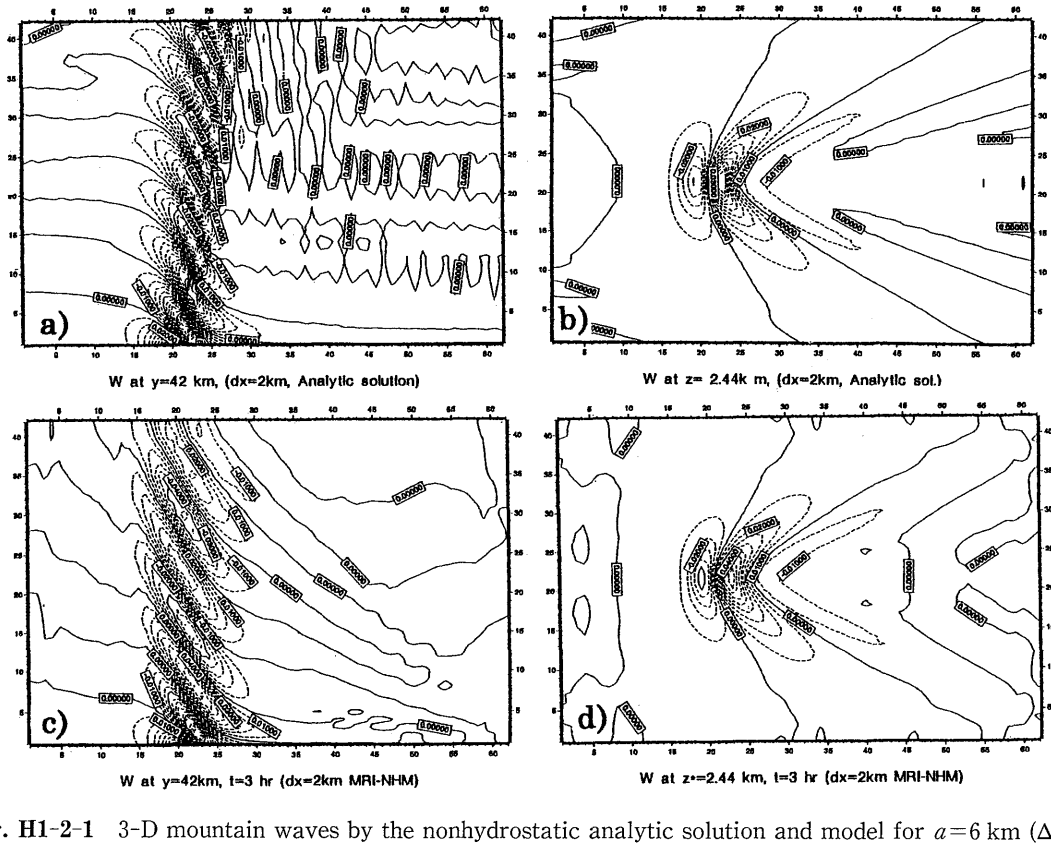

Fig. H1-2-1 3-D mountain waves by the nonhydrostatic analytic solution and model for $a=6$ km ($\Delta x=2$ km). a) Vertical cross-section of w through the mountaintop by the analytic solution. The contour interval is 1 cm s^{-1}. The graduations on the vertical and horizontal axes correspond to 400 m and 2 km, respectively. b) Horizontal cross-section of w at $z=2.44$ km by the analytic solution. The graduations on the x- and y- axes correspond to 2 km. c) Same as in a), but by the numerical model at $t=3$ h. d) Same as in b), but by the model at $t=3$ h.

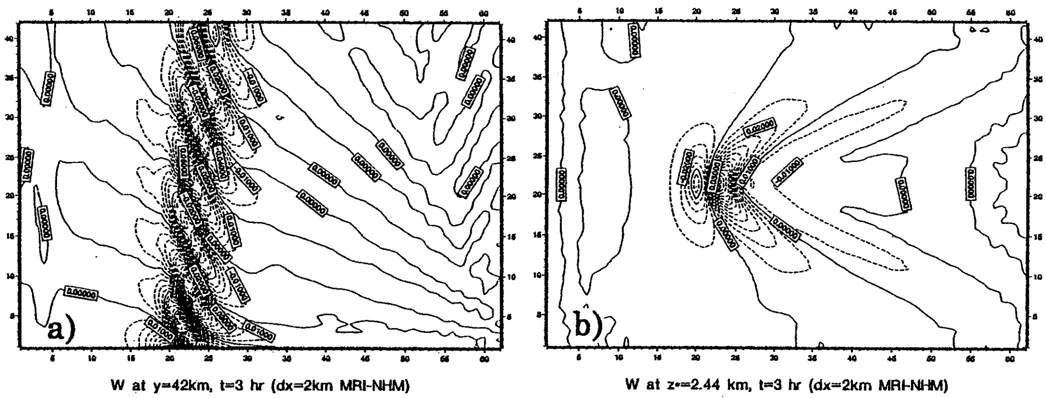

Fig. H1-2-2 Same as in Figs. H1-2-1 b) and d) but the fourth-order advection scheme is used.

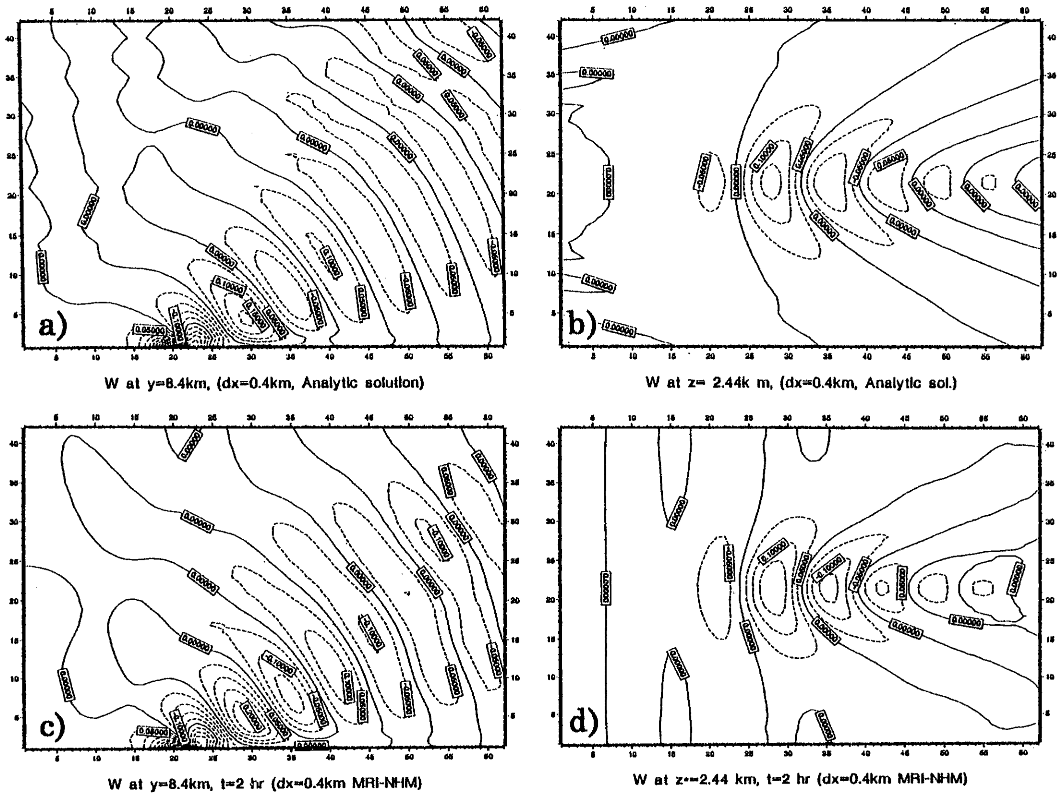

Fig. H1-2-3 Same as in Fig. H1-2-1 but for $a=1.2$ km ($\Delta x=0.4$ km). The contour interval is 5 cm s^{-1}. The scales on the x- and y- axes correspond to 0.4 km. Numerical model solutions are for the results at $t=2$ h.

H-2. Forecast experiment of the 1993 Kagoshima torrential rain[1]

H-2-1 Observation

Next we demonstrate the performance of the nonhydrostatic model as a regional forecast model. The event is the heavy rain that occurred in southern Kyushu, western Japan, in 1993. Figure H2-1-1 shows the surface weather map at 0900 JST 6 August. A stationary front runs from a depression around the east coast of China to south of Japan through Kyushu. Figure H2-1-2 shows the hourly rainfall analyses from 1600 JST to 2000 JST. An intense rainfall area corresponding to the mesoscale convective system moved east-southeastward, slowly passing over the southwestern part of Kyushu. Heavy rain exceeding 90 mm/hour was observed around Kagoshima City. The most intense period of the rainfall was from 1700 JST to 1900 JST. As seen in Fig. H2-1-3, a cyclonic circulation was analyzed in the observational surface wind pattern.

H-2-2 Forecast with 25 km horizontal resolution

First, we show the result of the forecast experiment with 25 km horizontal resolution (25 km-NHM). The model is nested with the Japan Spectral Model (JSM), an operational hydrostatic model of JMA. The nonhydrostatic model contains 82×82 grid points horizontally, which covers a domain of $(2000\ \mathrm{km})^2$ shown by a square in Fig. H-2-1. Vertically, 32-levels with variable grid intervals of $\Delta z = 40$ to 1160 m are employed. The time step is 30 s. Convective adjustment parameterization (Kato and Saito, 1995) is used jointly with warm-rain explicit cloud microphysics.

Figure H2-2-1 shows the sea-level pressure field at 1800 JST and three-hour precipitation from 1500 JST to 1800 JST forecasted by JSM and the nonhydrostatic model. Both models predict heavy rainfall in the southern part of Kyushu Island. As a whole, the nonhydrostatic model reproduces the forecast of JSM well. The mean surface pressure of the nonhydrostatic model decreases about 3.2 hPa from 0900 JST to 2400 JST, as shown in Fig. H2-2-2. This decrease of mean pressure corresponds to JSM's counterpart in the same domain. If we use the anelastic model, the decrease of the mean pressure for the 15 hours was only 0.6 hPa. The anelastic model cannot express the variation of mean surface pressure correctly because it assumes the preservation of total mass in the entire model domain.

H-2-3 Forecast with 5 km horizontal resolution

Forecast experiments were conducted with 10 km and 5 km horizontal resolutions. Here, we show the result of the 5 km simulation (5 km-NHM). The model domain consists of 122×122 grid points, which covers $(600\ \mathrm{km})^2$ around Kyushu. The vertical grid structure is the same as in 25 km-NHM. The initial and boundary conditions are supplied from JSM, while the initial time of the nonhydrostatic model is 1500 JST. As for cloud microphysics, a warm rain explicit scheme is used. The time step is 15 s, and the simulation is conducted up to 1440 Δt (6 hours).

Figure H2-3-1 shows the hourly rainfall predicted by 5 km-NHM, which corresponds to Fig. H-2-2. The maximum rainfall of each hour is 60 mm to 80 mm, and the correspondence between the observation and simulation is generally good except in north-south deviation (about 20 km) in the location of rainfall areas.

Figure H2-3-2a shows the horizontal wind at the lowest level of 5 km-NHM at 1800 JST. A cyclonic

[1]Part of this section was extracted from the results reported in Saito *et al.* (1998).

circulation appears northwest of the intense rainfall area. As seen in Fig. H2-3-2b, this circulation is a mesoscale depression with a circular contour of 1001 hPa. This mesoscale cyclone corresponds to Fig. H2-1-3 ; it is not seen in the initial condition and is predicted by neither JSM nor 25 km-NHM.

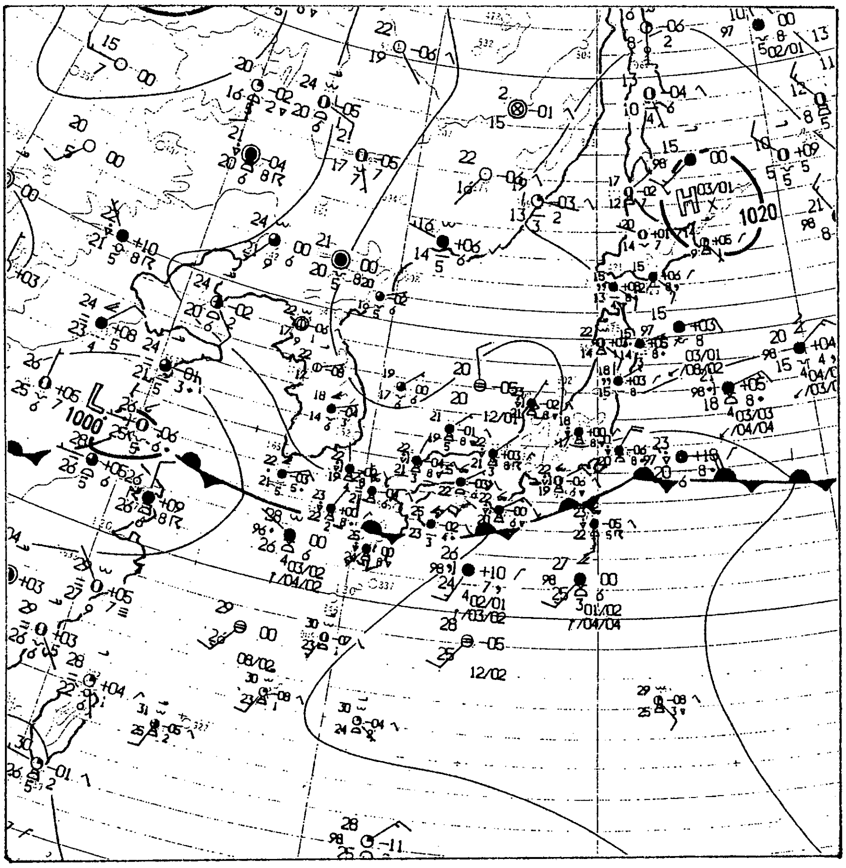

Fig. H2-1-1 Surface weather map at 0900 JST 6 August 1993. Contour interval is 4 hPa. After Saito (1997).

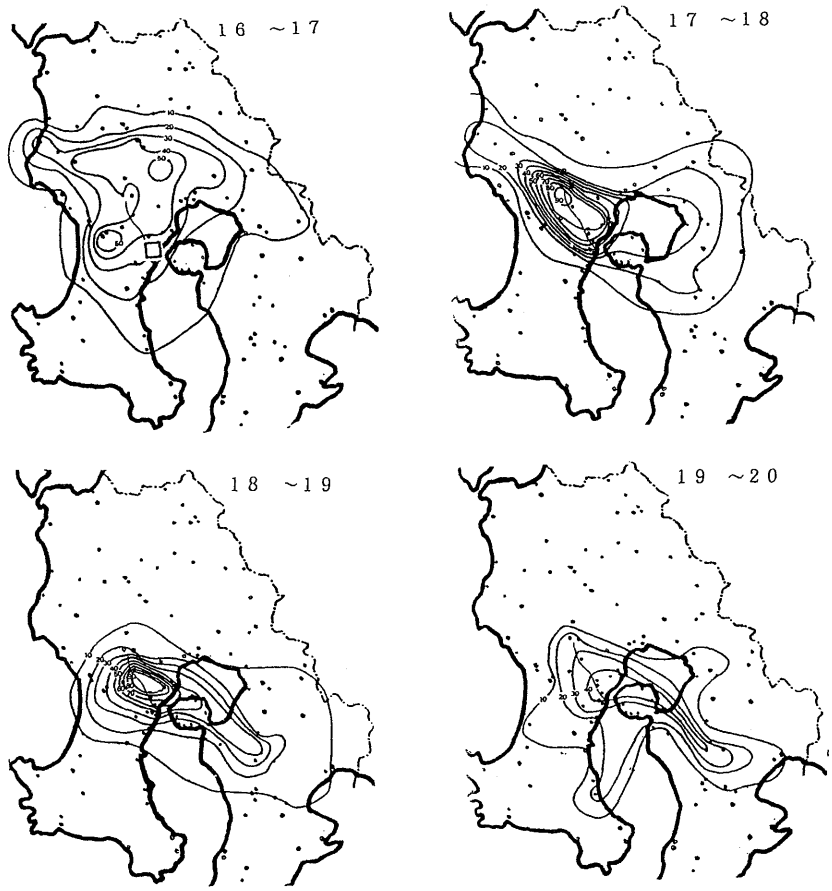

Fig. H2-1-2 Hourly rainfall from 1600 JST to 2000 JST, adopted from Sakurai and Hosoyamada (1994). Numbers in the upper right corner of each section show the local time (JST). Contour interval is 10 mm. Small square in the upper-left panel shows the location of Kagoshima City.

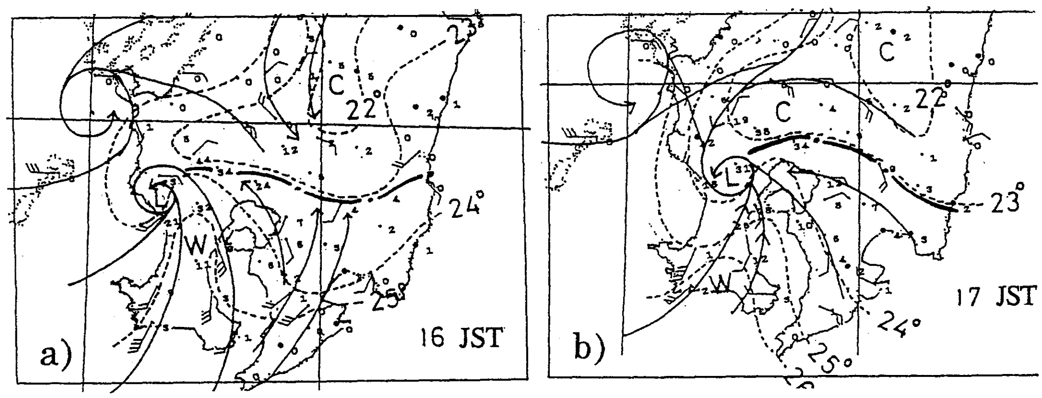

Fig. H2-1-3 Mesoscale analyses of local surface circulation adopted from Izumi (1994). The full barb and pennant indicate 1 knot and 5 knots, respectively.

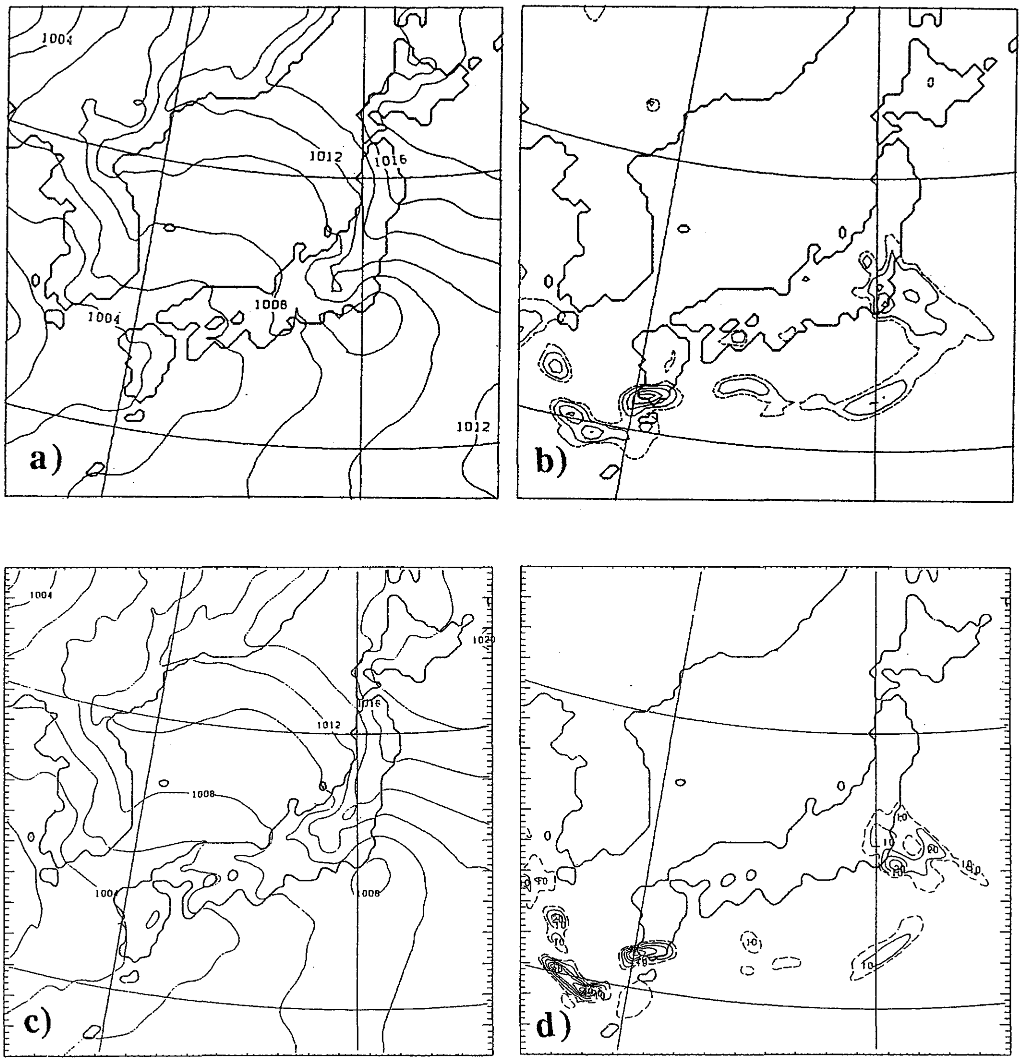

Fig. H2-2-1 **a)** Sea-level pressure field by JSM at 1800 JST. Contour interval is 2 hPa. **b)** Three-hour rainfall from 1500 JST to 1800 JST by JSM. Contour interval is 10 mm, while broken lines indicate 5 mm. **c)** Same as in a) but by the model. **d)** Same as in b) but by the model.

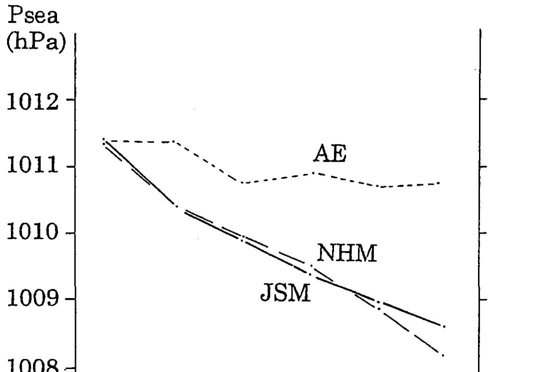

Fig. H2-2-2 Time sequence of mean sea-level pressure by JSM (solid line), 25 km-NHM (broken line) and AE-NHM (dotted line). The pressure is averaged over the domain of 25 km-NHM.

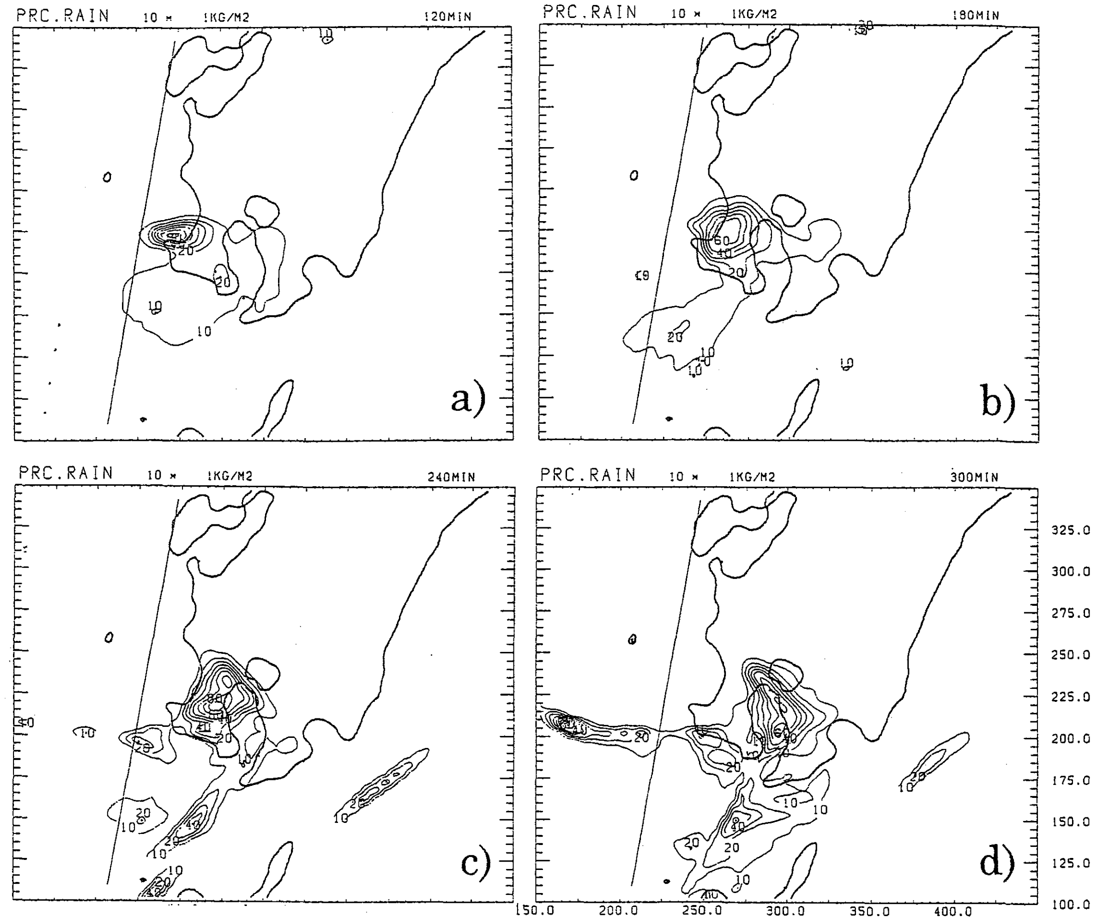

Fig. H2-3-1 Hourly rainfall by 5 km-NHM. Contour interval is 10 mm. **a)** 1600 JST to 1700 JST. **b)** 1700 JST to 1800 JST. **c)** 1800 JST to 1900 JST. **d)** 1900 JST to 2000 JST.

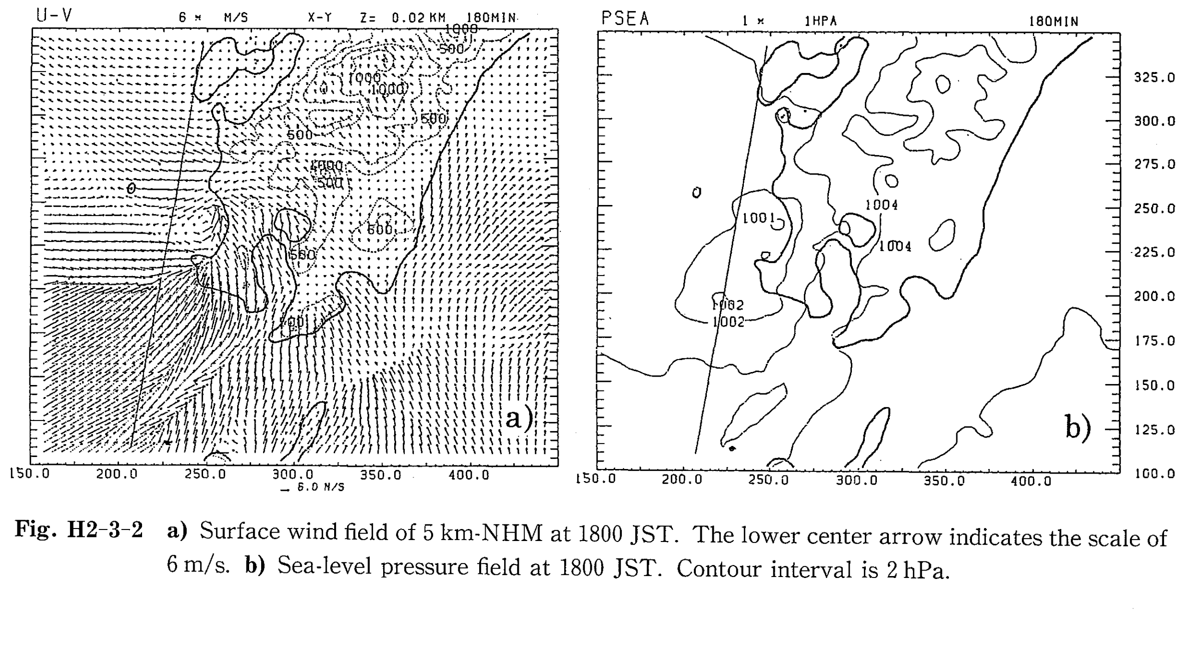

Fig. H2-3-2 **a)** Surface wind field of 5 km-NHM at 1800 JST. The lower center arrow indicates the scale of 6 m/s. **b)** Sea-level pressure field at 1800 JST. Contour interval is 2 hPa.

H-3. Statistical verification of rainfall prediction

H-3-1 Background and design of verification

The rainfall predicted by the MRI-NHM with a 10-km grid (NHM10) was verified during the 1996 Baiu season. The verification was compared with the results of RSM. These results were reported by Kato *et al.* (1988) and Saito and Kato (1999) in detail. This comparison is thought to have been conducted to examine the nonhydrostatic effect, because the RSM is a hydrostatic model. However, there are many differences between the model specifications of MRI-NHM and RSM, in addition to their dynamic frameworks. The most notable difference is found in the precipitation scheme employed in each model. Either the warm rain scheme that explicitly predicts the mixing ratios of cloud water and rainwater or the cold rain scheme that predicts those of cloud ice, snow and graupel in addition is employed in NHM10. In contrast, two parameterized convective schemes (*e.g.,* the Arakawa-Schubert and moist convective adjustment schemes) are used in conjunction with large-scale condensation in the RSM. A detailed comparison between hydrostatic and nonhydrostatic simulations of the development of moist convection has been conducted by Kato and Saito (1995).

Kurihara and Kato (1997) demonstrated that a clear diurnal variation of precipitation amount and intensity appeared in Kyushu during the 1996 Baiu season. They indicated that this variation comes from the effect of atmospheric radiation. The clouds suppressed the development of convections during the day and increased the convective instability at night. The effect of atmospheric radiation was also examined by excluding the atmospheric radiation process from NHM10. The atmospheric radiation is calculated by using the relative humidity (see G5-1-1).

Through use of the RSM with a resolution of about 20 km (operational RSM), the JMA provides a 51-hour weather forecast for the region in Fig. H3-1-1a twice a day. The RSM model specifications are summarized in Table 2 in Kato *et al.* (1998). The domain of RSM (RSM20) used in the present study covers about a quarter that of the operational RSM. Furthermore, the 10 km-resolution version of RSM (RSM10) is used to examine the influence of horizontal resolution. The domain of each model shown in Fig. H3-1-1a has $129\times129\times36$ grid points (the operational one is $257\times217\times36$). The orography of RSM20 is almost the same as that shown in Fig. H3-1-1a, and that of RSM10 is shown in Fig. H3-1-1b. The initial data of RSM10 and RSM20 (RSMs) are provided by the regional analysis, and the boundary conditions are provided by the output of the Global Spectral Model (GSM).

The horizontal domain for the MRI-NHM has 122×122 grid points while the vertical grid contains 38 levels with variable grid intervals of 40 m (near the surface) to 1120 m (at the top of the domain). The model top is located at 19.82 km. Each z-level almost corresponds to the σ-level in the RSMs. The domain is shown by the dashed square box in Fig. H3-1-1; the orography is almost the same as that of RSM10 (Fig. H3-1-1b).

Figure H3-1-2 shows the nesting procedure between GSM and RSM20 (RSM10) and between RSM20 and NHM10. The RSMs are one-way nested within the GSM forecast, and the integration time is 24 hours. The NHM10 is one-way nested within the RSM20 forecast, the initial time of which is 0000 UTC or 1200 UTC. The six-hour forecast of RSM20 (valid at 0600 UTC or 1800 UTC) is used for the initial data of NHM10. The integration time is 18 hours.

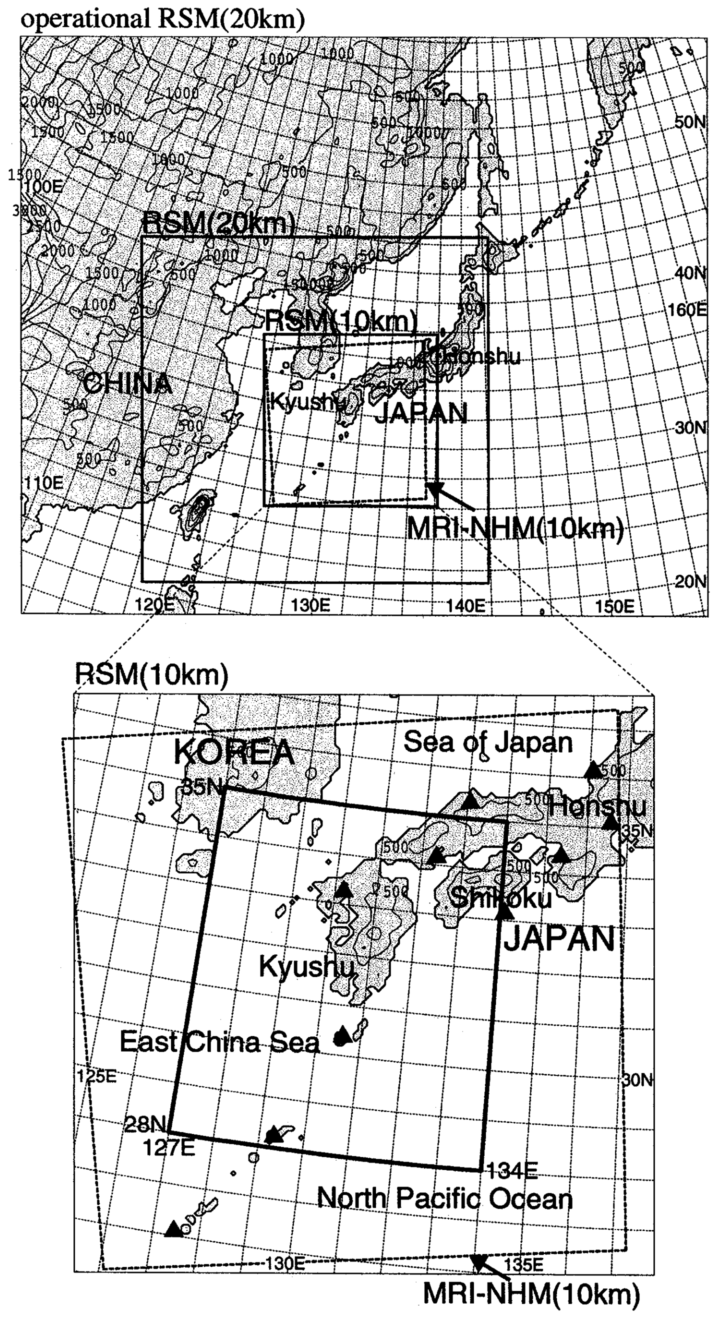

Fig. H3-1-1 (a) Domain and orography of the operational RSM. The domains of RSM10 and RSM20 are also shown by the small and large solid square boxes, respectively. The dashed square box represents the domain of NHM10. The orography of RSM20 is almost the same as that of the operational RSM. (b) Domain and orography of RSM10. The verification regionis endosed by thick colid lines (i.e., 28°N, 35°N, 127°E and 132°E). The solid triangle denotes the location of the JMA radars (from Kato *et al.*, 1998).

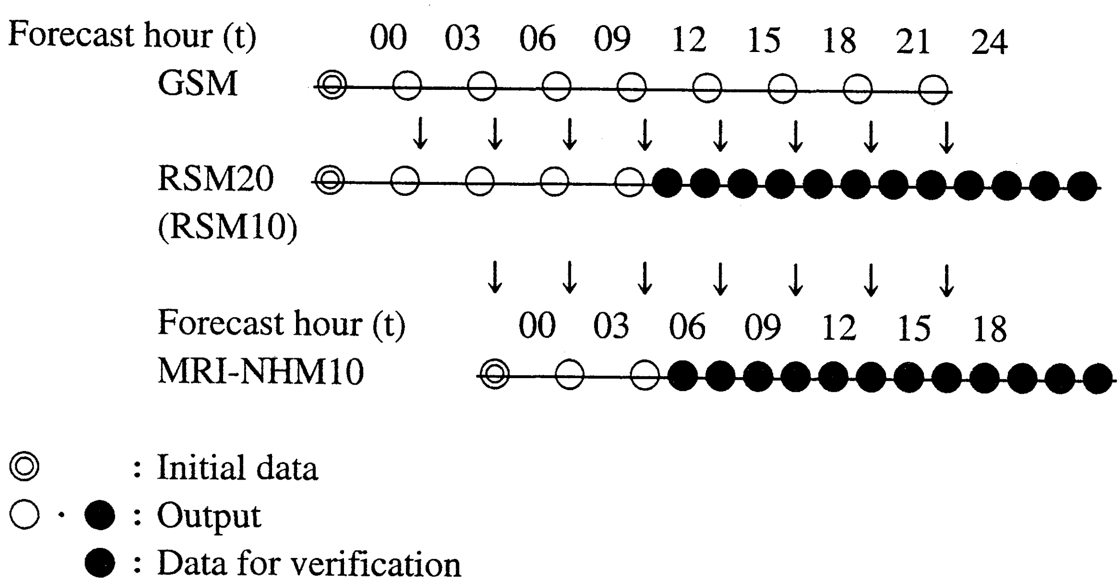

Fig. H3-1-2 Nesting procedure between numerical models

H-3-2 Verification method

The hourly accumulated rainfall simulated by NHM10 from the forecast time of 7 hours to 18 hours (FT=7 to 18), and those by RSM10 and RSM20 from FT=13 to 24 (Fig. H3-1-2) are verified using Radar-AMeDAS analyzed rainfall (R-AR). The R-AR is a composite of the radar estimated fields, calibrated by AMeDAS raingauge data, for hourly-accumulated precipitation. The R-AR is obtained not only on land but also on the sea. The region of the verification is shown in the area surrounded by the thick solid lines in Fig. H3-1-1b (*i.e.,* the lines of 28°N, 35°N, 127°E, and 132°E). This region is almost covered by the operational radars of JMA (whose positions are denoted by the solid triangles in Fig. H3-1-1b). The period of verification is between the valid times of 0100 UTC, 20 June and 1200 UTC, 10 July.

The statistical accuracy is calculated as follows. Hourly accumulated rainfall is divided into grids of 0.5 degree ($\sim 50 \times 50$ km^2), whose horizontal size is almost equal to the smallest resolved scale of the phenomena by 10 km-resolution models. Figure H3-2-1 shows the conditions of hits, passes, and false alarms of predicted rainfall to R-AR. The rainfall in the neighboring grids and at earlier and later hours is included in each condition to allow for slight differences in the space and time between the prediction and analysis. The following statistical measures of accuracy were calculated in the region near Kyushu Island by counting the number of hits, passes, and false alarms.

$$\text{Threat score} = \frac{N_{\text{hit}}}{N_{\text{hit}} + N_{\text{pass}} + N_{\text{false}}}, \qquad \text{(H3-2-1)}$$

$$\text{Bias score} = \frac{N_{\text{hit}} + N_{\text{false}}}{N_{\text{hit}} + N_{\text{pass}}}, \qquad \text{(H3-2-2)}$$

$$\text{Hit rate} = \frac{N_{\text{hit}}}{N_{\text{hit}} + N_{\text{pass}}}, \qquad \text{(H3-2-3)}$$

and

$$\text{False rate} = \frac{N_{\text{false}}}{N_{\text{hit}} + N_{\text{pass}}}, \qquad \text{(H3-2-4).}$$

where N_{hit}, N_{pass}, and N_{false} are the numbers of hits, passes, and false alarms. The threat score is the statistical measure of accuracy taking into account the numbers of passes and false alarms; the prediction accuracy improves as the threat score comes closer to 1. The bias score represents the rate of the numbers of predicted times to observed times, *i.e.,* the prediction overestimates for bias scores >1 and underestimates for bias scores <1. The hit and false rates represent the rates of the numbers of hits and false alarms to the observed times.

H-3-3 Verification results

Table H3-3-1 presents the average of the total hourly-accumulated rainfall. The total rainfall predicted by all models tends to be overestimated in comparison with the R-AR. The RSM in particular has overestimated it by close to 50%; the RSM has a tendency to predict precipitation greater than the observation, even considering that the R-AR tends to be underestimated on the sea where no AMeDAS station exists (Forecast Division/JMA, 1995). This overestimation could be a result of a weak precipitation area, since a precipitation area over 1 mm h^{-1} has been predicted almost twice by the RSM (not shown). In contrast, the NHM10 predicted smaller areas for weak precipitation and larger areas for heavy precipitation than the RSM, due to the explicit treatment of convection without any convection-parameterization scheme. The overestimation of heavy rainfall is greater in the results with a warm rain scheme than those with a cold rain scheme. The effect of an ice phase could suppress the excess development of convections.

Atmospheric radiation hardly affects the heavy precipitation and total rainfall, while its effect appears clearly in the diurnal variation of precipitation (Fig. H3-3-1). The peak of precipitation has a time lag with the NHM10 without an atmospheric radiation scheme, because it takes several hours for the influence of the boundary condition supplied by the RSM to spread to the center of the model domain. The diurnal variation of precipitation agrees well with the R-AR for the NHM10 with an atmospheric radiation scheme.

Figure H3-3-2 shows the threat and bias scores and the hit and false rates of NHM10, RSM10, and RSM20. The results for the NHM10 are presented for cases with a warm rain scheme and without an atmospheric radiation scheme (NHM10(Warm)) and for those with both cold rain and atmospheric radiation schemes (NHM10(C+R)). The threat scores of NHM10 are slightly worse, but considerably better than those of RSM10.

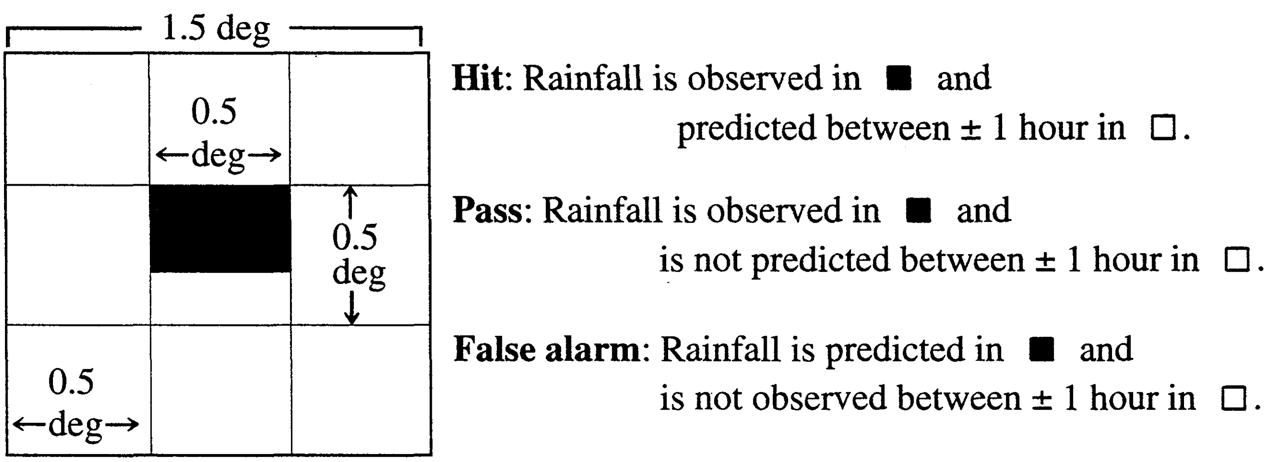

Fig. H3-2-1 Conditions of hits, passes, and false alarms of predicted rainfall for Radar-AMeDAS analyzed rainfall.

The NHM10(C+R) has good accuracy for weak precipitation in particular, close to that of RSM10. NHM10(C+R) has better bias scores than NHM10(Warm) over the whole precipitation intensity. However, the small bias scores of RSM (*e.g.,* 10 to 20 mm h^{-1}) indicate that the RSM can predict heavy rainfall to a small extent. The RSM10 has a high hit rate for weak precipitation, while the NHM10 has a relatively high hit rate for heavy precipitation. The NHM10 hits almost half the numbers for precipitation of 10 to 20 mm h^{-1}. In the results of both NHM10 and RSM10, the precipitation intensity with a relatively high false rate has also a relatively high hit rate (*e.g.,* 1 to 2 mm h^{-1} for the RSM10, and 20 mm h^{-1} for the NHM10). Therefore, a good threat score is obtained when the precipitation intensity is overestimated.

Although a 10-km grid cannot resolve individual convective cells, the NHM10 with an explicit precipitation scheme improved the prediction of heavy rainfall compared to the RSM10. This could be because explicit treatment of cloud-scale processes strongly influences the formation of heavy rainfall during the Baiu season. This improvement indicates that the NHM10 with an explicit precipitation scheme has good accuracy for a numerical weather prediction model, even when any convection-parameterized scheme is used conjunctionally. However, a new precipitation scheme suitable for a 5 to 10 km model must be developed to improve the prediction of weak precipitation and suppress the overestimation of heavy precipitation.

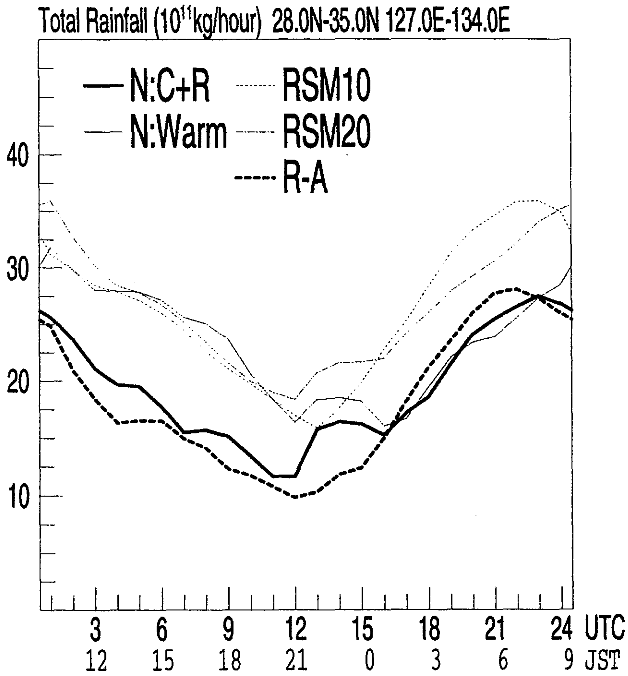

Fig. H3-3-1 Diurnal variation of the total rainfall. The thick solid line indicates the variation of NHM10 with an atmospheric radiation scheme, the thick dashed line represents that of NHM10 without an atmospheric radiation scheme, the thin solid line indicates that of RSM10, the dash-dotted line that of RSM20, and the thick dashed line that of R-AR (from Saito and Kato, 1999).

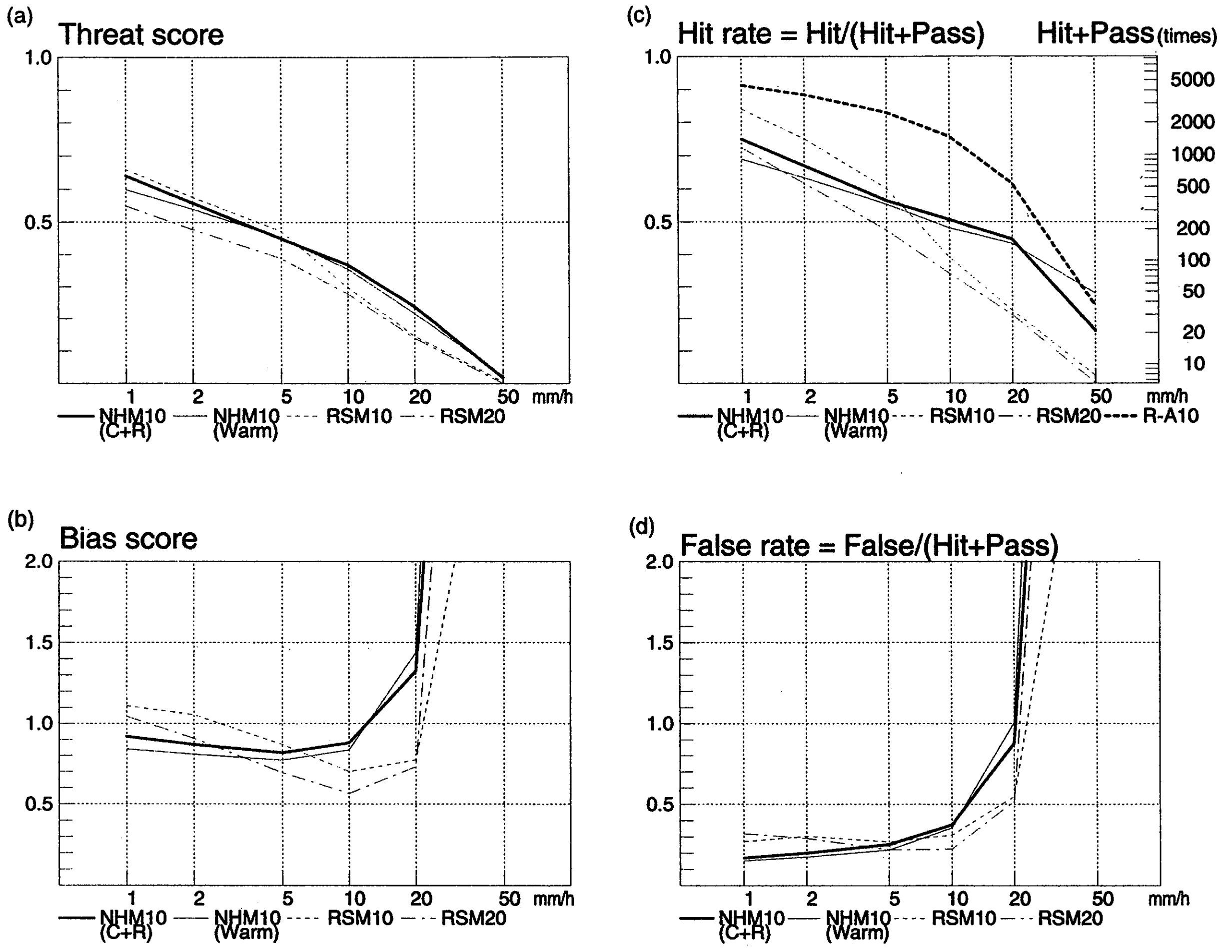

Fig. H3-3-2 Statistical scores of NHM10 with an atmospheric radiation scheme (thick solid line), NHM10 without an atmospheric radiation scheme (thin solid line), RSM10 (thin dashed line), and RSM20 (thin dash-dotted line). The abscissa denotes the hourly-accumulated rainfall. (a) Threat score. (b) Bias score. (c) Hit rate. (d) False rate. The numbers of observed times for R-A10 are shown by the thick dashed lines in (c) (from Saito and Kato, 1999).

Table H3-3-1 Average of total precipitation and precipitation area

	Total Rainfall [10^{11} kg h^{-1}]	Area of Rainfall [100 km^2] >20 mm	>10 mm	>5 mm	>1 mm
NHM10 (C+R)	19.01	17.66	46.88	93.6	175.7
NHM10 (Warm)	22.99	26.53	56.64	102.9	272.7
RSM10	26.03	8.41	37.65	115.5	595.6
RSM20	26.05	5.45	36.53	118.7	612.7
R-A10	17.75	8.82	42.85	112.3	385.4
R-A20	17.75	6.20	35.84	100.7	332.8

H-4. Cloud resolving simulation — winter marine stratocumulus

In winter, a continental cold air mass sometimes flows out over a warmer sea, supplying a great amount of heat and water vapor. As a consequence of this air-mass transformation, a maritime mixed layer develops, and stratocumulus is generated in its upper layer. In the Japanese Cloud and Climate Study (JACCS), aircraft observations of cloud physics and radiation were performed for lower clouds around the Japanese Islands during FY1996 and FY1997 winter seasons. The FY1996 experiment was conducted for marine stratocumulus in the cloud streets west of Kyushu in January 1997. In this study, we tried to reproduce observed features of stratocumulus by using a 3-D non-hydrostatic model and investigated the heat balance in the mixed layer.

H-4-1 Outline of numerical experiment

The elastic version of MRI-NHM (Ikawa and Saito, 1991 ; Saito and Kato, 1996) with a horizontal grid size of 1km was used. The calculation domain has a $300 \times 300 \times 38$ horizontal and vertical grid. In this study, the cloud physics in the model contains the cold rain scheme, and the atmospheric radiation scheme for the cloud-resolving model (G-5-2) is used. The initial and boundary conditions for MRI-NHM are provided from the output produced by RSM. MRI-NHM is one-way nested within the RSM forecast with an initial time of 2100 JST, 21 January 1997.

H-4-2 Results

Figure H4-2-1 shows the horizontal map of the liquid water path (LWP) simulated by MRI-NHM at 0300 UTC on 22 January 1997 (nine-hour forecast). Several cloud streets are obtained and roughly correspond with satellite observations (Fig. H4-2-2). They are about 10km wide and extend north and south. Figure H4-2-3 presents the vertical profile of liquid water content (LWC) along the cloud street. Aircraft observations (Fig. H4-2-3a) show that clouds contain LWC of about 0.7 gm^{-3} and extend from 1 to 2 km in height. The vertical distribution and the magnitude of LWC simulated by MRI-NHM are similar to observations (Fig. H-4-2-3b).

Figure H4-2-4 shows the vertical profiles of the components of heating rate averaged in the box in Fig. 1. The heating is seen in the whole layer. In the sub-cloud layer, the heating due to convergence of the upward sensible heat flux is greater than the cooling due to large-scale advection. In the under part of the cloud layer, the sum of the heating due to the convergence of the upward sensible heat flux, condensation and radiation is greater than the cooling due to large-scale advection. In the upper part of the cloud layer, the sum of the cooling due to the divergence of the upward sensible heat flux, evaporation and radiation is almost balanced by the heating due to large-scale advection. Above the cloud, the heating due to large-scale advection, especially subsidence, is dominant. Furthermore, the radiative heating and cooling is not small compared with other terms.

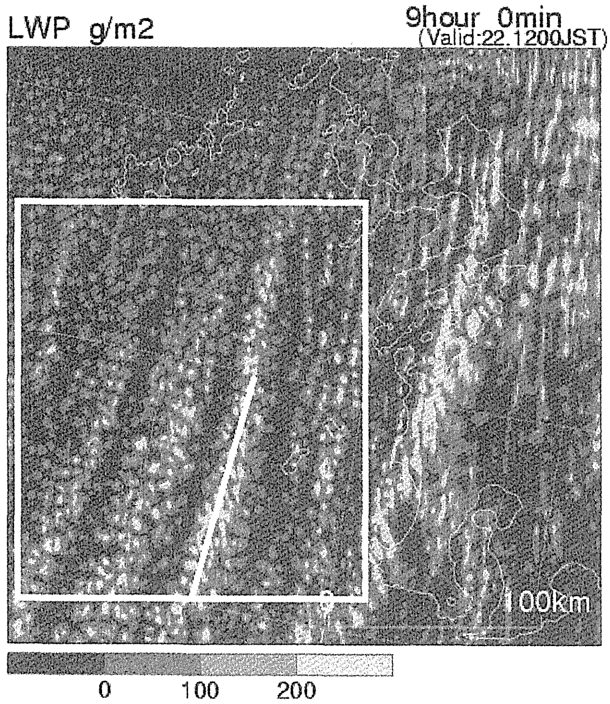

Fig. H4-2-1 Horizontal distribution of LWP at 0300 UTC on 22 January 1997 (nine-hour forecast). Solid line (box) is used in Fig. H-4-2-3 (Fig. H-4-2-4).

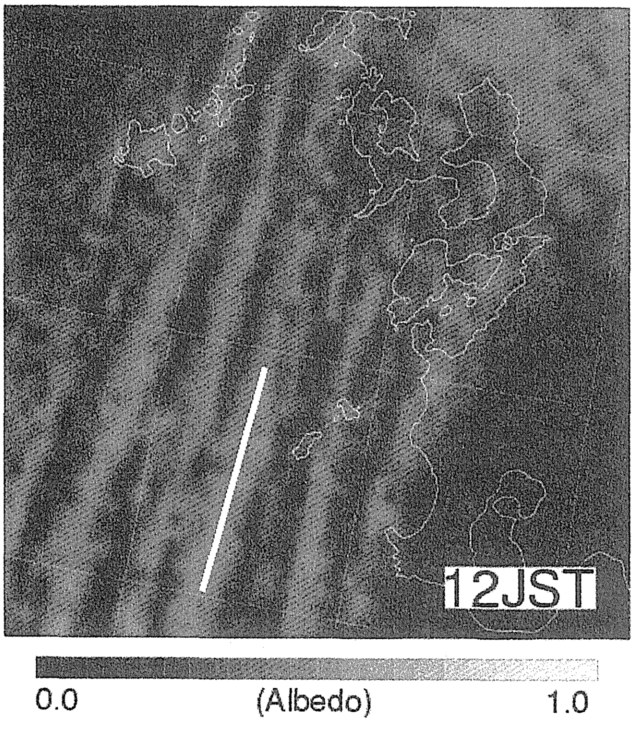

Fig. H4-2-2 Visible satellite image at 0300 UTC on 22 January 1997. Solid line denotes flight path of the aircraft.

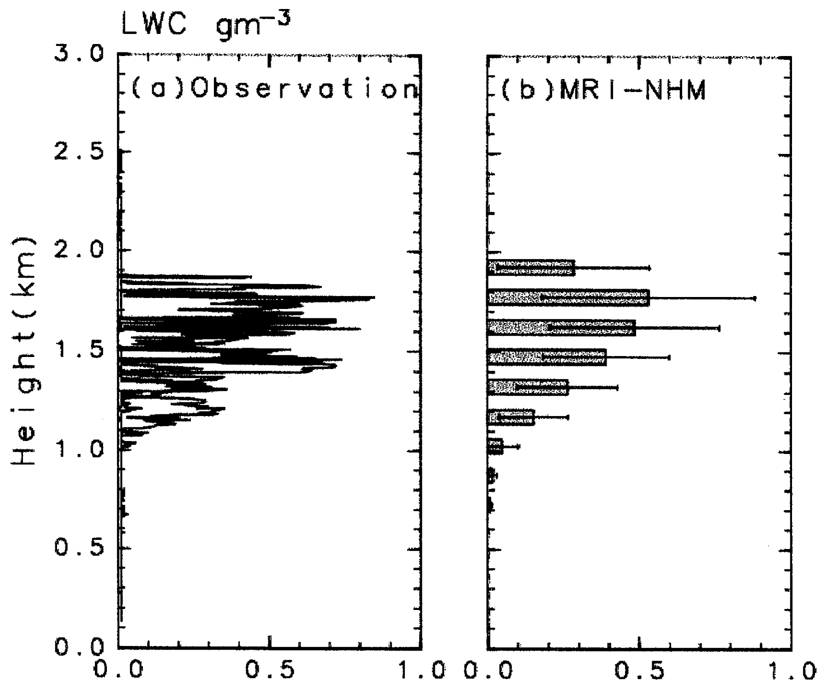

Fig. H4-2-3 Vertical profile of LWC of (a) aircraft observations along the solid line in Fig. H4-2-2 and (b) MRI-NHM simulation along the solid line in Fig. H4-2-1. Bar graphs (error bars) in (b) denote mean value (standard deviation).

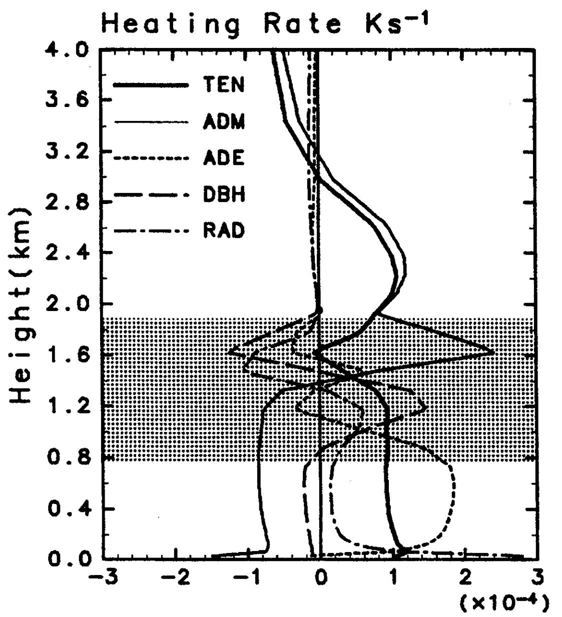

Fig. H4-2-4 Vertical profiles of heating rate components, averaged in solid box area in Fig.H-4-2-1, at 0300 UTC on 22 January 1997. Local time tendency is indicated by a thick solid line, area-scale advection by a thin solid line, convergence of the convective heat flux by a dotted line, the effect of condensation and evaporation by a dashed line, and the effect of radiation by a dash-dotted line. The hatched area denotes a cloud layer.

I. Model code structure

I-1. Model structure and job step

Job is divided into 4 steps currently.

Job Step 1

Preparation of orography file (Section K-1).

Job Step 2

Preparation of initial and boundary files (Section K-2).

Job Step 3

Running the model (Section K-3).

Job Step 4

Plotting the results (Section K-4).

I-2. Members and subroutine list of Job Step 3

I-2-1 Member list

In job step 3, following members exist. Here asterisk in each member name is the wild card, which stands for the source code version.

main*.f : main program

subadj*.f : convective adjustment

subadv*.f : computation of advection terms

subchk*.f : subroutines for check

subcvp*.f : computation of velocity

subdif*.f : subroutines for diffusion

subhel*.f : pressure equation solver

subhevi*.f : subroutines for E-HE-VI scheme

subhyd*.f : hydrostatic version

subini*.f : initial model setting

subios*.f : I/O subroutines

sublbc*.f : boundary condition

subpgf*.f : pressure gradient and forcing terms

subptg*.f : prediction ground temperature

subrad*.f : atmospheric radiation using relative humidity for cloud amount

subrade*.f : atmospheric radiation using cloud water and cloud ice

subsnw*.f : cloud microphysics

subtrb*.f : turbulent closure model

deigs.f : eigen function by Jacobi method

gamma.f : gamma function

comm.f : subroutines for data copy for HE-VI scheme

wrtfct.f : write forecast values for GrADS

I-2-2 Subroutine list

Following subroutines and functions are included in the above members.

a. subadj.f*

ADJUST : moist convective adjustment

CLBASE : calculation condensation level

RRMDFY : evaporation during the rain dropping to the surface

b. subadv.f*

CADVE1M : advection term for scholar variables

CADVC4W : compute advection term for W

CADV4UV : compute advection terms for U and V

CADVUP : upstream advection

CADVE3M : compute advection term for cloud water

CADVQN : compute advection term of number concentration

DVDNS : divide by density (currently not used)

UVMEAN : compute u/m and v/m at scholar point

CWMEAN : compute w/m at scholar point

DEFORM : compute deformation term

CLEARH : zero setting

LTRLB2 : adjust boundary values for cyclic condition (P point)

LTRLBU : adjust boundary values for cyclic condition (U point)

LTRLBV : adjust boundary values for cyclic condition (V point)

LTRLUV : adjust boundary values for cyclic condition (deformation terms)

ADJ2D1 : adjust boundary values for cyclic condition

MODADV : modify advection term in E-HI-VI scheme

c. subchk.f*

CHKEN3 : advection term for scholar variables

CHKMX : check maximum and minimum

CHKDIV : check maximum divergence in each level

CHKVAP : check total amount of Qv, Qc, Qr (currently not used)

CHKVAL : output values

CHKBDV : check boundary values (currently not used)

CHKFLX : check vertical flux

CHKFXM : check momentum flux (currently not used)

CHKAVR : check average value

CHKMNS : simple check of minus values

CHKMN0 : check of minus values

CHKMN2 : set u, v, w^* for modifed advection scheme

CHKMN20 : modify advection term by modified advection scheme

CHKMN21 : compute maximum and minimum of advection term

CHKMN22 : compute maximum of advection term (for MSWSYS(30)=3)

)CHKMN2-CHKMN22 are used for dry model or advection terms of U, V, W

CHKMN23 : prepare minimum values for modified advection scheme

CHKMN3 : modify advection terms of physical variables by modified advection scheme

CHKMN30 : compute advection flux of physical variables for modified advection scheme

CHKMN31 : compute maximum and minimum of advection term

CHKMN32 : compute maximum of advection term (for MSWSYS(30)=3)

*)CHKMN3-CHKMN32 are used for advection terms of physical variables

CHKBGT : check budget for cloud microphysics

CHKSUM : check sum

CHKMN1 : check minus values (for TKE)

d. subcvp.f*

SVELCH : time integration of velocity

ORUCHH : compute Orlanski's radiation condition phase velocity for U

ORVCHH : compute Orlanski's radiation condition phase velocity for V

EXTRX1 : extrapolation scholar values at x-boundary

EXTRY1 : extrapolation scholar values at y-boundary

EXTRX2 : extrapolation Qv at x-boundary

EXTRY2 : extrapolation Qv at y-boundary

EXTWX2 : extrapolation W at x-boundary

EXTWY2 : extrapolation W at y-boundary

EXTPX2 : extrapolation θ at x-boundary

EXTPY2 : extrapolation θ at y-boundary

EXTVX2 : extrapolation V at x-boundary

EXTUY2 : extrapolation U at y-boundary

EXTNUH : extrapolation U at x-boundary

EXTNVH : extrapolation V at y-boundary

CPSEA : compute sea level pressure

ADJPRS : adjust press at top boundary (currently not used)

e. subdif.f*

DAMPCN : computation of numerical diffusion

SETDCF : set diffusion coefficients

TSMOTH : Asselin's time filter

TSMTUV : Asselin's time filter for U and V

OSAVEH : save old value for time filter

COPYH : copy data set

RLDAMP3 : Rayleigh damping

f. subhel.f*

CPRESS : compute pressure

CPAI3 : solve pressure equation

VHELMH : Helmholtz equation solver

TRIDGH : Gaussian elimination method

TREGXH : Fourier transformation for x-direction

TREGYH : Fourier transformation for y-direction

GENCIN : set tri-diagonal matrix for pressure solver

UVPBD : lateral boundary treatment for U and V

INIVG1 : set eigen vector function by Jacobi method

INIVG2 : set eigen vector function for uniform grid

GMATD1 : set eigen vector matrix

g. subhevi.f*

TRIMAT : set matrix coefficient

SNDUV : update horizontal velocity with forward scheme

SNDWP : update vertical velocity and pressure with backward scheme

BUNDRY : apply boundary conditions

ASELIN : apply time filter

h. subhyd.f*

CHYDPRE : compute pressure for hydrostatic version

CHYPAI2 : compute surface pressure by solving pressure equation

CHYPAIA : compute pressure vertically

CPFHYI : set invariant forcing term

CPFHYV : set variant forcing term

HYVSTCO : compute co-efficient of pressure for surface pressure

HYVSTC1 : compute vertical sum of advection term and DU(V)DTBC

ZEROEIGV : set number of eigen value which is zero CHYDPRE :

i. subini.f*

INIT3 : read orographic file and set initial constants

INIUVD : initial set U and V from the parameter card

SETREF : set reference atmosphere

HRMEAN : compute horizontal mean

CSTATP : compute hydrostatic pressure

INIEX1 : interpolate initial reference field

RANDOM : make random perturbation (currently not used)

SETPTD : set barotropic geostrophically balanced field

CPTGRD : set ground temperature

DIVFLOW : set divergent flow (currently not used)

RELAX1 : Poisson equation solver by successive over relaxation

CADJP1 : adjust initial field by the variable calculus

SETOMW : set initial field of W^*

VRGDIS : compute variable grid distances

ORGIN3 : set metric tensors and their mean values

CPTRFT : compute reference atmosphere

INTRF3 : interpolate reference atmosphere to 3-D model planes

INTRF2 : interpolate reference atmosphere to 3-D model planes for half level

SETZRP : set height of full levels

SETZRW : set height of half levels

SETVDZ2 : set depth of half levels

READZS : read orography file

SETVRG : set variable grid levels

j. subios.f*

RDPAR1 : read parameter card

STRMTS : store grid point values

STRMTS2 : store grid point values with compression

COMPRE : compress GPVs into 2 byte integer

RESTFL : store restart file

SFTRCD : shift record number in case of restart

LOADPS : load sea-level pressure from the boundary file

LOADUV : load grid point values from the boundary file

LOADOM : load adjusted wind at the lateral boundary

STOROM : store adjusted wind at the lateral boundary

LOADBD : load boundary condition

STORBD : store boundary values and their tendencies

STMTC1 : store basic variables

LOADTG : load ground temperature from the ground temperature file

TIMSTP : time control

k. sublbc.f*

SETEXT : set time tendency of prognostic variables

SETEX2 : set time tendency of prognostic variables at lateral boundary

SETEXU : set time tendency of U at lateral boundary

SETEXV : set time tendency of V at lateral boundary

CDMFDT2 : compute time tendency of mass flux through lateral boundary

SETEXW : set time tendency of W at lateral boundary

SETEXP : set time tendency of θ at lateral boundary

CEXTBD : set value of prognostic variables at lateral boundary

JYSET2 : set start and end of JY

PRSTR1 : print out variables

CONDQV : compute condensation

PTCOND : compute condensation level

WDGROW : wind grow procedure

CDMFDT : compute time tendency of mass flux in case of wind grow

ADJFLX : adjust U and V according to mass flux at lateral boundary

CHKMFX : compute mass flux at lateral boundary

SETEXT2 : set time tendency of prognostic variables using SETEX3

SETEX3 : set time tendency of external wind and potential temperature

LOADEX : load external reference value and time tendency at boundary

ADJEXT : adjust external reference wind according to precipitation rates

l. subpgf.f*

CPFORI : compute invariant part of forcing term for pressure equation

CPFRV1 : compute variant part of forcing term for pressure equation

CFPBDV : compute boundary condition for pressure equation

WCVOMWM : convert W to W^*

OMWCVWM : convert W^* to W

UCVDNUM : convert u and v to U and V

WCVDNWM : convert w to W

ADJUVW : adjust wind in case of mountain grow initial start up

CPFX1 : compute pressure gradient force for x-direction

CPFY1 : compute pressure gradient force for y-direction

CPFZ : compute pressure gradient force for z-direction

CDIVTM : compute total divergence

CDIVS : compute separable part of divergence

CPTM : compute mass-virtual potential temperature

CDENS : compute density from state equation

CBUOYD : compute buoyancy term

m. subptg.f*

TGFCST : compute ground temperature

RADIAT : compute short and long wave radiations

GNCLD : compute cloud amount by diagnosis of relative humidity

GNCLOUD : sub program of GNCLD

RADIATD : compute solar and long wave radiation for dry model

GNCLDD : compute shade area for dry model

TGCONC : initial setting of the wetness, albedo, .. *etc.* for no-nesting model

TGSET : set initial ground temperature for no-nesting model

SETDAY : set UTC from the boundary file

n. subrad.f*

RADIAT3 : main program for atmospheric radiation

ZENITH : compute zenith angle

SPMNEW : compute short and long wave radiations

SCALEL : compute scale of Qv, carbon, ozone for long wave radiation

SCALES : compute scale of Qv, carbon, ozone for short wave radiation

QTINT : interpolate T, Qv vertically

LGWAVE : compute energy flux of long wave radiation

LGTRNS : set transmission function (TAU)

FTTRNS : set TAU for vertical surrounding grids

GTTRNS : set total TAU from bottom and top

TAUTBL : compute TAU

SOLAR : compute atmospheric absorption for short wave radiation

SOLSC : compute absorption of scattered part of solar radiation

SOLAB : compute absorption of absorbed part of solar radiation

MTOG : program for saving cpu time

GCLNEW : compute cloud amount by diagnosis of relative humidity

GCLNEW2 : compute cloud rate between vertical grids

TGFCST2 : compute ground temperature

o. subrade.f*

RADIAT3E : main program for atmospheric radiation using cloud water

ZENITHE : compute zenith angle

SPMNEWE : compute short and long wave radiations

SCALELE : compute scale of Qv, carbon, ozone for long wave radiation

SCALESE : compute scale of Qv, carbon, ozone for short wave radiation

QTINTE : interpolate T, Qv vertically

LGWAVEE : compute energy flux of long wave radiation

CTRNSE : compute transmission function (TAU) in cloud grids

LGTRNSE : compute total TAU of Qv, carbon, ozone for each level

FTTRNSE : compute total *TAU* of *Qv*, carbon, ozone for vertical surrounding

GTTRNSE : compute total *TAU* of *Qv*, carbon, ozone for bottom and top

TAUTBLE : compute *TAU* of each band by broad band models

SOLARE : compute atmospheric absorption for short wave radiation

SOLSCE : compute absorption of scattered part of solar radiation

SOLABE : compute absorption of absorbed part of solar radiation

MTOGE : program for saving cpu time

TGFCSTE : compute ground temperature

*p. subsnw * .f*

CPTQVN : compute potential temperature

CLDPHN : main program of cloud microphysics

CLDBG2 : cloud budget

CDTV : molecular dynamic viscosity of air

KOENIG : depositional growth of ice crystal

CLCWR1 : calculation of warm rain process

CLCWR2 : computation of cloud water in warm rain

CLRSHN : conversion from snow to graupel

CLVSHN : depositional growth of snow and graupel

CPICE : product of ice crystal

OUT03N : output list

OUT04N : output list

OUT05 : output list

CVRSH1 : melting of snow and graupel

CTRVF2 : compute terminal fall velocity

CTRVD2 : compute precipitation (Box Lagrangian scheme)

CTRVFM : compute precipitation (Euler scheme)

CQS3 : time integration of *Qc, Qr, Qs, Qg* and *Qi*

CQS2 : time integration of *Qv*

ADJNUM : adjust number concentration

CPT5 : compute time tendency of potential temperature

CPTQV1 : time integration of potential temperature

ADJQVH : adjust *Qv* after condensation and sublimation

ADJQCW : adjust *Qc* after condensation and sublimation

CGMMA : compute functions for terminal fall velocity etc.

FSUERM : error message

CQVSAT : compute saturation mixing ratio

CQVSAT1 : compute saturation mixing ratio for reference atmosphere *q. subtrb*.f*

CETUR5 : compute turbulent kinetic energy

CNVED3 : diagnose diffusion coefficients

CDIFET : compute diffusion term of turbulent energy

STRSED : compute stress terms

SETEMX : set maximum eddy diffusion coefficients

CRSTUV : compute Reynolds stress

KONDOH : compute bulk transfer coefficients over sea surface

GRDFXH : compute bulk transfer coefficients over ground surface

r. comm.f

SCATTER : copy from longtime step data to short time step data

GATHER : copy from short time step data to long time step data

I-3. Flow chart of Job Step 3

The flow of Job Step 3 (model run) is as follows :

I-3-1 Initial declaration and setting

a. Setting parameter

b. Declaration of arrays, common variables.

c. Setting of model constants

RDPAR1 — read parameter card

VRGDIS — set variable grid distance

SETZRP, SETZRW — set levels's heights

d. INIVG1 or INIVG2 — set eigen functions

e. Setting of constants for diffusion processes

SETEMX — set maximum eddy diffusion coefficients

SETDCF — set diffusion coefficients

f. Setting of orography file

INIT3 — read orography file and set initial constants

ORGIN3 — set metric tensors and their mean values

I-3-2 Model initiation

Two model initiation procedures are available ; stand alone initiation and nesting initiation, described in Chapter E. The control parameter is mode switch MSWSYS(12).

if (MSWSYS(12)=<2) then

a. Stand alone initiation

(==Stand alone initiation start==)

INIUVD — set of wind field (U and V) from the parameter card

SETREF — set reference atmosphere

CPTRFT — compute reference atmosphere

INTRF3 — interpolate reference atmosphere to 3-D model planes (for Qv)

CSTATP — compute hydrostatic pressure

CPTM — compute mass-virtual potential temperature

CDENSE — compute density from the state equation

GENCIN — set tri-diagonal matrix for pressure solver

UCVDNUM — convert u and v to U and V, multiplying reference density

CLEARH — set $W^*=0$

OMWCVWM — compute W from U and V (assuming $W^*=0$)

SETEXT — set external values for u, v, w, θ, Qv, and P

SETEXT2 — set zero for time tendency of external values of u, v and θ

LOADEX — load time tendency of external values of u, v and θ

(══ Stand alone initiation end ══)

else if (MSWSYS(12)>=3) then

b. Nesting initiation

(══ Nesting initiation start ══)

LOADUV — load grid point values from the boundary file

HRMEAN — compute horizontal mean state

CPTRFT — compute the reference atmosphere

CSTATP — compute hydrostatic pressure

CPTM — compute mass-virtual potential temperature

CDENSE — compute density from the state equation

GENCIN — set tri-diagonal matrix for pressure solver

LOADPS — load sea level pressure from the boundary file to set the total mass tendency

UCVDNUM — convert u and v to U and V, by multiplying reference density

WCVDNWM — convert w to W, by multiplying reference density

ADJFLX — adjust U and V according to mass flux at lateral boundary

CHKMFX — compute mass flux at lateral boundary

SETOMW — set initial field of W^*

CDIVTM, CHGKDIV — check divergence

if (MSWSYS(20)=0) then

══ anelastic, variational calculus start ══

RELAX — mass-consistent variational calculus

CADJP1 — adust U. V and W

══ variational calculus end ══

OMWCVWM — convert W to W^*

else if (MSWSYS(20)>0) then

OMWCVWM — convert W to W^*

end if

STOROM

do KTREAD = KTSTO + KTDTO,KTENO,KTDT

LOADUV — load grid point values from the boundary file

UCVDNUM — convert u and v to U and V, multiplying reference density

WCVDNWM — convert w to W, by multiplying reference density

CSTATP — compute hydrostatic pressure

CPTM — compute mass-virtual potential temperature

CDENSE — compute density from the state equation

GENCIN — set tri-diagonal matrix for pressure solver

UCVDNUM — convert u and v to U and V, by multiplying reference density

WCVDNWM — convert w to W, by multiplying reference density

ADJFLX — adjust U and V according to mass flux at lateral boundary

CHKMFX — compute mass flux at lateral boundary

SETOMW — set initial field of W^*

OMWCVWM — convert W to W^*

SETEXT — set external values for u, v, w, θ, Qv, and P

SETEX2 — set time tendency of prognostic variables at lateral boundary

SETEXT2 — set zero for time tendency of external values of u, v and θ

CDMFDT2 — compute time tendency of mass flux through lateral boundary

STORBD — store boundary values and their tendencies

enddo

(══ Nesting initiation end══)

c. Initiation of ground temperature

if (MSWSYS(12) =<2) then

TGCONC : initial setting of the wetness, albedo, etc., for stand alone run

TGSET : set initial ground temperature for stand alone run

else if (MSWSYS(12)>=3) then

LOADTG : load ground temperature from the ground temperature file

endif

d. Reset of initial value of model at start (restart) time

if (ITST=1) then

STMTC1 — store basic variables

LOADUV : load grid point values from the boundary file

LOADOM : load adjusted wind at the lateral boundary

CHKMFX — compute mass flux at lateral boundary

SETDAY — set universal time

CSTATP — compute hydrostatic pressure

CPTM — compute mass-virtual potential temperature

CDENSE — compute density from the state equation

CDIVT, CHKDIV — check divergence

else if (ITST>=2) then

RESTFL — read the restart file

CDIVT, CHKDIV — check divergence

SFTRCD — shift record number of the output file

end if

I-3-3 Time integration

do IT=ITST, ITEN

a. Setting of time step, model time

b. Diagnosis of density and set tri-diagonal matrix

CDENSE — compute density from the state equation

GENCIN — set tri-diagonal matrix for pressure solver

c. Computation

CEXTBD, SETEXW, ADJEXT — compute external value at boundary

CADVC4W, CADV4UV — compute advection terms

CRSTUV — compute stress terms

if (MSWSYS(13)>=8) then

RADIATE3E, TGFCST2E — cloud radiation process

else if (MSWSYS(13)>=6) then

RADIAT3, TGFCST2 — radiation relative humidity

else if (MSWSYS(13)>=2) then

TGFCST — no atmospheric radiation

end if

CETUR5 — Compute the turbulent kinetic energy

CPTQVN — Compute potential temperature with cloud microphysics

CNVED3 — Diagnose diffusion coefficients

CBUOYD — Diagnose buoyancy term

UVPBD — Treatment of lateral boundary condition

if (MSWSYS(20)<2) then

if (MSWSYS(20)=-1) then

*** HYDROSTTATIC VERSION ***

CHYDPRE — compute pressure for hydrostatic version

else if MSWSYS(20)>=0) then

*** ANELASTIC, ELASTIC-HI-VI VERSION ***

if (MSWSYS(20)=1) then

MODADV — Modify advection term

end if

CPRESS — compute pressure for non-hydrostatic version

end if

SVELCH — compute velocity

else if (MSWSYS(20)=2) then

* * * ELASTIC-HE-VI VERSION * * *

TRIMAT – set matrix coefficient

do m=1, nsound

SNDUV – update horizontal velocity with forward scheme

SNDWP – update vertical velocity and pressure with backward scheme

end do

BUNDRY – apply boundary conditions

ASELIN – apply time filter

end if

CPTM — Diagnose mass-virtual potential temperature

d. Output

STRMTS, STRMTS2 — Output grid point values

RESTFL — Output restart file

end do

J. Relevant utilities

J-1. Setting orography

The first step of the model structure (Job Step 1) is preparing the orography file. The file may be stored in a directory @data/ and named org**.

J-1-1 Format of the orography file

a. Record format

REC. 1	IXTST, IXTEN,JYMST, JYMEN, ZS, SL, FCORI, ROUGHL, FLATIT, FLONGI
REC. 2	NPROJC

b. Contents

Name	Type	Contents	Default	Unit
IXTST	I*4	Start number for x-direction	1	...
IXTEN	I*4	End number for x-direction	NX	...
JYMST	I*4	Start number for y-direction	1	...
JYMEN	I*4	End number for y-direction	NY	...
ZS(NX,NY)	R*4	Orographic height	...	M
SL(NX,NY)	R*4	Land coverage rate	1.0	0.01×%
FCORI(NX,NY)	R*4	Coriolis parameter f_3	...	s^{-1}
ROUGHL(NX,NY)	R*4	Roughness length	0.1	M
FLATIT(NX,NY)	R*4	Latitude	FLAT	degree
FLONGI(NX,NY)	R*4	Longitude	FLON	degree
NPROJC	C*4	Map projection	DES	...

J-1-2 Simple orography for idealized tests

For an ideal test, the orography is given by the following functions. For three-dimensional simulation, the orographic height is given by an isolated mountain as

$$Z_x(x,y)=\frac{h_m}{\{1+(\frac{x-x_0}{a})^2+(\frac{y-y_0}{b})^2\}^{\frac{3}{2}}}, \tag{J1-2-1}$$

where h_m is the height of the mountain top and, a and b are the horizontal scale for the x- and y-directions. For two-dimensional simulation, the orography is simply given by

$$Z_x(x)=\frac{h_m}{1+(\frac{x-x_0}{a})^2}, \tag{J1-2-2}$$

where a is the half width.

For simple orography, the Descart coordinate is assumed, and 'DES' should be set as NPROJC.

P. G. The above equations are given by the function ZSFN in org*.f in /srcenv. See K-1-2 for details.

J-1-3 Real orography for arbitrary conformal projection

a. GTOPO30 dataset

Real orography is provided by the GTOPO30 dataset, which is global digital elevation data with a horizontal grid spacing of 30 arc seconds (approximately 1 kilometer) developed at the US Geological Survey's EROS Data Center. Detailed information on the characteristics of GTOPO30, including the data distribution format, the data sources, production methods, accuracy, and hints for users, is found in the GTOPO30 URL

http://edcdaac.usgs.gov/gtopo30/gtopo30.html

and its README file

http://edcdaac.usgs.gov/gtopo30/README.html.

The original GTOPO30 data is a global data set covering the full extent of latitude from 90 degrees south to 90 degrees north ; MRI/NPD-NHM provides limited data of latitude from 10 to 50 degrees north and longitude from 110 to 150 degrees east. See K-2-2 for details.

b. Conversion to conformal projection map

The orography file is transformed into a conformal map projection. The model can accommodate the following three conformal map projections :

1) Polar stereo graphic projection

The horizontal coordinate (x, y) is a projected plane transformed by

$$\begin{pmatrix} x \\ y \end{pmatrix} = \begin{pmatrix} x_p + ma\cos\varphi\sin\Delta\lambda \\ y_p - ma\cos\varphi\cos\Delta\lambda \end{pmatrix}, \qquad \text{(J1-3-1)}$$

where (x_p, y_p) is the position of the north pole in the projected map, (φ, λ) the latitude and longitude, $\Delta\lambda$ the deflection of longitude from the standard longitude λ_0, and a the radius of the Earth (Fig. J1-3-1). The map factor, m, is defined by

$$m = \frac{1+\sin\varphi_0}{1+\sin\varphi}, \qquad \text{(J1-3-2)}$$

where φ_0 is the standard latitude and m is unity at $\varphi = \varphi_0$. For a position (x, y), the inverse transformation of (J1-3-1) is given by

$$\begin{pmatrix} \lambda \\ \varphi \end{pmatrix} = \begin{pmatrix} \lambda_0 + \tan^{-1}\dfrac{x-x_p}{y_p-y} \\ \sin^{-1}\dfrac{A^2-r^2}{A^2+r^2} \end{pmatrix}, \qquad \text{(J1-3-3)}$$

where

$$A = a(1+\sin\varphi_0), \qquad \text{(J1-3-4)}$$

$$r = \frac{y_p-y}{\cos\Delta\lambda}, \qquad \text{(J1-3-5)}$$

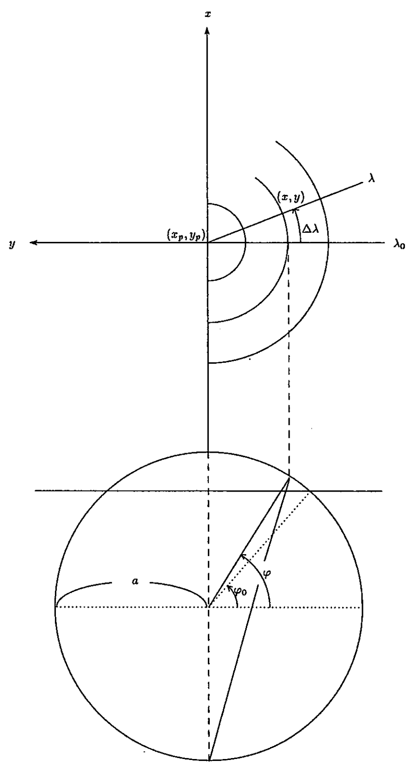

Fig. J1-3-1 Polar stereographic projection.

2) Lambert conformal projection

In a Lambert projection (Fig. J1-3-2), the horizontal coordinate (x, y) is given by

$$\begin{pmatrix} x \\ y \end{pmatrix} = \begin{pmatrix} x_p + \dfrac{m}{c} a \cos\varphi \sin c\Delta\lambda \\ y_p - \dfrac{m}{c} a \cos\varphi \cos c\Delta\lambda \end{pmatrix}, \tag{J1-3-6}$$

where

$$m = \left(\frac{\cos\varphi}{\cos\varphi_1}\right)^{c-1} \left(\frac{1+\sin\varphi_1}{1+\sin\varphi}\right)^{c}, \tag{J1-3-7}$$

and

$$c = \ln\left(\frac{\cos\varphi_1}{\cos\varphi_2}\right) / \ln\left\{\frac{\tan\left(\frac{\pi}{4}-\frac{\varphi_1}{2}\right)}{\tan\left(\frac{\pi}{4}-\frac{\varphi_2}{2}\right)}\right\}. \tag{J1-3-8}$$

The map factor m is unity at $\varphi=\varphi_1$ $(\pi/6)$ and $\varphi=\varphi_1$ $(\pi/3)$. c is about 0.72 when $\varphi_1=\pi/6$ and $\varphi_1=\pi/3$. The inverse transformation of (J1-3-6) is given by

$$\begin{pmatrix} \lambda \\ \varphi \end{pmatrix} = \begin{pmatrix} \lambda_0 + \dfrac{1}{c} \tan^{-1}\dfrac{x-x_p}{y_p-y} \\ \sin^{-1}\dfrac{B^2-r^2}{B^2+r^2} \end{pmatrix}, \tag{J1-3-9}$$

where

$$B = \frac{a(1+\sin\varphi_1)^{c}}{c(\cos\varphi_1)^{c-1}}, \tag{J1-3-10}$$

$$r = \frac{y_p - y}{\cos\{c(\lambda-\lambda_0)\}}. \tag{J1-3-11}$$

The polar stereographic projection (J1-3-1) to (J1-3-5) is a special case of $c=1$ in (J1-3-6) to (J1-3-11).

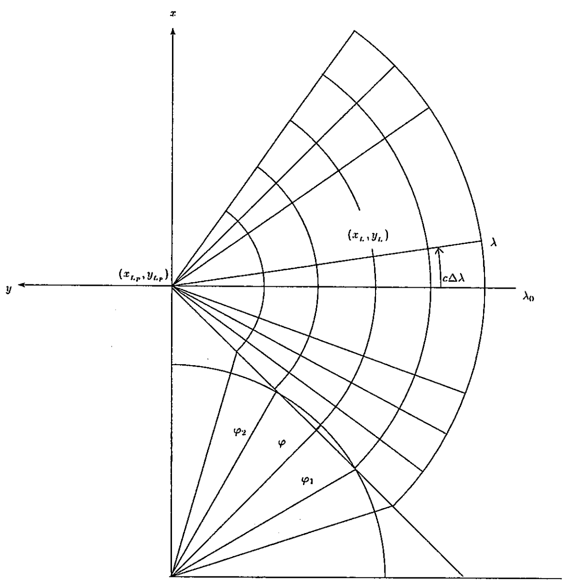

Fig. J1-3-2 Lambert conformal projection.

3) Mercator projection

In a Mercator projection (Fig. J1-3-3), the horizontal coordinate (x, y) is defined by

$$\begin{pmatrix} x \\ y \end{pmatrix} = \begin{pmatrix} x_o + a\cos\varphi_0 \Delta\lambda \\ y_o + a\cos\varphi_0 \ln\left(\dfrac{1+\sin\varphi}{\cos\varphi}\right) \end{pmatrix}, \tag{J1-3-12}$$

where (x_0, y_0) is the position of a point whose latitude and longitude are (0., λ_0) in the projected map. The map factor is given by

$$m = \frac{\cos\varphi_0}{\cos\varphi}. \tag{J1-3-13}$$

The inverse transformation of (J1-3-12) is given by

$$\begin{pmatrix} \lambda \\ \varphi \end{pmatrix} = \begin{pmatrix} \lambda_0 + \dfrac{x - x_0}{a\cos\varphi_0} \\ \sin^{-1}\dfrac{C-1}{C+1} \end{pmatrix}, \tag{J1-3-14}$$

where

$$C = e^{\frac{2(y-y_0)}{a\cos\varphi_0}}. \tag{J1-3-15}$$

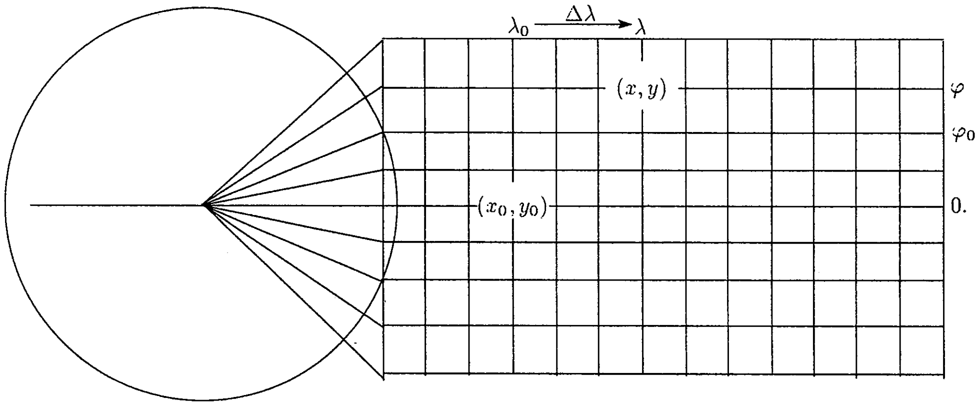

Fig. J1-3-3 Mercator projection.

J-2. File conversion for nesting with RSM

So far, the model has been used for several realistic simulations. The outer models that supply the initial and boundary conditions are the Japan Spectral Model of JMA (JSM) (Saito, 1994, 1997 ; Saito and Kato, 1996 ; Kato, 1996, 1998 ; Seino and Saito, 1999 ; Murata *et al.,* 1999), Regional Spectral Model of JMA (RSM) (Saito, 1996 ; Kato *et al.,* 1998 ; Eito *et al.,* 1999 ; Yoshizaki *et al.,* 2000) and Limited Area Assimilation and Prediction System of BMRC (LAPS) (Saito *et al.,* 2001a). Recently, Saito (2000) has tested nesting the nonhydrostatic model with Global Analysis data of JMA. In this section, we present the nesting utility for RSM as an example.

J-2-1 Input and output files

a. Input file from RSM

The following four files are required from RSM for file conversion for nesting. These files are obtained by running RSM. For details of the files and the 'GVS1' format, see the RSM user's guide (Goda, 1996).

File	Contents	Format	Remarks
RSM.HM	RSM's orography file	GVS1	
RFEB**Z	RSM's eta plane file	GVS1	forecast file
RF2M**Z	RSM's physical monitor	GVS1	forecast file
RASB**Z	RSM's surface file		

b. Temporary file

The following four temporary files are made by running 'readrsm' step. These files (NXO, NYO, NZO) may be smaller than RSM's original size (257,217,36) since they are cut out from RSM's output files according to the nonhydrostatic model domain.

File	Array	Content	Unit	Remarks
@rsm.org	ZS(NXO,NYO), SL(NXO,NYO)	Orography height Land coverage	m 0.01%	Cut out from RSM.HM
@rsm.gpv	RAINO(NXO,NYO), PSEA(NXO,NYO), PAIO(NXO,NYO), UO(NXO,NYO,NZO), VO(NXO,NYO,NZO), TO(NXO,NYO,NZO), QVO(NXO,NYO,NZO)	Accumulated rain Sea-level pressur Surface pressure x-direction wind y-direction wind Temperature Water vapor	mm Pa m/s m/s K Kg/Kg	Cut-out from RFEB**Z
@rsm.sfc	SSTO(NXO,NYO), TINO(NXO,NYO,4)	sea surface temp. ground temperature		cut-out from RASB**Z
@rsm.phy	WETO(NXO,NYO), KINDO(NXO,NYO), ROUGHO(NXO,NYO), TINO(NXO,NYO,4)	wetness land use roughness length ground temperature	0.01% --- m K	cut-out from RF2M**Z

c. Other file

The real orography file for nonhydrostatic model as in J-1-1 is required.

File Name	Array	Content	Unit	Remarks
org**	see J-1-1	see J-1-1	···	···

d. output file

File Name	Array	Content	Unit	Remarks
uvptq**	PSEAM, PTOPM, IDATE(5), U(NX,NY,NZ), V(NX,NY,NZ), W(NX,NY,NZ), PT(NX,NY,NZ) QV(NX,NY,NZ) PTGRD(NX,NY), PTGRDT(NX,NY), PTSEA(NX,NY), PAI(NX,NY), TIN(NX,NY,4)	mean sea level pressure mean model top pressure date x-direction wind y-direction wind z-direction wind potential temperature (θ) water vapor θ at ground (θ_g) time tendency of θ_g θ at sea surface (θ_s) surface pressure ground temperature	Pa Pa ··· m/s m/s m/s K Kg/Kg K K/s K Pa K	

ptgrd**	IDATE(5), WET(NX,NY), FKTG(NX,NY), ROCTG(NX,NY), ALBED(NX,NY)	date (yy/mm/dd/hh/wk) wetness heat diffusion heat capacity surface albedo	 0.01% m^2/s^4 $J/K/m^3$ 0.01%	
org**.x	see J-1-1	see J-1-1	…	…
sst**	SSTI(NX,NY,4)	sea surface temperature	K	
newfl**.ps	Post Script file	for monitor		

J-2-2 Flowchart of Jobstep 2.

Main program of Jobstep 2 is in srcenv/newflrsm***.f*. The job flow is as follows:

a. Setting parameter

b. Declare arrays, common variables.

c. Set model constants and definition of graphic environments

d. Read RSM orography and surface files (@rsm.org, @rsm.sfc)

e. Set outer model projection

LATLON, REVERSE

g. Define NHM model grids

VRGDIS, SETXRP, SETXRU, SETZRP, SETZRW

f. Read NHM orography file (org**) and setting of NHM model projection

MAPJPN, PRJCT2, RLTLN

g. Interpolate RSM orography and make adjusted NHM orography (org**.x)

NINTR2D, ZSTRNS3

h. Store adjusted NHM orography and surface file (ptgrd**)

NINTR2D, STORTG

do KT=KTST, KTEN

i. Read RSM's forecast file (@rsm.gpv, @rsm.phy)

REVERSE

j. Compute height of eta planes

PHICAL

k. Compute mean pressure at top of NHM

l. horizontal interpolation of RSM's forecast

NINTR2D

m. Adjust ground temperature

n. interpolation of RSM's forecast into NHM grids

INTERJ, NINTRP, NTRANSG

o. Store interpolated value (uvptq**)

STORUV

end do

J-2-3 Subroutine list of Jobstep 2.

Following subroutines are included in each member. Subroutines in the member 'nflutnpd2.f' are developed by the Numerical Prediction Division of JMA.

a. nflutlty2.f :

STORUV : store interpolated values to the file uvptq**

INTERJ : vertical interpolation

NINTRP : three dimensional interpolation

NINTRPT : three dimensional interpolation for θ

INTERZ : vertical interpolation for θ

NINTR2D : horizontal interpolation

VRGDIS : set variable grid distances

SETXRP : set absolute position of scalar points

SETXRU : set absolute position of vector points (U and V)

SETZRP : set height of full level

SETZRW : set height of half level

ZSTRNS3 : adjust NHM orography

REVERSE : change arrays' order in the y-direction

NTRANSG : rotate interpolated model's horizontal wind direction

LOADMT : load grid point values from NHM's output file

STORTG : store ground surface data to ptgrd**

b. nflutplt1.f :

PLTLO2 : plot latitude and longitude lines

PLTLN2 : plot projected lines

PCONTSL : plot contour with coast lines

c. nflutnpd2.f :

LATLON : compute latitude and longitude of each grid of RSM

LLTOIJ : compute RSM grid point from latitude and longitude

RLTLN : compute RSM grid position from latitude and longitude

PHICAL : compute height from pressure and temperature

SPLINX : Spline interpolation

J-3. Plot job

Source program of the plot job is in the directory ../srcplt. Basically the job is similar to that described in Chapter E of Ikawa and Saito (1991), while multi images and shade pattern are supported, and a postscript file is made. For the detail of parameter setting, see Section K.

J-3-1 Model output file (1)

In Job Step 3, STRMTS outputs grid point values of the model integration. The format is as follows. They can be selectively output according to parameter card file KDD (see K-4-3). An economical, compressed file can also be output by STRMTS2.

Record	Output	Contents of GPV
REC.1	ITDT, KD(1), U	x-direction momentum
REC.2	ITDT, KD(2), V	y-direction momentum
REC.3	ITDT, KD(3), W	z-direction momentum
REC.4	ITDT, KD(4), PT, TIN	potential temperature, ground temperature (4 layers)
REC.5	ITDT, KD(5), QV	mixing ratio of water vapor
REC.6	ITDT, KD(6), QC, QM	mixing ratio of cloud water, cloud amount
REC.7	ITDT, KD(7), QR	mixing ratio of rain
REC.8	ITDT, KD(8), ETURB	turbulent kinetic energy
REC.9	ITDT, KD(9), EDDYKM, EDDYKH, DLEN	eddy diffusion coefficients for momentum and heat mixing length
REC.10	ITDT, KD(10), PRS, PSEA, PTOPAV, SMQR, SMQS, SMQH	pressure, sea level pressure, average pressure at model top, accumulated rain, snow and graupel
REC.11	ITDT, KD(11), PQV, PQCW, PPT	production term of water vapor and cloud water, tendency of potential temperature
REC.12	ITDT, KD(12), PQR, PQCI	production term of rain and cloud ice
REC.13	ITDT, KD(13), QCI	mixing ratio of cloud ice
REC.14	ITDT, KD(14), QS	mixing ratio of snow
REC.15	ITDT, KD(15), QH	mixing ratio of graupel
REC.16	ITDT, KD(16), PQS, PQH	production term of snow and graupel
REC.17	ITDT, KD(17), DNSG2, ZS, SL	density*$G^{1/2}$ ground height, land coverage rate
REC.18	ITDT, KD(18), CPHU, CPHV	phase velocity of gravity wave for x- and y- directions
REC.19	ITDT, KD(19), QNCI	number density of cloud ice
REC.20	ITDT, KD(20), QNS	number density of snow

J-3-2 Model output file compressed by using integer*2

The subroutine of STRMTS2 outputs a compressed result file. With this file the plot job illustrated in subsection K-5-2 can be used conveniently. Output kinds can be selected according to the parameter card file KDD (see, K-4-3). The output file produced in the restart run does not make REC.1-REC.10+NZ.

Record	Output	Contents of GPV
REC.1	DT,DX,DY,DZ,PTRF,PRESRF,ZRP,ZRW,ISTRMT, IDATE,KTSTO,STDLAT,N1,C1,N2,C3,C4,C5,CO	Refer to the following remarks
REC.2	(I*4) 0, (C*5) 'ZS', (I*4) 1	Height of terrain
REC.3	(R*4) WMAX,WMIN, (I*2) ZS	
REC.4	(I*4) 0, (C*5) 'SL', (I*4) 1	Sea-land parameter
REC.5	(R*4) WMAX,WMIN, (I*2) SL	
REC.6	(I*4) 0, (C*5) 'FLAT', (I*4) 1	Latitude
REC.7	(R*4) WMAX,WMIN, (I*2) FLAT	
REC.8	(I*4) 0, (C*5) 'FLON', (I*4) 1	Longitude
REC.9	(R*4) WMAX,WMIN, (I*2) FLON	

REC.10	(I*4) 0, (C*5) 'PAIRF', (I*4) NZ	Base of Exner function
REC.11	(R*4) WMAX,WMIN, (I*2) PAIRF(,,1)	
REC.10+NZ	(R*4) WMAX,WMIN, (I*2) PAIRF(,,NZ)	
	(I*4) 1, (C*5) CMSYS, (I*4) NZ	Predicted values of 'F' at 1-th time step
REC.I1	(R*4) FMAX,FMIN, (I*2) F(,,1)	
REC.I1+NZ	(R*4) FMAX,FMIN, (I*2) F(,,NZ)	
	(I*4) 1, (C*5) 'END', (I*4) 0	End of output at 1-th time step
	(I*4) ISTRMT, (C*5) CMSYS, (I*4) NZ	Predicted values of 'F' at *ISTRMT*-th time step
REC.I2	(R*4) FMAX,FMIN, (I*2) F(,,1)	
REC.I2+NZ	(R*4) FMAX,FMIN, (I*2) F(,,NZ)	
	(I*4) ISTRMT, (C*5) 'END', (I*4) 0	End of output at *ISTRMT*-th time step
	(I*4) ISTRMT*J, (C*5) CMSYS, (I*4) NZ	Predicted values of 'F' at *ISTRMT***J*-th time step
REC.I*	(R*4) FMAX,FMIN, (I*2) F(,,1)	
REC.I*+NZ	(R*4) FMAX,FMIN, (I*2) F(,,NZ)	
	(I*4) ISTRMT*J, (C*5) 'END', (I*4) 0	End of output at *ISTRMT***J*-th time step

Here (I*4) denotes integer*4, (I*2) integer*2, (R*4) real*4, and (C*5) character*5. The compressed formula is

```
REAL*4 F4(*),FMAX,FMIN
INTEGER*2 F(*)
WD=(FMAX-FMIN)/64000.0
F(,)=NINT((F4(,)-FMIN)/WD-32000.0).
```

(J3-2-1)

Remark)

Name	Type	Meaning	Name	Type	Meaning
DT	R*4	Time step interval	DX	R*4	x-direction grid distance
DY	R*4	y-direction grid distance	DZ	R*4	z-direction grid distance
PTRF	R*4	base of potential temperature	PRESRF	R*4	base of pressure for Exner function
ZRP(NZ)	R*4	vertical levels except vertical velocity	ZRW (NZ)	R*4	vertical levels of vertical velocity
ISTRMT	I*4	time step interval of GPV output, date	IDATE (5)	I*4	Date (year, month, day, hour, day of the week)
KTSTO	I*4	Start time of nesting file	STDLAT	R*4	standard latitude
N1	I*4		N2	I*4	
C1(N1)	C*5	Name list of predicted values	C3(N2)	C*5	Name list of predicted values
C4(N2)	C*5	Name list of predicted values	C5(N2)	C*5	Name list of predicted values
CO(N2)	C*5	Name list of predicted values			

K. User's guide to running the model

K-1. Getting started

The UNIX combined model environment is supplied by a tar file *mrinpd.tgz* To decompress and expand the code, type the following commands:

gzip -cd *mrinpd.tgz* | tar -xvf -

The following subdirectories are found in the directory *mrinpd***.

shl** : unix shell script

srcenv : source program for environment settings

src** : source program for model run

srcplt : source program for plot job (1)

card : parameter card to control jobs

data : data file for radiation, etc.

shlplt2 : unix shell script for plot job (2)

srcplt : source program for plot job (2)

@data : temporary dataset to store output data

@src997lib : temporary dataset to store object modules

K-2. Setting the orography file

K-2-1 Simple orography for ideal test

The Unix shell for preparing a simple orography file for an ideal test is in shl**/#orbel**. The following is an example of the shell script (shl997/#orbel32an) for model size (32,32,NZ).

```
cd srcenv
echo'     PARAMETER (NX=32,NY=32)'>zsize.h
f90 -o org3232.out org3dm.f
  org3232.out<<EOF
  &NAMORG
  IXTST=1,IXTEN=32,JYMST=1,JYMEN=32,XCENT=16.5,YCENT=16.5,
  PWX=3.0,PWY=3.0,ZTOP=100.0,THETA=0.0,LTBDRY=0,
  FLAT=0., FLON=140., FZLAND=0.1
  &END
  &NAMSST
  PTGRDS=288.3
  &END
  &NAMPRJ
  NPROJC='DES'
  &END
EOF
mv fort.50 ../@data/org.bell32an
```

The namelists as the input parameter are as follows:

1) Namelist &NAMORG

Name	Type	Meaning	Default	remarks
IXTST	int	start number for x-direction	1	
IXTEN	int	end number for x-direction	NX	

Name	Type	Meaning	Default	remarks
JYMST	int	start number for y-direction	1	
JYMEN	int	end number for y-direction	NX	
XCENT	real	location of mountain top in x-direction	NX/2	x_0 in (J1-2-1)/Δx
YCENT	real	location of mountain top in y-direction	NY/2	y_0 in (J1-2-1)/Δy
PWX	real	half width in x-direction	···	a in (J1-2-1)/Δx
PWY	real	half width in y-direction	···	b in (J1-2-1)/Δy
ZTOP	real	mountaintop height	···	h_m in (J1-2-1)
THETA	real	angular of rotation	0.	no other choice
LTBDRY	real	lateral boundary condition	0	1 : cyclic for x-direction 2 : cyclic for x- and y-directions
FLAT	real	latitude (degree)	0.0	
FLON	real	longitude (degree)	140.0	
FZLAND	real	roughness length (m)	0.1	

2) Namelist &NAMSST

Name	Type	Meaning	Default	remarks
PTGRDS	real	potential temperature at sea surface (K)	---	not used in ordinary setting

3) Namelist &NAMPRJ

Name	Type	Meaning	Default	remarks
NPROJC	c*4	map projection	'DES'	Descart coordinate

The output file is stored in @data/org.bell** (fort.50), and its format is described in J-1-1.

K-2-2 Real orography for arbitrary conformal projection

Setting of the real orography file is performed using gtopo30 dataset. To decompress and expand the dataset, type the following commands:

gzip -cd *mrinpd.tgz* | tar -xvf -

In the directory *gtopo30*, *step2.dx10.sh* is a sample shell script for 10 km resolution real orography around Kyushu.

```
step2 -F'PORT(STDUF)'<domain.card.LMN102.dx10
mv fort.80 ../mrinpd997/@data/org.kyushu.102dx10
```

Here, domain.card specifies namelist for orography information such as the domain size, horizontal resolution, map projection, *etc*..

```
&NAMDOM
  NX= 102
  NY= 102
  NPROJC='LMN'
  DX= 10000.
  DY= 10000.
  SLAT= 32.5
  SLON= 140.
  FLATC= 32.5
```

```
  FLONC= 130.5
  XI= 61.
  XJ= 165.
  XLAT= 30.
  XLON= 140.
&END
```

The contents of the namelist is as follows:

1) Namelist &NAMDOM

Name	Type	Meaning	Default	remarks
NX	int	model array size x-direction		…
NY	int	model array size y-direction		…
NPROJC	c*4	map projection	…	'PSN': Polar stereo 'LMN': Lambert 'MER': Mercator
DX	real	data resolution x-direction (m)	…	
DY	real	data resolution y-direction (m)	…	
SLAT	real	standard latitude	…	φ_0 in J1-3-2
SLON	real	standard longitude	…	λ_0 in J1-3-1
FLATC	real	latitude of map's center	…	
FLONC	real	longitude of map's center	…	
XI	int	grid number x-direction of (XLAT,XLON)	…	dummy if FLATC is specified
XJ	real	grid number y-direction of (XLAT,XLON)	…	dummy if FLATC is specified
XLAT	real	latitude of standard point	…	dummy if FLATC is specified
XLON	real	Longitude of standard point	…	dummy if FLATC is specified

A temporary file is output in mrinpd**/@data/org.kyushu102.dx10 (fort.80), whose format is same as in J-1-1. By running shlplt2/zsls.sh, a postscript file can be made in @data/zs.ps (fort.60) to monitor the model domain. Figure K2-2-1 shows the domain and orography made in the example shell script.

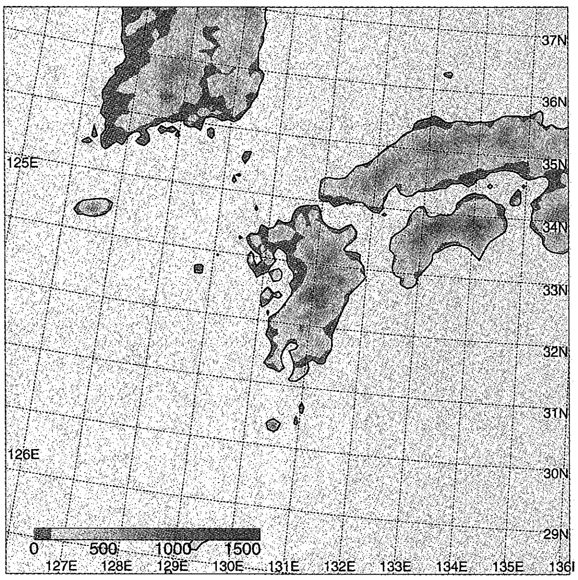

Fig. K2-2-1 Domain and orography produced in the example shell script in K-2-2.

K-3. File conversion for nesting

K-3-1. Nesting with RSM

The Unix shell for file conversion for nesting with RSM is in ../shl/#nflrsm**. The following is an example of the shell script (shl997/#nflmprsm) for model size (102,102,38).

```
echo '#*----- Compile -----'
setenv DATE y9906.d2500
  cd srcenv
  f90 -O3 -c nflutlty2.f nflutplt1.f nflutnpd2.f
echo'  PARAMETER (NX=102,NY=102,NZ=38)'>mdlsize.h
  f90 -O3 nflmprsm.f nflutlty2.o nflutplt1.o nflutnpd2.o ../srcplt/nflutplt2.o ..
/srcplt/plotpswk.o -o nflmprsm102.out
cd ..
echo '#*----- convert to Arakawa-C, z* coordinate -----'
rm fort.*
ln -s  @data/@rsmdata.org fort.10
ln -s  @data/@rsmdata.gpv fort.11
ln -s  @data/@rsmdata.sfc fort.12
ln -s  @data/@rsmdata.phy fort.13
ln -s  data/MAPJPN fort.43
ln -s  @data/org.kyushu.102dx10 fort.51
ln -s  data/PSDATA fort.9
srcenv/nflmprsm102.out <<EOF
  &NAMMAPO
  SCALE=3000.,FLSTP=10.,XSW=20.,YSW=20.
  &END
  &NAMMAPI
  FLATSI=25.5, FLATNI=39.5, FLONWI=125.0, FLONEI=140.5, SCALEI=1000.,
  SLONI=140., SLATI=32.5, FLSTPI=2., XSWI=20., YSWI=20., IFILEI=51,
  NPROJC='LMN'
  &END
  &NAMORGI
  FLATC=32.5, FLONC=130.5, DX=10000., DY=10000.,
  THI=0., NXIN=102, NYIN=102, IWDTH=5, IMERG=5, GRMAX=0.15
  &END
  &NAMGRDI
  DXI=10000., DX1I=10000., DX2I=10000., IX1I=10, IX2I=20,
  DYI=10000., DY1I=10000., DY2I=10000., IY1I=10, IY2I=20,
  DZI=1120., DZ1I=40., DZ2I=1120., IZ1I=38, IZ2I=38
  &END
  &NAMNEST
  KTST=9, KTEN=15, KTDEL=3,
  &END
EOF
mv fort.23 @data/uvptq.102.$DATE
mv fort.25 @data/ptgrd.102.$DATE
```

The dataset @rsm** are obtained by running shl997/#readrsm, and their format is described in J-2-1. The namelists as the input parameter are as follows:

1) Namelist &NAMMAPO

This namelist defines the map to show the forecast of RSM.

Name	Type	Meaning	Default	remarks
SCALE	real	scale of map projection	···	

Name	Type	Meaning	Default	remarks
XSW	real	x position of under-left of map	…	
FLSTP	real	interval for depict latitude and longitude lines	…	
YSW	real	y position of under-left of map	…	

2) Namelist &NAMMAPI

This namelist defines the map to show the domain of NHM.

Name	Type	Meaning	Default	remarks
FLATSI	real	latitude of under-left of map	…	
FLATNI	real	latitude of upper-right of map	…	
FLONWI	real	longitude of under-left of map	…	
FLONEI	real	longitude of upper-right of map	…	
SCALEI	real	scale of map projection	…	
SLONI	real	standard latitude	…	φ_0 in J1-3-2
SLATI	real	standard longitude	…	λ_0 in J1-3-1
FLSTPI	real	interval for depict latitude and longitude lines	…	
XSWI	real	x position of under-left of map	…	
YSWI	real	y position of under-left of map	…	
IFILEI	int	device number for output file	51	
NPROJC	c*4	map projection	…	'PSN': Polar stereo 'LMN': Lambert 'MER': Mercator

3) Namelist &NAMORGI

This namelist transfers domain information of the NHM orography. The parameter values must be consistent with the namelist NAMORG of the orography setting.

Name	Type	Meaning	Default	remarks
FLATC	real	center latitude (degree)		
FLONC	real	center longitude (degree)		
DX	real	x-direction resolution (m)	…	
DY	real	y-direction resolution (m)	…	
THI	real	angular of rotation	0.	no ther choice
NXIN	int	model array size in x-direction	NX	
NYIN	int	model array size in y-direction	NY	
IWIDTH	int	width of rim to use the RSM orography	>4	
IMERG	int	width of rim to merge the RSM orography	>4	
GRMAX	real	maximum steepness of orography		

4) Namelist &NAMGRDI

This namelist is to define the grid structure of NHM.

Name	Type	Meaning	Default	remarks
DXI	real	x-direction grid distance (m)		
DX1I	real	x-direction left-most grid distance (m)	DXI	Dx_l in D-4 in Ikawa and Saito (1991)
DX2I	real	x-direction right-most grid distance (m)	DXI	Dx_r in D-4 in Ikawa and Saito (1991)
IX1I	int	start index for constant grid distance (x-direction)	…	i_l in D-4 in Ikawa and Saito (1991)
IX2I	int	start index for constant grid distance (x-direction)	…	i_r in D-4 in Ikawa and Saito (1991)
DYI	real	y-direction grid distance (m)		
DY1I	real	y-direction left-most grid distance (m)	DYI	
DY2I	real	x-direction rihgt-most grid distance (m)	DYI	
IY1I	int	start index for constant grid distance (y-direction)	…	
IY2I	int	start index for constant grid distance (y-direction)	…	
DZI	real	z-direction grid distance	…	
DZ1I	real	grid distance at lowest level (m)	…	
DZ2I	real	grid distance at highest level (m)	DZI	
IZ1I	int	start index for constant grid distance (z-direction)	1	
IZ2I	int	end index for constant grid distance (z-direction)	NZ	

5) Namelist &NAMNEST

This namelist defines the period of the nesting run.

Name	Type	Meaning	Default	remarks
KTST	int	Start time of nesting in terms of the forecast time of RSM	…	
KTEN	int	End time of nesting	…	
KTDEL	int	Time interval of RSM GPV	3	

A postscript file is made in @data/nflmprsm.ps (fort.60) to monitor the file conversion. Figure K3-1-1 indicates the domain and orography of RSM and the nonhydrostatic model for the sample shell script. Figure K3-1-2 shows the RSM forecast at KT=12 and for monitoring the file conversion.

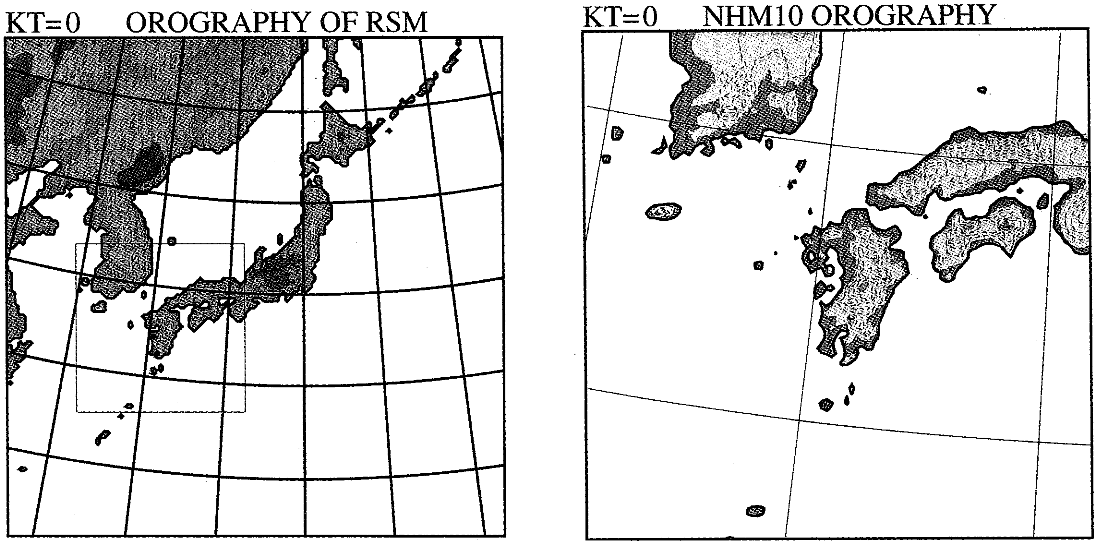

Fig. K3-1-1 Domain and orography of NHM monitored in the file conversion.

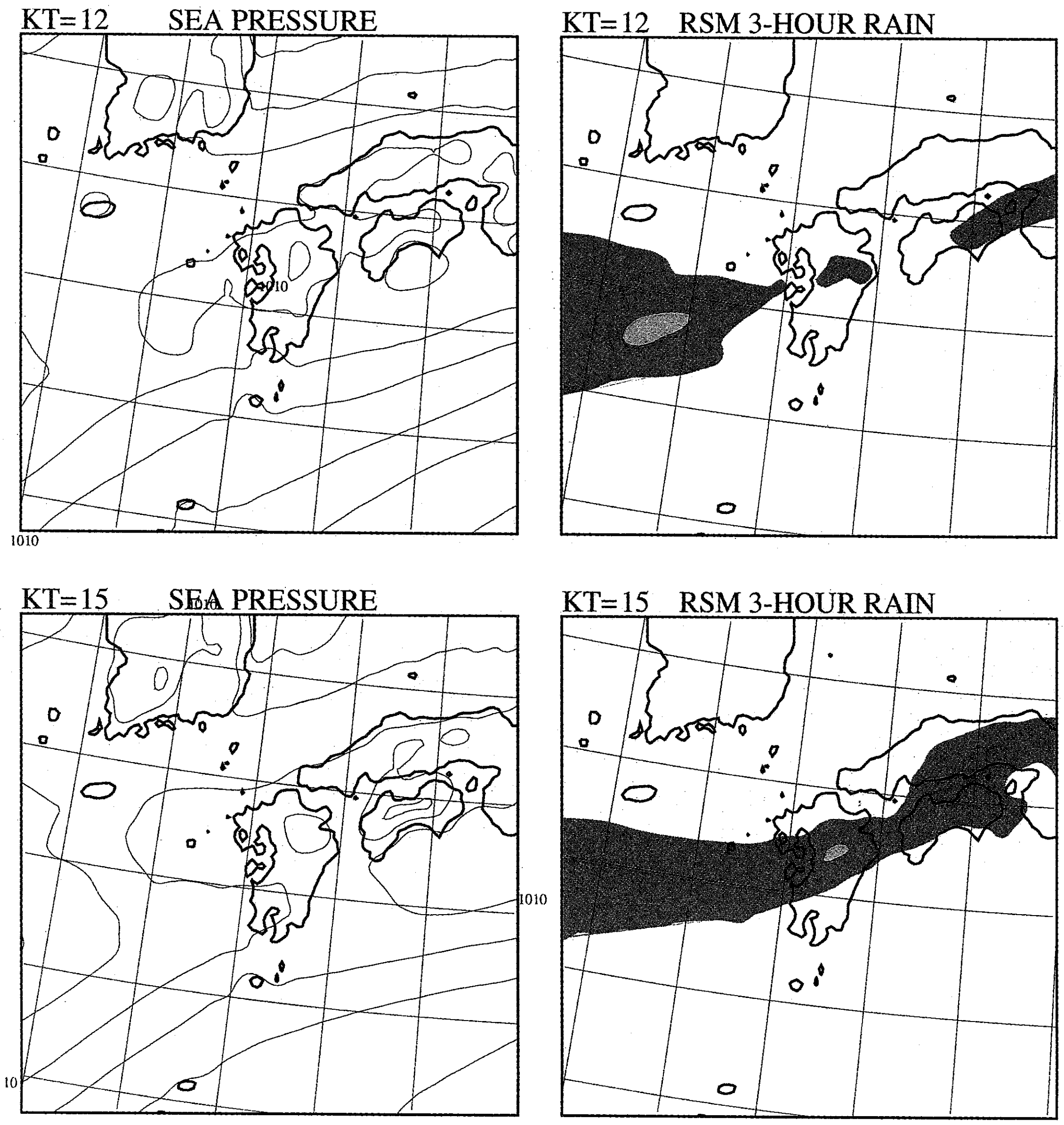

Fig. K3-1-2 RSM forecast (surface pressure and three-hour precipitation) at 1200 UTC and 1500 UTC 1999 Jun 25 for monitoring.

K-3-2. Self-nesting

A Unix shell of file conversion for self-nesting is also prepared (shl997/#nflmpnhm) ; it converts the model output files J-3-1 or J-3-2 to the boundary file described in J-2-1-d. This utility is available for double- or triple-nesting with RSM as well as a nesting run within the stand-alone run of the nonhydrostatic model.

K-4. Model run

K-4-1. Stand alone run

An example of the shell script for 2 km resolution linear mountain waves (shl997/#glmwv3232) is as follows.

```
echo '#### Compile started ####'
cd src997-2000
  mv ../@src997lib/*.o .
  cp prm.inc32 prm.inc
  rm mainy2.o comm.o wrtfct.o subhevi.o
make
mv*.o ../@src997lib
mv a.out ../@src997lib/main32.out
#------------------------------------------------------------
cd ..
rm fort.50
ln -s @data/org.bell32an fort.50
echo '#### Time integration started ####'
time @src997lib/main32.out<card/LMWV32HI
# time @src997lib/main32.out<card/LMWV32HE
  mv fort.8 @data/strmts2.list
  mv fort.62 @data/strmts2.lmwv.file1
echo '#### Time integration end ####'
  rm fort.*
```

The control parameter card (card/LMWV32HI) for above example is as follows:

```
3-DIM SIMULATION OF STEADY-STATE LINEAR MOUNTAIN WAVE OVER A
BELL-SHAPED MOUNTAIN
NX,NY,NZ=32,32,32, DX=2000.0M, DZ=40 - 1240M OPEN BOUNDARY CONDITION
  &NAMMSW
  MSWSYS( 1)=0, MSWSYS( 2)=1, MSWSYS( 3)=2, MSWSYS( 4)=2, MSWSYS( 5)=2,
  MSWSYS( 6)=-1,MSWSYS( 7)=1, MSWSYS( 8)=0, MSWSYS( 9)=3, MSWSYS(10)=0,
  MSWSYS(11)=0, MSWSYS(12)=2, MSWSYS(13)=0, MSWSYS(14)=0, MSWSYS(15)=2,
  MSWSYS(16)=0, MSWSYS(17)=2, MSWSYS(18)=2, MSWSYS(19)=0, MSWSYS(20)=1,
  MSWSYS(21)=0, MSWSYS(22)=0, MSWSYS(23)=0, MSWSYS(24)=0, MSWSYS(25)=0,
  MSWSYS(26)=0, MSWSYS(27)=0, MSWSYS(28)=0, MSWSYS(29)=0, MSWSYS(30)=0
  &END
  &NAMPAR
  ITST= 1, ITEND=120, ISTRMT=30, ISTRRS=1000, ITOUT=5000, ITCHK=5000,
  DT=30.0, DX=2000.0, DY=2000.0, DZ=1240.0, PTRF=300.0, PRESRF=100000.0
  &END
  &NAMGRD
  DXL=2000.0, DXR=2000.0, IX1=20,I X2=40, DYL=2000.0, DYR=2000.0,
  IY1=20, IY2=40, DZL=40.0, DZR=1240.0, IZ1=32, IZ2=32
  &END
  &NAMVAL
  RATIOI=0.5, RATIOO=0., RATIO2=0., RUVNI=0.5, RUVNO=0., RUVN2=0.,
  FNLTR=0.0, IDIFX=0, DIFNL=0.0, DIF2D=60.0, ASTFC=0.2,
  STDLON=140.0, STDLAT=0.0, KZDST=24, KZDEN=32,
```

```
  RLDMPX=0.0, RLDMPZ=30.0, RLDMPO=0.0,
  PTGRDS=288.3, PTGRDR=0.0, PTGRDL=0.0,
  ITGROW=0, UBIAS=0.0, VBIAS=0.0, ITSST=0, EOVER=0.5
  &END
  &NAMNST
  KTSTO=6, KTENO=12, KTDTO=3, DTRATIO=3600.,
  ALPHA=0.5, ITRMX=20000, RLXCON=1.0E-4, OVERLX=1.8
  &END
  &NAMRAD
  DTRADS=300.0
  &END
  &NAMPTG
  DAY0=90.0, GTIME0=0.0, ALBEDL=0.2, ALBEDS=0.6, WETL=0.1, WETS=1.0
  &END
  IN      Z(M)    U(M/S)    V(M/S)     PT(K)    RH(%)   QC(G/KG)   QR(G/KG)
   1       0.0       8.0       0.0     288.3      0.0        0.0        0.0
   2    3900.0       8.0       0.0     300.0      0.0        0.0        0.0
   3   11900.0       8.0       0.0     324.0      0.0        0.0        0.0
   4   19900.0       8.0       0.0     348.0      0.0        0.0        0.0
   5   20100.0       8.0       0.0     348.6      0.0        0.0        0.0
99
  &NAMKDD
  KDD( 1)=1, KDD( 2)=1, KDD( 3)=1, KDD( 4)=2, KDD( 5)=1,
  KDD( 6)=0, KDD( 7)=0, KDD( 8)=0, KDD( 9)=0, KDD(10)=1,
  KDD(11)=0, KDD(12)=0, KDD(13)=0, KDD(14)=0, KDD(15)=0,
  KDD(16)=0, KDD(17)=1, KDD(18)=0, KDD(19)=0, KDD(20)=0,
```

The control parameter card (card/LMWV32HE) is an alternative card for HE-VI scheme, where MSWSYS(15)=1 and MSWSYS(20)=2 are set instead of MSWSYS(15)=2 and MSWSYS(20)=1.

K-4-2. Nesting run with RSM

Following is an example of the shell script (shl997/#grsm10238) for nesting run with RSM by model size (102, 102, 38).

```
#  nesting simulation with RSM (102,102,38)
unlimit datasize
unlimit stacksize
setenv DATE y9906.d2500
echo '#### Compile started ####'
cd src997-2000
  mv ../@src997lib/*.o .
  cp prm.inc102 prm.inc
  rm mainy2.o comm.o wrtfct.o subhevi.o
make
  mv*.o ../@src997lib
  mv a.out ../@src997lib/main102.out
cd ..
#------------------------------------------------------------
  rm fort.*
ln -s  @data/uvptq.102.$DATE fort.23
ln -s  @data/ptgrd.102.$DATE fort.25
ln -s  @data/org.102dx10.$DATE fort.50
ln -s  data/BANDCNX fort.90
echo '#### Time integration started ####'
time @src997lib/main102.out<card/RSM10238
```

```
#time @src997lib/main102.out<card/RSM102HE
  mv fort.62 @data/rsm102dx10.$DATE
#
echo '#### END ####'
  rm fort.*
```

The example of the control parameter card (card/RSM10238) for nesting is as follows:

```
MRI/NPD UNIFIED NONHYDROSTAIC MODEL NESTING RUN
10 KM RESOLUTION WITH REAL OROGRAPHY
NX,NY,NZ=102,102,38, DX=10000.0M, DZ=40 - 1120M, NESTING WITH RSM20
 &NAMMSW
 MSWSYS( 1)=1, MSWSYS( 2)=1, MSWSYS( 3)=2, MSWSYS( 4)=2, MSWSYS( 5)=2,
 MSWSYS( 6)=-2,MSWSYS( 7)=1, MSWSYS( 8)=1, MSWSYS( 9)=3, MSWSYS(10)=0,
 MSWSYS(11)=0, MSWSYS(12)=7, MSWSYS(13)=8, MSWSYS(14)=0, MSWSYS(15)=2,
 MSWSYS(16)=0, MSWSYS(17)=2, MSWSYS(18)=1, MSWSYS(19)=0, MSWSYS(20)=1,
 MSWSYS(21)=1, MSWSYS(22)=0, MSWSYS(23)=2, MSWSYS(24)=0, MSWSYS(25)=1,
 MSWSYS(26)=2, MSWSYS(27)=0, MSWSYS(28)=0, MSWSYS(29)=0, MSWSYS(30)=0
 &END
 &NAMPAR
 ITST=1, ITEND=1080, ISTRMT=540, ISTRRS=1621, ITOUT=5000, ITCHK=5000,
 DT=20.0, DX=10000.0, DY=10000.0, DZ=1120.0, PTRF=300.0, PRESRF=100000.0
 &END
 &NAMGRD
 DXL=10000.0, DXR=10000.0, IX1=20, IX2=40, DYL=10000.0, DYR=10000.0,
 IY1=20, IY2=40, DZL=40.0, DZR=1120.0, IZ1=38, IZ2=38
 &END
 &NAMVAL
 RATIOI=1.0, RATIOO=0.5, RATIO2=0.5, RUVNI=1.0, RUVNO=0.5, RUVN2=0.5,
 FNLTR=0.0, IDIFX=10, DIFNL=150.0, DIF2D=60.0, ASTFC=0.2,
 STDLON=140.0, STDLAT=32.5, KZDST=30, KZDEN=38,
 RLDMPX=60.0, RLDMPZ=60.0, RLDMPO=0.0,
 PTGRDS=288.3, PTGRDR=0.0, PTGRDL=0.0,
 ITGROW=0, UBIAS=0.0, VBIAS=0.0,I TSST=0,E OVER=0.5
 &END
 &NAMNST
 KTSTO=09, KTENO=15, KTDTO=3, DTRATIO=3600.,
 ALPHA=0.5, ITRMX=20000, RLXCON=3.0E-4, OVERLX=1.8
 &END
 &NAMRAD
 DTRADS=300.0
 &END
 &NAMPTG
 DAY0=90.0, GTIME0=0.0, ALBEDL=0.2, ALBEDS=0.6, WETL=0.1, WETS=1.0
 &END
 IN      Z(M)    U(M/S)    V(M/S)     PT(K)     RH(%)  QC(G/KG)  QR(G/KG)
  1       0.0       8.0       0.0     288.3       0.0       0.0       0.0
  2    3900.0       8.0       0.0     300.0       0.0       0.0       0.0
  3   11900.0       8.0       0.0     324.0       0.0       0.0       0.0
  4   19900.0       8.0       0.0     348.0       0.0       0.0       0.0
  5   20100.0       8.0       0.0     348.6       0.0       0.0       0.0
99
 &NAMKDD
 KDD( 1)=1, KDD( 2)=1, KDD( 3)=1, KDD( 4)=2, KDD( 5)=1,
 KDD( 6)=1, KDD( 7)=1, KDD( 8)=0, KDD( 9)=0, KDD(10)=1,
 KDD(11)=0, KDD(12)=0, KDD(13)=0, KDD(14)=0, KDD(15)=0,
 KDD(16)=0, KDD(17)=1, KDD(18)=0, KDD(19)=0, KDD(20)=0,
```

```
KDD(21)=0, KDD(22)=0, KDD(23)=0, KDD(24)=0,
KDD(25)=0, KDD(26)=0
&END
```

K-4-3. Control parameter card

The specification of model run can be controlled by the control parameter card. Its contents are as follows.

1) First three lines (3A80) in the control parameter card are for user's comments.

2) Namelist &NAMMSW

This namelist sets the mode switch for basic condition of the model.

	Meaning	Value	Contents	Remarks
MSWSYS(1)	Lower boundary condition for momentum flux	0	free-slip	
		1	non-slip	
MSWSYS(2)	out flow lateral boundary condition for normal wind	1	Orlanski-type	no other choice
MSWSYS(3)	eigen function	0	read stored file	
		1	make by Jacobi method	for variable grid
		2	make using tri-gonometrical function	for uniform grid distance
MSWSYS(4)	out flow lateral boundary condition for wind component parallel to the boundary	0	use the value at inner closest point	
		1	Orlanski-radiation condition	
		2	extrapolate for space and time	
MSWSYS(5)	lateral boundary condition for turbulent energy and vari-ables in cloud physics	0	use the value at inner closest point	
		1	Orlanski-radiation condition	
		2	extrapolate for space and time	
MSWSYS(6)	Definition of density ($\rho G^{1/2}$)	-2	fully compressible (consider map factor)	
		-1	fully compressible	
		0	use the value of the reference atmosphere	anelastic/quasi-compressible
		1	Bousinesq approximation	
MSWSYS(7)	computation of wind at lateral boundary	1	time integration	no other choice
MSWSYS(8)	Coriolis parameter	0	not consider	
		1	consider $f_3=2\omega\sin\varphi$ only	
		2	full evaluation	
MSWSYS(9)	number of iteration in pressure equation solver	1	no iteration	for case of no orography or non-slip condition in elastic model

	Meaning	Value	Contents	Remarks
		3	three times iteration	
MSWSYS(10)	dimension of model	0	three-dimension	
		1	two-dimension	
MSWSYS(11)	upper boundary condition	0	free slip, rigid wall	no other choice
MSWSYS(12)	start-up procedure	0	mountain grow	until ITGROW
		1	wind grow	until ITGROW
		2	pre-existing wind and mountain	
		3	read pre-existing files	currently, not available
		4	nesting ($\omega=0$ at all levels)	
		5	nesting (ω is converted from w)	
		6	nesting (ω from continuity equation)	
		7	nesting (ω from continuity equation, $\omega=0$ at lateral boundary)	
MSWSYS(13)	ground temperature	0	no heat and moisture flux	
		1	vary by sin function	amplitude PTGRDR
		2	predict ground temperature	method of RSM
		3	predict ground temperature	consider ground steepness
		4	predict ground temperature	consider orographic shadow
		5	predict ground temperature	consider both 3 and 4
		6	predict ground temperature with atmospheric radiation	method of RSM
		7	predict ground temperature with atmospheric radiation	consider ground steepness
		8	predict ground temperature with atmospheric radiation	use cloud water and cloud ice
		9	predict ground temperature with atmospheric radiation	8+ consider ground steepness
MSWSYS(14)	lateral boundary condition	0	open for both x- and y-directions	
		1	open for x-direction periodic for y-direction	
		2	periodic for both x- and y-directions	
		−1	open for x-direction free-slip rigid wall for y-direction	
		−2	rigid wall for both x- and y-directions	
MSWSYS(15)	buoyancy	0	split and linearized	for anelastic model (AE)
		1	split but not linearized	for HE-VI scheme
		2	density perturbation	for HI-VI scheme

	Meaning	Value	Contents	Remarks
MSWSYS(16)	initial wind component	0	multiply $\rho G^{1/2}$	
		1	not multiply $\rho G^{1/2}$	for double nesting
MSWSYS(17)	outflow boundary condition for θ	0	use inner closest value	
		1	Orlanski-radiation condition	
		2	extrapolate for time and space	
MSWSYS(18)	cloud physics	2	dry model	
		1	Warm rain	
		0	Cold rain	predict *Ni*
		−1	Cold rain	predict *Ni, Ns*
		−2	Cold rain	predict *Ni, Ns, Ng*
MSWSYS(19)	turbulent closure model	0	level 2.5	no other choice
MSWSYS(20)	basic equation	−1	anelastic, hydrostatic	
		0	Anelastic (AE)	
		1	Elastic (HI-VI)	
		2	Elastic (HE-VI)	
MSWSYS(21)	fall-out of rain	0	Euler Scheme	
		1	Box-Lagrangian Scheme	
MSWSYS(22)	convection	0	not parameterized	
		1	cloud physics and convective adjustment	condensation in parameterization becomes cloud water
		2	cloud physics and convective adjustment	condensation in parameterization becomes precipitation instantly
		3	convective adjustment and large scale condensation only	not predict *Qc* and *Qr*
		4	large scale condensation only	not predict *Qc* and *Qr*
MSWSYS(23)	boundary condition for pressure	0	no sponge layers	
		1	Rayleigh-damping in upper layer	
		2	Rayleigh-damping in upper layer and near lateral boundary	
MSWSYS(25)	lateral boundary relaxation for *U, V, W* and θ	0	no boundary relaxation	
		1	boundary relaxation by Rayleigh-damping	
MSWSYS(26)	mass flux through lateral boundaries	0	no adjustment	
		1	adjust to preservetotal mass	
		2	adjust following mean pressure of mother model	effective in case of nesting

	Meaning	Value	Contents	Remarks
		3	adjust monitoring total mass	currently not available
MSWSYS(27)	vertical grid distance	0	stretching according to DZL, ZDR, IZ1, IZ2 in Namelist & NAMGRD	see sub.VRGDIS
		1	arbitrary setting of height of scalar level	see sub.SETVRG
MSWSYS(28)	advection scheme	0	second order, centered, flux form	
		1	horizontally upstream first order, advective form	advection scheme except wind component
		2	horizontally second order, centered advective form	
		3	horizontally upstream third order advective form	
		4	horizontally fourth order, centered advective form	
		5	horizontally fourth order, centered advective form	advection scheme except wind component
MSWSYS(29)	subgrid evaporation	0	not consider	
		1	consider by predicting cloud amount	see G-1-4
MSWSYS(30)	flux correction for advection	0	not employed	
		1	for U, V, W and Qv	
		2	for U, V, W, θ and Qv	
		3	for U, V and W	

3) Namelist &NAMPAR

This namelist sets basic parameters such as the time step.

Name	Type	Meaning	Default	remarks
ITST	int	start time step	1	restart when greater than 1
ITEND	int	end time step	⋯	
ISTRMT	int	time step interval of GPV out put	⋯	
ITOUT	int	time step interval of monitoring list	⋯	
ITCHK	int	time step interval of check	⋯	
DT	int	time step increment (s)	⋯	
DX	real	x-direction grid distance (m)	⋯	
DY	real	y-direction grid distance (m)	⋯	
DZ	real	z-direction grid distance (m)	⋯	set DZR when variable grid
PTRF	real	base of potential temperature	300.	θ in prognostic variables is the difference from PTRF
PRESRF		base of pressure for Exner function (Pa)	100000.	

4) Namelist &NAMGRD

This namelist is for setting of the variable grid distances. In case of nesting, the values must be consistent with those of the namelist NAMGRDI in K-3.

Name	Type	Meaning	Default	remarks
DXL	real	x-direction left-most grid distance (m)	DX	
DXR	real	x-direction right-most grid distance (m)	DX	
IX1	int	start index for constant grid distance (x-direction)	⋯	
IX2	int	start index for constant grid distance (x-direction)	⋯	
DYL	real	y-direction left-most grid distance (m)	DY	
DYR	real	y-direction right-most grid distance (m)	DY	
IY1	int	start index for constant grid distance (y-direction)	⋯	
IY2	int	start index for constant grid distance (y-direction)	⋯	
DZL	real	grid distance at lowest level (m)	⋯	
DZR	real	grid distance at highest level (m)	DZ	
IZ1	int	start index for constant grid distance (z-direction)	1	
IZ2	int	end index for constant grid distance (z-direction)	NZ	

5) Namelist &NAMVAL

This namelist specifies some basic values for the boundary conditions and other model options.

Name	Type	Meaning	Default	remarks
RATIOI	real	weighting parameter at inflow boundary	0.5–1.0	α_{in} in (F2-2-6)
RATIOO	real	weighting parameter at outflow boundary	0.0–1.0	α_{out1} in (F2-2-6)
RATIO2	real	weighting parameter at outflow boundary	0.0–1.0	α_{out2} in (F2-2-6)
RUVNI	real	weighting parameter at inflow boundary	0.5–1.0	β_{in} in (F2-2-10)
RUVNO	real	weighting parameter at outflow boundary	0.0–1.0	β_{out1} in (F2-2-10)
RUVN2	real	weighting parameter at outflow boundary	0.0–1.0	β_{out2} in (F2-2-10)
FNLTR	real	start index for constant grid distance (y-direction)	⋯	
IDIFX	int	width of lateral boundary relaxation sponge layers	0	
DIFNL	real	coefficient for nonlinear numerical damping	0.	m_{NL} in (G4-1)
DIF2D	real	coefficient for 4-th order numerical damping	90.	m_{2D} in (G4-2)
ASTFC	real	coefficient for Asselins time filter	0.2	ν in (G4-3)
STDLON	real	standard longitude (λ_0)	140.0	see Fig. J1-3-1, 2

Name	Type	Meaning	Default	remarks
STDLAT	real	standard latitude (φ_0)	36.0	see (C1-3-2)
KZDST	int	start index for upper Rayleigh damping layer (z-direction)	NZ-8	zd in (F3-3) is ZRP(KZDST)
KZDEN	int	end index for upper Rayleigh damping layer (z-direction)	NZ	
RLDMPX	real	coefficients for lateral boundary relaxation	0.0	m_R in (F2-4-1)
RLDMPZ	real	coefficients for upper Rayleigh damping layer	90.0	m_{Rz} in (F3-2-1)
RLDMPO	real	coefficients for whole domain Rayleigh damping	0.0	
PTGRDS	real	sea surface potential temperature (K)	288.0	
PTGRDR	real	amplitude for diurnal change of ground potential temperature (K)	0.0	
PTGRDL	real	ground surface potential temperature (K)	0.0	Deviation from PTGRDS
ITGROW	int	end time step for wind grow initiation	0	
UBIAS	real	bias for u (m/s)	0.0	
VBIAS	real	bias for v (m/s)	0.0	
ITSST	int	start time step of elastic equation	0	
EOVER	real	coefficient for implicit treatment for HI-VI	0.5	α in (C3-1-6)

6) Namelist &NAMNST

This namelist specifies some basic values for nesting.

Name	Type	Meaning	Default	remarks
KTSTO	int	start time of nesting file	0	
KTENO	int	end time of nesting file	24	
KTDTO	int	interval of nesting file	3	
DTRATIO	real	unit of nesting file (s)	3600.	
ALPHA	real	ratio of weighting parameter at variational calculus	0.5	α_1/α_2 in (E2-3-7)
ITRMX	int	maximum iteration number for successive over relaxation in variational calculus	20000	
RLXCON	real	Minimum to stop the iteration	1.0E-4	
OVERLX	real	coefficients in over relaxation	1.8	

7) Namelist &NAMRAD

This namelist specifies time interval of radiation calculation.

Name	Type	Meaning	Default	remarks
DTRADS	real	time interval of radiation calculation (s)	300.	

8) Namelist &NAMPTG

This namelist specifies some basic values for calculation of ground temperature when the model is not nested.

Name	Type	Meaning	Default	remarks
DAY0	real	day at it=0	…	
GTIME0	real	time at it=0 (UTC)	24	
ALBEDL	real	ground albedo	0.2	
ALBEDS	real	sea albedo	0.6	not used currently
WETL	real	ground wetness	0.1	
WETS	real	sea surface wetness	1.0	

9) Vertical profile

In the stand-alone run (K-4-1), a horizontally uniform atmosphere is used for initial and boundary conditions. A vertical profile is given by lines of numbers that specify u (m/s), v (m/s), θ (K), RH (relative humidity ; %, or mixing ratio ; g/Kg), Q_c (g/Kg) and Q_r (g/Kg) at the denoted altitudes from ground level z (m). The value at each model grid point is determined by linear interpolation. When MSWSYS(27)=1 is given in the namelist & NAMMSW, the model plane height is set by z in the prameter card.

10) Namelist &NAMKDD

This namelist specifies the kind of data stored in the model output file (J-3-1 or J-3-2). Details of data kind of each number are given by comment lines at the bottom of the parameter card.

K-5. Visualization

Several tools for visualizing simulation results are provided. Since these are written in Fortran language, they can be used with any workstation or personal computer employing Unix OS. The figures are output as a postscript file, which can be seen on a display by using the 'gs' Unix command. Tools producing a postscript file are also written in Fortran language and are described in Kato (2001).

K-5-1 Plot job (1)

The Unix shell for plot utility (1) is in ../shl**/#p**. This job is based on the plot utility described in Chapter E in Ikawa and Saito (1991), but multiple figures can be depicted by a postscript file in one page with shade patterns. The following is an example of the shell script (shl997/#plmw3232) for plotting mountain waves of model size (32,32,32).

```
#  plmw3232 excecute plot job, and make ps.file
echo '#/*----- Compilie Started -----'
cd srcplt
echo ' PARAMETER (LX=32, LY=32, LZ=32)'>psize.h
rm PLOTMAIN.o a.out
make
cd ../shl997
#echo '#/*----- PLOT STARTED -----'
```

```
rm fort.*
ln -s ../card/PDLMWV32 fort.31
ln -s ../@data/org.bell32an fort.50
ln -s ../@data/strmts2.lmwv.file1 fort.62
ln -s ../data/PSDATA fort.99
../srcplt/a.out<../card/LMWV32HI
mv fort.60 ../@data/lmwv32.ps
rm fort.*
```

The plot parameter card card/PDLMWV32 is as follows:

```
4       DEVISE(2--XY       4--GLASER)
 20000 24000 130 156    2         CANVAS
   60
11                        DATA KIND W (I2)

   10                     INTVAL      1 CM/S     (0.1*I5)

2 16    1  32    1    31      10      90     1     (I1,I3,X,7I5)
@
5
   90
11                        DATA KIND W
   10                     INTVAL      1 CM/S
2 16    1  32    1    31      10      50     1     (I1,I3,X,7I5)
@
5
  120
11                        DATA KIND W
   10                     INTVAL      1 CM/S
2 16    1  32    1    31      10      10     1     (I1,I3,X,7I5)
@
4
11                        DATA KIND W
   10                     INTVAL      1 CM/S
1  7    1  32    1    32      55      10     1     (I1,I3,X,7I5)
@
1
1  9    1  32    1    32      55      50     1
@
1
1 12    1  32    1    32      55      90     1
@
9
```

The above parameters are basically similar to E-4 in Ikawa and Saito (1991), but "change parameter" after the @ mark is modified as follows:

1. CHANGE THE POSITION OF CROSS SECTION
2. CHANGE KIND OF DAT AS IN SMALL ITEM
3. CHANGE COMPUTER TIME STEP
4. SAME AS IN 2, BUT VSTERM IS NOT CALLED
5. SAME AS IN 3, BUT VSTERM IS NOT CALLED
6. SAME AS IN 2, BUT DEPICT SHADE PATTERN
7. SAME AS IN 3, BUT DEPICT SHADE PATTERN

8. SAME AS IN 4, BUT DEPICT SHADE PATTERN

9. END OF PLOT

The postscript file made in @data/lmwv32.ps (fort.60) is shown in Fig. K5-1-1. The UNIX shell script and relevant input card for a nesting run with RSM are in shl997/#prsm10238 and card/PD10238, respectively, and the result is shown in Fig. K5-1-2

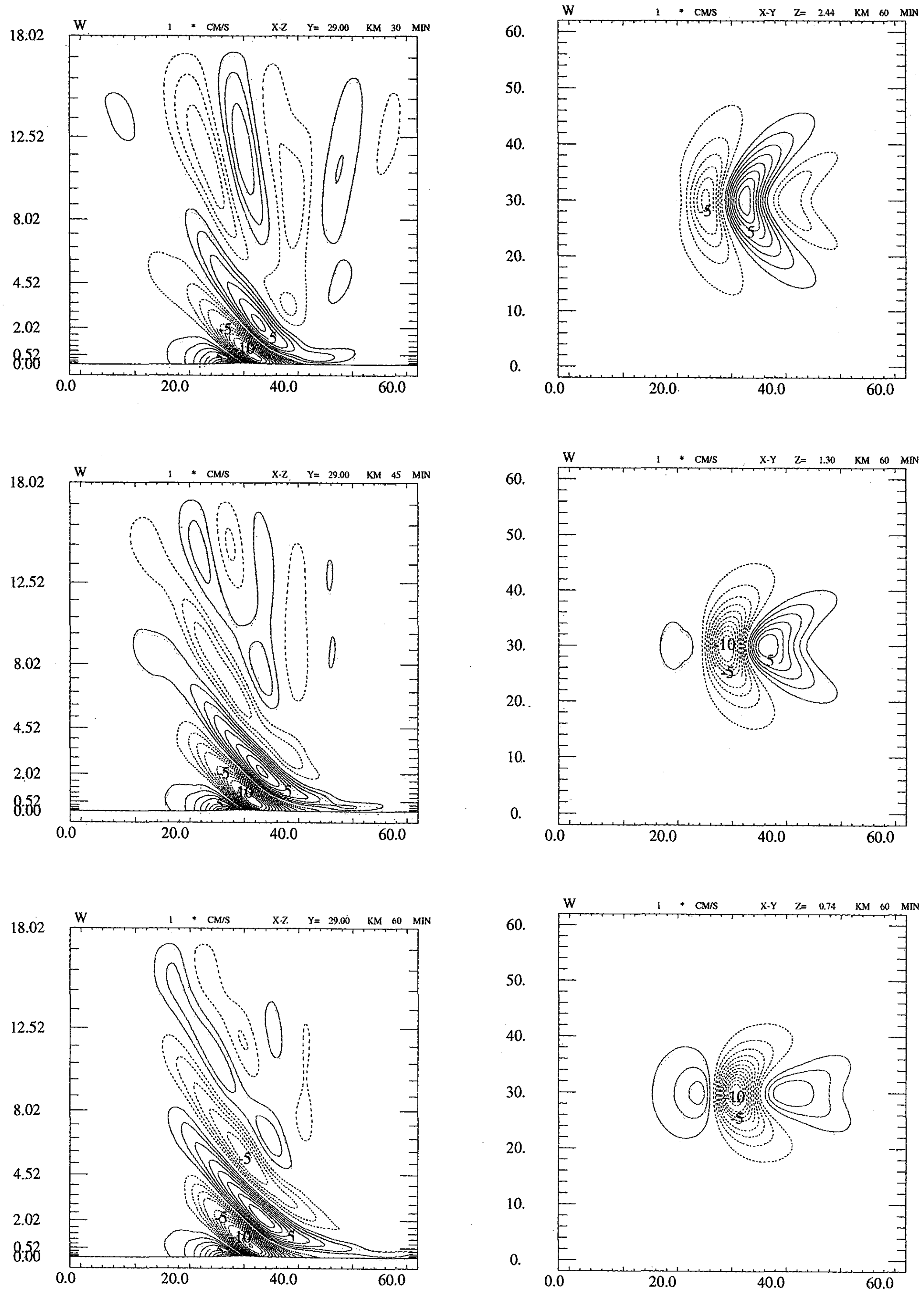

Fig. K5-1-1 Linear mountain waves simulated by the sample script described in K-4-1.
Left: Vertical section of w through mountain top at $t=30$, 45, 60 min.
Right: Horizontal cross-section of w at $t=60$ min at $z=2.44$, 1.30, 0.74 km.

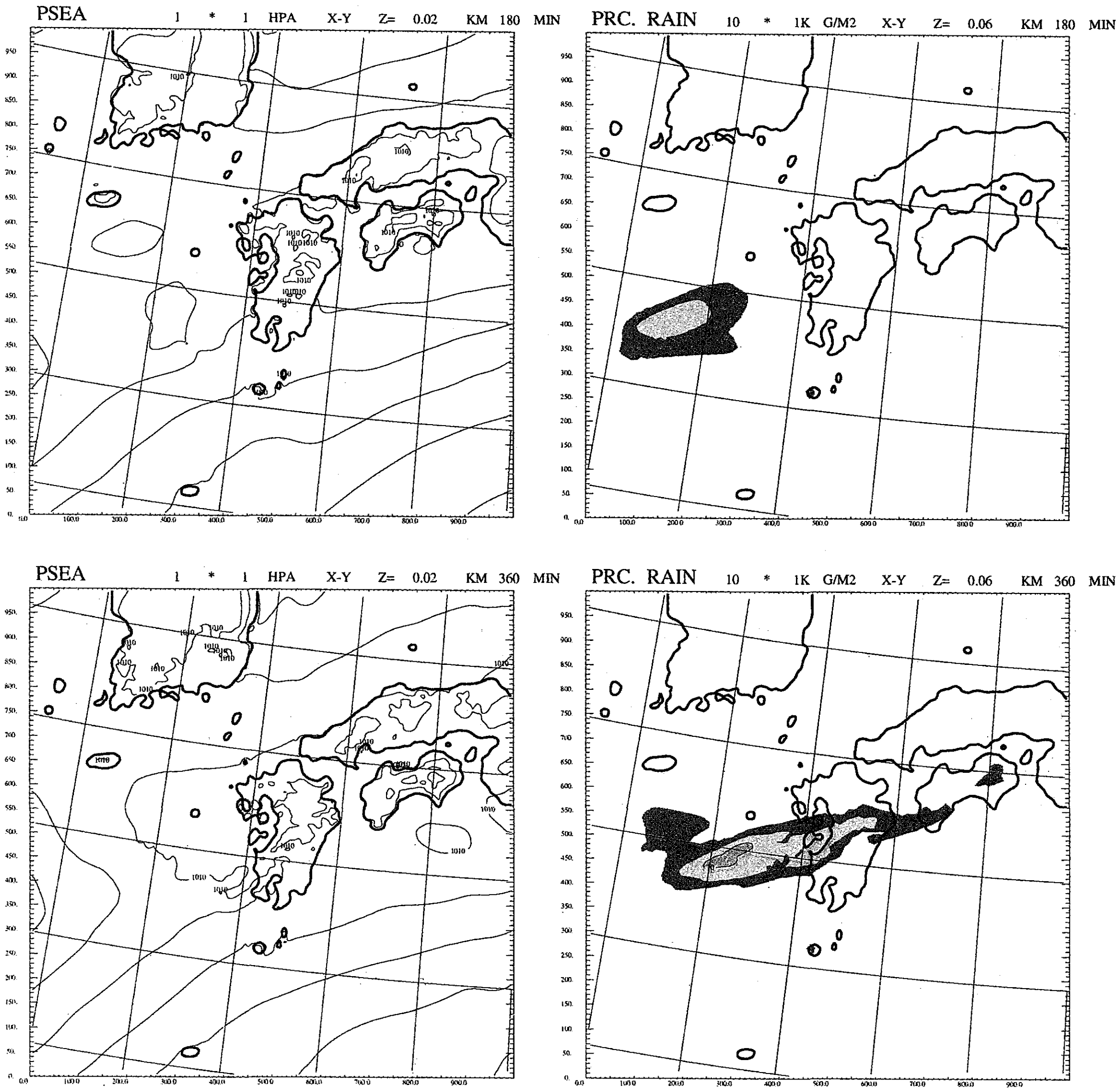

Fig. K5-1-2 NHM forecast (surface pressure and three hour precipitation) at 1200 UTC and 1500 UTC 1999 Jun 25 corresponding to Fig. K3-1-2.

K-5-2. Plot job (2)

The plot job introduced in this subsection is valid for a model output file compressed by using integer*2 (see J-3-2).

(a) Horizontal fields

The horizontal field on the terrain-following coordinate can be drawn by using shlplt2/cd**.sh. The results are output as a postscript file in @data/cd.**.dx10.ps (fort.60). The following shell (shlplt2/cd102.dx10.sh) is an example of the simulation with model size (102,102,38). For different model sizes, replace the numbers in parameters in c$NUM.f with those for the expected model size. The model output file is linked to fort.62. When the output file produced in the restart run is used, it is linked to fort.63. The output file for the next restart run is then linked to fort.64. An example shell is shown in Fig. K5-2-1.

```
#!/bin/csh

setenv DATE y9906.d2500
```

```
cd srcplt2
echo '  PARAMETER(NX=102, NY=102, NZ=38, NXC=NX, NYC=NY)'>cd_dim.h
f90 cdmain.f cdraws.f cutility.f ../srcplt/plotpswk.o -o cd.out

cd ../shlplt2
rm fort.62
ln -s ../@data/rsm102dx10.$DATE fort.62
../srcplt2/cd.out  <<EOF
   0                    0                    0    1.0    -1        2.5    4    /
MDRAIN,MDMAX,MDBAR,CDLTLN,MDUV,CUV,ISP
   1            0            0            0                                  /
MDCOL(0:SHADE,1:COLOR),MDMES,MDLINE,MDWHITE
  0.05    0.4    0.05    0.2          / XB1,YB1,XB2,YB2(POSITION OF BAR)
540   1080 540     1    6     C     / ITST,ITEN,ITD,NIT1,NRP,CRGB
   2     3    0      1   32.5     0 / NDX,NDY,IPST,IPDT,STLAT,NELASTIC
   1 102    1    102   2  RAIN 10.0 0.0 10.0 / IST,IEN,JST,JEN,KEN,MSYS,CD
   1 102    1    102   5  RH    2.0 30.0 100.0 / IST,IEN,JST,JEN,KEN,MSYS,CD
   1 102    1    102  18  RH    2.0 30.0 100.0 / IST,IEN,JST,JEN,KEN,MSYS,CD
   1 102    1    102   2  SLP  0.2 1008.0 1011.0 / IST,IEN,JST,JEN,KEN,MSYS,CD
   1 102    1    102   5  PTE  1.0 325.0 350.0 / IST,IEN,JST,JEN,KEN,MSYS,CD
   1 102    1    102  18  PTE  1.0 325.0 350.0 / IST,IEN,JST,JEN,KEN,MSYS,CD
EOF
mv fort.60 ../@data/cd.$DATE.dx10.ps
rm fort.*
```

Name	Type	Meaning
MDRAIN	INT	0
MDMAX	INT	1 : drawing maximum value 0 : not drawing
MDBAR	INT	0
CDLTLN	REAL	Interval degree of drawing latitude and longitude 0.0 : not drawing
MDUV	INT	Vertical level of plotting wind vectors 0 : not drawing -1 : same level of drawing field.
CUV	REAL	Amplitude ($m\ s^{-1}$) of wind vectors for a horizontal grid
ISP	INT	Grid interval of plotting wind vectors
MDCOL	INT	0
MDMES	INT	1 : plotting grid marks at every boundaries 0 : plotting the horizontal scale
MDLINE	INT	0
MDWHITE	INT	0 : using black color for drawing coastal lines, wind vectors, etc 1 : using white color
MDNANAME	REAL	0.0
X0,Y0,XM,YM	REAL	Left-bottom position, width and height for NDX=NDY=1
ITST	INT	Starting time step for drawing 0 must be set for time step=1
ITEN	INT	Ending time step for drawing
ITD	INT	Interval of time step for drawing
NIT1	INT	1 : not changing the page for drawing the other field 0 : changing the page

Name	Type	Meaning
NRP	INT	Numbers of drawing field
CRGB	CHAR	A : painting field with optional values and color or hatch pattern (Refer the following remark1) B : painting field with gray scale C : coloring field automatically N : plotting contours
NDX	INT	Dividing numbers of panel in a x-direction
NDY	INT	Dividing numbers of panel in a y-direction
IPST	INT	0
IPDT	INT	1
STLAT	REAL	Standard latitude
NELASTIC	INT	0 : Using map factors 1 : Not using map factors
IST	INT	Left position for drawing field
IEN	INT	Right position for drawing field
JST	INT	Bottom position for drawing field
JEN	INT	Top position for drawing field
KEN	INT	Vertical level for drawing field
MSYS	CHAR	Kind of drawing field (Refer to remark 2 below.)
CD	REAL	Contour interval for CRGB='N' Divided interval value for CRGB='B','C' Default for CRGB='A' Amplitude ($m\ s^{-1}$) of wind vectors for a horizontal grid for MSYS='UV'
CDST	REAL	Starting value for painting field Default for CRGB='A', 'N'
CDEN	REAL	Ending value for painting field Default for CRGB='A', 'N'

Remark 1. When CRGB is set to 'A', on the next line of 'IST,IEN,----', color and/or hatch index and boundary values must be inserted as follows.

$N\ I_1\ B_1\ I_2\ B_2 ---- I_N\ B_N\ I_{N+1},$

where N is the number of boundary values, I_I color and/or hatch indexes, and B_I boundary values. Here $B_N > B_{N-1} > ---- > B_1$ must be satisfied. Color and hatch indexes are presented in Kato (2000).

Remark 2. The kinds of drawing fields are shown below. Predicted values must be output by selecting the parameter card file KDD (see I-3).

MSYS	KIND	MSYS	KIND
PT	Potential temperature (K)	T	Temperature (°C)
PTE	Equivalent PT (K)	PTGRD	Ground PT (K)
RADPT	PT time change due to atmospheric radiation ($K\ s^{-1}$)	U	x-directional wind ($m\ s^{-1}$)
V	y-directional wind ($m\ s^{-1}$)	W	Vertical wind ($cm\ s^{-1}$)
VEL	Horizontal wind speed ($m\ s^{-1}$)	VOL	Horizontal vorticity ($10^{-4}\ s^{-1}$)

MSYS	KIND	MSYS	KIND
SLP	Sea-level pressure (hPa)	UV	Horizontal wind vectors
DP	Pressure disturbance from the basic state (Pa)	P	Pressure (hPa)
ETURB	Turbulence energy (J)	QC	Mixing ratio of cloud water ($g\ kg^{-1}$)
QR	Mixing ratio of rainwater (0.1 $g\ kg^{-1}$)	QCI	Mixing ratio of cloud ice (0.1 $g\ kg^{-1}$)
QH	Mixing ratio of graupel (0.1 $g\ kg^{-1}$)	QS	Mixing ratio of snow (0.1 $g\ kg^{-1}$)
RH	Relative humidity (%)	RAIN	Rainfall intensity ($mm\ h^{-1}$)
PREC	Precipitation intensity ($mm\ h^{-1}$)	SNOW	Snowfall intensity ($mm\ h^{-1}$)

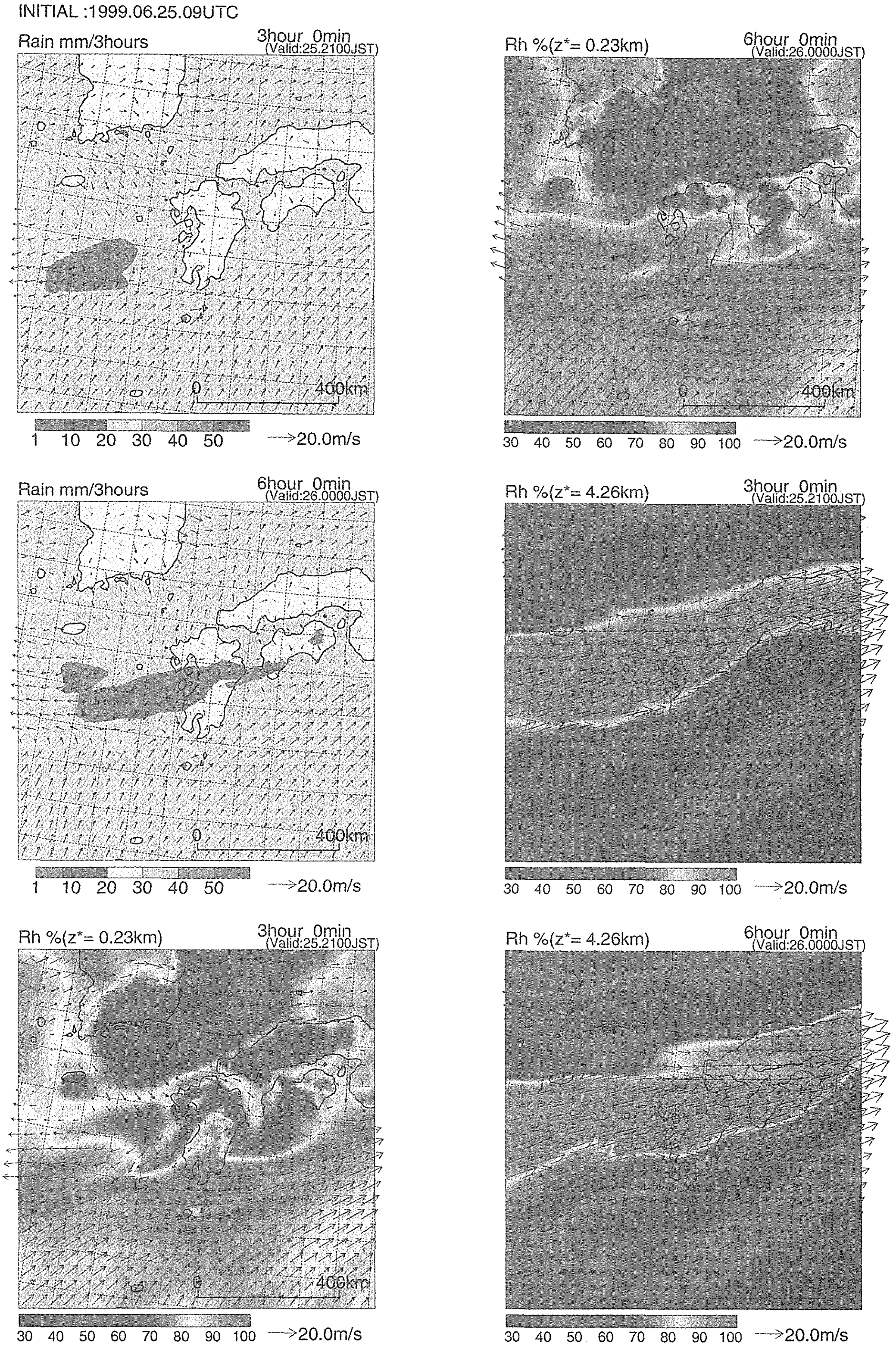

Fig. K5-2-1 NHM forecast (three hour precipitation and Relative humidity) at 1200 UC and 1500 UTC 1999 Jun 25 corresponding to Fig. K5-1-2.

(b) Vertical fields

The vertical field can be drawn by using the unix shell shlplt2/vd**.sh. The results are output as a postscript file in @data/vd.**.ps (fort.60). The following shell is an example (shlplt2/vd102.dx10.sh) of the simulation with model size (102,102,38). For a different model size, replace the numbers in the parameters in v$NUM.f with those for the expected model size. The model output file is linked to fort.62. When the output file produced in the restart run is used, it is linked to fort.63. The output file for the next restart rún is then linked to fort.64. An example shell is shown in Fig. K5-2-2.

```
#!/bin/csh

setenv DATE y9906.d2500

cd srcplt2
echo '     PARAMETER(MX=102, MY=102, MZ=38, NXC=MX, NYC=MY)'>vd_dim.h
echo '     PARAMETER(NX=102, NY=102, NZ=38)'>>vd_dim.h
f90 vdmain.f vdraws.f vutility.f ../srcplt/plotpswk.o -o vd.out

cd ../shlplt2
rm fort.62
ln -s ../@data/rsm102dx10.$DATE fort.62
../srcplt2/vd.out  <<EOF
           1     0    1    5.0   / MDVL,MDMAX,MDUV,CDUV
  540   1080   540    1    2  C / ITST,ITEN,ITD,NIT1,NRP,CRGB
    2     2     0    1 32.5  0 / NDX,NDY,IPST,IPDT,STLAT,NELSTIC
   72 81  100   20   27  RH     5.0  30.0 100.0 / IST,IEN,JST,JEN,KEN,MSYS,CD
   72 81  100   20   27  PTE    2.0 330.0 350.0 / IST,IEN,JST,JEN,KEN,MSYS,CD
/*
//* MDVL=1 : DRAWING VALUES OF CONTOUR, MDMAX=1 : DRAWING THE MAXIMUM VALUE
//* MDUV : LEVEL OF UVPLOT, CUV : CONTOUR INTERVAL OF UVPLOT
//* MDUV=1 : DRAWING UVW, >1 : DRAWING UV WITH INTERVAL OF MDUV GRIDS
//* CDUV : ARROW STANDARD(MDUV=1)  OR CONTOUR INTERVAL OF VEL(MDUV>1)
EOF
mv fort.60 ../@data/vd.$DATE.dx10.ps
rm fort.*
```

Name	Type	Meaning
MDVL	INT	1 : drawing contour values 0 : not drawing
MDMAX	INT	1 : drawing maximum value 0 : not drawing
MDUV	INT	1 : plotting wind vectors on the cross section >1 : plotting horizontal arrows every MDUV grids 0 : not drawing
CDUV	REAL	Amplitude ($m\ s^{-1}$) of wind vectors for a horizontal grid for MDUV>1
ITST	INT	Starting time step for drawing 0 must be set for time step=1
ITEN	INT	Ending time step for drawing
ITD	INT	Interval of time step for drawing
NIT1	INT	1 : not changing the page for drawing the other field 0 : changing the page

Name	Type	Meaning
NRP	INT	Numbers of drawing field
CRGB	CHAR	A : painting field with optional values and color or hatch pattern (Refer the following remark1) B : painting field with gray scale C : coloring field automatically N : plotting contours
NDX	INT	Dividing numbers of panel in a x-direction
NDY	INT	Dividing numbers of panel in a y-direction
IPST	INT	0
IPDT	INT	1
STLAT	REAL	Standard latitude
NELASTIC	INT	0 : using map factors 1 : not using map factors
IST	INT	Left position in a x-direction for drawing field (IST≦IEN)
IEN	INT	Right position in a x-direction for drawing field
JST	INT	Left position in a y-direction for drawing field
JEN	INT	Right position in a y-direction for drawing field
KEN	INT	Vertical top level for drawing field
MSYS	CHAR	Kind of drawing field (Refer the following remark2)
CD	REAL	Contour interval for CRGB='N' Divided interval value for CRGB='B','C' Default for CRGB='A' Amplitude ($m\ s^{-1}$) of wind vectors for a horizontal grid for MSYS='UW','VW','UVW'
CDST	REAL	Starting value for painting field Default for CRGB='A', 'N'
CDEN	REAL	Ending value for painting field Default for CRGB='A', 'N'

Remark 1) Refer the remark1 in K5.2(a).

Remark 2) Kinds of drawing field are shown as follows. Predicted values must be output by selecting the parameter card file KDD (see, I-3).

MSYS	KIND	MSYS	KIND
PT	Potential temperature (K)	T	Temperature ($C°$)
PTE	Equivalent PT (K)	U	x-directional wind ($m\ s^{-1}$)
V	y-directional wind ($m\ s^{-1}$)	W	Veritical wind ($cm\ s^{-1}$)
UW	Wind vectors in x- and z-direction	VW	Wind vectors in y- and z-direction
UVW	Wind vectors on the cross section	UV	Horizontal wind arrow
VEL	Horizontal wind speed ($m\ s^{-1}$)	TE	Turbulence energy (J)
DP	Pressure disturbance from the basic state (hPa)	QC	Mixing ratio of cloud water ($g\ kg^{-1}$)
QR	Mixing ratio of rainwater (0.1 $g\ kg^{-1}$)	QCI	Mixing ratio of cloud ice (0.1 $g\ kg^{-1}$)
QH	Mixing ratio of graupel (0.1 $g\ kg^{-1}$)	QS	Mixing ratio of snow (0.1 $g\ kg^{-1}$)
RH	Relative humidity (%)	STB	Brunt-Vaisala frequency (0.01 s^{-1})

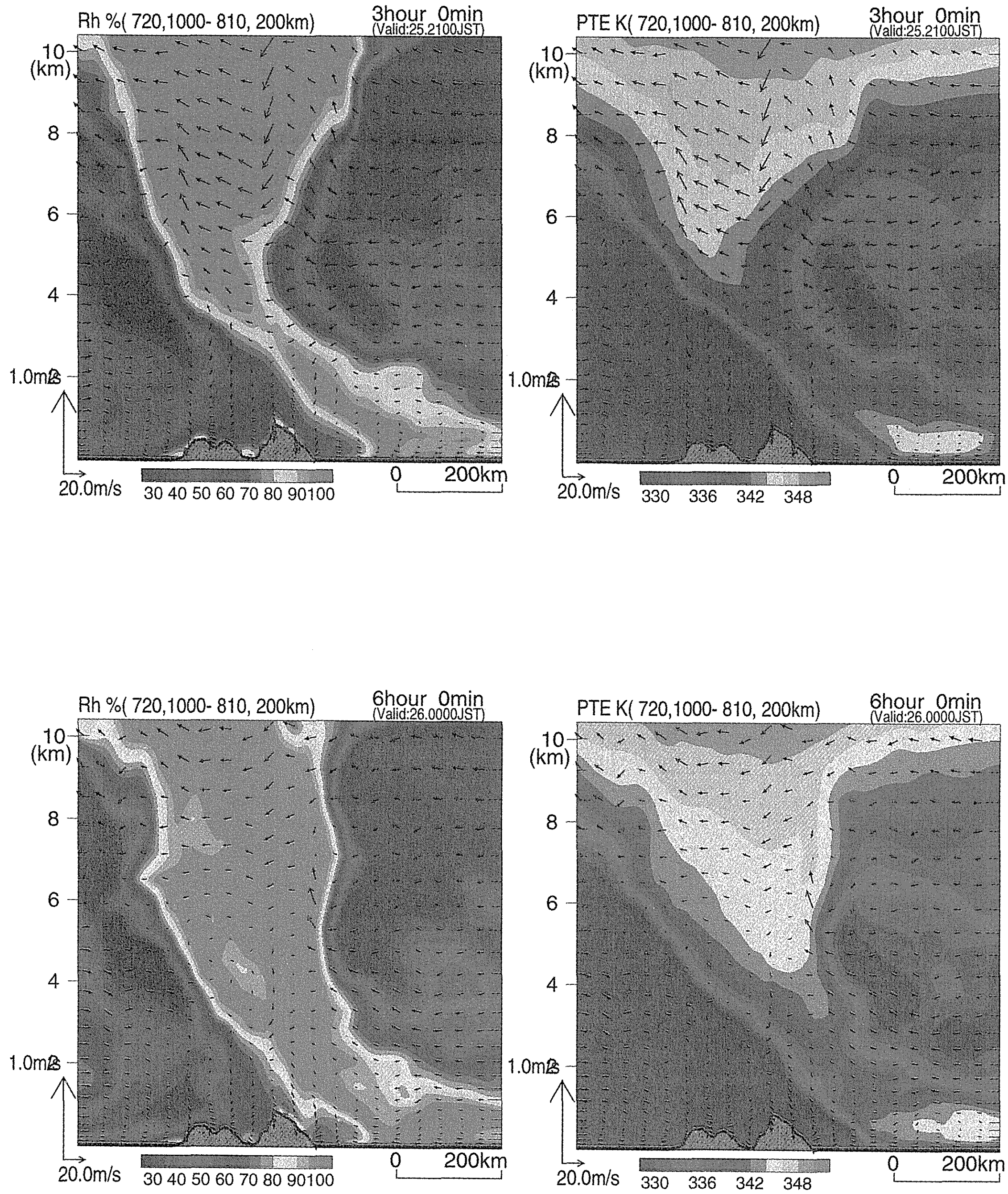

Fig. K5-2-2 Vertical profile of NHM forecast (relative humidity and equivalent potential temperature) at 1200 UC and 1500 UTC 1999 Jun 21.

L. Remarks on developments underway

L-1. Code parallelization

Code parallelization of the model to handle the distributed memory parallel computers has begun, in collaboration with the Numerical Prediction Division of JMA and the Research Organization for Information Science and Technology (RIST ; http://www.tokyo.rist.or.jp/). This program is related to the "*Earth Simulator Project*", planned by the Science and Technology Agency of Japan and is being conducted by the Earth Simulator Research and Development Center (ESRDC ; http://www.gaia.jaeri.go.jp/). A ultra parallel computer with vector processors will be constructed for this project, and will theoretically attain 40 TFLOPS in FY2001. The purpose of the project is to clarify and predict the global climate changes, reproducing a "virtual earth" in the ultra computer. One of the targets is establishment of "1 km meteorology" using cloud-resolving simulations for a several-thousand kilometer square area. A prototype parallel version of MRI/NPD-NHM was developed for this purpose (Saito *et al.,* 1999 ; 2000) and its expansion, "JMA-NHM," has been under development (Muroi *et al.,* 2000 ; see L-2). An MPI (Message Passing Interface) is employed for the communications library.

An elliptic pressure tendency equation (D3-1-1) exists in an HI-VI scheme, and is solved by the dimension reduction method in MRI/NPD-NHM, as described in D-3. However, a simple application of the direct method to the distributed memory parallel environment requires the "all to all" communication between the parallel nodes. To avoid this problem, we divide the model domain in the y-direction, and employ a pre-process just before the Fourier transform (operation of inverse matrix of D3-3-2) in the y-direction, where the matrix of the finite discretization form of the pressure equation is re-arranged.

Figure L-1-2 shows the vertically accumulated water content at 1000 JST, 22 January 1997, simulated by the parallelized nonhydrostatic model (HI-VI version of JMA-NHM). The case is the same as in H-4-2, but the nonhydrostatic model is nested with the 9 hour forecast of RSM, the initial time for which is 2100 JST, 21 January 1997. Four nodes of the HITAC SR8000 of MRI were employed as a test case in this simulation, wherein the model domain was enlarged to $(2160\ \mathrm{km})^2$ but the horizontal resolution and the number of the vertical levels were were reduced to 3 km and 20 levels, respectively. The cloud microphysics were simplified to the warm rain process. We used a Mercator map projection with a standard latitude of 36 degrees north, and the computed LWP was remapped to the " longitude-latitude grid " for visualization to compare with the visible satellite image of the day (Fig. L-1-1).

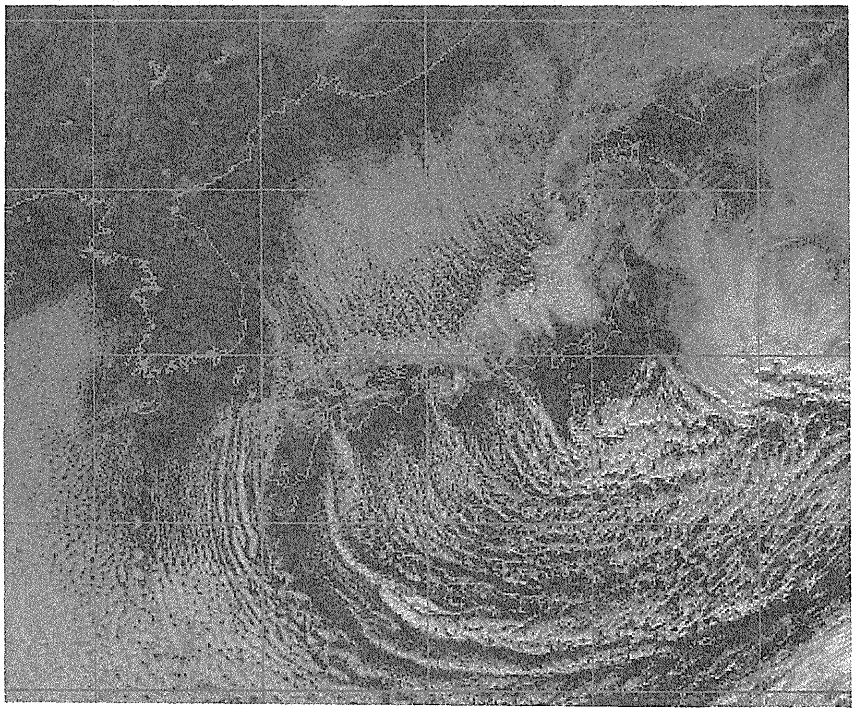

Fig. L-1-1 Visible satellite image at 0200 UTC 1997 JAN 22.

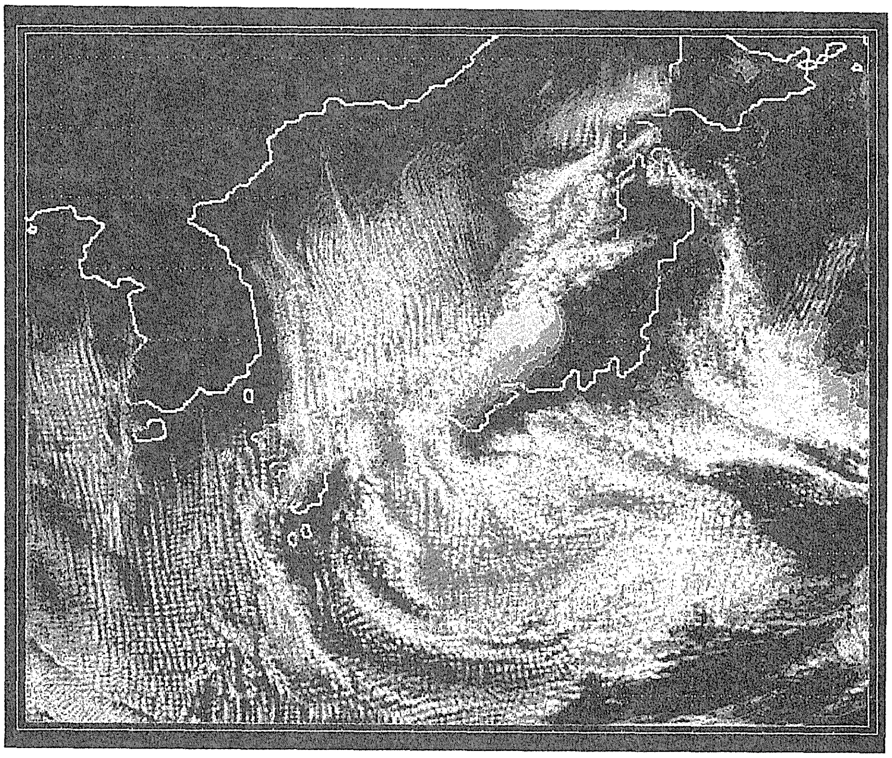

Fig. L-1-2 Accumulated water content of 0100 UTC 1997 JAN 22 simulated by the parallelized nonhydrostatic model. Contours of 0.05, 0.2, 0.5 and 1.0 Kgm^{-2} are depicted. Areas above 0.2 Kgm^{-2} are shaded. After Saito *et al.* (2001b).

L-2. Development for an operational NWP model at JMA

The rapid increase of computer power in recent decades will makes it possible to operate a nonhydrostatic model for numerical weather prediction (NWP); and many operational centers are presently developing their nonhydrostatic models. A joint program with the Numerical Prediction Division (NPD) of JMA has been underway since February 1999 (Muroi *et al.,* 1999; 2000). A One goal of this program is to develop a unified nonhydrostatic model (MRI/NPD-NHM) for both for research and operational purposes.

A hydrostatic regional spectral model (RSM) is operated at JMA to support short-range forecasts. The horizontal resolution of the model is about 20 km. In 2001, JMA has started operation of a 10 km mesh regional model for to preventing natural disasters; however, though it is still a hydrostatic model. Demands for more accurate weather information is still increaseing. Improvement of the precipitation amount forecast is one of the biggest primary targets of mesoscale predictions over Japan. Current existing operational model doesn't predict severe rainfall well. Nonhydrostatic models with microphysical processes are highly recommended for a higher-resolution NWP model.

NPD previously developed its a nonhydrostatic model previously (Muroi, 1998; 1999a). But MRI and NPD consent an agreement to develop a unified nonhydrostatic model in February 1999, and started a joint program for the development of a next-generation numerical prediction model.

The major primary mission of this project is to optimize the source code and revise the physical processes and pre-post procedures, which will to be suitable for an operational suite. Implementation of an HE-VI scheme is one of the major issues of in this project. In MRI-NHM, semi-implicit (HI-VI) time integration is originally applied. But the HE-VI scheme would be suitable for a higher and wider resolution model on the a distributed memory parallel machine. Theoretically, a semi-implicit scheme requires all-to-all communication in each time step. A split-explicit scheme, however, needs communications only with the neighbors of each node. So it is worthwhile to try a split-explicit scheme on a parallel machine. The detailed specification of the scheme is described in C-3-2.

We conducted a test to examine the efficiency of the HE-VI scheme on HITAC SR2201. The grid numbers of this test is $114\times114\times38$, and the horizontal resolution is 10 km, and the forecast period is 12 hours. The elapsed times of simulation in the base HE-VI and HI-VI cases are

HE-VI scheme: 260 minutes,

HI-VI scheme: 420 minutes,

when 4 processors are used. All other processes, except for the time integration methods, are the same and the cloud microphysics were simplified to the warm rain process. This result indicates that the HE-VI scheme is suitable for a parallel machine.

Development of a data assimilation system, the initialization procedure, and the economic microphysical processes would be other issues of in this project.

A standard coding rule will be required to establish fruitful collaboration between many researchers to develop a unified model. A prototype of this programming rule has been built and refinement of all the source code of the unified model according to this rule will be conducted.

L-3. A spherical coordinate version for a global nonhydrostatic model.

Development of a spherical, curvilinear orthogonal coordinate version of MRI/NPD-NHM is underway. In the new model, we introduce two map factors, m_1 and m_2, along the x- and y- (longitudinal and latitudinal) directions instead of the single map factor m in the conformal projection. The curvature terms (C1-3-15) and (C1-3-16) become

$$Crv_1 = m_1 m_2 v \{ v\frac{\partial}{\partial x}(\frac{1}{m_2}) - u\frac{\partial}{\partial y}(\frac{1}{m_1}) \} - \frac{uw}{a}, \quad \text{(L-3-1)}$$

$$Crv_2 = m_1 m_2 u \{ v\frac{\partial}{\partial x}(\frac{1}{m_2}) - u\frac{\partial}{\partial y}(\frac{1}{m_1}) \} - \frac{vw}{a}, \quad \text{(L-3-2)}$$

In a longitude-latitude grid, if we take

$$m_1 = \frac{1}{a \cos \varphi}, \ m_2 = \frac{1}{a}, \quad \text{(L-3-3)}$$

$$w = a \cos\varphi \frac{d\lambda}{dt}, \ v = a\frac{d\varphi}{dt}, \quad \text{(L-3-4)}$$

basic equations (C1-3-9)-(C1-3-11) are reduced to the following conventional momentum equations in spherical coordinates.

$$\frac{du}{dt} - \frac{uv \tan \varphi}{a} + \frac{uw}{a} + \frac{1}{\rho}\frac{\partial p}{a \cos \varphi \partial \lambda}$$
$$= 2\Omega v \sin \varphi - 2\Omega w \cos \varphi + DIF.u, \quad \text{(L-3-5)}$$

$$\frac{dv}{dt} + \frac{u^2 \tan \varphi}{a} + \frac{vw}{a} + \frac{1}{\rho}\frac{\partial p}{a\partial\varphi} = -2\Omega u \sin \varphi + DIF.v, \quad \text{(L-3-6)}$$

$$\frac{dw}{dt} - \frac{u^2+v^2}{a} + \frac{1}{\rho}\frac{\partial p}{\partial z} + g = 2\Omega u \cos \varphi + DIF.w, \quad \text{(L-3-7)}$$

In the new model, we use the Cylindrical Equidistant projection,

$$m_1 = \frac{\cos \varphi_0}{\cos \varphi}, \ m_2 = 1, \quad \text{(L-3-8)}$$

whose map factors become unity at the standard latitude φ_0, and the basic equations are rewritten into the flux form in terrain-following coordinates.

Figure L-3-2 shows an example of 18- and 36-hour forecasts of the sea-level pressure predicted by the new model nested with the global analysis data of JMA (GNANL ; 1.25×1.25 degrees, pressure plain, 17 levels). The horizontal resolution of the nonhydrostatic model is 1.45×1.45 degrees. Vertically, 38 layers are employed, and vertical resolution at the lowest level is 40 m, where the horizontal wind is computed at 20 m level above the ground surface. The domain covers from 80 degrees north to 80 degrees south and from 5 degrees east to 7 degrees west, which corresponds to about 95% of the global surface. For simplicity, a dry model is used, and the lowest level temperature in GANAL is used for the initial value of the ground and sea-surface temperatures. The surface pressure pattern of the model generally follows the global analysis well at the corresponding valid times (figures not shown).

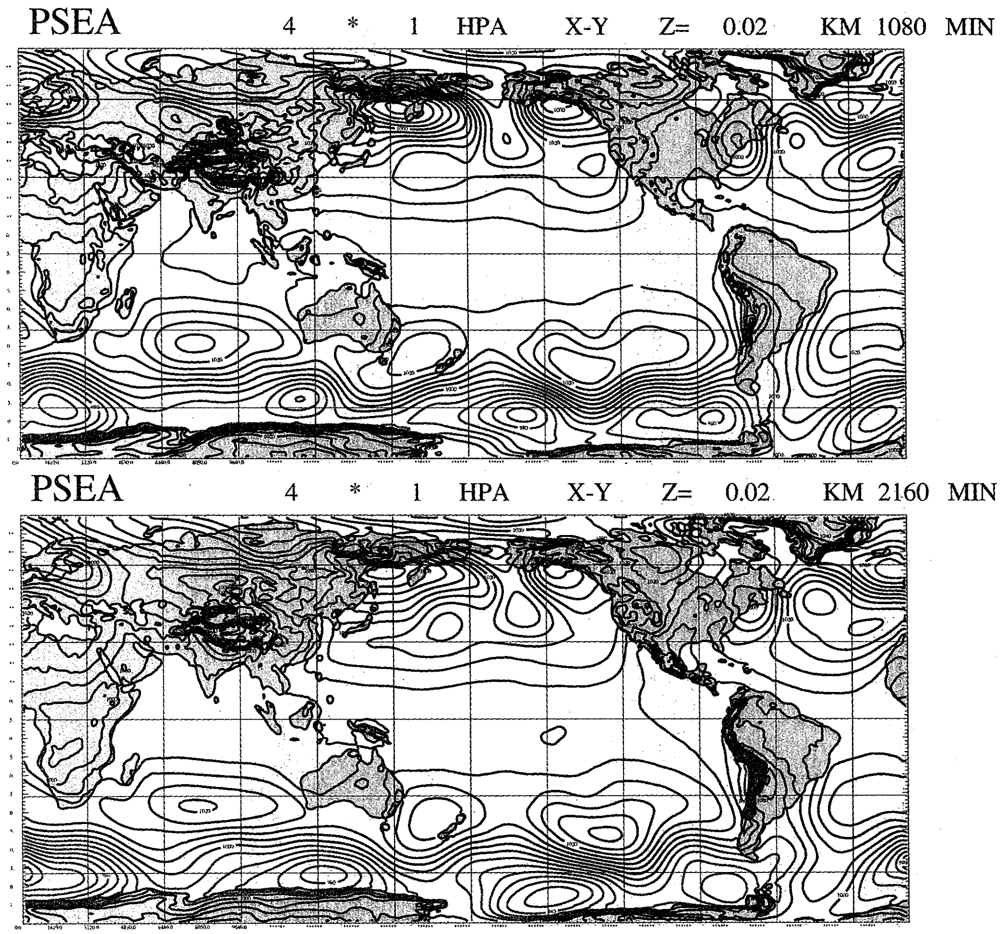

Fig. L-3-2 Sea-level pressure at $t = 18$ and 36 hours predicted by the nonhydrostatic model. Contour interval is 4 hPa. Model initial time is 2400 UTC 1 March 1999. After Saito (2001).

M. References

Clark, T. L., 1977 : A small-scale dynamic model using terrain following coordinate transformation. *J. Comp. Phys.,* **24**, 186-215.

Clark, T. L. and W. D. Hall, 1991 : Multi-domain simulations of the time dependent Navier Stokes equations : error analysis of nesting procedures. *J. Comp. Phys.,* **92**, 456-481.

Deardorff, J. W., 1980 : Stratocumulus-capped mixed layers derived from a three-dimensional model. *Boundary-Layer Meteorol.,* **18**, 495-527.

DWD, 1999 : Quarterly Report of the operational NWP-models of the Deutscher Wetterdienst, Deutscher Wetterdienst, 63 pp.

Doms, G. and U. Schaettler, 1997 : The nonhydrostatic limited-area model LM (Lokal-Modell) of DWD. Part I : Scientific Documentation. *Deutscher Wetterdienst,* 155 pp.

Dudhia, J., 1993 : A nonhydrostatic version of the Penn State-NCAR mesoscale model : Validation tests and simulation of an Atlantic cyclone and cold front. *Mon. Wea. Rev.,* **121**, 1493-1513.

Eito, H., M., Yoshizaki, T., Kato, K., Saito and Y., Mano, 1999 : 3-D Numerical experiments of marine stratocumulus observed around Japan islands in winter. *CAS/JSC WGNE Res. Act. Atmos. Ocea. Model.,* **28**, 5.21-5.22.

Forecast Division/Japan Meteorological Agency, 1995 : Analysis process and accuracy of the estimated amount of rainfall based on radar and AMeDAS observation. *Weather Service Bulletin JMA,* **62**, 279-339 (in Japanese).

Fujibe, F., K. Saito, D. S. Wratt and S. G. Bradley, 1999 : A numerical study on the diurnal variation of low-level wind in the lee of a two-dimensional mountain. *J. Meteor. Soc. Japan,* **77**, 827-843.

Gadd, A. and J. Keers, 1970 : Surface exchanges of sensible heat in a 10-level model atmosphere. *J. Atmos. Sci.,* **96**, 297-308.

Gal-Chen, T. and R. C. J. Somerville, 1975 : On the use of a coordinate transform for the solution of the Navier-Stokes equation. *J. Comp. Phys.,* **17**, 209-228.

Goda, H., 1996 : Users' guide of the Reginal Spectral Model of JMA, *Numerical Prediction Division of JMA* (in Japanese).

Goda, H. and K. Kurihara, 1991 : Development of nonhydrostatic model, *Suuchiyoho-ka Houkokku Bessatsu,* **37**, 67-82 (in Japanese).

Golding, B. W., 1992 : An efficient non-hydrostatic forecast model. *Meteorol. Atmos. Phys.,* 50, 89-103.

Goldman, A. and T. G. Kyle, 1968 : A comparison between statistical model and line calculation with application to the 9.6 μm ozone and the 2.7 μm water vapor bands. *Appl. Opt.,* **7**, 1167-1177.

Goody, R. M., 1952 : A statistical model for water vapor absorption. *Quart. J. Roy. Meteor. Soc.,* **78**, 165-169.

Houghton, J. T., 1977 : The physics of atmospheres. Cambridge Univ. Press. 203 pp.

Hsu, Y. and A. Arakawa, 1990 : Numerical modeling of the atmosphere with an isentropic vertical coordinate. *Mon. Wea. Rev.,* **118**, 1933-1959.

Ikawa, M., 1981 : The energy conserving scheme of invariant form for the shallow convection. *Pap. Met. Geophys.,* **32**, 65-78.

Ikawa, M., 1988 : Comparison of some schemes for nonhydrostatic models with orography. *J. Meteor. Soc. Japan,* **66**, 753-776.

Ikawa M. and K. Saito, 1991 : Description of a non-hydrostatic model developed at the Forecast Research Department of the MRI. *Tec. Rep. MRI,* **28**, 238 pp.

Ikawa M., H. Mizuno, T. Matsuo, M. Murakami, Y. Yamada and K. Saito, 1991 : Numerical modeling of the convective snow cloud over the Sea of Japan. *J. Meteor. Soc. Japan,* **69**, 641-667.

Izumi, K., 1994 : Analysis of the torrential rain over southern Kyushu on 6 August 1993. *Prep. Autumn Conf. MSJ.,* **66**, C358 (in Japanese).

Kato, T., 1995 : Box-Lagrangian rain-drop scheme. *J. Meteor. Soc. Japan,* **73**, 241-245.

Kato, T., 1996 : Hydrostatic and non-hydrostatic simulations of the 6 August 1993 Kagoshima torrential rain. *J. Meteor. Soc. Japan,* **74**, 355-363.

Kato, T., 1998 : Numerical simulation of the band-shaped torrential rain observed southern Kyushu, Japan on 1 August

1993. *J. Meteor. Soc. Japan,* **76**, 97-128.

Kato, T., 1999 : Verification of the MRI-nonhydrostatic-model predicted rainfall during the 1996 BAIU season. Part 2 : Effects of ice-phase and atmospheric radiation. *CAS/JSC WGNE Research Activities in Atmospheric and Oceanic Modelling,* **28**, 4.11-4.12.

Kato, T., 2001 : Tools making a postscript files based on 'GPSL' (to be submitted *Tech. Rep. MRI*).

Kato, T. and K. Saito, 1995 : Hydrostatic and non-hydrostatic simulation of moist convection : Applicability of hydrostatic approximation to a high-resolutionmodel. *J. Meteor. Soc. Japan,* **73**, 59-77.

Kato, T., K. Kurihara, H. Seko, K. Saito and H. Goda, 1998 : Verification of the MRI nonhydrostatic model model predicted rainfall during the 1996 Baiu season. *J. Meteor. Soc. Japan,* **76**, 719-735.

Kikuchi, Y., 1975 : Governing equations, *Suuchiyoho-ka Houkokku Bessatsu,* **21**, 4-17 (in Japanese).

Klemp, J. B. and R. Wilhelmson, 1978 : The simulation of three-dimensional convective storm dynamics. *J. Atmos. Sci.,* 35, 1070-1096.

Kondo, J., 1975 : Air-sea bulk transfer coefficients in diabatic conditions. *Boundary-Layer Meteor.,* 9, 91-112.

Kondo, J., 1976 : Heat balance of the East China Sea during the air mass transformation experiment. *J. Meteor. Soc. Japan,* 54, 382-398.

Kurihara, K. and T. Kato, 1997 : Characteristics of diurnal variation of precipitation around Kyushu Distinct during the Baiu season. *Tenki,* **44**, 631-636 (in Japanese).

Lacis, A. A., and J. E. Hansen, 1974 : A parameterization for the absorption of solar radiation in the earth's atmosphere. *J. Atmos. Sce.,* **31**, 118-133.

Lin, Y. H., R. D. Farley and H. D. Orville, 1983 : Bulk parameterization of the snow field in a cloud model. *J. Clim. Appl. Meteor.,* **22**, 1065-1092.

Liou, K. N., 1992 : Radiation and Cloud Processes in the Atmosphere. *Oxford University Press, New York,* 487 pp.

Manabe, S., J. Smatorinsky, and R. F. Strickler, 1965 : Simulated climatology of a general circulation model with a hydrologic cycle. *Mon. Wea. Rev.,* **93**, 769-798.

Murakami, M., 1990 : Numerical modeling of dynamical and microphysical evolution of an isolated convective cloud — The 19 July 1981 CCOPE cloud. *J. Meteor. Soc. Japan,* **68**, 107-128.

Murata, A., K. Saito, and M. Ueno, 1999 : A numerical simulation of typhoon Flo (1990) using the MRI mesoscale nonhydrostatic model, *Proceedings of Workshop on Mesoscale Numerical Weather Prediction and its Application,* 31-34.

Muroi, C., 1998 : Development of nonhydrostatic model. *Suuchiyoho-ka Houkokku Bessatsu,* **44**, 25-41 (in Japanese).

Muroi, C., 1999a : Development of JMA nonhydrostatic model. *Prep. Spring Conf. MSJ.,* **75**, P 127 (in Japanese).

Muroi, C., 1999b : On the next generation NWP models in JMA. *NWP newsletter,* 18, No. 1, 1-4 (in Japanese).

Muroi, C., K. Saito, T. Kato and H. Eito, 1999 : Development of the MRI/NPD nonhydrostatic model, *Proceedings of Workshop on Mesoscale Numerical Weather Prediction and its Application,* 83-86.

Muroi, C., K. Saito, T. Kato and H. Eito, 2000 : Development of JMA nonhydrostatic mesoscale model and its computational efficiency, *Prep. Spring Conf. MSJ.,* **77**, P 124 (in Japanese).

Nakamura, H., 1978 : Dynamical effects of mountains on the general circulation of the atmosphere : 1. Development of finite-difference schemes suitable for incorporating mountains. *J. Meteor. Soc. Japan,* **56**, 317-339.

Numerical Prediction Division/Japan Meteorological Agency, 1997 : Outline of the operational numerical weather prediction of the Japan Meteorological Agency. 126 pp. [Available from JMA, 1-3-4 Otemachi, Chiyoda-ku, Tokyo 100-8122, Japan.]

Ogura, M. 1969 : A direct method of Poisson equation by Dimension Reduction Method, *J. Meteor. Soc. Japan,* **47**, 319-323.

Ohno, H. and M. Isa, 1984 : A statistical relation between GMS-viewed cloud amount and relative humidity. *Tenki,* 31, 493-495 (in Japanese).

Orlanski, I., 1976 : A simple boundary condition for unbounded hyperbolic flows. *J. Comp. Phys.,* **21**, 251-269.

Pielke, R. A., W. R. Cotton, R. L. Walko, C. J. Tremback, W. A. Lyons, L. D. Grasso, M. E. Nicholls, M. D. Moran, D. A. Wesley, T. J. Lee, and J. H. Copeland, 1992 : A comprehensive meteorological modeling system -RAMS. *Meteor. Atmos. Phys.,* **49**, 69-91.

Redelsperger, J. L., P. Brown, F. Guichard, C. Hoff, M. Kawasima, S. Lang, T. Montmerle, K. Nakamura, K. Saito, C. Seman, and W. K. Tao, 2000 : A GCSS model intercomparison for a tropical squall line observed during TOGA-COARE. Part 1 : Cloud-Resolving Models. *Q. J. R. Met. Soc.,* **126**, 823-863.

Robert, A. J., 1966 : The integration of low order spectral form of the primitive meteorological equations. *J. Atmos. Sci.,* **44**, 237-245.

Roberts, R. E., J. A. Selby and L. M. Bibermann, 1976 : Infrared continuum absorption by atmospheric water vapor in the 8-12 μm window. *Appl. Opt.,* **15**, 2085-2090.

Rodgers, C. D. and C. D. Walshaw, 1966 : The computation of infrared cooling rate in planetary atmospheres. *Quart. J. Roy. Meteor. Soc.,* **92**, 67-92.

Saito, K., 1993 : A numerical study of the local downslope wind "Yamaji-kaze" in Japan Part 2 : Non-linear aspect of the 3-D flow over a mountain range with a col. *J. Meteor. Soc. Japan,* **71**, 247-271.

Saito, K., 1994a : A numerical study of the local downslope wind "Yamaji-kaze" in Japan Part 3 : Numerical simulation of the 27 September 1991 windstorm with a non-hydrostatic multi-nested model. *J. Meteor. Soc. Japan,* **72**, 301-329.

Saito, K., 1994b : On the MRI nonhydrostatic nesting model. (2) Modification to a fully compressible model. *Technical Report submitted to the annual meeting of the JMA for improvement of forecasting technique, MRI, Forecast Research Department.* 1-17 (in Japanese).

Saito, K., 1996 : On the MRI mesoscale nonhydrostatic model (2) —nesting with RSM—. *Prep. Spring Conf. MSJ.,* **70**, B213 (in Japanese).

Saito, K., 1997: Semi-implicit fully compressible version of the MRI mesoscale nonhydrostatic model—Forecast experiment of the 6 August 1993 Kagoshima torrential rain—. *Geophys. Mag. Ser. 2,* **2**, 109-137.

Saito, K., 1998 : Recent modification of the MRI-NHM—Higher order advection schemes and adjustment of mass-flux through lateral boundaries according to the precipitation rates—. *CAS/JSC WGNE Res. Act. Atmos. Ocea. Model.,* **27**, 5.44-5.45.

Saito, K., 2000 : Modification of the MRI nonhydrostatic model—arbitrary conformal projection mapping and nesting with the global analysis data—. *CAS/JSC WGNE Res. Act. Atmos. Ocea. Model.,* **29**, 5.35-5.36.

Saito, K., 2001 : Development of a global nonhydrostatic model. *Tenki,* **48**, 103-104 (in Japanese).

Saito, K. and A. Baba, 1988 : A statistical relation between relative humidity and the GMS observed cloud amount, *J. Meteor. Soc. Japan,* **66**, 187-192.

Saito, K. and M. Ikawa, 1991 : A numerical study of the local downslope wind "Yamaji-kaze" in Japan. *J. Meteor. Soc. Japan,* **69**, 31-56.

Saito, K. and M. Ikawa, 1992 : Numerical simulation of local wind by a nonhydrostatic nested model. *Tenki,* **39**, 615-625 (in Japanese).

Saito, K., L. Thanh and T. Takeda, 1994 : Airflow over the Kii Peninsula and its Takeda, 1994 relation to the orographic enhancement of rainfall. *Pap. Met. Geophys.,* **45**, 65-90.

Saito, K., M. Murakami, T. Matsuo and H. Mizuno, 1996 : Sensitivity experiments on the orographic snowfall over the mountainous region of northern Japan. *J. Meteor. Soc. Japan,* **74**, 793-813.

Saito K. and T. Kato, 1996 : On the modification of the MRI nonhydrostatic nesting model. *Tenki,* **43**, 101-114 (in Japanese).

Saito, K. and M. Yamasaki, 1997: GEWEX Cloud System Studies model intercomparions on a squall line of TOGA-COARE. *CAS/JSC WGNE Res. Act. Atmos. Ocea. Model.,* **25**, 5.31-5.32.

Saito, K., G. Doms, U. Schaettler and J. Steppeler, 1998 : 3-D mountain waves by the Lokal-Modell of DWD and the MRI mesoscale nonhydrostatic model. *Pap. Met. Geophys.,* **49**, 7-19.

Saito K. and T. Kato, 1999 : The MRI mesoscale nonhydrostatic model. *Met. Res. Note,* **196**, 169-195 (in Japanese).

Saito, K., T. Kato, H. Eito, C. Muroi, K. Gopal, Y. Yamagishi and T. Yonemura, 1999 : On the parallelization of the MRI nonhydrostatic model. *Prep. Spring Conf. MSJ.,* **76**, B306 (in Japanese).

Saito, K., T. Kato, H. Eito, C. Muroi, K. Gopal and Y. Yamagishi, 2000 : Parallelization of a cloud resolving nonhydrostatic model (2). *Prep. Spring Conf. MSJ.,* **77**, B305 (in Japanese).

Saito, K., T. Keenan, G. Holland and K. Puri, 2001a : Numerical simulation of tropical diurnal thunderstorms over the Maritime Continent. *Mon. Wea. Rev.,* **129**, 378-400.

Saito, K., T. Kato, H. Eito and C. Muroi, 2001b : Cloud resolving simulation over (2000 km)^2 with a parallel nonhydrostatic model. *CAS/JSC WGNE Res. Act. Atmos. Ocea. Model. (submitted)*

Sakurai, H. and S. Hosoyamada, 1994 : Actual condition of the Kagoshima torrential rain. *Rep. Kagoshima University research group,* 1-12 (in Japanese).

Segami, A., K. Kurihara, H. Nakamura, M. Ueno and I. Takano, 1989 : Description of Japan Spectral Model. *JMA/NPD Technical Report,* **25**, 41 pp.

Seino, N. and K., Saito, 1999 : A numerical study of the local front in the Kanto Region, Japan. *CAS/JSC WGNE Research Activities in Atmospheric and Oceanic Modelling,* **28**, 5.50-5.51.

Seko, H., T. Kato, K. Saito, M. Yoshizaki, K. Kusunoki and H. Okamura, 1997 : Analytical and numerical studies of a quasi-stationary precipitation band observed over Kanto area associated with Typhoon 9426 (Orchid). *J. Meteor. Soc. Japan,* **77**, 929-928.

Sherman, C. A., 1978 : A mass-consistent model for wind fields over complex terrain. *J. Appli. Meteor.,* **17**, 312-319.

Smolarkiewicz P., 1983 : A simple positive definite advection scheme with small implicit diffusion. *Mon. Wea. Rev.,* **111**, 479-486.

Smith, R. B., 1980 : Linear theory of stratified hydrostatic flow past an isolated mountain. *Tellus,* **32**, 348-364.

Sommeria, G., 1976 : Three-dimensional simulation of turbulent processes in an undisturbed trade wind boundary layer. *J. Atmos. Sci.,* **33**, 216-241.

Stephens, G. L., 1978 : Radiation profiles in extended water clouds. II. Parameterization schemes. *J. Atmos. Sci.,* **35**, 2123-2132.

Sugi, M., K. Kuma, K. Tada, K. Tamiya, N. Hasegawa, T. Iwasaki, S. Yamada and T. Kitade, 1990 : Description and performance of the JMA operational global spectral model (JMA-GSM88). *Geophys. Mag.,* **43**, 105-130.

Tapp, M. C. and P. W. White, 1976 : A non-hydrostatic mesoscale model. *Q. J. R. Meteorol. Soc.,* **102**, 277-296.

Thomas, S., C. Girard, G. Doms and U. Schaettler, 1999 : Semi-implicit scheme for the DWD Lokal-Modell. *Met. Atmos. Phys.* (to be submitted).

Tanguay, M. A., A. Robert and R. Laprise, 1990 : A semi-implicit semi-Lagrangian fully compressible regional forecast model. *Mon. Wea. Rev.,* **118**, 1970-1980.

Yamamoto, A. and T. Satomura, 1994 : An introduction of a radiation scheme in non-hydrostatic model. *Prep. Spring Conf. MSJ.,* **65**, A103 (in Japanese).

Yamasaki, M., 1977: A preliminary experiment of the tropical cyclone without parameterizing the effects of cumulus convection. *J. Meteor. Soc. Japan,* **55**, 11-31.

Yoshizaki, M., T. Kato, Y. Tanaka, H. Takayama, S. Shoji, H. Seko, K. Arao and K. Manabe, 2000 : Analytical and numerical study of the 26 June 1998 orographic rainband observed in the western Kyusyu, Japan. *J. Meteor. Soc. Japan,* **77**, 835-856.

気象研究所技術報告一覧表

第１号　バックグラウンド大気汚染の測定法の開発（地球規模大気汚染特別研究班，1978）
Development of Monitoring Techniques for Global Background Air Pollution. (MRI Special Research Group on Global Atmospheric Pollution, 1978)

第２号　主要活火山の地殻変動並びに地熱状態の調査研究（地震火山研究部，1979）
Investigation of Ground Movement and Geothermal State of Main Active Volcanoes in Japan. (Seismology and volcanology Research division, 1979)

第３号　筑波研究学園都市に新設された気象観測用鉄塔施設（花房龍男・藤谷徳之助・伴野　登・魚津　博，1979）
On the Meteorological Tower and Its Observational System at Tsukuba Science City. (T. Hanafusa, T. Fujitani, N. Banno, and H. Uozu, 1979)

第４号　海底地震常時観測システムの開発（地震癌研究部，1980）
Permanent Ocean − Bottom Seismograph Observation System. (Seismology and Volcanology Research Dvision, 1980)

第５号　本州南方海域水温図−400m（又は500m）深と1,000m深−（1934−1943年及び1954−1980年）（海洋研究部，1981）
Horizontal Distribution of Temperature in 400m (or 500m) and 1,000m Depth in Sea South of Honshu, Japan and Western − North Pacific Ocean from 1934 to 1943 and from 1954 to 1980. (Oceanographical Research Division, 1981)

第６号　成層圏オゾンの破壊につながる大気成分及び紫外日射の観測（高層物理研究部，1982）
Observations of the Atmospheric Constituents Related to the Stratospheric ozon Depletion and the Ultraviolet Radiation. (Upper Atmosphere Physics Research Division, 1982)

第７号　83型強震計の開発（地震火山研究部，1983）
Strong − Motion Seismograph Model 83 for the Japan Meteorological Agency Network. (Seismology and Volcanology Research Division, 1983)

第８号　大気中における雪片の融解現象に関する研究（物理気象研究部，1984）
The Study of Melting of Snowflakes in the Atmosphere. (Physical Meterology Research Division, 1984)

第９号　御前崎南方沖における海底水圧観測（地震火山研究部・海洋研究部，1984）
Bottom Pressure Observation South off Omaezaki, Central Honsyu. (Seismology and Volcanology Research Division and Oceanographical Research Division, 1984)

第10号　日本付近の低気圧の統計（予報研究部，1984）
Statistics on Cyclones around Japan. (Forecast Research Division, 1984)

第11号　局地風と大気汚染質の輸送に関する研究（応用気象研究部，1984）
Observations and Numerical Experiments on Local circulation and Medium − Range Transport of Air Pollutions. (Applied Meteorology Research Division, 1984)

第12号　火山活動監視手法に関する研究（地震火山研究部，1984）
Investigation on the Techniques for Volcanic Activity Surveillance. (Seismology and volcanology Research Division, 1984)

第13号　気象研究所大気大循環モデル－Ｉ（MRI・GCM－I）（予報研究部，1984）

A Description of the MRI Atmospheric General circulation Model (The MRI・GCM－I). (Forecast Research Division, 1984)

第14号　台風の構造の変化と移動に関する研究―台風7916の一生―（台風研究部，1985）

A Study on the Changes of the Three - Dimensional Structure and the Movement Speed of the Typhoon through its Life Time. (Typhoon Research Division, 1985)

第15号　波浪推算モデルMRIとMRI―IIの相互比較研究―計算結果図集―（海洋気象研究部，1985）

An Intercamparion Study between the Wave Models MRI and MRI－II － A Compilation of Results －(Oceanographical Research Division, 1985)

第16号　地震予知に関する実験的及び理論的研究（地震火山研究部，1985）

Study on Earthquake Prediction by Geophysical Method. (Seismology and Volcanology Research Division, 1985)

第17号　北半球地上月平均気温偏差図（予報研究部，1986）

Maps of Monthly Mean Surface Temperature Anomalies over the Northern Hemisphere for 1981－1981. (Forecast Research Division, 1986)

第18号　中層大気の研究（高層物理研究部・気象衛星研究部・予報研究部・地磁気観測所，1986）

Studies of the Middle Atmosphere. (Upper Atmosphere Physics Research Division, Meteorological Satellite Research Division, Forecast Research Division, MRI and the Magnetic Observatory, 1986)

第19号　ドップラーレーダーによる気象・海象の研究（気象衛星研究部・台風研究部・予報研究部・応用気象研究部・海洋研究部,1986）

Studies on Meteorological and Sea Surface Phenomena by Doppler Radear. (Meteorological Satellite Research Division, Typhoon Research Division, Forecast Research Division, Applied Meteorology Research Division and Oceanographical Research Dvision, 1986)

第20号　気象研究所対流圏大気大循環モデル（MRI・GCM―Ｉ）による12年間分の積分（予報研究部，1986）

Mean Statistics of the Tropospheric MRI・GCM－I based on 12－year Integration. (Forecast Research Division, 1986)

第21号　宇宙線中間子強度1983－1986（高層物理研究部，1987）

Multi － Directional Cosmic Ray Meson Intensity 1983－1986. (Upper Atmosphere Physics Research Divison, 1987)

第22号　静止気象衛星「ひまわり」画像の噴火噴煙データに基づく噴火活動の解析に関する研究（地震火山研究部，1987）

Study on Analysis of Volcanic Eruptions based on Eruption Cloud Image Data obtained by thd Geostationary Meteorological satellite 'GMS). (Seismology and Volcanology Research Division, 1987)

第23号　オホーツク海海洋気候図（篠原吉雄・四竈信行，1988）

Marine Climatological Atlas of the sea of Okhotsk. (Y. Shinohara and N. Shikama, 1988)

第24号　海洋大循環モデルを用いた風の応力異常に対する太平洋の応答実験（海洋研究部，1989）

Response Experiment of Pacific Ocean to Anomalous Wind Stress with Ocean General Circulation Model. (Oceanographical Research Division, 1989)

第25号　太平洋における海洋諸要素の季節平均分布（海洋研究部，1989）

Seasonal Mean distribution of Sea Properties in the Pacific. (Oceanographical Research Division, 1989)

第26号　地震前兆現象のデータベース（地震火山研究部，1990）
Database of Earchquake Precursors. (Seismology and Volcanology Research Division, 1990)

第27号　沖縄地方における梅雨期の降水システムの特性（台風研究部，1991）
Characteristics of Precipitation Systems During the Baiu Season in the Okinawa Area. (Typhoon Research Dvision, 1991)

第28号　気象研究所・予報研究部で開発された非静水圧モデル（猪川元興・斉藤和雄，1991）
Description of a Nonhydrostatic Model Developed at the Forecast Research Department of the MRI. (M. Ikawa and K. Saito, 1991)

第29号　雲の放射過程に関する総合的研究（気候研究部・物理気象研究部・応用気象研究部・気象衛星・観測システム研究部・台風研究部，1992）
A Synthetic Study on Cloud－Radiation Processes. (Climate Research Department, Physical Meteorology Research Department, Applied Meteorology Research Department, Meteorological Satellite and Observation system Research Department, and Typhoon Research Department, 1992)

第30号　大気と海洋・地表とのエネルギー交換過程に関する研究（三上正男・遠藤昌宏・新野　宏・山崎孝宇，1992）
Studies of Energy Exchange Processes between the Ocean－Ground Surface and Atmosphere. (M. Mikami, M. Endoh, H. Niino, and K. Yamazaki, 1992)

第31号　降水日の出現頻度からみた日本の季節推移―30年間の日降水量資料に基づく統計―（秋山孝子，1993）
Seasonal Transition in Japan, as Revealed by Appearance Frequency of Precipitating-Days. － Statistics of Daily Precipitation Data During 30 Years － (T. Akiyama, 1993)

第32号　直下型地震予知に関する観測的研究（地震火山研究部，1994）
Observational Study on the Predictiona of Disastrous Intraplate Earthquakes. (Seismology and Volcanology Research Department, 1994)

第33号　各種気象観測機器による比較観測（気象衛星・観測システム研究部，1994）
Intercomparisons of Meteorological Observation Instruments. (Meteorological Satellite and Observation System Research Department, 1994)

第34号　硫黄酸化物の長距離輸送モデルと東アジア地域への適用（応用気象研究部，1995）
The Long－Range Transport Model of Sulfur Oxides and Its Application to the East Asian Region. (Applied Meteorology Research Department, 1995)

第35号　ウインドプロファイラーによる気象の観測法の研究（気象衛星・観測システム研究部，1995）
Studies on Wind Profiler Techniques for the Measurements of Winds. (Meteorological Satellite and Observation System Research Department, 1995)

第36号　降水・落下塵中の人工放射性核種の分析法及びその地球化学的研究（地球科学研究部，1996）
Geochemical Studies and Analytical Methods of Anthropogenic Radionuclides in Fallout Samples. (Geochemical Research Department, 1996)

第37号　大気と海洋の地球化学的研究（1995年及び1996年）（地球化学研究部，1998）
Geochemical Study of the Atmosphere and Ocean in 1995 and 1996. (Geochemical Research Department, 1998)

第38号　鉛直２次元非線形問題（金久博忠，1999）
Vertically 2-dmensional Nonlinear Problem, (H. Kanehisa, 1999)

第39号　客観的予報技術の研究（予報研究部，2000）

Study on the Objective Forecasting Techniques (Forecast Research Department)

第40号　南関東地域における応力場と地震活動予測に関する研究（地震火山研究部，2000）

Study on Stress Field and Forecast of Seismic Activity in the Kanto Region. (Seismology and Volcanology Research Department, 2000)

第41号　電量滴定法による海水中の全炭酸濃度の高精度分析および大気中の二酸化炭素と海水中の全炭酸の放射性炭素同位体比の測定（地球化学研究部，2000）

Coulometric Precise Analysis of Total Inorganic Carbon in Seawater and Measurements of Radiocarbon for the Carbon Dioxide in the Atmosphere and for the Total Inorganic Carbon in Seawater (Geochemical Research Department, 2000)

気 象 研 究 所

1946（昭和21）年 設立

所長： 中山 嵩

気象研究所技術報告

気象研究所技術報告は，1978年（昭和53）年の初刊以来，気象研究所が必要の都度発行する刊行物であり，原則として気象研究所職員及びその共同研究者による気象学，海洋学，地震学その他関連の地球科学に関する技術報告，資料報告および総合報告（以下報告という）を掲載する。

気象研究所技術報告の編集は，編集委員会が行う。編集委員会は原稿の掲載の可否を判定する。

気象研究所技術報告 ISSN 0386-4049
第 42 号

平成13年3月 発 行

編集兼発行者 気 象 研 究 所

〒305-0052 茨城県つくば市長峰1－1
TEL. (0298) 53-8535

印刷所 有限会社 アレス

〒305-0032 茨城県つくば市竹園2－11－6